Guacira Costa de Oliveira

Advances in Multi-Terminal HVDC Transmission Systems: Nonlinear controllers for Modular Multilevel Converters

São Paulo
2021

Guacira Costa de Oliveira

Advances in Multi-Terminal HVDC Transmission Systems: Nonlinear controllers for Modular Multilevel Converters

Corrected Version

Doctoral thesis presented to the Polytechnic School of the University of São Paulo to obtain the title of Doctor of Science and to the Université Paris-Saclay to obtain the title of Doctorat en Automatique.
Doctoral specialty: Automatics and Power systems

Supervisor: Renato Machado Monaro
Supervisor: Gilney Damm
Supervisor: Françoise Lamnabhi-Lagarrigue

São Paulo
2021

Este exemplar foi revisado e corrigido em relação à versão original, sob responsabilidade única do autor e com a anuência de seu orientador.

São Paulo, 18 de Fevereiro de 2021

Assinatura do autor: Guacira Costa de Oliveira

Assinatura do orientador: Renato M. Monaro

Catalogação-na-publicação

Oliveira, Guacira Costa de
Advances in Multi-Terminal HVDC Transmission Systems: Nonlinear controllers for Modular Multilevel Converters / G. C. Oliveira -- versão corr. -- São Paulo, 2021.
221 p.

Tese (Doutorado) - Escola Politécnica da Universidade de São Paulo. Departamento de Engenharia de Energia e Automação Elétricas.

1.Modular Multilevel Converter 2.Nonlinear Control 3.Lyapunov Theory 4.MMC Average Bilinear Model I.Universidade de São Paulo. Escola Politécnica. Departamento de Engenharia de Energia e Automação Elétricas II.t.

Acknowledgment

First of all, I would like to address my acknowledgments to my Brazilian supervisor Renato Machado Monaro. I appreciate his many contributions, constant incentive, and encouragement for this research. I am also very grateful to my advisor, Gilney Damm, to support me and share his knowledge and experience during the time I worked at the L2S Laboratory. Equally important, I thank my thesis director Françoise Lamnabhi-Lagarrigue for her guidelines.

I want to thank the reviewers and the jury for the time and dedication to read this thesis and add valuable comments on this research.

Moreover, I am thankful to Dr. Filipe Perez for sharing his knowledge of control and mathematics and his constant incentive and support.

Furthermore, I appreciate Miguel Jiménez Carrizosa for sharing his nonlinear controller experience and have received me at Centro de Eléctronica Industrial - UPM. As well, I thank Professor Elena Panteley for her contributions to the development of the bilinear controller.

I am also grateful to Supelec staff Anne, Maryvonne, and Raul; also, USP staff Fatima, Eliana e Elias, to help me with the bureaucracies so often.

Besides research, I have made many friends at L2S, which turned my days at work even better: Hidayet Zaimaga, Fernando Bottura, Paulo, Abdelkrim, Janailson, Juan, Sabah, Alessio, Higor, Ricardo, Leonardo Doin, and Kuba. I am equally grateful to João Neto and Helton for joy times.

I also would like to express gratitude to my colleagues from LGrid at USP, especially Luis Lourenço, who has shared many of his knowledge and contribute to many technical discussions.

Also, I was very fortunate during my stay in Paris because I met many people who welcomed me as family. Eleonore Schiller and Matheus to be the best hosts that I could have. Adrien Falce and his family for receive me and show many of the French culture. Zilda and her family for welcome in my first days in Orsay. Barbara and her family for the often warm greeting. In particular, my friend Olivier Barbeau for providing me with unfailing support and continuous encouragement throughout my years of study and through the process of researching and writing this thesis.

Above all, I would like to thank my long term friends in which I always receive positive

messages and encouragement: Marina, Leiviane, Thayna, Alice, Rene, Renaira, Luciana, Athila, Marsolla, Larissa Lima, Luciano, Ailton Jr., and Priscilla Vale. I also have to thank Lais Campos to support me psychologically in overcoming numerous obstacles I have been facing through my Ph.D.

I want to express my deepest gratitude to my mother, Maria Nilca da Costa, and my brother Rafaell da Costa Bezerra for being the best example of thankful and honest people and their constant support and encouragement. Additionally, thank my father, Manoel Joaquim de Oliveira Neto (in memory), for his many advice concerning studies.

I couldn't forget mention my nephew Ravel, my sister-in-law Renania, my cousins Rafaella, Vanessa, Vânia, Rodolfo, João Paulo, Fernando, Lara e Manoel and my uncles Nilma, Nilda, Nilza, Antônio, Francisco, Damião, Mizael, José and Manoel that are always celebrating the achievements that I have in my career.

Finally, I would like to acknowledge the Erasmus Mundus SMART 2 (Project Reference: 552042-EM-1-2014-1-FR-ERA MUNDUS-EMA2) coordinated by Centrale SUPELEC, and the Coordination for the Improvement of Higher Education Personnel (CAPES) for the financial support.

Gyuacira Costa de Oliveira

October, 2020

Abstract

Oliveira, G. C **Advances in Multi-Terminal HVDC Transmission Systems: Nonlinear controllers for Modular Multilevel Converters**. 228 p. Ph.D. Thesis – Polytechnic School, University of São Paulo, and Laboratory of Signals and Systems, University of Paris-Saclay, 2021.

Modular Multilevel Converter (MMC) is a very important topic in the context of high voltage direct-current transmission systems applications. This topology is suitable for several applications, as a result of smaller switching losses due to lower switching frequency, low alternating-current harmonic distortion, modular structure enabling scalability construction and practical maintenance. However, a more complex control strategy is required to control circulating current, to compensate the voltage imbalance between legs and voltage balancing of Submodules (SMs), such as to maintain SM's capacitors voltages constant. This thesis presents two nonlinear controllers for an MMC, able to control circulating currents, and the energy in the converter. First proposed controller is developed using Lyapunov theory, strongly based on singular perturbation and feedback linearization techniques. Second one is designed following bilinear theory based on quadratic feedback control. For both, a mathematical proof is given for its stability, which is based on Lyapunov's theory. This result provides asymptotic stabilization for the three-phases MMC. The use of a Lyapunov function implies a formal verification of stability and a broad region of attraction for the considered model. Both control techniques are developed by means of an average bilinear model and performances are verified by means of a detailed MMC switching model at Matlab Simscape Electrical environment. The evaluation includes active and reactive power reference variations, grid imbalance conditions, parameters uncertainties and even a comparison with a standard PI controller. Also, for the nonlinear controllers, it is studied the effect of control gains on the system's dynamics. The main thesis' contributions can then be stated as the two distinct nonlinear control algorithms, based on a bilinear mathematical model, designed for MMC converters; Both algorithms are able to control circulating currents and converter's energy at the switching MMC model; There are formal

stability analysis by Lyapunov theory for these controllers; and once these proposed controllers are not based on a linearized model, a broad operation region is obtained.

Keywords: Modular Multilevel Converter, Nonlinear Control, Lyapunov Theory, MMC Average Bilinear Model.

Resumo

Oliveira, G. C **Advances in Multi-Terminal HVDC Transmission Systems: Nonlinear controllers for Modular Multilevel Converters**. 228 p. Tese de doutorado – Escola Politécnica, Universidade de São Paulo, and Laboratory of Signals and Systems, University of Paris-Saclay, 2021.

O conversor multinível modular é o tópico de interesse amplo e atual no contexto de aplicações de sistemas de transmissão de corrente contínua de alta tensão. Essa topologia é adequada para várias aplicações, como resultado de menores perdas de chaveamento, devido à menor frequência de comutação dos IGBTs, baixa distorção harmônica na corrente alternada, estrutura modular que permite escalabilidade na construção e manutenção prática. No entanto, é necessária uma estratégia de controle mais complexa para controlar a corrente circulante, para compensar o desequilíbrio de tensão entre as pernas e o equilíbrio de tensão dos sub-módulos, de forma a manter constantes as tensões dos capacitores dos sub-módulos. Esta tese apresenta dois controles não-lineares para conversores MMC, capazes de controlar correntes circulantes e a energia no conversor. O primeiro é projetado seguindo a teoria bilinear baseada no controle de feedback quadrático. O segundo controlador proposto é desenvolvido usando a teoria de Lyapunov, fortemente baseada em técnicas *singular perturbation* e *feedback linearization*. Para ambos, é definida uma prova matemática de sua estabilidade, baseada na teoria de Lyapunov. Este resultado fornece estabilização assintotica para as três fases MMC. O uso de uma função de Lyapunov implica uma verificação formal da estabilidade e uma região explícita de atração para o modelo considerado. Ambas as técnicas de controle são desenvolvidas por meio de um modelo médio bilinear e a robustez e o desempenho são verificados por meio de um modelo chaveado de conversores MMC nas simulações do Matlab Simscape Electrical. A avaliação inclui variações de referência de potência ativa e reativa, condições de desequilíbrio da rede, incertezas de parâmetros e até uma comparação com um controlador PI. Além disso, para os controladores não lineares, são estudados: o efeito do controle de ganho na dinâmica do sistema e no desempenho do controlador em caso de alteração no ponto de operação. As principais contribuições da tese

são os dois algoritmos distintos de controle não-linear, baseados em um modelo matemático bilinear, projetados para conversores MMC; Ambos os algoritmos são capazes de controlar o equilíbrio de corrente circulante e a energia do conversor; Há uma análise formal de estabilidade pela teoria de Lyapunov para esse sistema; e uma vez que os controles propostos não se baseiam em um modelo linearizado, uma vasta região de operação é alcançável.

Palavras-chave: Conversores Modulares Multiníveis, Controle Não-linear, Teoria de Lyapunov, Modelo Médio Bilinear de MMC.

Résumé

Oliveira, G. C **Advances in Multi-Terminal HVDC Transmission Systems: Nonlinear controllers for Modular Multilevel Converters**. 228 p. Tese de doutorado – Escola Politécnica, Universidade de São Paulo, and Laboratory of Signals and Systems, University of Paris-Saclay, 2021.

Le convertisseur modulaire à plusieurs niveaux est un sujet d'intérêt important et actuel dans le contexte des applications de systèmes de transmission haute tension à courant continu. Cette topologie convient à plusieurs applications, en raison de pertes de commutation plus faibles dues à une fréquence de commutation plus petite, à une faible distorsion harmonique de courant alternatif, à une structure modulaire permettant une construction évolutive, et une maintenance plus simple. Cependant, une stratégie de contrôle plus complexe est nécessaire pour contrôler le courant circulant, pour compenser le déséquilibre de tension entre les circuits et l'équilibrage de tension de SMs, de manière à maintenir constantes les tensions des condensateurs de SM. Cette thèse présente deux contrôleurs non linéaires pour un MMC, capables de contrôler les courants circulants et l'énergie dans le convertisseur. Le premier est conçu selon la théorie bilinéaire basée sur le contrôle de rétroaction quadratique. Le deuxième contrôleur proposé est développé en utilisant la théorie de Lyapunov, fortement basé sur des techniques de perturbation singulière et de linéarisation par bouclage. Pour les deux, une étude mathématique est réalisée sur la stabilité, basée sur la théorie de Lyapunov. Ce résultat assure une stabilisation asymptotique pour les trois phases MMC. L'utilisation d'une fonction de Lyapunov implique une vérification formelle de la stabilité et une région explicite d'attraction pour le modèle considéré. Les deux techniques de contrôle sont développées à partir d'un modèle bilinéaire moyen, et la robustesse et les performances sont vérifiées au moyen d'un modèle de commutation MMC provenant des simulations électriques Matlab Simscape. L'évaluation comprend des variations de référence de puissance active et réactive, des conditions de déséquilibre du réseau, des incertitudes de paramètres et même une comparaison avec un contrôleur PI standard. Aussi, pour les contrôleurs non linéaires sont étudiés: l'effet des gains du contrôle sur la dynamique du système et les

performances du contrôleur en cas de changement du point de fonctionnement. Les contributions principales de la thèse sont les deux algorithmes de contrôle non linéaires distincts, basés sur un modèle mathématique bilinéaire, conçus pour les convertisseurs MMC; Les deux algorithmes sont capables de contrôler l'équilibrage du courant et énergie du convertisseur au niveau du modèle détaillé du MMC par commutation; Il existe une analyse formelle de la stabilité par la théorie de Lyapunov pour ces systèmes; et une fois que le contrôle proposé n'est pas basé sur un modèle linéarisé, une vaste région d'opération est garantie.

Mots-clé: Convertisseurs modulaires à plusieurs niveaux, contrôle non linéaire, théorie de Lyapunov, modèle MMC bilinéaire moyen.

List of Figures

List of Tables

List of Acronyms

AC Alternating Current

AVM Average-model

CAPES Coordination for the Improvement of Higher Education Personnel

CCC Capacitor-Commutated Converters

DC Direct Current

EPS Electric Power System

ECB Equivalent Circuit Based

HVDC High Voltage Direct Current

IGBT Insulated Gate Bipolar Transistor

LCC Line Commutated Converter

LS Least Squares

MMC Modular Multilevel Converter

MTDC Multi-terminal HVDC

NL Nearest-Level

NPC Neutral-Point Clamped

PLL Phase Locked Loop

PWM Pulse Width Modulation

PCC Point of Common Coupling

PLQR Periodic Linear Quadratic Regulator

PR Proportional-resonant

PI Proportional-integral

SM Submodule

SHE Selective Harmonic Elimination

SVM Space Vector Modulation

SPWM Sinusoidal Pulse Width Modulation

TE Thevenin's Equivalent

VSC Voltage Source Converter

List of Symbols

$\bar{V}_C^{SM}$	SM's nominal capacitor voltage
i_{cirj}	MMC circulating current per phase
$i_{cirj}^{2\omega}$	Double fundamental frequency circulating current per phase j
i_{dc}	DC current
i_{mj}	MMC arm current per phase
i_{vdq}	dq components of AC side currents
i_{vd}	Direct d component of AC side currents
i_{vj}	AC side currents per phase in ABC
i_{vq}	Quadrature q component of AC side currents
k_i^x	Integral gain of state x
k_p^x	Proportional gain of state x
L_c	AC phase inductance
P_e	Active power
P_{ej}^{AC}	AC active power on phase j
P_{ej}^{DC}	DC active power on phase j
Q_e	Reactive power
R_c	AC phase impedance
V_{arm}^j	Output voltage on the arm linked with phase j
V_o^n	SM n, output voltage

v_{Cn}^{SM} Capacitor's voltage

v_{Ctot_j} Sum of all capacitors voltage on the leg linked with phase j

$v_{Ctot_{mj}}$ Sum of all capacitors voltage on arm m of phase j

v_{d0} DC voltage component

V_{DC} DC output voltage

v_{fd} Direct d component of AC voltage per phase at the PCC

v_{fq} Quadrature q component of AC voltage per phase at the PCC

v_j AC voltage per phase at the PCC

v_{mj} Equivalent arm voltage produced by SMs per phase

W_C^{SM} stored energy per SM

W_h Total converter energy

W_v Energy difference between MMC upper and lower part

W_l Total energy in lower converter arms

W_u Total energy in upper converter arms

avm MMC average-model

j AC phases

L MMC arm inductance

l MMC lower arm

m MMC upper or lower arm

N Number of series SMs per arm

R SM switching power losses

swit MMC switching-model

u MMC upper arm

Contents

CHAPTER 1

Introduction

Green energy systems have been expanding considerably worldwide in the last decades. In 2017, for the first time, 30 % of the electricity generated in Europe was produced by renewable sources. This amount was the combination of solar, biomass, and, meaningfully, the wind, which has grown to 20.9 % of the production [1]. Figure 1 shows that in 2018 thirteen of twenty-seven European countries had already reached the targeted 20% of renewable share [2]. However, the target has been updated to at least a 32% share of renewable energy in 2030 [3]. Therefore, European renewable energy ambitions are close to those targeted, and the electrical grid infrastructure is changing to support the power consumption.

Figure 1 – Share of energy from renewable sources in the Europe Member States in % of the gross final energy consumption.

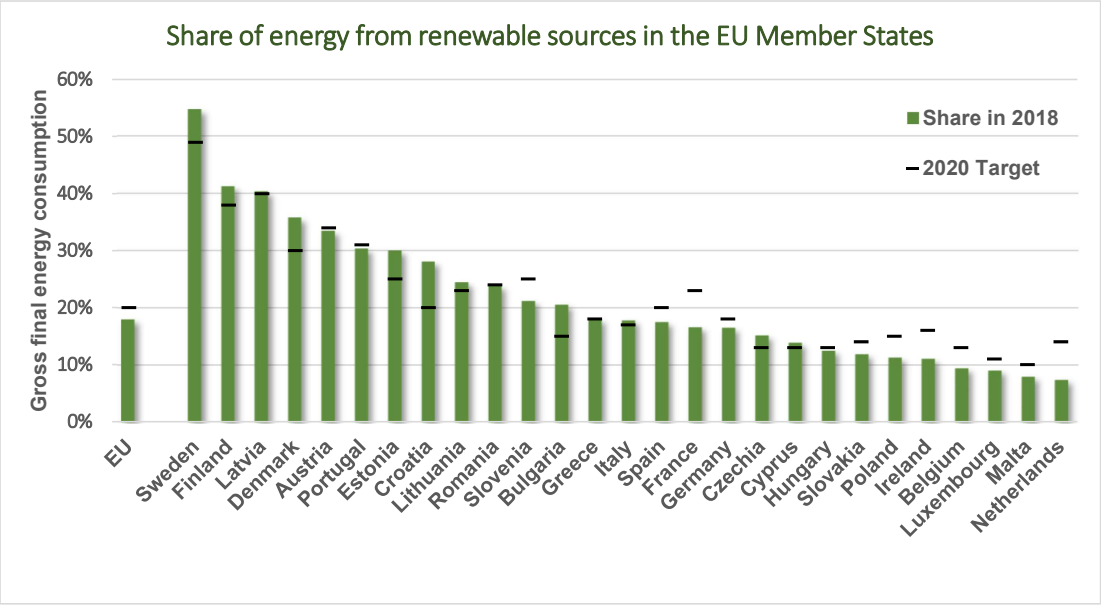

Source: [2]

The new grid layout consists of both Alternating Current (AC) transmission and Direct Current (DC) systems. DC technology performs suitable solutions, such as high voltage transmission of large-scale power either for long distances or for offshore energy sources and underground lines. Moreover, the electricity market stimulates the European *SuperGrid* construction, allowing it to conduct electricity inside its borders and neighboring countries. The European *SuperGrid* aims to integrate $10\ \%$ of the European electrical production by 2020 [4], and to rise to 15% by 2030 to ensure stability and a more sustainable energy supply [5].

A 1000 MW $\pm$ 320 kV part of the European *SuperGrid* that connects France and Spain is already operating with the MMC technology [6]. Nowadays there is a project to link offshore wind reserves in the North Sea to high population zones in the south region of Germany; and there is a link connecting France and Italy that is under development to date [4]. The European *SuperGrid* is a concrete plan along with distinct technical requirements related to control automation, DC protection, and grid stability.

An electrical grid with a variety of power sources creates new challenges for the system operation. Long electrical transmission lines may present power limiting to transmit high power levels and face oscillatory stability problems. Currently, High Voltage Direct Current (HVDC) is currently applied to interconnect asynchronous systems, large-scale power transfer in long-distance projects, and underwater and underground transmission, which is also a less expensive solution after a break-even distance. The cost of the DC stations is higher than AC ones, while DC lines are more affordable. Besides, losses in DC lines are smaller than in AC lines since there are no capacitive and inductive effects. Figure 2 presents break-even distance, which represents the length of the transmission line where the cost of DC station plus DC lines becomes equal to the price of AC station plus AC lines [7; 8].

Figure 3 shows an electrical grid from the AC generation to the final consumer. The most important equipment of a AC-DC station is the converter. It transforms the AC produced power into DC, which will flow through DC lines and supply consumers.

The Modular Multilevel Converter (MMC) is the most recent converter topology used

Figure 2 – Relation between HVDC and HVAC cost: the break-even distance to system which uses cables is near to $50\ km$, and using overhead transmission line is near to $600\ km$.

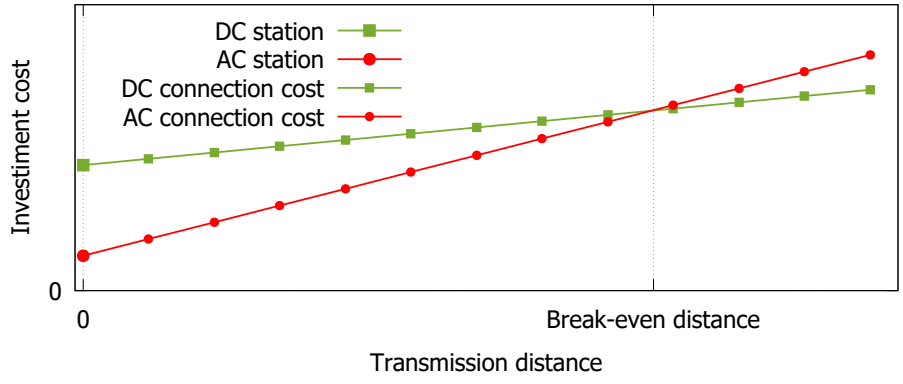

Source: [7]

Figure 3 – Sketch of electrical grid.

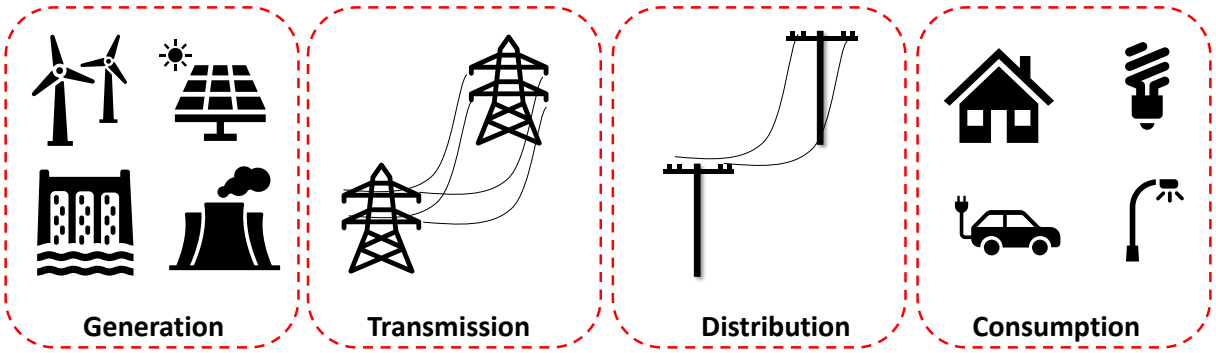

Source: Author

at HVDC stations. This converter topology outperforms the previous technology, especially concerning smaller switching losses due to the low switching frequency, lower AC harmonic distortion, modular structure enabling a scalable construction, and practical maintenance. On the other hand, the MMC presents a complex control and higher building cost than the previous topology. On the other hand, circulating current management and the voltage balancing of SMs are some challenges related to the use of this technology. Therefore, this thesis aims to develop a nonlinear control strategy for HVDC stations, particularly, an adequate solution for circulating currents and converter energy. Furthermore, the controller will be designed to assure system stabilization.

1.1 History and background

The first use of direct current was in 1882, in a long-distance electrical energy transmission line, to connect two German cities: Miesbach and Munich [9]. At the same time, New York was lighted by DC circuits. However, technical constraints limited the DC application on power systems. Since the relationship between power losses and voltage transmission level is inversely proportional, the drawback was how to change the DC voltage between the transmission and the consumption level. On the other hand, it is not difficult to convert the voltage level in AC systems using transformers. Also, AC generators are more efficient and have a more straightforward structure and maintenance compared to the DC ones. Therefore, AC power generation, transmission, and distribution is the most dominant process in Electric Power System (EPS).

Meaningful development of power electronic devices has been noticed in the past few decades. In addition to that, many technical limitations on EPS have been overcome by DC applications, such as:

- ❏ Offshore applications;
- ❏ Connection between unsynchronized AC networks;

- ❏ Power transmission capacity of underground and undersea cables and overhead transmission lines, since there was a reduction in the capacitive and inductive effects;

- ❏ Large renewable energy generation connected to the main grid since renewable energies have a seasonal power production, DC converters maintain the voltage at the PCC, so the power variations will not affect the PCC voltage.

The progress in the field of power electronics is the result of many people's efforts and research. Figure 4 presents some important events in the power electronics development. At the beginning of the EPS's research, around 1882, DC projects were limited by lighting and simple line transmission applications. DC systems advanced in the creation of mercury-vapor valves (1901), and its first applications were the German project Elbe-Berlin (although it did not work due to the second world war) and the Gotland island commercial project, in Sweden. However, mercury-vapor valves had some limitations, including electrical arcs inside the mercury tube, limited useful voltage, mercury heating time; the flexibility of small voltage levels; and the environmental issues related to exposure to mercury. As a result of these limitations, mercury-vapor valves were replaced by valves with thyristors (1970). They brought together the device's conversion and control, providing less space and weight, but their losses were higher compared to the valves.

Funding and research to develop thyristor valves in the 1960s ensured a technical improvement. For this reason, the Gotland island project was rebuilt using thyristors in the 1970s. This state-of-the-art thyristor technology is still used nowadays and has been called Line Commutated Converter (LCC).

In the late 1990s, the Capacitor-Commutated Converterss (CCCs) were created using a combination of thyristors and capacitors, and they were able to provide reactive power control. Also, a back-to-back application of an asynchronous electrical system connection $2200\ MW$ between Argentina and Brazil. In 2013, a $2385\ km$ of HVDC system was built to interconnect south hydro power plants to the major load centers of southeastern Brazil.

Nowadays, there is almost no use of CCC in projects, as the advancement of the next technologies followed their development. High rated semiconductor devices (IGBTs, IGCTs, and GCOs) define the new concept of HVDC systems. The self-commutated devices principle allowed the construction of Voltage Source Converters (VSCs). The VSC first application was executed, once again, in Sweden, on the Gotland island.

The MMC concept is the latest advancement in HVDC technology, published in 2003 by professor Rainer Marquardt [11]. MMC has several advantages, such as lower switching losses, voltage level scalability, since they have a modular structure, more straightforward maintenance, and low AC current distortion, along with other benefits. The Siemens Trans Bay Cable Project in San Francisco, USA, employs the MMC [12].

Figure 4 – Direct transmission technology evolution over the years

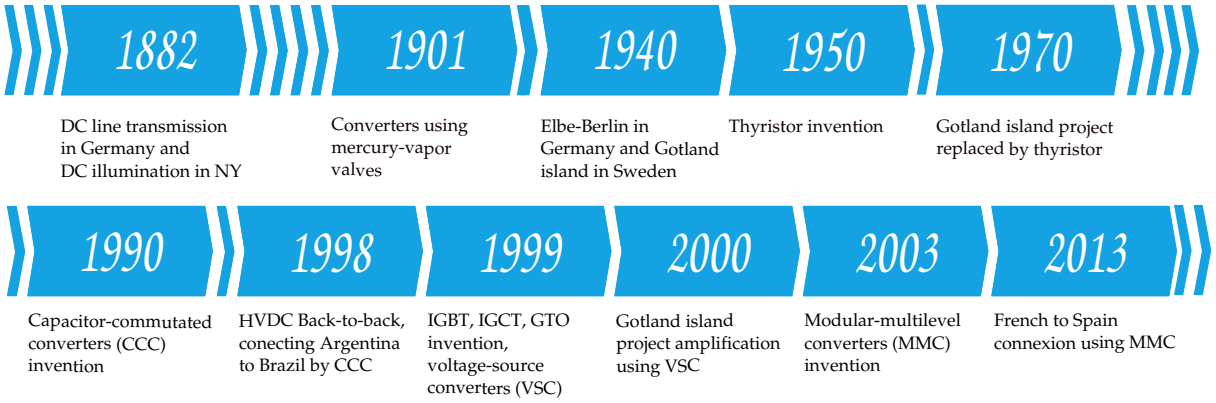

Source: [10]

Nowadays, the LCC, VSC and MMC projects coexist. Furthermore, the first connection of more than two DC stations is operated by China Southern Power Grid since 2013, using VSC [1].

1.2 Equipment

HVDC systems are mainly composed of converters that connect the AC to DC electrical bar. Between them, transformers and phase reactors complete the interface. Transformers adjust the AC voltage level to converter operational voltage. Phase reactors are composed of a large inductor connected in series at each phase to smooth the AC current and promote the power flow control. Essential components of HVDC transmission are converters that are capable of converting AC to DC, and also the opposite, DC to AC.

These converters are composed of semiconductors connected in series, and they generate the desired voltage level. There are different types of converters, depending on the semiconductors technology used. The LCCs uses thyristors, while the VSCs employs transistors. LCCs features lower switching losses, and they are suitable for high power applications. On the other hand, VSCs transistors allow the switching control in both on and off positions, implying control of the power flow direction.

1.2.1 HVDC topologies

In the literature, there are many HVDC topologies. These variabilities allow flexibility concerning power demand, stability, operations, and implementing costs.

Distinct topologies, also based on LCC and VSC, are named as back-to-back, monopolar and bipolar, regarding DC transmission line as arrangement. Other features are obtained by combining these three topologies. HVDC systems based on back-to-back topology are about two directly linked converters, without transmission line. This topology is usually applied to connect

[1] The history described in this section was based on [13; 10; 9; 14]

unsynchronized systems in which each system has a distinguished frequency or different control method.

Figure (5) shows the most common HVDC topologies. Each subfigure is described as:

- ❏ Monopoles have a single converter per terminal connected by one or two transmission lines and a current return path. Two types of the return path for current are possible: by ground or sea and metallic conductor. The ground/sea return is often favorite due to the cost reduction.

  (a) Symmetric monopole topology is widely employed on VSC system projects. This topology links two converters by two transmission lines. Each one will assume a positive or negative polarity, while the ground reference will be taken on the capacitors' grounding filters. Despite the fact there are two transmission lines, in case of a line-ground fault, the other line will not be able to maintain the operation by ground return;

  (b) Asymmetric monopole topology with ground return comprehends two converters linked by a single transmission line. The pole is usually negative due to the reduced corona effect [15]. This configuration uses the ground as the return. About this configuration, just the transmission line works to keep the system voltage levels. In case of a fault, stop operation cannot be avoided. This topology has a cost advantage due to the use of just one line. However, there aren't many projects using it, because environmental aspects linked with the ground current return;

  (c) Asymmetric Monopole with the metallic return is similar to ground return. However, it uses a metallic conductor as a return. This topology can be easily upgraded to bipolar.

- ❏ Bipolar topology combines two asymmetric monopoles. They operate with opposite polarity. In this topology, each line can work independently, by ground return or metallic, in the other line's unavailability. Bipolar topologies, compared to monopolar topologies, duplicate the power rating operation and create a redundancy, in case of one converter to be out of service. On the other hand, it is a more costly option since it uses the two converters. Furthermore, the ac side's connection is more tricky: it is necessary to provide two different transformers or a transformer with two secondary windings. The connection design need to manage issues as ac-side harmonic distortion and high direct voltage stresses — besides, bipolar installation demands attention concerning insulation;

  (d) Bipole with ground return presents a higher cost than the respective monopolar topology. Also, introduces environmental concerns resulting from ground currents if there is an unbalance between poles, such as pole outages and maintenance periods. In case of no grounding on bipolar configuration, the advantage of redundancy is

loose because the return path for the current is necessary for the half system be available during faults;

(e) Bipole with a metallic return is even costly once it needs an extra low-voltage insulated neutral conductor. However, this topology reduces environmental concerns.

Figure 5 – HVDC transmission line topologies. (a) Symmetric monopole. (b) Asymmetric monopole with ground return. (c) Asymmetric monopole with metallic return. (d) Bipolar with ground return. (e) Bipolar with metallic return.

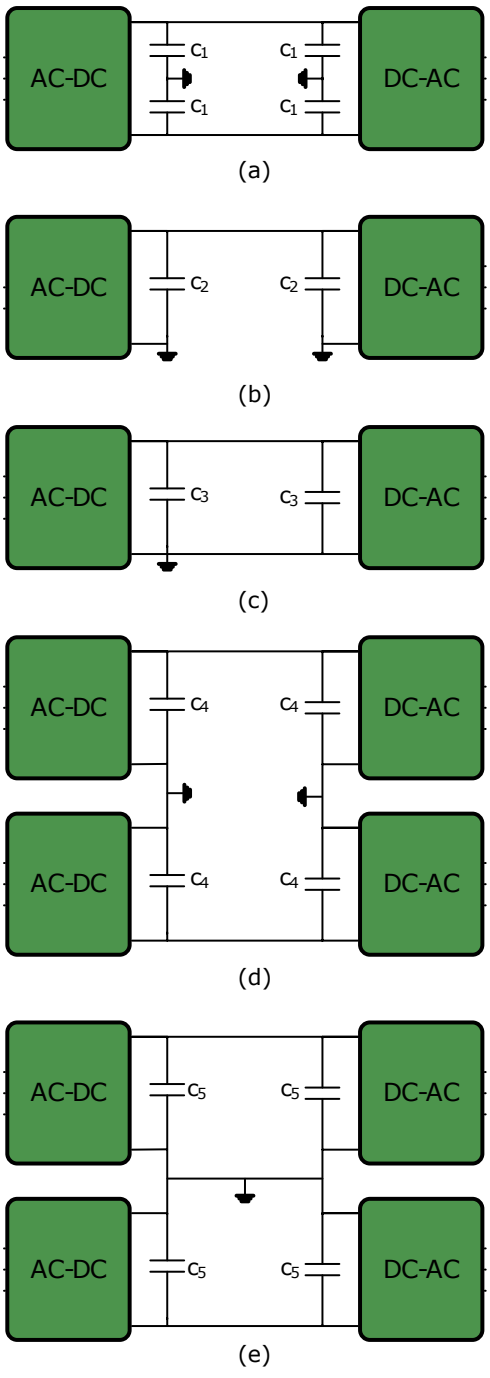

Source: [16]

Grids with more than two stations are called multi-terminal. They may combine two or more topologies. Figure 6 presents a multi-terminal test system proposed by *Conseil International des Grands Réseaux Électriques* (CIGRÉ). There is a diversity of connections in this CIGRÉ's system test, including the connection between AC and DC grid, symmetric monopole lines, and bipolar links. Also, includes the underground, oversea, and overhead lines.

Figure 6 – Multi-terminal test system proposed by CIGRÉ.

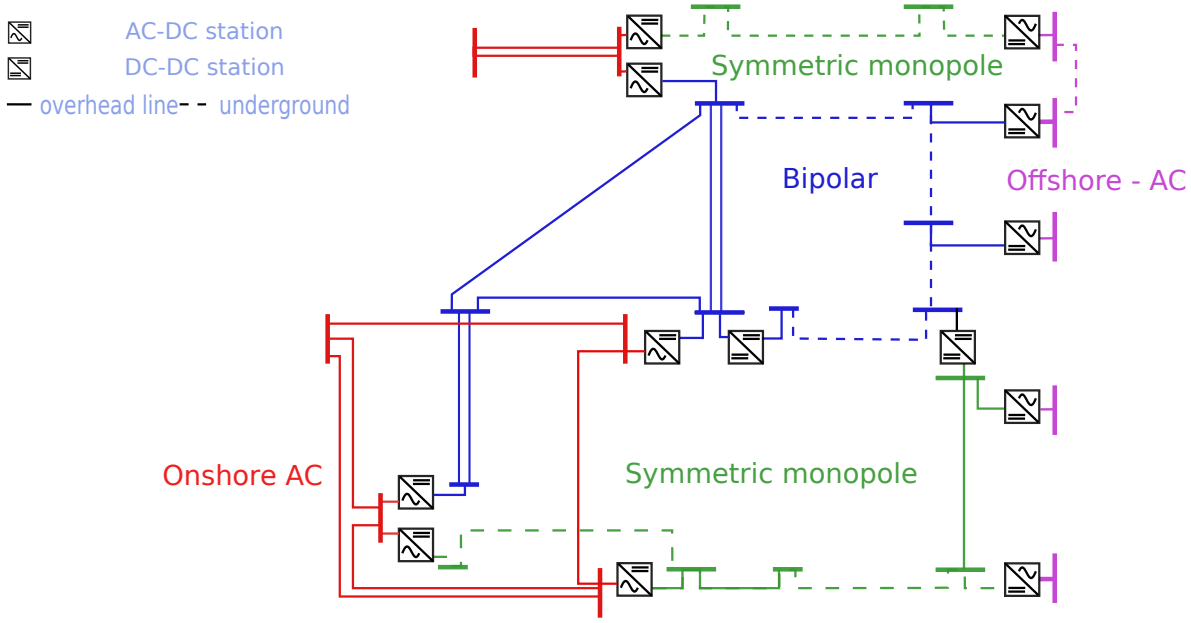

Source: [17]

1.2.2 Line-commuted converters

LCCs use thyristor valves to convert between AC and DC currents. Each phase connects two thyristor valves (one to the top and another to the bottom of the converter), so a three-phase converter consists of a six-pulse thyristor bridge, as show in figure (7). This topology produces an AC current and a DC voltage with high harmonic distortion, once each phase changes every 60^{o}. Another challenge in the six-bridge LCC is to reach the operational voltage level. Usually, thyristors are connected in series to increase the operational performance. For modern LCC applications, the twelve-pulse thyristor bridge is dominant [9].

In LCC systems, the power flow inversion is obtained by the output voltage polarity inversion. Voltage polarity inversion is not allowed in weak bars, so the LCC application needs to consider this restriction [18].

Figure 7 – Line-commuted converter topology.

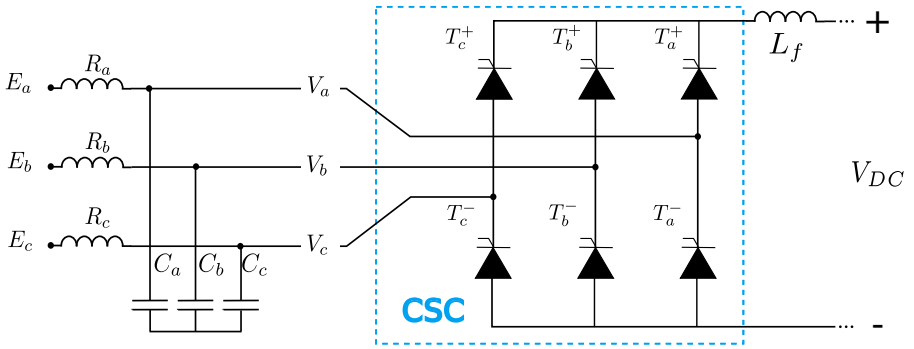

Source: [10]

1.2.3 Voltage-source converters

VSCs uses transistors, usually IGBTs. Transistors have two degrees of freedom, therefore, on and off switching control (see figure 8). A PWM, which produces a high-frequency signal, provides this switching control. As a result, VSC with PWM modulation has a wide range of voltage amplitude and the desired phase angle.

Due to the high-frequency modulation produced by PWM to switch IGBTs, there are fewer harmonic components in the current and voltage produced by VSC compared to LCC. Additionally, the on and off switching control allows VSC to control the active and reactive power by inverting the current direction and maintaining the output voltage polarity.

LCCs needs to absorb reactive power to maintain the output voltage at the desired value, so the PCC short circuit capacity must be high. On the other hand, there is no reactive power request for VSCs, so their connection can be made in both weak or strong AC grids.

Figure 8 – Voltage Source Converter topology.

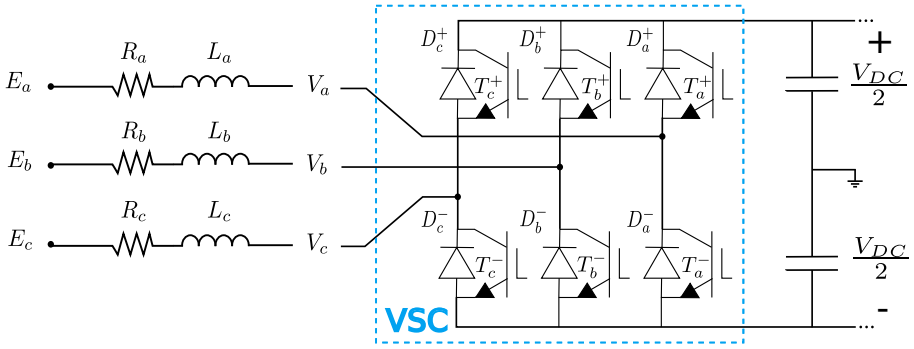

Source: [10]

1.2.4 Modular-multilevel converter

In 2003, the conception of modular converters was developed to reduce harmonic distortions in the output AC voltage, requiring little or no filters and increasing the operative voltage range. MMCs can produce an output voltage smooth and nearly an ideal sinusoidal because of the number of Submodules (SMs) used to construct the converter, see figure 9. *N* SMs imply in a output voltage with $N + 1$ levels (considering that each sub-module is a two level converter). By increasing the converter levels, there is switching loss reduction since the IGBT switching frequency is smaller. Converters that have scalability assets and produce output voltage with many levels are denoted as Modular Multilevel Converters (MMCs).

For instance, some completed projects using this technology (e.g., Siemens TransBay Cable project in San Francisco), and several other projects are still in progress (e.g., Siemens project to France-Spain connection). As aforementioned, the power production from renewable energy generations is increasing across the world. However, green sources have inherent seasonal power production. Especially wind power plants since they have a dependence on wind speed and solar power plants, due to shadowing condition dependence. These inherent characteristics may affect EPS performance regarding protection, stability, and power dispatch [19; 20]. Integrating large renewable production to the main electrical grid is currently a challenge, and much research focuses on this issue [21; 22; 23]. Multi-terminal HVDC (MTDC) based on MMC is a suitable solution to solve these challenges. A MTDC is an arrange of more than two DC stations with a few more DC or AC stations.

MTDC is an outstanding solution to offshore wind plants, due to the higher oversea cable's capacitance, and also to the power generation variability in Europe and the *Supergrid* project [24].

Figure 9 – Modular Multilevel Converter topology.

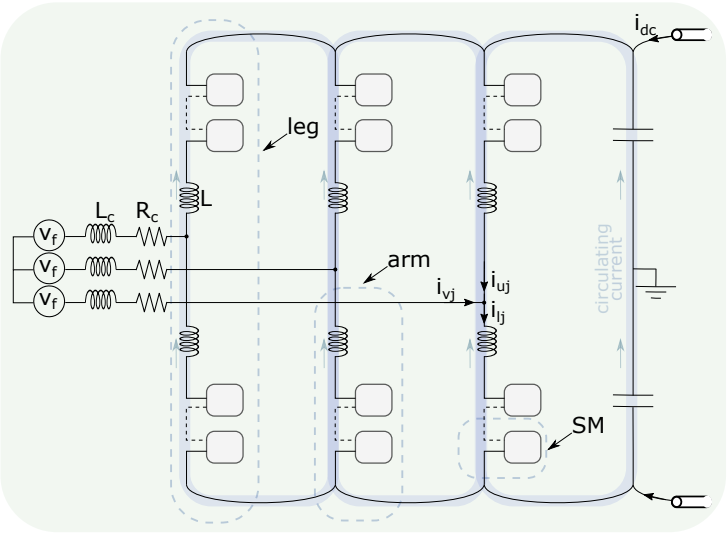

Source: Author

1.3 Controlling Modular Multilevel Converters

The control of MMC has additional challenges in comparison to other converters' topology. The control method may have to deal with:

- ❏ Externally, manage active and reactive power flow, and AC and DC voltage;
- ❏ Internally, deal with converter's dynamics as circulating currents, SM capacitor's voltage, arm balancing, phase balancing, and converter's energy control.

MMCs also have a complex modeling technique because of the high number of Submodule (SM), which requires simultaneous control to attain capacitor voltage balancing. There are many MMC modeling approaches, and models directly affect the control design. In this thesis, a mathematical model based on the average arm is used to develop the controllers, and a switching model is used to verify controls' performances. Concerning the average model, there are many approaches in the literature. In [25], the average model considers a switching function model that accurately includes each SM's capacitors' dynamic.

Additionally, in [26], there is a continuous model where arms are represented by variable voltage sources function. However, a more complex average model will increase the system order, so the complexity of the proposed solution. In this way, the average model used in this research is based on [27], which uses an equivalent SM voltage, per arm.

A switching model is simulated using the proposed controller to verify the control performance. The switching model has a low-level controller, which properly attain SMs voltage balancing. The sorting algorithm implemented in the low-level control is based on the standard technique proposed by [24].

Concerning control, most of the existing results for MMCs consist of linear controllers, as vector control. There, only one point of operation is considered in its design and system's nonlinearities are disregarded [28; 29; 30].

In this point of view, one may cite works as [31], where the nonlinear MMC model is first linearized, and then linear controllers are designed for it. In a different way, [27] proposes a discrete-time bilinear model of an MMC, controlled by a sum-of-squares decomposition method, following a nonlinear analysis.

These studies are motivated by the relevance of designing nonlinear controllers that can assure stability throughout large electrical grid operation regions, including rigorous stability analysis [32; 33]. The next chapter will discuss with more detail about modeling and control of MMC.

1.4 Main objective of the thesis

This thesis's main goal is to develop an MMC's control method suitable to ensure the system state's stability, in particular circulating currents and converter stored energy.

1.4.1 Specific objectives

The following specific objectives must be accomplished:

- ❏ To develop a control method able to minimize the circulating currents and converter stored energy for an MMC converter;
- ❏ To prove the system's stabilization;
- ❏ To evaluate the control robustness for the converter's parameter variation;
- ❏ To evaluate the control gains' impacts on converter dynamics.

1.5 Main contributions

The main contributions of this thesis are to present two new nonlinear controllers applied to the MMC. The proposed techniques allow the control of the AC and DC voltages, circulating currents, and the total and balancing converter energy. Mathematical proofs are presented for its stability, which is based on Lyapunov's theory. These controllers provide asymptotically stabilization for the three-phases MMC.

1.6 Thesis's organization

This chapter presents a general discussion on this research's motivation and the state-of-the-art concerning HVDC transmission systems. Chapter 2 presents an overview regarding equipment and topologies that describe an HVDC system, and MMC modeling aspects are discussed. Additionally, the chapter presents dynamic equations of the MMC average model, represented in a bilinear form, followed by MMC switching model considerations and an overview of control design to MMC. Chapter 3 is dedicated to present the two used system tests and to a PI controller design. In chapter 4, a nonlinear controller is proposed for an MMC. In chapter 5, a bilinear control is designed. Finally, the conclusions, further research, and publications are presented in Chapter 6.

CHAPTER 2

Modular Multilevel Converters

Modular Multilevel Converter (MMC) is a type of VSC for large scale power transmission. This technology has been considered the most viable solution for integrating renewable energy on the main grid, either AC or DC. Electrical grids composed of more than two nodes, connecting renewable generations, have been called Multi-terminal HVDC (MTDC), in which MMC is a suitable solution. MMC has high scalability and easy maintenance since the power level is directly related to the number of modules (SM) used.

The number of SM used on a MMC also implies the shape of the sinusoidal output voltage. A high number of SM units smooths the output voltage, reducing the need for filters. Each converter's leg produces a DC output voltage. However, the unbalance between voltage legs generates the circulating currents, for which the control is one of the challenges of this new technology.

Circulating currents are composed mainly of second and third harmonics and a DC component. The DC component is responsible for the converter's active power transfer, and the harmonics are mitigated. Other operational aspects related to MMC operation as SMs topology, modulation, and sorting algorithm of MMC are also introduced in this chapter. Furthermore, the feature related to modeling aspects and the detailed average model descriptions are presented. At last, MMC's control design is discussed.

2.1 MMC internal topology

In [11] it is first presented the MMC technology. These converters are suited to a high power scale, with even less distortion at the output voltage than the standard VSC. Although less distortion may not require filters, there is always a compromise with the cost when the converter uses many switches.

This thesis considers the symmetric monopole topology using half-bridge SM, as shown in Figure 10. So, a three-phase MMC with symmetric monopole topology comprehends three legs, one per phase of AC side [16]. On the other side, there is the DC terminal with two poles, positive and negative. At each leg, there are two branches, which are called arms. One of them

Figure 10 – Modular Multilevel Converter (MMC) based in the symmetric monopole topology and half-bridge's SMs.

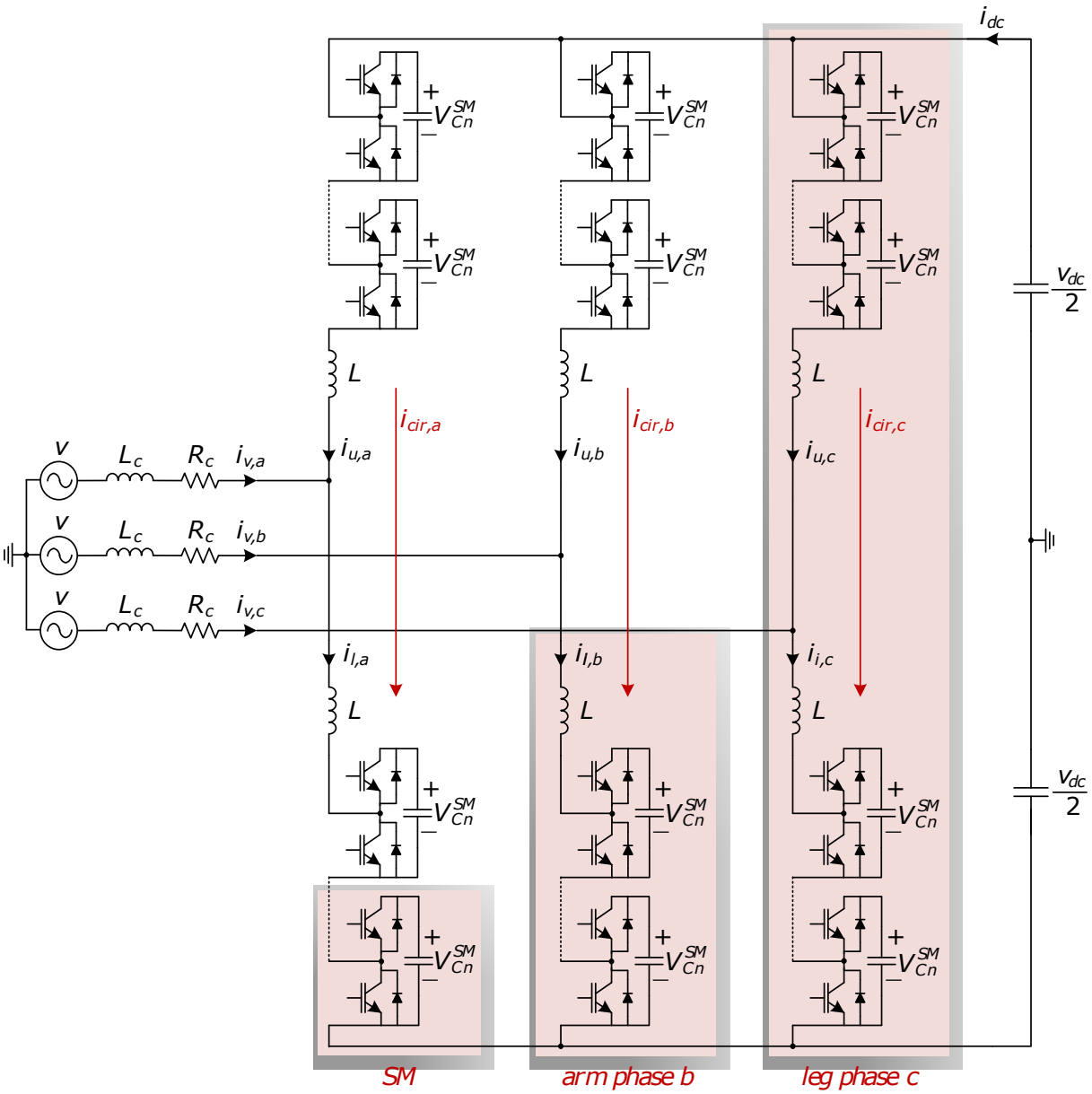

Source: Author

is connected to the positive pole and the other connected to the negative pole of the DC side terminal. The subscript m denotes the physical location of the arm concerning the DC side terminal to which it is connected. Therefore, m can assume the value u or l: referring to the upper arms, for the ones in which link the AC side and the positive pole of DC side, while the l denotes the lower arms ones, that in turn is the link between the ac side and the negative pole of DC side terminal.

Converter's arm comprise N SMs connected in series and followed by an inductance L. The design of this inductor takes into account the external fault criterion. However, a large L, imply a slower system dynamic [34].

Regarding the modeling, it is reasonable to consider a resistance R, in series with L, which summarises the resistive behavior of the MMC. R must be the equivalent of the resistive voltage drop across conducting switches, cables, connections, and the inductor resistances. However, these effects should be minimized as much as possible since they are directly related to losses [34].

Converter dimensioning is mainly defined by the application goals. It essentially consists of the chosen number of SM per arm, which is directly related to the output voltage level. However it is necessary to consider a compromise between the number of SM and the associated cost, and even the nominal voltage of each capacitor at SM.

Converter's Submodule (SM)s are composed of IGBTs, freewheeling diode, and capacitors. These devices can be arranged in different ways: half-bridge, full-bridge, or hybrid configuration. Therefore, it allows for distinct project features.

- ❑ **Full-bridge**: A MMC based on full-bridge SM has more switching devices than the half-bridge based. Consequently, this configuration presents higher losses once two devices are in conduction per active SM. Meanwhile, DC cable fault can be handled by full-bridge SM. This topology allows the SM to generate a negative voltage, which opposes to AC voltage and restrain the short-circuit current from the DC side. This ability suits full-bridge converters to applications in overhead transmission lines, since these are more susceptible to faults [35].

Figure 11 – Full-bridge SM and the related output voltage.

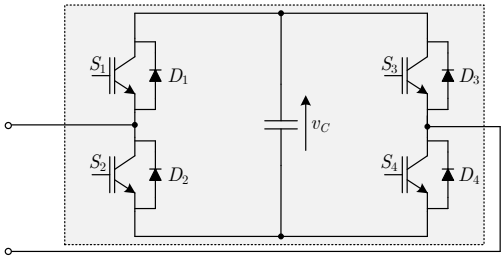

Source: Author

❏ **Half-bridge**: HVDC projects usually employ half-bridge based converters; mainly in underground and submarine HVDC transmission systems. The reduced numbers of semiconductor devices reduce losses and cost compared to the full-bridge topology. However, half-bridge SMs do not have DC fault suppression ability since this configuration cannot produce a negative voltage. Therefore, it is necessary to include breakers at the terminals [36].

Due to its vast applicability, the half-bridge topology was chosen for the following analyses in this thesis.

Figure 12 – Half-bridge SM and the related output voltage.

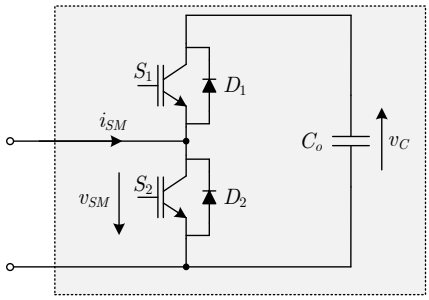

Source: Author

SM's operation

In general, MMC based on half-bridge SM synthesizes the output voltage defined by the PWM strategy, which manages the insertion of SMs. Each SM can produce an output voltage of two levels, $0\ V$ and the capacitor voltage (V_{Cn}^{SM}), as shown in figure 12. The inserted modules are called active SM and, simultaneously, some SMs that are not active are called bypassed SM. It is possible to summarise four operation modes of half-bridge SM by figure 13. Active SMs are represented by a short-circuit. As noticed in this figure, the arrangement between current polarization and capacitor generates that diversity of modes [37]. The descriptions of each mode are:

(a) S_1 is on and S_2 is off. The current has positive polarity, and the diode charges the capacitor. In this mode the SM is active;

(b) S_1 is off and S_2 is on. The current has a positive polarity, and the capacitor is not connected. In this mode, the SM is bypassed;

(c) S_1 is on and S_2 is off. The current has a negative polarity, and the capacitor is discharged through IGBT S_1. In this mode the SM is active;

(d) S_1 is off and S_2 is on. The current has a negative polarity, and the capacitor is not connected. In this mode, the SM is bypassed.

(e) This state is out of work condition. In this case, both IGBTs, S_1 and S_2 are off, and just the freewheel diodes are used to submodule operation.

(f) This state is out of work condition. In this case, both IGBTs, S_1 and S_2 are off, and just the freewheel diodes are used to submodule operation.

Figure 13 – Possible SM operations. a) active SM with positive current; b) bypassed SM with positive current; c) active SM with negative current; d) bypassed SM with negative current and; (e) and (f) submodule equivalent blocked state.

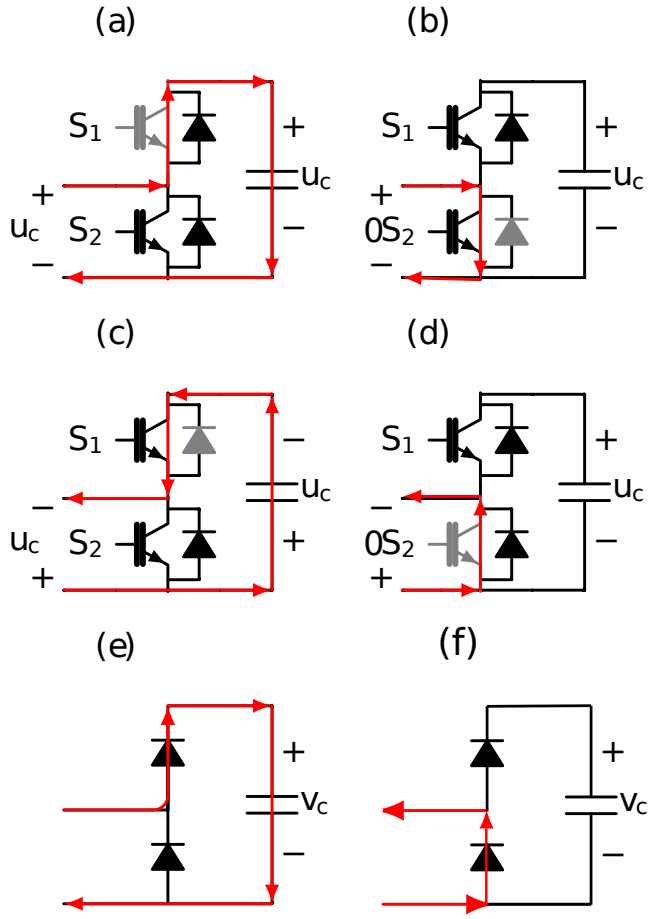

Source: Author

The direction that currents are flowing in Figure 13 are linked with the active power flow between the AC and DC side.

Modulations

A MMC's leg consist of N SM connected in series. SMs are activated to ensure the desired output voltage. Modulation defines the exact time instants to change the status of each SM between active or bypassed. By modulating the commands of the SM, it is possible to generate a signal as the desired output voltage. To attain the desired reference voltage, the converter's

controller generates the modulation, defining the exact moment to activate each SM. Modulation is the synthesis of a reference signal using pulse trains with the same average voltage at any instant [24].

There are several types of modulation strategies. They affect the total converter losses, the energy balance on the converter's arms, and voltage balancing across SMs capacitors. A proper modulation method choice implies significant dynamic effects, as mentioned above, with no further controllers [36; 38; 39; 40; 41].

In [24], modulation techniques are classified according to the switching frequency imposed on the converters, as high-switching PWM and fundamental-frequency modulation (also known as Staircase modulation).

The high switching PWM comprehends Space Vector Modulation (SVM) and Sinusoidal Pulse Width Modulation (SPWM), and also their variations. They are popular thanks to their simple implementation obtained from the two-level conventional PWM.

In [42], SPWM techniques are classified as follow:

- ❏ PWM carrier:
  - carrier-disposition:
    - phase disposition;
    - phase opposition disposition;
    - alternate phase opposition disposition.
  - subharmonic techniques:
    - saw-tooth;
    - phase-shifted carrier-based.
- ❏ Reference signal:
  - one reference;
  - two references;
  - multiple references.

At fundamental-frequency modulation, the submodule switches once per cycle, and this became attractive thanks to the reduction of switching losses. This class of modulation comprehends Selective Harmonic Elimination (SHE) and Nearest-Level (NL) [43]. These techniques are often designed for practical applications on MMC [44].

This research will not attain to describe further details concerning each modulation; however, table 1 summarises the most traditional modulation techniques and their features.

While performing MMC simulation, the modulation must be considered. For an average model approach, it is necessary to have a well-performed modulation to produce a smooth and nearly to ideal sinusoidal output voltage per arm. Therefore, when using average model

Table 1 – Modulation features.

Switching frequency	Modulation method	Feature
fundamental frequency modulation	SHE	This modulation define switching patterns which can eliminates the low-order harmonics of the output voltage waveform. The method calculates switching patterns and saves in tables for various modulation indices and the output-voltage phase angle [45; 46].
Fundamental frequency modulation	NL	This method is suitable for high-level MMC. Consists of choosing the output voltage level nearest to the reference. The harmonic content of the output voltage is inversely related to the converter level: as bigger the number of submodules, the harmonic content on the output is smaller. Compared to SHE, the implementation of this technique is less complex and requires less computational effort [42].
high switching PWM	SVM	This method consists of determining the switching sequences and the duty cycle of switching. An algorithm determines the vectors adjacent to the reference signal. A diagram composed of state vectors is used. Thus, the algorithm decides the vectors and vector zero-order, finally defining each switching device's states. [47] propose a general scheme for performing the SVM for multilevel inverters, in addition to a method for calculating the duty cycle and determining the switching sequence.
high switching PWM	SPWM	The SPWM consists of comparing a sinusoidal reference signal (modulation) with a triangular high-frequency waveform (carrier), thus generating a sequence of pulses. For multilevel converters, PWM can be performed through one or more modulating waveform, comparing them to multiple carriers. Thus, [42] summarize some SPWM modulation techniques according to the carriers' provisions and the number of modulators as presented above [48; 38].

this research considers that the modulation is already well designed and able to balance SM capacitors' voltage. These previous conditions are necessary to the mathematical propositions on controllers on chapter 4 and chapter 5, where an MMC average model is considered. On the other hand, a phase-shift PWM is considered for the switching model performed on SIMULINK.

SM capacitor voltage balancing and sorting algorithm

Modulation techniques can be combined with sorting algorithms to regulate SM capacitor voltages. A sorting algorithm is a low-level control strategy that can be used as an interface between modulation and SM's activation. It is in charge of the capacitor voltage balancing. The use of these algorithms can help to reduce switching losses and circulate currents. Therefore

a sorting algorithm can adequately choose the SM activation sequence in a way to balance the SM's capacitor charge.

An active SM contributes to the output voltage in the arm in which it is placed. Regarding the SM capacitor voltage, it is expected to maintain an average value in all SMs to produce the same output voltage level per phase and smaller circulating currents, which reduces converter losses. For this purpose, the sorting algorithm is used to sort the SM arms to be active, considering their voltage. As a result, the desired output voltage is produced, and SM capacitor's loads are balanced.

There are many sorting algorithm techniques [42; 44; 49], and the traditional one is described in the flowchart in figure 14.

By using the traditional sorting algorithm presented on figure 14, the SMs capacitors voltage share of each converter arms at each period of PWM is accomplished. Modulation defines the number of submodules N to be activated in the arm m. SM capacitor voltages are measured and classified per arm. If the current arm m is positive, the algorithm identifies and activates the N submodules with the lowest voltages. Consequently, the current charges the corresponding inserted SM capacitors, and their voltages increase.

On the other hand, if the current is negative, the algorithm identifies and activates the SMs with the highest voltages. So, the current discharges the corresponding inserted SM capacitors, and their voltages decrease. Capacitors of bypassed submodules remain unchanged.

Despite the advantages mentioned above, there are disadvantages to the use of the traditional sorting algorithm. Although it achieves the capacitors' voltage share for the MMC operating points, it increases the number of switching transitions among the SMs. Because of the sorting algorithm may change the submodule status (inserted/bypassed) through two consecutive PWM periods in which there is no change of inserted number N. The higher switching frequency also raises the power losses, which are undesirable in high-power systems projects.

This thesis use a sorting algorithm presented by [24]. The author considers that the phase-shift modulation technique combined with the sorting algorithm provides sufficient capacitor voltage share and contributes with a discussion concerning the attained results.

Circulating Current

DC voltage generated by each leg is not necessarily balanced. Because of this unbalance, currents circulate in the three phases of the converter, and they are called circulating currents. They do not affect AC side currents, but produce the equivalent DC current (i_{dc}) [50].

Circulating currents ($i_{cir,abc}$ presented in figure (10)) are composed of a DC component and AC component, with the double of the grid nominal frequency. While the DC component is essential for the transmission of real power, the AC component needs to be mitigated. This comprehends one of the technical challenges of MMC technology, once these circulating currents can increase converter's losses.

Figure 14 – Traditional sorting algorithm achievement during one PWM period.

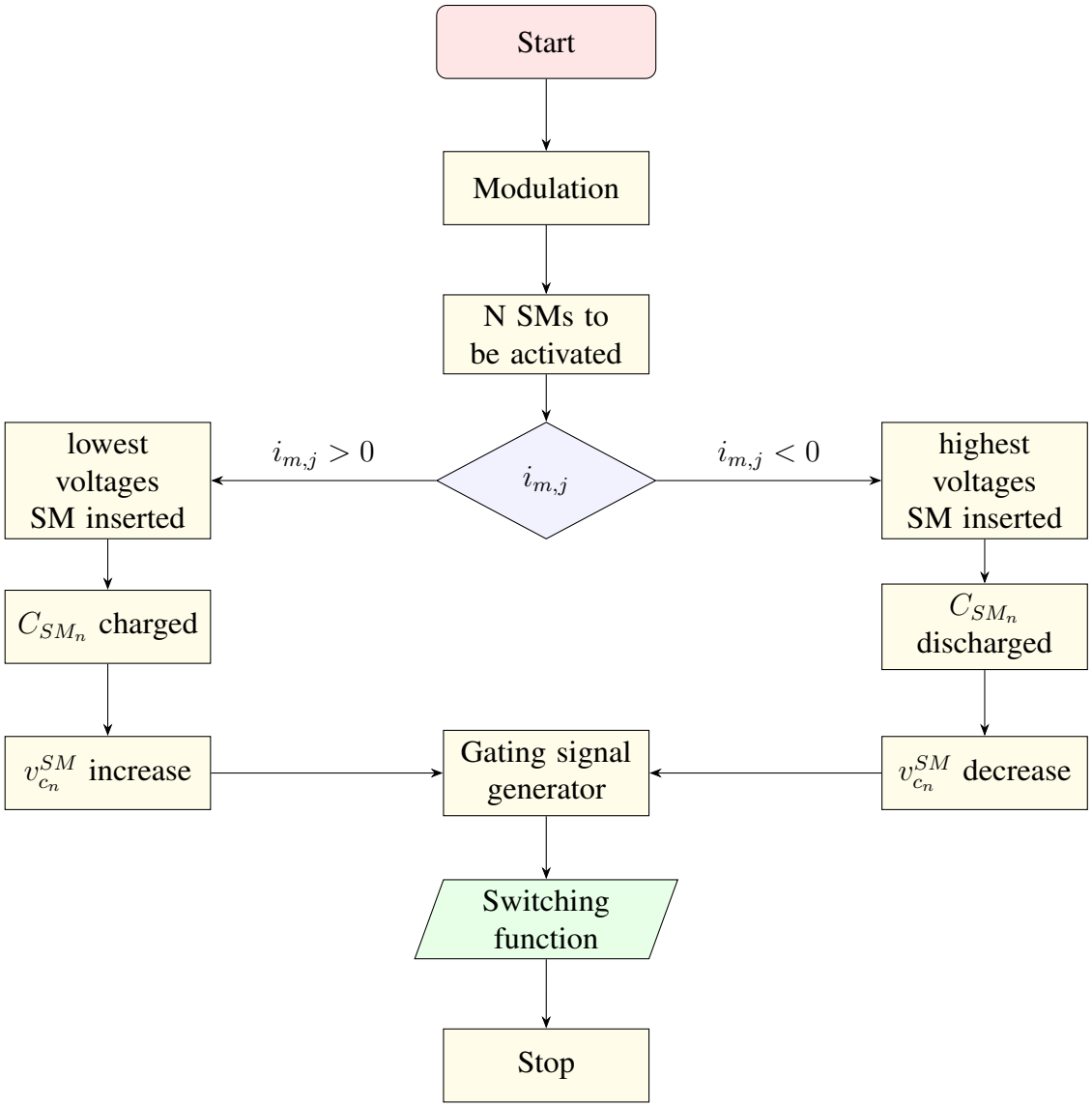

Source: Author

Phase Locked Loop

It is fundamental to consider proper synchronization with the AC grid voltages and the MMC control. The synchronization process detects the positive-sequence voltage component at the fundamental frequency, so the magnitude and angle are used to convert voltage and control variables into rotating reference frames [51].

In this thesis, Phase Locked Loop (PLL) technique is used to detect positive-sequence voltages for the MMC switched model. In order to do that, the rotating reference frame (*dq0*) will follow the vectors of the alternating system (*abc*), with the same frequency and angle.

In Figure 15, the PLL schematic is presented. This circuit generates, using Park transformation, the signal $v_{f,d}$ which is synchronized with the fundamental component of v_a (see Figure 10). Also, frequency and phase angle θ are estimated either in steady state or during electromagnetic transients.

The quadrature axis produced ($v_{f,q}$) is the phase difference between the *abc* signal and the direct rotating frame. $v_{f,q}$ is controlled by PI to be equal to zero, and the angular velocity ω_0 is obtained. Integrating angular velocity, the phase angle θ is achieved. Additionally, homopolar component zero is null for balanced AC systems.

Figure 15 – PLL internal diagram.

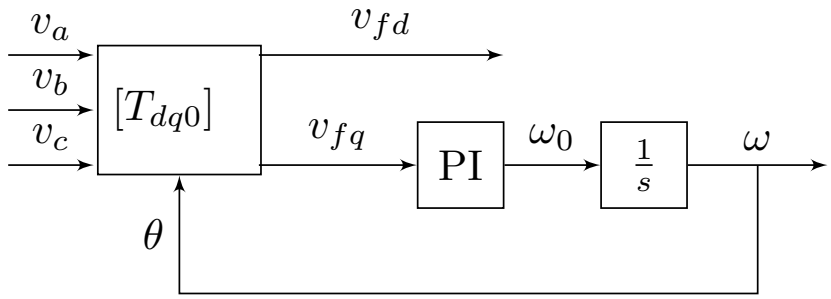

Source: [51]

2.2 Modeling

In order to develop an accurate MMC model, it should consider a high number of electrical nodes, a strong coupling effect among states, and an extensive set of operating points [52].

A MMC converter comprehends hundreds of SM independently controlled. Each arm of a MMC behaves as a variable voltage source, which allows controlling the output voltages (AC and DC) independently. Meanwhile, it results in an increase of the modeling complexity, in comparison with standard VSCs. A MMC model, which comprehends all intrinsic switching dynamics, is a computational challenge, once a high number of switching devices [36]. However, there are many simplified and computationally realizable models proposed by the literature.

Figure 16, adapted from [52], summarises different model types, often discussed in the literature. In this figure, the computational effort increases from left to right. There are two main divisions: full order models and reduced-order average models. Full order models describe each element and reduced-order models combine elements and describe it by a combined behavior.

2.2.1 Full order models

Concerning more complex model representations, they use the classical nodal admittance method to describe the system. Usually, lumped elements are integrated by trapezoidal rule, as shown in figure 17 and the distributed elements are modeled by Bergeron's method. Also, subsequent time-dependent topology represents non-linear elements, like semiconductors, which results in a simulation computationally intensive [36]. In figure 17 lumped elements on the left side and equivalent elements on the right, as: (a) resistor, (b) inductor and equivalent Bergeron,

Figure 16 – Summary of MMC models.

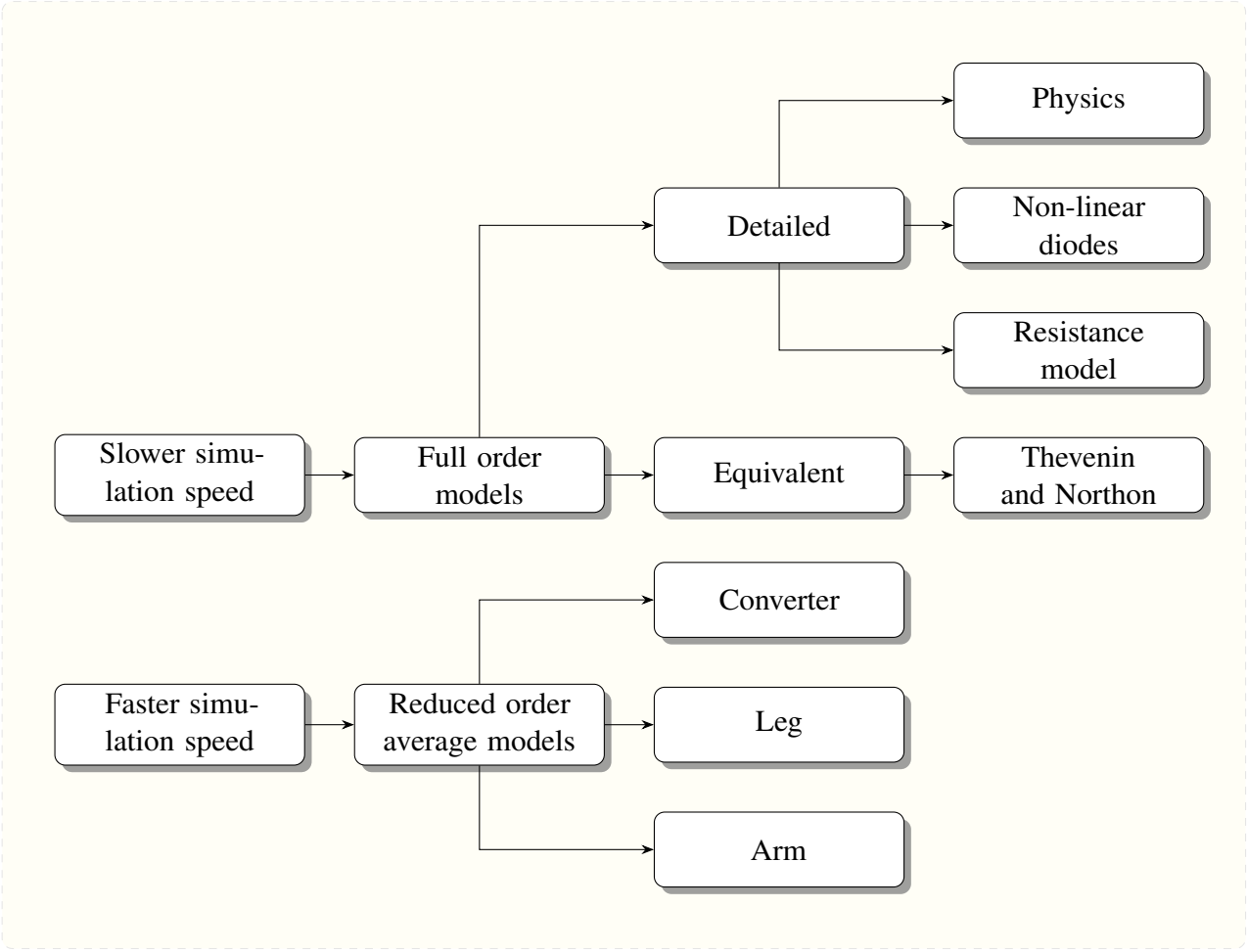

Source: Author

(c) capacitor and equivalent Bergeron (d) a IGBT and the representation using two resistors which represent the active and the bypassed state of the switching element. This model simplify the complexity imposed by IGBTs. With this goal, IGBTs are replaced by a large resistor (R_{off}), for the no conduction state, and a small resistor (R_{on}), for the conduction state. The resistance is defined by the signal and current direction on a node that represents the gate of the IGBT.

This group of methods can reproduce the internal converter's dynamics, including all capacitor voltages and the circulating current. Therefore, the model describes with high accuracy all system phenomena. This modeling usually is used to validate another MMC simplified model.

Regarding detailed models, these can also use different representations of semiconductors since the full physics model is one of the closest representations of a MMC. Detailed models use the exactly equivalent circuit or their differential equation for the IGBTs. Also, use nonlinear functions or other representations [36; 53]. However, full order models have a hundred nodes to be simulated, which results in a large admittance matrix that is inverted for each converter switch. This process requires an excessive computational load resulting in a slow simulation [52].

In the literature, there are many MMC models that have moderate processing time and present an adequate performance in transient and steady-state as the real system behaviors. One of these

Figure 17 – Lumped elements on the left side and equivalent elements on the right. (a) resistor, (b) inductor, (c) capacitor and (d) IGBT.

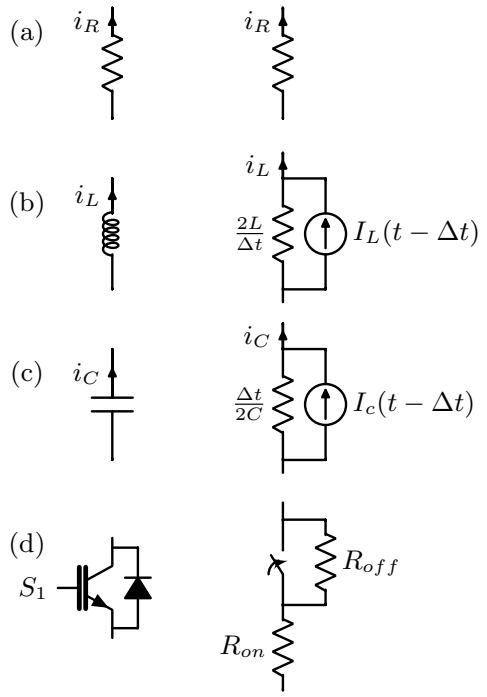

Source: [10]

Figure 18 – Thevenin equivalent SM.

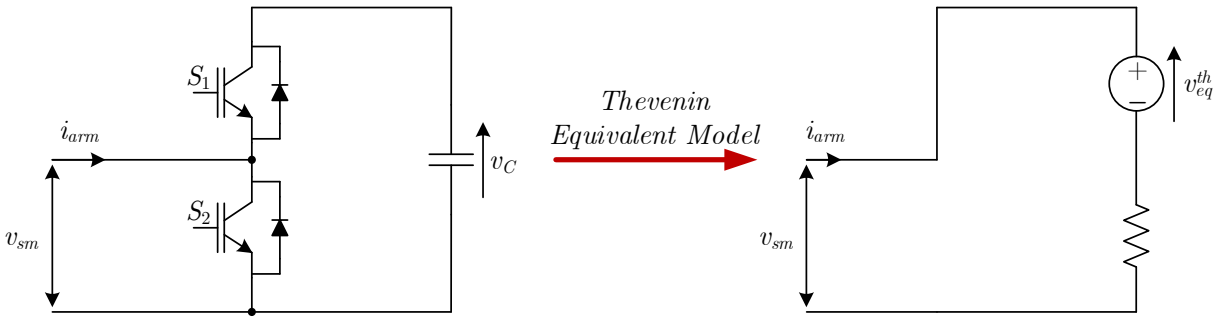

Source: [54]

modeling methods is the Equivalent Circuit Based (ECB) Model as Thevenin's Equivalent (TE) in which SMs are replaced by the Thevenin or Norton equivalent circuit [25; 53; 54], as shown figure 18.

This method drastically reduces the number of nodes on the system. It is solved by linear algebraic relations which enables real-time simulation and is ideal for parallelization. Another option for real-time simulation and parallelization is the switching function models that use state-space formulation [55]. This model reduces the system dynamics to a controlled current and voltage sources. However, it is computationally intense and does not enable fault study [36].

2.2.2 Reduced order average model

In order to achieve a faster simulation of MMC, reduced-order models have been proposed in the literature. These models are called Average-model (AVM) and consist of reducing the number of state variables inside the model by making some hypotheses. The AVM approximates the switching effects of all SMs in an arm by the continuous voltage source, and it is assumed perfect balancing between the SM capacitor voltages [27; 52; 56; 57; 58] . These models integrate the dynamic of capacitors and their coupling effects with the arm current [55].

AVM are considered as very straightforward and easy to use for control design [55]. The approach of AVM considers the hypothesis that modulation can do SMs capacitor voltage balancing. This hypothesis is the critical point for an accurate representation of a MMC. However, this modeling is suited for many signal analysis, steady-state studies, and power-flow analyses. Indeed average model is robust and easily scalable, as well as it is much faster than a detailed model (about 370 times) and quicker than a simplified equivalent model (about seven times) [57].

For all these reasons, the reduced-order average model will be considered in this thesis to design the controllers.

2.2.3 Derivation of reduced order average model

Regarding mathematical modeling, state-space is used to describe the dynamics of the systems. This approach is often adopted in general and MMC modeling literature due to the ease of manipulation it offers. Most models presented above can be represented by state-space, where the difference lies in the chosen state variables [55; 56].

Two hypotheses are considered for the MMC circuit modeled for this thesis:

- ❑ As aforementioned, considering the hypothesis that modulation can provide SMs capacitor voltage balancing, the reduced-order average model circuit is shown in figure (19);
- ❑ The voltage on the DC link, imposed over the capacitors, is controlled by the converter at the other end of the DC link, so two ideal voltage sources are connected in series in the DC circuit, each one with $V_{DC}/2$ voltage.

This circuit is the main model considered in this thesis, it is based on [27]. There are no capacitors directly described in this model, so this state-space model neglects the coupling effect between the inductor currents and capacitor voltages. AC current ($i_{v,abc}$), circulating current ($i_{cir,abc}$), total stored energy (W_h), and balancing stored energy (W_v) were chosen as state variables.

From the illustration of a MMC in figure 19 the state-space can be constructed. The N SMs connected per arm produce an equivalent voltage source equal to $v_{m,j}$. It is a three-phase converter and each phase (*j = a, b and c*) is connected with a leg that consists of upper and lower arms (*m = u or l*).

Figure 19 – Average model of a three-phase MMC.

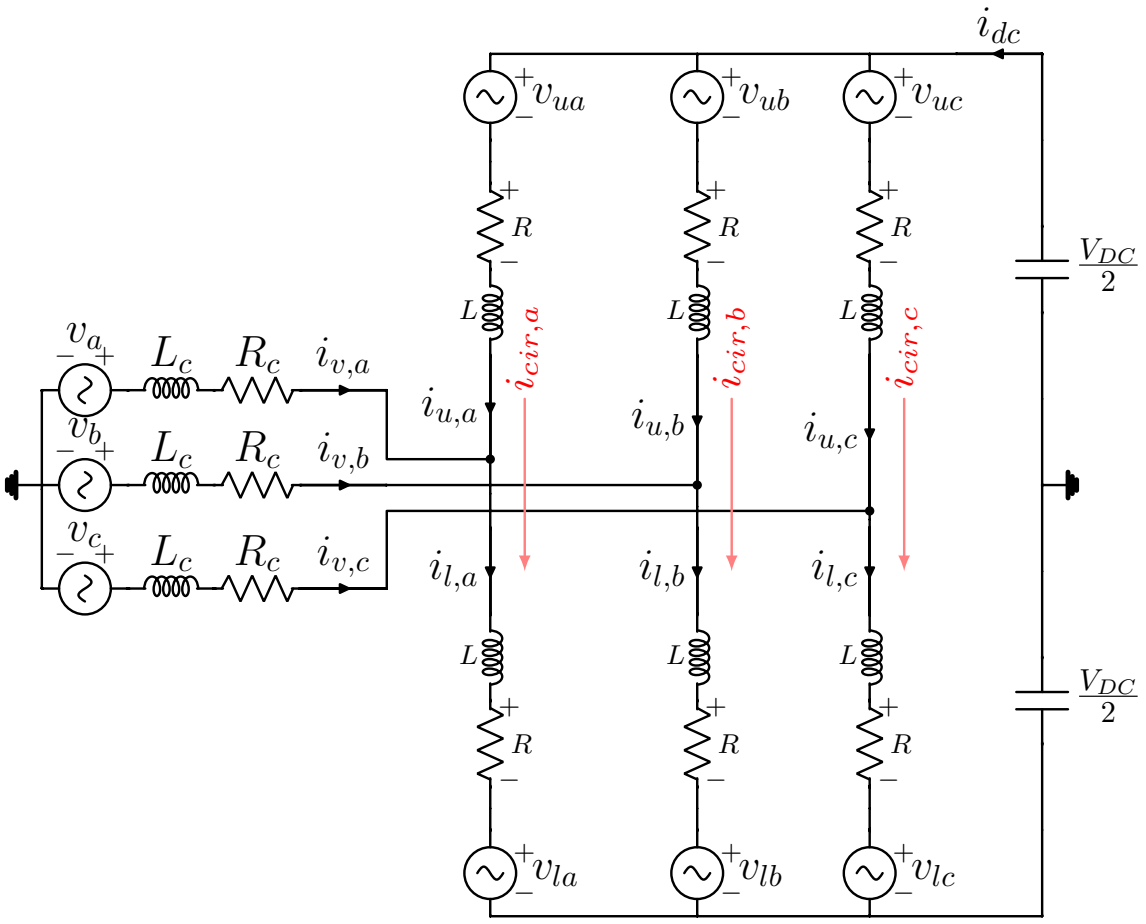

Source: Author

An inductance L follows the equivalent voltage source in series with resistance R. L needs to consider the external fault criterion, while R summarises the resistive behavior of the MMC (resistive voltage drop across conducting switches, cables, connections, and the inductor resistances). On the AC side, an RL filter is considered per phase (R_c and L_c).

In figure 20 it is considered phase j from the MMC average model circuit shown in figure 19. Applying Kirchhoff's voltage law on upper arm (figure 20(a)), from V_{DC} to $v_{f,j}$ is obtained equation 1. If equation (1) is equal to zero, equation (2) is obtained. About the lower arm (figure 20 (b)) from V_{DC} to $v_{f,j}$ there is equation 3 and rearranging it, one obtains equation 4.

$$\frac{V_{DC}}{2} - v_{u,j} - Ri_{u,j} - L\dot{i}_{u,j} + R_c i_{v,j} + L_c \dot{i}_{v,j} - v_{f,j} = 0 \tag{1}$$

$$-\frac{V_{DC}}{2} = -v_{u,j} - Ri_{u,j} - L\dot{i}_{u,j} + R_c i_{v,j} + L_c \dot{i}_{v,j} - v_{f,j} \tag{2}$$

$$-\frac{V_{DC}}{2} + v_{l,j} + R\dot{i}_{l,j} + L\dot{i}_{l,j} + R_c i_{v,j} + L_c \dot{i}_{v,j} - v_{f,j} = 0 \tag{3}$$

Figure 20 – Kirchhoff's voltage law for upper arm (a) and lower arm (b) at phase j.

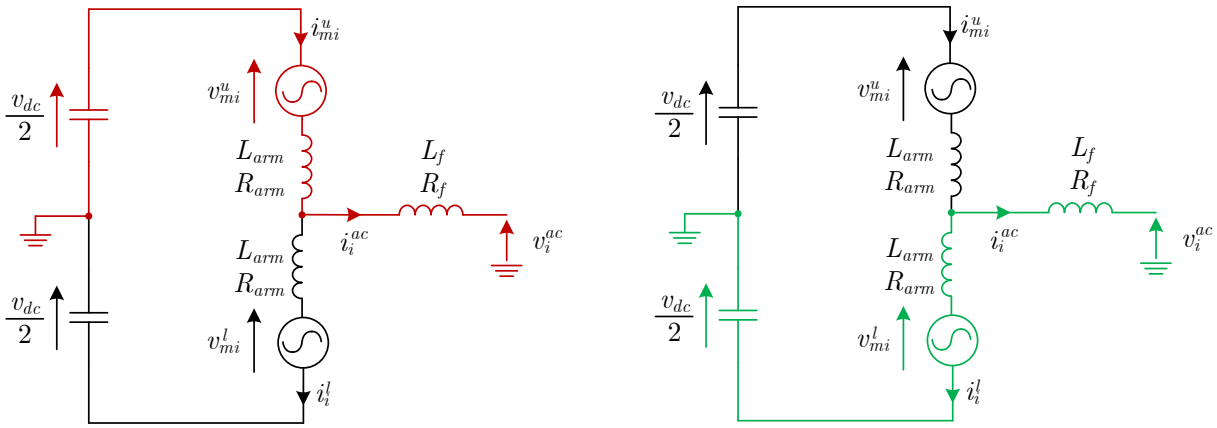

Source: Author

$$\frac{V_{DC}}{2} = v_{l,j} + R_{l,j} + L\dot{i}_{l,j} + R_c i_{v,j} + L_c \dot{i}_{v,j} - v_{f,j}. \tag{4}$$

Kirchhoff's current law on the node identified in figure 20 defines AC current $i_{v,j}$, related to upper and lower current:

$$i_{v,j} = -i_{u,j} + i_{l,j} \tag{5}$$

The arm currents ($i_{u,j}$ and $i_{l,j}$) can be rewritten in terms of circulating current ($i_{cir,j}$) and AC side current ($i_{v,j}$). It is considered that $i_{v,j}$ is equally distributed to upper and lower arms and that there are circulating currents flowing between legs, defined in (6) and (7).

$$i_{u,j} = -\frac{i_{v,j}}{2} + i_{cir,j} \tag{6}$$

$$i_{l,j} = \frac{i_{v,j}}{2} + i_{cir,j} \tag{7}$$

Adding (6) and (7), it is obtained circulating currents' expression (8).

$$i_{cir,j} = \frac{i_{u,j} + i_{l,j}}{2} \tag{8}$$

Power-flow equations

Adding (2) to (4):

$$0 = -v_{u,j} + v_{l,j} + R(-i_{u,j} + i_{l,j}) + L(-\dot{i}_{u,j} + \dot{i}_{l,j}) + 2R_c i_{v,j} + 2L_c \dot{i}_{v,j} \tag{9}$$

Replacing (5) in (9):

$$L\dot{i}_{v,j} + 2L_c\dot{i}_{v,j} = v_{u,j} - v_{l,j} - Ri_{v,j} - 2R_c i_{v,j} \tag{10}$$

Considering the following notation:

$$R_{eq} = R + 2R_c \tag{11}$$

$$L_{eq} = L + 2L_c \tag{12}$$

Rearranging (10) one obtains the current dynamic (13), for the phase *j* from the AC side. This equation describes and enables the control of active and reactive power at AC side.

$$\dot{i}_{v,j} = -\frac{R_{eq}}{L_{eq}} i_{v,j} + \frac{v_{u,j} - v_{l,j}}{L_{eq}} + \frac{2v_{f,j}}{Leq} \tag{13}$$

By subtracting (4) from (2):

$$-V_{DC} = -v_{u,j} - v_{l,j} - R(i_{u,j} + i_{l,j}) - L(\dot{i}_{u,j} + \dot{i}_{l,j}) \tag{14}$$

Substituting (8) in (14):

$$-V_{DC} = -v_{u,j} - v_{l,j} - 2Ri_{cir,j} - 2L\dot{i}_{cir,j} \tag{15}$$

Rearranging (15) it is obtained the dynamic equation for the circulating current, which describes and enables DC power control.

$$\dot{i}_{cir,j} = -\frac{R}{L} i_{cir,j} - \frac{v_{u,j} + v_{l,j}}{2L} + \frac{V_{DC}}{2L} \tag{16}$$

Converter energies equation

Even though the average model neglects SM capacitor effect, their combined contribution to converter dynamics is included in the model by the energy expression.

MMC is the first technology of converter to enable independent control of AC and DC current. This control is directly linked to converter power input and output. This power difference results in the SMs capacitors load. In other words, the real operation of a MMC implies voltage changes of SM's capacitor. In this way, SMs will be suitable to synthesize the output DC voltage, and, consequently, the output currents are driven.

Based on this, achieving the voltage on SMs's capacitor results in a certain amount of stored energy per SM. Therefore, the total amount of energy stored (also called in the literature as horizontal balancing) in MMC will be considered as a state, as well as the difference between the energy stored on the upper and lower arms (also called vertical balancing).

- ❏ Total energy or horizontal balancing (W_h): describes an energy distribution in horizontal direction (through AC to DC side), summing the energy of each arm, to achieve the desired total converter energy.

- ❏ Energy balancing or vertical balancing (W_v): describes an energy distribution through all upper arms in comparison with all lower arms, to achieve equal energy distribution between converter's upper and lower arms.

MMC energy control is mandatory to converter proper operation. Also, it is possible to use the internal energy to propose new control objectives, either for fast frequency support (or inertial support) or for imbalanced operation with different upper and lower arm's energy, as presented in [59].

So, converter total energy derivative is described at equation (17), where each equivalent source per arm times arm current are considered. Finally, total converter power is represented by the derivative of energy.

$$\dot{W}_h = \sum_{m=u}^{l} \sum_{j=a}^{c} v_{m,j} i_{m,j} \tag{17}$$

Equations (6) and (7) replaced at equation (17) leads to the final equation, based on $i_{v,j}$ and $i_{cir,j}$ which are chosen as state variables. So, equation (18) is obtained.

$$\dot{W}_h = \sum_{j=a}^{c} v_{u,j}(-\frac{i_{v,j}}{2} + i_{cir,j}) + \sum_{j=a}^{c} v_{l,j}(\frac{i_{v,j}}{2} + i_{cir,j}) \tag{18}$$

Considering the AC and DC power produced by either converter's part (upper or lower),the converter balancing energy is defined as in equation (19):

$$\dot{W}_v = \sum_{j=a}^{c} v_{u,j} i_{u,j} - \sum_{j=a}^{c} v_{l,j} i_{l,j} \tag{19}$$

Equation 6 and equation 7 are replaced in equation 19 to obtain the final equation based on $i_{v,j}$ and $i_{cir,j}$, which are the chosen state variables. So, equation 20 is obtained.

$$\dot{W}_v = \sum_{j=a}^{c} v_{u,j}(-\frac{i_{v,j}}{2} + i_{cir,j}) - \sum_{j=a}^{c} v_{l,j}(\frac{i_{v,j}}{2} + i_{cir,j}) \tag{20}$$

In other words, the energy related state variable W_h corresponds to the total energy stored in the SM capacitors and can also be obtained as:

$$W_h = W_u + W_l \tag{21}$$

where W_u is the energy stored in the upper arm SM capacitors and W_l the energy stored in the lower arm SM capacitors. As for the energy balancing W_v it can be obtained as difference

between upper and lower arm's stored energy as:

$$W_v = W_u - W_l. \tag{22}$$

The stored energy in the upper and the lower arm can be obtained from the SM capacitor's voltage as:

$\mathrm{W}_k = \frac{C_{SM}}{2} \sum_{j=1}^{3} \sum_{i=1}^{N} v_{C,ki,j}^2$(23)where k indicates upper u or lower l arms, j the phases of the converter and i indicates the SMs.

Change of reference by Park's transformation

Park's transformation is widely used in the electrical power system to simplify three-phase system analyses. Park's transformation uses a rotational matrix that transforms a balanced three-phase system (AC) into a two-phase system (DC). The two-phase system is rotating by a reference frame. The frequency of the rotation is linked with the frequency of one AC phase.

An *abc* system can be transformed in *dq0* by using the matrix T bellow

$$T = \frac{2}{3} \begin{bmatrix} cos(\theta) & cos(\theta - \frac{2\pi}{3}) & cos(\theta + \frac{2\pi}{3}) \\ -sin(\theta) & -sin(\theta - \frac{2\pi}{3}) & -sin(\theta + \frac{2\pi}{3}) \\ \frac{1}{2} & \frac{1}{2} & \frac{1}{2} \end{bmatrix} \tag{24}$$

$$x_{qd0} = T x_{abc} \tag{25}$$

and the inverse transformation (*dq0* to *abc*) can be obtained by

$$T^1 = \begin{bmatrix} cos(\theta) & -sin(\theta) & \frac{1}{2} \\ cos(\theta - \frac{2\pi}{3}) & -sin(\theta - \frac{2\pi}{3}) & \frac{1}{2} \\ cos(\theta + \frac{2\pi}{3}) & -sin(\theta + \frac{2\pi}{3}) & \frac{1}{2} \end{bmatrix} \tag{26}$$

$$x_{abc} = T^{-1} x_{dq0} \tag{27}$$

MMC reduced order average model in *dq0* reference frame

Considering Park's transformation matrix T, the three-phase MMC system will turns into *dq0* reference frame. To illustrate the transformation process (13) is rewritten in (28).

$$\begin{bmatrix} \dot{i}_{v,a} \\ \dot{i}_{v,b} \\ \dot{i}_{v,c} \end{bmatrix} = \begin{bmatrix} -\frac{R_{eq}}{L_{eq}} & 0 & 0 \\ 0 & -\frac{R_{eq}}{L_{eq}} & 0 \\ 0 & 0 & -\frac{R_{eq}}{L_{eq}} \end{bmatrix} \begin{bmatrix} i_{v,a} \\ i_{v,b} \\ i_{v,c} \end{bmatrix} + \begin{bmatrix} \frac{1}{L_{eq}} & 0 & 0 \\ 0 & \frac{1}{L_{eq}} & 0 \\ 0 & 0 & \frac{1}{L_{eq}} \end{bmatrix} \begin{bmatrix} v_{u,a} - v_{l,a} \\ v_{u,b} - v_{l,b} \\ v_{u,c} - v_{l,c} \end{bmatrix} + \begin{bmatrix} \frac{2}{Leq} & 0 & 0 \\ 0 & \frac{2}{Leq} & 0 \\ 0 & 0 & \frac{2}{Leq} \end{bmatrix} \begin{bmatrix} v_{f,a} \\ v_{f,b} \\ v_{f,c} \end{bmatrix} \tag{28}$$

Using matrix T of Park's transformation in equation (28) equation (29) is obtained.

$$\begin{bmatrix} \dot{i}_{v,d} \\ \dot{i}_{v,q} \\ \boxed{\dot{i}_{v,0}} \end{bmatrix} = \begin{bmatrix} -\frac{R_{eq}}{L_{eq}} & w & 0 \\ -w & -\frac{R_{eq}}{L_{eq}} & 0 \\ 0 & 0 & -\frac{R_{eq}}{L_{eq}} \end{bmatrix} \begin{bmatrix} i_{v,d} \\ i_{v,q} \\ \boxed{i_{v,0}} \end{bmatrix} +$$

$$+ \begin{bmatrix} \frac{1}{L_{eq}} & 0 & 0 \\ 0 & \frac{1}{L_{eq}} & 0 \\ 0 & 0 & \frac{1}{L_{eq}} \end{bmatrix} \begin{bmatrix} v_{u,d} - v_{l,d} \\ v_{u,q} - v_{l,q} \\ \boxed{v_{u,0} - v_{l,0}} \end{bmatrix} + \begin{bmatrix} \frac{2}{Leq} & 0 & 0 \\ 0 & \frac{2}{Leq} & 0 \\ 0 & 0 & \frac{2}{Leq} \end{bmatrix} \begin{bmatrix} v_{f,d} \\ v_{f,q} \\ \boxed{v_{f,0}} \end{bmatrix} \tag{29}$$

Taking into account that in the equilibrium of balanced systems, the zero components are equal to zero (boxed terms in (29)), then equation (29) can be rewritten as a system (30), which describes the AC current state variables that should be controlled.

$$\begin{bmatrix} \dot{i}_{v,d} \\ \dot{i}_{v,q} \end{bmatrix} = \begin{bmatrix} -\frac{R_{eq}}{L_{eq}} & w \\ -w & -\frac{R_{eq}}{L_{eq}} \end{bmatrix} \begin{bmatrix} i_{v,d} \\ i_{v,q} \end{bmatrix} + \begin{bmatrix} \frac{1}{L_{eq}} & 0 \\ 0 & \frac{1}{L_{eq}} \end{bmatrix} \begin{bmatrix} v_{u,d} - v_{l,d} \\ v_{u,q} - v_{l,q} \end{bmatrix} + \begin{bmatrix} \frac{2}{Leq} & 0 \\ 0 & \frac{2}{Leq} \end{bmatrix} \begin{bmatrix} v_{f,d} \\ v_{f,q} \end{bmatrix} \tag{30}$$

In the same way, (16) can be rewritten as the system (31) in the *dq0* frame. Where $v_{u,0}+v_{l,0} = v_{d0}$ means the DC component in the converter legs. Then, system (31) describes the circulating current dynamics in *dq0* reference that should be controlled.

$$\begin{bmatrix} \dot{i}_{cir,d} \\ \dot{i}_{cir,q} \\ \dot{i}_{cir,0} \end{bmatrix} = \begin{bmatrix} -\frac{R}{L} & w & 0 \\ -w & -\frac{R}{L} & 0 \\ 0 & 0 & -\frac{R}{L} \end{bmatrix} \begin{bmatrix} i_{cir,d} \\ i_{cir,q} \\ i_{cir,0} \end{bmatrix} + \begin{bmatrix} -\frac{1}{2L} & 0 & 0 \\ 0 & -\frac{1}{2L} & 0 \\ 0 & 0 & -\frac{1}{2L} \end{bmatrix} \begin{bmatrix} v_{u,d} + v_{l,d} \\ v_{u,q} + v_{l,q} \\ v_{d0} \end{bmatrix} + \begin{bmatrix} 0 \\ 0 \\ \frac{v_{dc}}{2L} \end{bmatrix} \tag{31}$$

Concerning the converter total stored energy in (18) and energy balancing at (20), these values on the referential $f = d, q, 0$ are presented in (32) and (33), respectively.

$$\begin{aligned} \dot{W}_h &= \frac{3}{2}\sum_{f=d}^{0} v_{u,f}(-\frac{i_{v,f}}{2} + i_{cir,f}) + \frac{3}{2}\sum_{f=d}^{0} v_{l,f}(\frac{i_{v,f}}{2} + i_{cir,f}) \\ &= -\frac{3}{4}v_{u,d}i_{v,d} + \frac{3}{2}v_{u,d}i_{cir,d} - \frac{3}{4}v_{u,q}i_{v,q} + \frac{3}{2}v_{u,q}i_{cir,q} + \frac{3}{4}v_{l,d}i_{v,d} + \frac{3}{2}v_{l,d}i_{cir,d} + \\ &+ \frac{3}{4}v_{l,q}i_{v,q} + \frac{3}{2}v_{l,q}i_{cir,q} + 3i_{cir,0}v_{d,0} \end{aligned} \tag{32}$$

$$\begin{aligned} \dot{W}_v &= \frac{3}{2}\sum_{f=d}^{0} v_{u,f}(-\frac{i_{v,f}}{2} + i_{cir,f}) - \frac{3}{2}\sum_{f=d}^{0} v_{l,f}(\frac{i_{v,f}}{2} + i_{cir,f}) \\ &= -\frac{3}{4}v_{u,d}i_{v,d} + \frac{3}{2}v_{u,d}i_{cir,d} - \frac{3}{4}v_{u,q}i_{v,q} + \frac{3}{2}v_{u,q}i_{cir,q} - \frac{3}{4}v_{l,d}i_{v,d} - \frac{3}{2}v_{l,d}i_{cir,d} - \\ &+ \frac{3}{4}v_{l,q}i_{v,q} - \frac{3}{2}v_{l,q}i_{cir,q} \end{aligned} \tag{33}$$

Finally, considering the state vector as $x = [i_{v,d}\ i_{v,q}\ i_{cir,d}\ i_{cir,q}\ i_{cir,0}\ W_h\ W_v]^T$ and the controller input as $u = [v_{u,d}\ v_{u,q}\ v_{l,d}\ v_{l,q}\ v_{d0}\ ]^T$, the three-phase MMC can be represented by the bilinear form shown in (34) and at (36).

$$\dot{x} = Ax + \sum_{k=1}^{\rho} B_k u_k x + b_k u_k + z \tag{34}$$

where, considering $\rho = 5$.

The model in system (35) can be summarized in (36).

$$\begin{cases}
\dot{i}_{v,d} = -\dfrac{R_{eq}}{L_{eq}} i_{v,d} + \omega \cdot i_{v,q} + \dfrac{v_{u,d} - v_{l,d}}{L_{eq}} + \dfrac{2v_{f,d}}{L_{eq}} \\
\dot{i}_{v,q} = -\dfrac{R_{eq}}{L_{eq}} i_{v,q} - \omega \cdot i_{v,d} + \dfrac{v_{u,q} - v_{l,q}}{L_{eq}} + \dfrac{2v_{f,q}}{L_{eq}} \\
\dot{i}_{cir,d} = -\dfrac{R}{L} i_{cir,d} + \omega \cdot i_{cir,q} - \dfrac{v_{u,d} + v_{l,d}}{2L} \\
\dot{i}_{cir,q} = -\dfrac{R}{L} i_{cir,q} - \omega \cdot i_{cir,d} - \dfrac{v_{u,q} + v_{l,q}}{2L} \\
\dot{i}_{cir,0} = -\dfrac{R}{L} i_{cir,0} - \dfrac{v_{d0}}{2L} + \dfrac{V_{DC}}{2L} \\
\dot{W}_h = -\dfrac{3}{4} v_{u,d} i_{v,d} + \dfrac{3}{2} v_{u,d} i_{cir,d} - \dfrac{3}{4} v_{u,q} i_{v,q} + \dfrac{3}{2} v_{u,q} i_{cir,q} + \\
\qquad + \dfrac{3}{4} v_{l,d} i_{v,d} + \dfrac{3}{2} v_{l,d} i_{cir,d} + \dfrac{3}{4} v_{l,q} i_{v,q} + \dfrac{3}{2} v_{l,q} i_{cir,q} + 3 v_{d0} i_{cir,0} \\
\dot{W}_v = -\dfrac{3}{4} v_{u,d} i_{v,d} + \dfrac{3}{2} v_{u,d} i_{cir,d} - \dfrac{3}{4} v_{u,q} i_{v,q} + \dfrac{3}{2} v_{u,q} i_{cir,q} + \\
\qquad - \dfrac{3}{4} v_{l,d} i_{v,d} - \dfrac{3}{2} v_{l,d} i_{cir,d} - \dfrac{3}{4} v_{l,q} i_{v,q} - \dfrac{3}{2} v_{l,q} i_{cir,q}
\end{cases} \tag{35}$$

$$
\begin{bmatrix} \dot{i}_{v,d} \\ \dot{i}_{v,q} \\ \dot{i}_{cir,d} \\ \dot{i}_{cir,q} \\ \dot{i}_{cir,0} \\ \dot{W}_h \\ \dot{W}_v \end{bmatrix} = \begin{bmatrix} \frac{-R-2R_c}{L+2L_c} & \omega & 0 & 0 & 0 & 0 & 0 \\ -\omega & \frac{-R-2R_c}{L+2L_c} & 0 & 0 & 0 & 0 & 0 \\ 0 & 0 & -\frac{R}{L} & \omega & 0 & 0 & 0 \\ 0 & 0 & -\omega & -\frac{R}{L} & 0 & 0 & 0 \\ 0 & 0 & 0 & 0 & -\frac{R}{L} & 0 & 0 \\ 0 & 0 & 0 & 0 & 0 & 0 & 0 \\ 0 & 0 & 0 & 0 & 0 & 0 & 0 \end{bmatrix} \begin{bmatrix} i_{v,d} \\ i_{v,q} \\ i_{cir,d} \\ i_{cir,q} \\ i_{cir,0} \\ W_h \\ W_v \end{bmatrix} + \begin{bmatrix} 0 & 0 & 0 & 0 & 0 & 0 & 0 \\ 0 & 0 & 0 & 0 & 0 & 0 & 0 \\ 0 & 0 & 0 & 0 & 0 & 0 & 0 \\ 0 & 0 & 0 & 0 & 0 & 0 & 0 \\ 0 & 0 & 0 & 0 & 0 & 0 & 0 \\ -\frac{3}{4} & 0 & \frac{3}{2} & 0 & 0 & 0 & 0 \\ -\frac{3}{4} & 0 & \frac{3}{2} & 0 & 0 & 0 & 0 \end{bmatrix} \begin{bmatrix} i_{v,d} \\ i_{v,q} \\ i_{cir,d} \\ i_{cir,q} \\ i_{cir,0} \\ W_h \\ W_v \end{bmatrix} v_{u,d} +
$$

$$
+ \begin{bmatrix} 0 & 0 & 0 & 0 & 0 & 0 & 0 \\ 0 & 0 & 0 & 0 & 0 & 0 & 0 \\ 0 & 0 & 0 & 0 & 0 & 0 & 0 \\ 0 & 0 & 0 & 0 & 0 & 0 & 0 \\ 0 & 0 & 0 & 0 & 0 & 0 & 0 \\ 0 & -\frac{3}{4} & 0 & \frac{3}{2} & 0 & 0 & 0 \\ 0 & -\frac{3}{4} & 0 & \frac{3}{2} & 0 & 0 & 0 \end{bmatrix} \begin{bmatrix} i_{v,d} \\ i_{v,q} \\ i_{cir,d} \\ i_{cir,q} \\ i_{cir,0} \\ W_h \\ W_v \end{bmatrix} v_{u,q} + \begin{bmatrix} 0 & 0 & 0 & 0 & 0 & 0 & 0 \\ 0 & 0 & 0 & 0 & 0 & 0 & 0 \\ 0 & 0 & 0 & 0 & 0 & 0 & 0 \\ 0 & 0 & 0 & 0 & 0 & 0 & 0 \\ 0 & 0 & 0 & 0 & 0 & 0 & 0 \\ \frac{3}{4} & 0 & \frac{3}{2} & 0 & 0 & 0 & 0 \\ -\frac{3}{4} & 0 & -\frac{3}{2} & 0 & 0 & 0 & 0 \end{bmatrix} \begin{bmatrix} i_{v,d} \\ i_{v,q} \\ i_{cir,d} \\ i_{cir,q} \\ i_{cir,0} \\ W_h \\ W_v \end{bmatrix} v_{l,d} +
$$

$$
+ \begin{bmatrix} 0 & 0 & 0 & 0 & 0 & 0 & 0 \\ 0 & 0 & 0 & 0 & 0 & 0 & 0 \\ 0 & 0 & 0 & 0 & 0 & 0 & 0 \\ 0 & 0 & 0 & 0 & 0 & 0 & 0 \\ 0 & 0 & 0 & 0 & 0 & 0 & 0 \\ 0 & \frac{3}{4} & 0 & \frac{3}{2} & 0 & 0 & 0 \\ 0 & -\frac{3}{4} & 0 & -\frac{3}{2} & 0 & 0 & 0 \end{bmatrix} \begin{bmatrix} i_{v,d} \\ i_{v,q} \\ i_{cir,d} \\ i_{cir,q} \\ i_{cir,0} \\ W_h \\ W_v \end{bmatrix} v_{l,q} + \begin{bmatrix} 0 & 0 & 0 & 0 & 0 & 0 & 0 \\ 0 & 0 & 0 & 0 & 0 & 0 & 0 \\ 0 & 0 & 0 & 0 & 0 & 0 & 0 \\ 0 & 0 & 0 & 0 & 0 & 0 & 0 \\ 0 & 0 & 0 & 0 & 0 & 0 & 0 \\ 0 & 0 & 0 & 0 & 3 & 0 & 0 \\ 0 & 0 & 0 & 0 & 0 & 0 & 0 \end{bmatrix} \begin{bmatrix} i_{v,d} \\ i_{v,q} \\ i_{cir,d} \\ i_{cir,q} \\ i_{cir,0} \\ W_h \\ W_v \end{bmatrix} v_{d,0} +
$$

$$
+ \begin{bmatrix} \frac{1}{L+2L_c} \\ 0 \\ -\frac{1}{2L} \\ 0 \\ 0 \\ 0 \\ 0 \end{bmatrix} v_{u,d} + \begin{bmatrix} 0 \\ \frac{1}{L+2L_c} \\ 0 \\ -\frac{1}{2L} \\ 0 \\ 0 \\ 0 \end{bmatrix} v_{u,q} + \begin{bmatrix} -\frac{1}{L+2L_c} \\ 0 \\ -\frac{1}{2L} \\ 0 \\ 0 \\ 0 \\ 0 \end{bmatrix} v_{l,d} + \begin{bmatrix} 0 \\ -\frac{1}{L+2L_c} \\ 0 \\ -\frac{1}{2L} \\ 0 \\ 0 \\ 0 \end{bmatrix} v_{l,q} +
$$

$$
+ \begin{bmatrix} 0 \\ 0 \\ 0 \\ 0 \\ -\frac{1}{2L} \\ 0 \\ 0 \end{bmatrix} v_{d,0} + \begin{bmatrix} \frac{2v_{f,d}}{L+2L_c} \\ \frac{2v_{f,q}}{L+2L_c} \\ 0 \\ 0 \\ \frac{V_{DC}}{2L} \\ 0 \\ 0 \end{bmatrix} \tag{36}
$$

The control of MMC has additional chalenges in comparison with other converters topology. The control method may have to deal with

- ❏ Externally, manage active and reactive power flow, AC and DC voltage,
- ❏ Internally, deal with converter dynamics as circulating currents, SM capacitor voltage, arm balancing, phase balancing, and converter energy control.

MMCs also have a complex modeling technique because of the high number of Submodule (SM), which requires simultaneous control to attain capacitor voltage balancing. There are many MMC modeling approaches, and models that directly affect the control design. In this thesis, a mathematical model based on the average arm is used to develop the controllers, and a switching model is used to verify controls performances. Concerning the average model, there are many approaches in the literature. In [25], the average model considers a switching function model that accurately includes each SM's capacitors' dynamic.

Additionally, in [26], authors introduce a continuous model where arms are represented by variable voltage sources function. However, a more complex average model will increase the system order, as well as the complexity of the proposed solution. In this way, the average model used in this research is based in [27], which consider per arm, an equivalent SM voltage.

A switching model is simulated with the proposed controller to verify the control performance. The switching model has a low-level controller, which properly attain SMs voltage balancing. The sorting algorithm implemented in the low-level control is based on the standard technique proposed by [24].

Concerning control, most of the existing results on the control strategy for MMCs consist of linear controllers, such as vector control, which may not have guaranteed stability. This is because only one point of operation is considered in its design and also because the system's nonlinearities are approximated [28; 29; 30].

In this point of view, one may cite works as [31], where the nonlinear MMC model is first linearized, and then linear controllers are designed for it. In a different way, [27] proposes a discrete-time bilinear model of an MMC, controlled by a sum-of-squares decomposition method, following a nonlinear analysis.

These studies are motivated by the relevance of designing nonlinear controllers that can assure stability throughout large electrical grid operation regions, including rigorous stability analysis [32; 33]. The next chapter will discuss with more detail about modeling and control to MMC.

2.3 Control designs for MMC systems

The control algorithm regulates systems' variables, in order to attain application requirements. System operation and user requests may change the power demand and voltage levels.

Furthermore, the control provides equipment protection from current and voltage over nominal values. Also, it must provide system stability and suitable responses during transients resulting in all expected operating conditions. In addition, control can address AC grid support: inertial and frequency stabilization to low-inertia grids [60], and voltage stabilization to high-impedance grids [24].

Besides the aforementioned applications, MMC controller will also deal with circulating current, most about the second harmonic suppression goal [61], and capacitor voltage balancing. Arm current also needs to be measured and controlled once it is directly related to SM capacitor voltage.

As discussed above, and highlighted by [24], when using MMC topology, there are additional concerns with dynamics that the control must take into account. They are summarized below:

- ❏ upper level controls: they are common for two-level VSC controller.
  - DC voltage to ensure low level losses and no damage to the cables' insulation.
  - AC voltage, in weak AC grids.
  - Active power transfer to attend the power demand.
  - Reactive power requirement.
- ❏ second-harmonic circulating current suppression
- ❏ SM capacitor voltage balancing
- ❏ arm, phase, pole balancing
- ❏ energy charge

The literature states the above mentioned controllers by two-level: high-level control and low-level control, as summarized in figure 21, adapted from [62]. The high-level control comprehends the power flow between the DC and AC sides. The power flow is given by setting voltage references for upper and lower arms. These definitions also comprehend DC voltage, AC voltage, and frequency. Low-level control of MMC deals with internal converter aspects as control of circulating current, SM capacitor voltage regulation, and arm energy balancing. These aspects rely on the management of SMs switching. A proper switch method may attend the requested arm voltage and ensure SMs capacitor balance [63; 52].

The literature has investigated the control aspects, which are particular to the use of MMC. Several methods are addressed to MMCs' control, as [61; 50; 64]. They are mostly based on PWM approach and standard linear control, using an open-loop or closed-loop approach.

Circulating current control

One of the goals of the control in the MMC applications is the circulating currents suppression. They flow through the converter phase legs of the MMC and come from the voltage

Figure 21 – MMC-HVDC necessary controls.

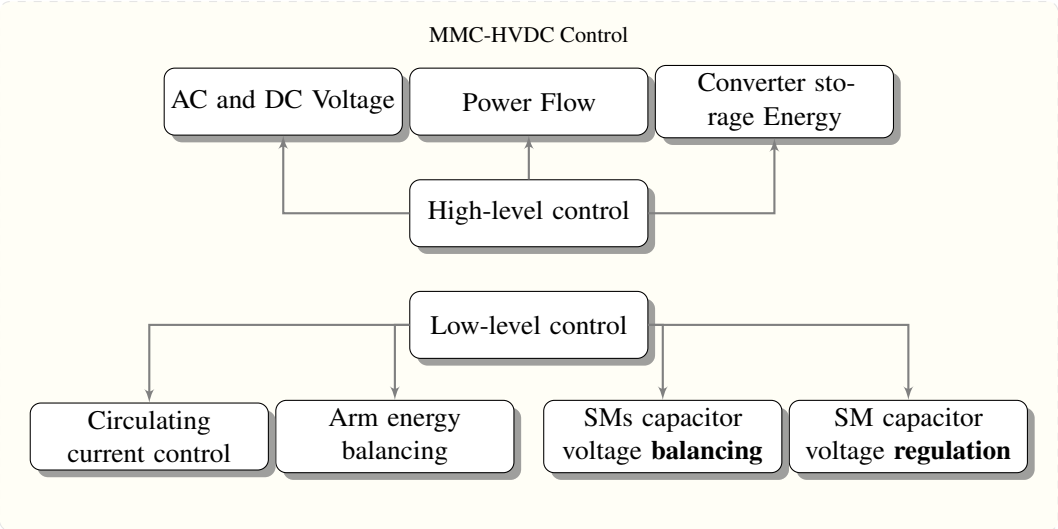

Source: Author

differences among the phase legs [65]. The circulating current controller is often mentioned in the literature as "inner"or "inner-loop". In circulating current, there are DC and harmonic components. DC components play a crucial role in the DC power dispatch, while the fundamental frequency component can transport energy between the upper and lower arms [65]. The remaining circulating current components result in current signal depreciation and the increased capacitor voltage ripple, mainly the second harmonic component [61; 65].

The open-loop approach is based on the estimation of internal parameters, such as the value of the SM capacitor voltages, total voltage per arm, and arm current. In [61], a new controller is proposed, like circulating current suppressing controller (CCSC). The control is based on an open-loop modulation that uses SM capacitor voltage. CCSC control is integrated to DC-loop control in stationary $\alpha\beta\theta$ frame. A proportional-resonant regulator is integrated due to the internal model principle. The authors point out that the CCSC methods suppress just the second harmonic component. However, they highlight that this component is the dominant one at circulating current. Therefore, the proposed controller focuses on the second harmonic, while the DC component is neglected, also because it has no effect on circulating current. Finally, the control achieves a steady-state performance, which has a compromise with dynamic performance. In [50] and [66], a dq reference frame control is implemented to suppress the second harmonic on circulating current. It was combined with a Phase shifted carrier PWM with switching frequency reduction. The proposed controller is efficient in suppressing the double harmonic circulating current and, as a consequence, improve SM capacitor voltage balancing.

In [65], a thorough investigation demonstrates the interaction between arm currents and capacitor voltages. It is derived from an equation describing circulating current components, and the analytical expression is verified by experimental results. The authors conclude that second-order harmonic is directly proportional to the amplitude of the AC side current. They can validate the analytical equation on a $10\ kVA$ prototype with five SM per arm. Finally, the results

improve the sizing of the components: arm inductor and the SM capacitors. This improvement may reduce the alternating components in the circulating currents.

Capacitor voltage balancing control strategy

In an MMC, the SM capacitor voltages deviate from their nominal value during regular operation. This is the result of different conduction intervals for each SM. So, a method to attain voltages' balancing is required to have a proper converter operation. The technique needs to charge or discharge particular SM to achieve the desired nominal value of capacitor voltage [24]. This control is often implemented within the modulation strategy [67]. However, it can be implemented by a sorting control method [68; 69; 70; 71; 40].

Capacitor voltage balancing is then assured by the modulation, for this reason it must be taken care for correctly adjusting the modulation reference wave to accomplish a proper SM switching, which maintains the capacitor voltage balanced.

The proposal presented by [67] is a simplified control technique in order to control the voltage of capacitors that are used in the DC bus of a three-phase three-level Neutral-Point Clamped (NPC) rectifier. In addition, it is highlighted that SVM-PWM is the best technique applied to converters. Most voltage balancing techniques are based on modifying the switching sequences, including extra hardware and modified SVM-PWM hexagon. The extra hardware included in the NPC converters not only makes the system expensive, but also adds complex calculation. The modification in the SVM-PWM hexagon used to balance the capacitor voltage affects the parameters on the source and load side beyond acceptable limits. Therefore, the authors concluded that the research reported in the literature is not sufficient with regard to capacitor voltage balance of a three-phase NPC bidirectional rectifier using optimized switching sequences. In this way, the researcher proposes a new modulation technique that reduces the potential variations of the neutral point and keeps the parameters of the source side and the load side within the acceptable and without the need for extra hardware. The results presented through the simulation demonstrate the effectiveness of the proposed control algorithm. One of the main points is that no additional hardware is needed for the stable operation of the NPC rectifier, which results in reduced volume and reduced component costs. The DC bus capacitor voltages are balanced within a narrow band. The voltage balancing effect of the DC bus capacitor is reflected on the source side and the load side.

In the **sorting control method**, the capacitor voltage balancing is separated from the modulation strategy. The modulation manages the number of active SMs, and the sorting control select which SMs will switch to perform the voltage balancing among submodules. In [72] the goal is to equalize and stabilize the SM capacitor voltages. The SM selection method, combined with the stored energy estimation, is proposed. A single-phase control is proposed, for the purpose of being scalable for the number of the converter phase. This approach provides the balancing of stored energy in each arm. However, small oscillation changes are not totally suppressed by this method. In [73], MMC control is accomplished by using a state observer. Two controllers are

proposed, and a comparison with an open-loop control is performed. One uses the state observer to estimate the total voltage per arm, and the other, the voltage balancing method is used with the state estimation of each SM voltage. The results show that both propositions improve voltage balancing control methods in comparison with the open-loop approach.

In [68] it is presented a sorting control method to minimize voltage fluctuation on submodule capacitors under low-frequency carrier modulation. The authors combine a sorting algorithm that selects submodules to be activated with a common-mode voltage and circulating current injection. The proposed methods can reduce energy fluctuation, and attain effective capacitor voltage balancing thanks to using the sorting algorithm. Furthermore, the circulating current fluctuation is decreased.

The authors of [40] highlight that phase-shift modulation has an equal power distribution between submodules resulting in a suitable inner current control and DC capacitor voltage balance. However, this method has a weak harmonic performance. Thus, the paper presents a phase-disposition modulation, combined with a hysteresis controller and a sorting algorithm, to control capacitor voltages balance, inner current control, and individual control of the DC capacitor voltages. Moreover, a hysteresis controller drives circulating currents into the desired range, arm voltage balancing, and individual voltage capacitors properly controlled are achieved.

Converter energy control

In [29], the authors deal with the total energy problem. The method is based on a rotating reference frame and uses a circulating current suppression technique. The proposed method is efficient in eliminating the oscillation on converter legs energy, and as a consequence, reduces voltage oscillation. This reduction is obtained by injection of differential current with a second harmonic component. The authors consider that it is the main drawback of the proposed method. Furthermore, in [74], besides controlling the total energy, they propose a difference in energy control. The energy control is obtained by the regulation of positive, negative, and zero sequences of circulating currents in dq0 reference frame, for both once and twice the fundamental frequency. The authors highlight that it is possible to cancel the oscillating terms of total energy and difference energy by driving circulating current to zero. For example, they are using the circulating current suppressing controller proposed by [66]. Although the method proposed by the authors consists of implementing a different reference to converter energy. This methodology effectively improve the capacitor oscillation reduction in comparison with [26] and improve the circulating current suppression in comparison with [66].

A full control system was proposed by [28]. The control is based on maximum and minimum functions to perform the submodules' selection. The proposed method can decouple DC voltage from submodules' voltage, enabling a different set point for DC bus and active submodules. Author call attention that there are no significant results on system dynamics from the energy balancing controller proposed by [49]; on the other hand, circulating current suppression presented

by [75], adequately supply arm energy balancing. The control proposition can drastically reduce submodules switching, per circle.

The previously mentioned researches focused on power and internal control aspects. However, there is another aspect to be addressed by AC-DC converter controllers: DC voltage bus control. There are three external aspects to be controlled (DC voltage bus, active and reactive power). However, technical restrictions allow each station to control just two of these aspects. Most of the mentioned researchers consider DC-bus voltage constant or controlled by another station. In [30], DC-bus voltage is attained by submodules' capacitor voltage. The converter energy model attains the solution in two ways: one in which stored energy does not depend on the DC-bus level and the other one which does. The presented solution can be used in multiterminal connections on the station, which control DC-bus voltage.

Nonlinear multivariable control

Besides, most of the researches presented above develop MMC controller based on cascaded control (e.g., PID control) [42]. This bias results from the simplification of the system in subsystems and step-by-step building and a well-known technique to implement control tuning [76]. In this case, each control loop is often associated with different response times, where the faster gives the reference to the slower. Furthermore, cascaded controls are designed to a specific operation point, on the other hand, the nonlinear one is designed to a wide operation region. Accordingly to this, there are solutions to MMC controllers which differ from conventional cascade control based.

In [77], a current and energy control, as well as energy balancing of a bilinear state-space MMC model, is achieved by a nonlinear multivariable control. All MMC internal parameters are modeled as a periodic bilinear time-varying system. The authors demonstrate a Periodic Linear Quadratic Regulator (PLQR), using currents and energies estimation by Least Squares (LS). The Linear-Quadratic problem is solved by an optimal time-invariant state feedback control law. The control is performed in a $430\ MVA$ MMC. Converter start up and arm balancing are showed.

In [27], the proposed MMC control is based on sum-of-square decomposition method. A bilinear discrete model with rotating reference frame is used for the design. A quadratic Lyapunov function is proposed to ensure system stability. Besides, an optimization process took place to maximize the convergence region of Lyapunov function. A three-phase switching model, with 41 levels, is used to validate the proposed control. State trajectories are shown. At last, a comparison with a PI controller is provided. The authors highlight that the proposed control is more demanding and need more computational effort. However can be easily implemented in real time.

A model-based nonlinear control is shown in [78], where is considered an MMC average model where a resulting submodule is represented per arm. A nonlinear coordinate transformation is used to point candidate states as output. The authors performed system linearization, based on the candidates output.

Multivariable control uses a nonlinear multivariable model. These methods request advanced control strategies to define the control laws and perform stability analyses [52]. The convenience of using a multivariable control approach is to design a direct control strategy of all the converter's state variables. State-space equations of the MMC system are integrated. Moreover, it allows the demonstration of the proposed scheme's suitability to asymptotically stabilize the MMC's complicated dynamics.

Stability analyses are substantial for the study of dynamic systems. In this thesis these will be achieved through Lyapunov theory [79] searching to establish that:

- ❏ An equilibrium point is stable if all solutions starting at nearby point, stay nearby, and;
- ❏ An equilibrium point is asymptotically stable if all solutions starting at a nearby point tend to the equilibrium point and time goes to infinity.

Since each operating point (P_e and Q_e) defines different values for all states, it is convenient to proceed with a change of variables, where the state x will be replaced by its error $\tilde{x}$ plus their steady state value $\bar{x}$.

$$x \triangleq \tilde{x} + \bar{x}$$

This change of variable is convenient because for all operating point $\tilde{x}$ its reference is zero. To attain this goal, the control can be designed focusing on asymptotically stabilize state error ($\tilde{x} = 0$), when time goes to infinity. Thus, state x will assume its reference value, $\bar{x}$.

In this thesis, two multivariable controls, based on Lyapunov theory, are addressed to achieve the MMC control challenges:

- ❏ **Chapter 4:** A nonlinear approach based on Feedback Linearization and Backstepping, and;
- ❏ **Chapter 5:** A bilinear approach based on Quadratic Feedback control.

Feedback linearization approach

Considering a nonlinear system as

$$\begin{aligned} \dot{x} &= f(x) + G(x)u \\ y &= h(x) \end{aligned} \tag{37}$$

the Feedback Linearization consists on finding a state feedback control, as

$$u = \alpha(x) + \beta(x)v \tag{38}$$

and a change of variables

$$z = T(x) \tag{39}$$

that transform the nonlinear system into an equivalent linear system. The feedback linearization of the MMC is investigated by [31]. The nonlinear model is presented, and an input-output feedback linearization is accomplished. However, the authors utilize linear controllers, Proportional-resonant (PR) and PI controller, to regulate the linearized system states. The zero-dynamic stability is investigated and proved. Furthermore, the proposed control well succeed to track reference, providing faster dynamic response and smooth transients for step response. In [80] the feedback linearization control based on Lyapunov theory is addressed for a DC/DC converter, in the context of multi-terminal HVDC. System model is bilinear in a state space representation. Controllability and stability are investigated. The system is modeled as a bilinear approach of an average dynamic model and computer simulations are addressed. The proposed control stabilizes the MMC system. In addition, authors designed a quadratic feedback control which will be further discussed along this chapter.

As presented above by equations 37-39, the proposed control is model dependent [81]. Thus modeling and parametric errors affect the control performance. It is possible to verify these effects by robustness validations. Furthermore, it is possible to ensure a degree of robustness, often stronger than linear controls, as said by Lemma 9.1 [79]. Accordingly, a nonlinear controller is able to operate in a wide region.

Quadratic Feedback control approach

Electrical circuits based on switching devices like MMC are often mathematically modeled as bilinear systems [77; 27; 80; 82; 83]. The system is described by linear differential equations and the control inputs are the coefficients. The general representation of bilinear system consists of:

$$\dot{x} = Ax + \sum_{k=1}^{\rho} (u_k B_k x + u_k b_k) \tag{40}$$

Considering a bilinear system in which the state variables are $x \in \mathbb{R}^n$, and the input variables are $u \in \mathbb{R}^\rho$.

The design of nonlinear control for the bilinear system is a tough problem, even worse for higher dimension systems [84]. To control this class of system raises many challenges, mostly: manage all states altogether, what results in states which are dynamically coupled.

In [84] it is derived conditions for the existence of a control Lyapunov function for a general bilinear system. The authors deals with two dimensional bilinear systems with one control input. It is presented a necessary and sufficient condition which ensures that the presented design condition can be satisfied. The condition is that $V(x) = x^T P x$, based on [85; 86], with a

symmetric and positive definite matrix P is a quadratic Lyapunov control function for the system in equation 40 if and only if equation 41 is valid.

$$Y(x) := x^T(A^TP + PA)x \leq 0 \forall x \in M := \left\{ x \in \mathbb{R}^n | x \neq 0, \sum_{k=1}^{\rho} \{(B_k x + b_k)^T P x\}^2 \neq 0 \right\} \tag{41}$$

Thus, the stated control Lyapunov function ensures asymptotic stability of the closed-loop system inside set M. In [80] asymptotic stability is guaranteed to a bilinear DC/DC converter, through a quadratic feedback control. The control assumptions were similar to the presented above by [84]. The model of DC/DC converter has dimension four. A change of variable is performed and control is designed to drive error $\tilde{x}$ to be zero, implying x to $\bar{x}$. The control simulations are performed on matlab. The authors consider the bilinear controller, for the presented system with dimension four, more accessible to implement than the feedback linearization approach. However, also highlight that feedback linearization is broader known and has established theory on the literature.

Thesis boundary conditions

The context created in this introduction surrounds the thesis proposition. The two above mentioned control approaches will take place in the following chapters. Additionally, asymptotic stability has been established. The controllers are designed for the three-phase MMC converters. They are based on the bilinear average model proposed by [77; 27]. The computer algebra systems, MAPLE and Mathematica 11.2, are the computational software used to attain the math computation. Furthermore, MATLAB R2019b at the SIMULINK Simscape Electrical environment simulates a switching MMC model and average-model. The MMC simulated on Simscape has a sorting algorithm implemented, based on [24].

2.4 Chapter conclusion

This chapter discussed the main points about MMC operational principles. The use of full-bridge SM instead of half-bridge SM would improve DC cable fault protection, although it increases switching losses. Modulation and sorting algorithm handle the voltage balancing across arms' SM. Furthermore, the modeling aspect concerning the decrease of the computational requirement for reduced-order models is discussed. Additionally, the mathematical modeling of the reduced-order average model was presented and used to develop the controllers proposed in this thesis. Finally a section concerning the control designs for MMC systems is presented.

CHAPTER 3

MMC Linear Control and Test System

As discussed in chapter 2, comparing MMC converters in respect to other VSCs, there are additional dynamics that controller must take into account: circulating current control, SM capacitor voltage balancing, and stored internal energy .

In this research, the three-phase MMC switching model uses phase-shift modulation. Here it is considered that the SM capacitor voltage balancing is solved by the modulation interface, which will be further analyzed. Among the drawbacks of using the MMC, this thesis has addressed the points of circulating current management, and stored internal energy and its balancing.

In the next chapters of this thesis, a reduced-order average model was used to develop the proposed control and to make the mathematical stability analysis. Meanwhile, a switched model was tested on Matlab Simscape Electrical to verify its performance. Two multivariable controllers are presented to solve the MMC control challenge. In addition, this chapter demonstrates, for comparison purposes, a cascaded control based on PI.

The cascade control presented here is adapted from the control proposed on [28]. These modifications are necessary to have the same state variables and control inputs as the proposed nonlinear controllers.

Two test systems with two different voltage levels are presented — one in medium voltage and the other in high-voltage. The goal is to verify nonlinear control performance and tuning for each particular case. The medium-voltage system is a $60\ kV$ DC voltage and nominal power of $50\ MVA$, based on the system proposed in [27]. Meanwhile, the high-voltage is a $400\ kV$ DC and $450\ MVA$, based on [87].

Simulations with average-model and with switching-model were performed. MMC state references are described in this chapter.

This chapter focuses on the performance of the MMC models using the PI controller adapted from [28].

3.1 Equilibrium points for state variables and control inputs

This section will establish the equilibrium point for states and the corresponding control inputs values ($\bar{x}$ and $\bar{u}$). However, since references may change in response to grid variations or disturbances, here it will be highlighted the corresponding modifications.

Current i_{vj} is defined in the previous chapter in rotating dq reference frame. Park's transformation was used to transform symmetrical and balanced AC system equations (28) into the syncronized rotating dq reference frame of (30), which is recalled here:

$$\begin{bmatrix} \dot{i}_{vd} \\ \dot{i}_{vq} \end{bmatrix} = \begin{bmatrix} -\frac{R_{eq}}{L_{eq}} & w \\ -w & -\frac{R_{eq}}{L_{eq}} \end{bmatrix} \begin{bmatrix} i_{vd} \\ i_{vq} \end{bmatrix} + \begin{bmatrix} \frac{1}{L_{eq}} & 0 \\ 0 & \frac{1}{L_{eq}} \end{bmatrix} \begin{bmatrix} v_{ud} - v_{ld} \\ v_{uq} - v_{lq} \end{bmatrix} + \begin{bmatrix} \frac{2}{Leq} & 0 \\ 0 & \frac{2}{Leq} \end{bmatrix} \begin{bmatrix} v_{fd} \\ v_{fq} \end{bmatrix}$$

In the rotating reference frame the power in the PCC can be described by (42).

$$S_e = P_e + jQ_e = \frac{3}{2}(v_{fd} + jv_{fq})(i_{vd} - ji_{vq}) \tag{42}$$

$$P_e = \frac{3}{2}(v_{fd}i_{vd} + v_{fq}i_{vq}) \tag{43}$$

$$Q_e = \frac{3}{2}(-v_{fd}i_{vq} + v_{fq}i_{vd}) \tag{44}$$

It is assumed that the rotating frame is aligned with the alternating terminal voltage, thus the voltage v_a is synchronized on the d axis. Thanks to this consideration, v_{fq} is equal to zero. Following this, the AC active and reactive power definitions are rewritten in (45) and (46).

$$P_e = \frac{3}{2}v_{fd}i_{vd} \tag{45}$$

$$Q_e = -\frac{3}{2}v_{fd}i_{vq} \tag{46}$$

As it is possible to see, active and reactive power flow are directly linked with states i_{vd} and i_{vq}. Thus they are used to define reference values. $\bar{P}_e$ and $\bar{Q}_e$ are the power references an are defined by the consumption demand. The desired values for the AC currents are defined in (47) and (48) as functions of the active and reactive power references coming from higher level controllers.

$$\bar{x}_1 = \bar{i}_{vd} = \frac{2\bar{P}_e}{3v_{fd}} \tag{47}$$

$$\bar{x}_2 = \bar{i}_{vq} = \frac{2\bar{Q}_e}{3v_{fd}} \tag{48}$$

Since components dq of circulating current in an MMC do not produce useful power and increase the converter losses, they should be minimized. For this reason, their references are taken as zero:

$$\bar{x}_3 = \bar{i}_{cird} = 0 \tag{49}$$

$$\bar{x}_4 = \bar{i}_{cirq} = 0 \tag{50}$$

The desired values for control inputs can be defined by system equation (31) (recalled below) in the equilibrium point of the steady-state, thus $\dot{x} = 0$.

$$\begin{bmatrix} \dot{i}_{cird} \\ \dot{i}_{cirq} \\ \dot{i}_{cir0} \end{bmatrix} = \begin{bmatrix} -\frac{R}{L} & w & 0 \\ -w & -\frac{R}{L} & 0 \\ 0 & 0 & -\frac{R}{L} \end{bmatrix} \begin{bmatrix} i_{cird} \\ i_{cirq} \\ i_{cir0} \end{bmatrix} + \begin{bmatrix} -\frac{1}{2L} & 0 & 0 \\ 0 & -\frac{1}{2L} & 0 \\ 0 & 0 & -\frac{1}{2L} \end{bmatrix} \begin{bmatrix} v_{ud} + v_{ld} \\ v_{uq} + v_{lq} \\ v_{d0} \end{bmatrix} + \begin{bmatrix} 0 \\ 0 \\ \frac{v_{dc}}{2L} \end{bmatrix}$$

In this way, (31) becomes (51), (52) and (53).

$$-\frac{R}{L}\bar{i}_{cird} + w \cdot \bar{i}_{cirq} - \frac{\bar{v}_{ud} + \bar{v}_{ld}}{2L} = 0 \tag{51}$$

$$-w \cdot \bar{i}_{cird} - \frac{R}{L}\bar{i}_{cirq} - \frac{\bar{v}_{uq} + \bar{v}_{lq}}{2L} = 0 \tag{52}$$

$$-\frac{R}{L}\bar{i}_{cir0} - \frac{\bar{v}_{d0}}{2L} + \frac{V_{DC}}{2L} = 0 \tag{53}$$

Replacing (49) and (50) in (51), we obtain:

$$\bar{v}_{ud} = -\bar{v}_{ld} \tag{54}$$

Also, replacing (49) and (50) in (52) obtains:

$$\bar{v}_{uq} = -\bar{v}_{lq} \tag{55}$$

Thus, replacing (54) and (55) in (30), at the equilibrium point, it becomes (56), (57), (58) and (59).

$$-\frac{R_{eq}}{L_{eq}}\bar{i}_{vd} + w \cdot \bar{i}_{vq} + \frac{2\bar{v}_{ud}}{L_{eq}} + \frac{2v_{fd}}{L_{eq}} = 0 \tag{56}$$

$$-\frac{R_{eq}}{L_{eq}}\bar{i}_{vd} + w \cdot \bar{i}_{vq} - \frac{2\bar{v}_{ld}}{L_{eq}} + \frac{2v_{fd}}{L_{eq}} = 0 \tag{57}$$

$$-w \cdot \bar{i}_{vd} - \frac{R_{eq}}{L_{eq}}\bar{i}_{vq} + \frac{2\bar{v}_{uq}}{L_{eq}} + \frac{2v_{fq}}{L_{eq}} = 0 \tag{58}$$

$$-w \cdot \bar{i}_{vd} - \frac{R_{eq}}{L_{eq}}\bar{i}_{vq} - \frac{2\bar{v}_{lq}}{L_{eq}} + \frac{2v_{fq}}{L_{eq}} = 0 \tag{59}$$

Collecting terms on (56), (57), (58), (59) and (53) the reference to the control inputs $\bar{v}_{ud}$, $\bar{v}_{ld}$, $\bar{v}_{uq}$, $\bar{v}_{lq}$ and $\bar{v}_{d0}$ are obtained:

$$\bar{v}_{ud} = \frac{R_{eq}}{2}\bar{i}_{vd} - \frac{wL_{eq}}{2} \cdot \bar{i}_{vq} - v_{fd} \tag{60}$$

$$\bar{v}_{ld} = -\frac{R_{eq}}{2}\bar{i}_{vd} + \frac{wL_{eq}}{2} \cdot \bar{i}_{vq} + v_{fd} \tag{61}$$

$$\bar{v}_{uq} = \frac{wL_{eq}}{2} \cdot \bar{i}_{vd} + \frac{R_{eq}}{2}\bar{i}_{vq} - v_{fq} \tag{62}$$

$$\bar{v}_{lq} = -\frac{wL_{eq}}{2} \cdot \bar{i}_{vd} - \frac{R_{eq}}{2}\bar{i}_{vq} + v_{fq} \tag{63}$$

$$\bar{v}_{d0} = -2R\bar{i}_{cir0} + V_{DC} \tag{64}$$

The desired value for the zero component of the circulating current ($\bar{i}_{cir0}$) comes from the equilibrium point at steady-state of equation (18), where derivative of the desired value is zero ($\dot{\bar{x}} = 0$). In (18) replacing (60) and (62) and collecting terms to obtain (65).

$$\bar{x}_5 = \bar{i}_{cir0} = \frac{V_{DC} - \sqrt{V_{DC}^2 - 4R(\bar{i}_{vd}\bar{v}_{ud} + \bar{i}_{vq}\bar{v}_{uq})}}{4R} \tag{65}$$

In (65), one of the roots is unfeasible since it takes the MMC to a very high dissipating mode, so the other is chosen.

The reference for SMs' energy is linked with SMs' capacitor voltage, and it can be expressed as in equation (66).

$$V_{DC} - 2Ri_{cirj} - 2L\dot{i}_{cirj} = 2NV_C^{SM} \tag{66}$$

Applying Park's transformation (T) in equation (66), the equilibrium point for capacitors' voltage is:

$$V_C^{SM} = \frac{V_{DC} - 2R\bar{x}_5}{2N} \tag{67}$$

then, the stored energy per SM can be calculated as:

$$W_C^{SM} = \frac{1}{2}C_{SM}\left(V_C^{SM}\right)^2 \tag{68}$$

By equation (68), considering all active SMs, the desired total energy of the converter is obtained in equation (69).

$$\bar{x}_6 = \bar{W}_h = 6 \cdot N \cdot W_C^{SM} = \frac{3C_{SM} \cdot (V_{DC} - 2R\bar{x}_5)^2}{4N} \tag{69}$$

Due to the symmetric configuration of the converters, upper and lower arms must have the same stored energy in steady-state, so the reference for the energy balance ($\bar{W}_v$) is defined as zero.

$$\bar{x}_7 = \bar{W}_v = W_u - W_l = 0 \tag{70}$$

The state reference and the stability condition defined above fuel the control development and simulations which will be presented in this thesis.

3.2 PI controller

A cascaded-control for the MMC is described in this section, which is based on a PI and is adapted from [25]. The modifications were necessary to obtain the same control inputs as the proposed nonlinear controllers, thus attaining a proper and fair performance comparison.

The result in [25] was chosen as the standard to be compared due to similarities in the control's objectives. The authors proposed an MMC control system, based on converter's stored internal energy. Furthermore, it points out the decoupling between the DC voltage produced by the converter and the voltage imposed by the DC bus. This result is also achieved by both nonlinear controllers proposed in this thesis.

An MMC converter with the same configuration as presented in figure 10 is considered by [25]. From there, equations (71) and (72) per phase j are obtained.

$$\frac{V_{DC}}{2} = v_{uj} + L\dot{i}_{uj} + Ri_{uj} - L_c\dot{i}_{vj} - Ri_{vj} + v_{fj} \tag{71}$$

$$\frac{V_{DC}}{2} = v_{lj} + L\dot{i}_{lj} + Ri_{lj} + L_c\dot{i}_{vj} + Ri_{vj} - v_{fj} \tag{72}$$

In the original control proposed by [25], there are two key variables which combine the controller inputs $v_{m,j}$, presented as: ($V_{conv_{acj}}$ and $V_{conv_{dcj}}$). They are respectively the total voltage on the leg j and the average voltage between upper and lower arm. They are presented in equation (73) and equation (74).

$$V_{conv_{acj}} = \frac{v_{lj} - v_{uj}}{2} \tag{73}$$

$$V_{conv_{dcj}} = v_{uj} + v_{lj} \tag{74}$$

Subtracting and adding (71) and (72), and also replacing the definition in (73) and (74) the equations (75) and (76) are obtained.

$$v_{fj} - v_{conv_{acj}} = \left(\frac{L}{2} + L_c\right)\dot{i}_{vj} + \left(\frac{R}{2} + R_c\right)i_{vj} \tag{75}$$

$$V_{DC} - v_{conv_{dcj}} = 2L\dot{i}_{cir_j} + 2Ri_{cir_j} \tag{76}$$

So, the following controllers in dq rotating reference frame are proposed to control AC current from (75).

$$\bar{v}_{conv_d} = -(\bar{i}_{vd} - i_{vd})C_{i_{ac}} + v_{fd} - \left(\frac{L}{2} + L_c\right)\omega i_{vq} \tag{77}$$

$$\bar{v}_{conv_q} = -(\bar{i}_{vq} - i_{vq})C_{i_{ac}} + v_{fq} - \left(\frac{L}{2} + L_c\right)\omega i_{vd} \tag{78}$$

Also, to control circulating current of equation (76), the control in equation (79) is proposed.

$$\bar{v}_{conv_{dc}} = -(\bar{i}_{cirj} - i_{cirj})C_{i_{cir}} + \frac{V_{DC}}{2} \tag{79}$$

where C_x is the PI control function in Laplace domain, in equation (80).

$$C_x = k_p^x + \frac{k_i^x}{s} \tag{80}$$

where x represents each of the considered states.

In [25] the relation between power variation and energy stored on SM capacitors are provided as:

$$C_{arm}\frac{d\left(v_{Ctot_{uj}}^2 + v_{Ctot_{lj}}^2\right)}{dt} = P_{ej}^{DC} - P_{ej}^{AC} \tag{81}$$

$$C_{arm}\frac{d\left(v_{Ctot_{lj}}^2 - v_{Ctot_{uj}}^2\right)}{dt} = i_{cir_j}v_{conv_{acj}} \tag{82}$$

The control of total energy (W_h) provides the regulation of energy exchange between AC and DC sides. It is obtained through the desired value of DC circulating current $\bar{i}_{cir0}$ by the PI control derived from (81) as shown in (83). Meanwhile, energy balancing (W_v) balance the energy between upper and lower arms, by the desired values of AC components of the circulating currents i_{cirdq}. The PI controller is derived from (82) and shown in (84).

$$\bar{i}_{cir0} = \left(\left(\bar{W}_h - W_h\right)C_{W_h} + P_e^{AC}\right)\frac{1}{V_{DC}} \tag{83}$$

$$\bar{i}_{cir_{dq}} = \left(\bar{W}_v - W_v\right)\frac{C_{W_v}}{V_{conv_{acdq}}} \tag{84}$$

In this thesis it is proposed an adaptation of the control shown above, from [25]. The power flow controllers consist in considering the control inputs $v_{m,j}$ separately. Equations (73) and (84) consider the combined voltage v_{uj} and v_{lj}, while in this thesis they are considered separately. Therefore, each control input, i.e. the arms' equivalent voltage ($v_{m,j}$), is derived below.

From the previous chapter, the power-flow equation (13) can be written as (85).

$$\frac{v_{lj} - v_{uj}}{2} = \frac{-L_{eq}\dot{i}_{vj}}{2} - \frac{R_{eq}i_{vj}}{2} + v_{fj} \tag{85}$$

So, Park's transformation is applied to equation (85), and by a change of variables it is obtained the AC current control (86) and (87).

$$\frac{\tilde{v}_{ld} - \tilde{v}_{ud}}{2} = -(\bar{i}_{vd} - i_{vd})C_{i_{ac}} + v_{fd} \tag{86}$$

$$\frac{\tilde{v}_{lq} - \tilde{v}_{uq}}{2} = -(\bar{i}_{vq} - i_{vq})C_{i_{ac}} + v_{fq} \tag{87}$$

In the same way, equation (16) can be written as (88). A change of variables and Park's transformation on (88), produces circulating currents' control (89), (90) and (91).

$$v_{uj} + v_{lj} = -2L\dot{i}_{cirj} - 2Ri_{cirj} + V_{DC} \tag{88}$$

$$\tilde{v}_{ud} + \tilde{v}_{ld} = -(\bar{i}_{cird} - i_{cird})C_{i_{cird}} \tag{89}$$

$$\tilde{v}_{uq} + \tilde{v}_{lq} = -(\bar{i}_{cirq} - i_{cirq})C_{i_{cirq}} \tag{90}$$

$$\tilde{v}_{d0} = -(\bar{i}_{cir0} - i_{cir0})C_{i_{cir0}} \tag{91}$$

Collecting terms from (86), (87), (89) and (90), one obtains the uncoupled control inputs at (92), (93), (94), and (95).

$$\tilde{v}_{ud} = -\frac{1}{2}(\bar{i}_{cird} - i_{cird})C_{i_{cird}} + (\bar{i}_{vd} - i_{vd})C_{i_{ac}} \tag{92}$$

$$\tilde{v}_{uq} = -\frac{-1}{2}(\bar{i}_{cirq} - i_{cirq})C_{i_{cirq}} + (\bar{i}_{vq} - i_{vq})C_{i_{ac}} \tag{93}$$

$$\tilde{v}_{ld} = \frac{1}{2}(\bar{i}_{cird} - i_{cird})C_{i_{cird}} + (\bar{i}_{vd} - i_{vd})C_{i_{ac}} \tag{94}$$

$$\tilde{v}_{lq} = \frac{1}{2}(\bar{i}_{cirq} - i_{cirq})C_{i_{cirq}} + (\bar{i}_{vq} - i_{vq})C_{i_{ac}} \tag{95}$$

Concerning total energy W_h and balancing energy W_v, the controller proposed by [25] in (83) and (84) is simplified and used. Where total energy's control provides the reference for i_{cir0}, which regulates DC power output, while the energy balance control provides i_{cird} reference.

$$\bar{i}_{cir0} = -(\bar{W}_h - W_h)C_{W_h} \tag{96}$$

$$\bar{i}_{cird} = -(\bar{W}_v - W_v)C_{W_v} \tag{97}$$

Therefore, all states of a three-phase MMC can be controlled by the cascade-control adapted from [25]. Including energy states which aren't directly controlled by controller inputs.

The PI controllers developed in this section are summarized by the block diagrams in figure 22 to figure 26. Also, the firing pulses generation is depicted in figure 27 based on phase-shift PWM.

Figure 22 – Block diagram of control input v_{ud}.

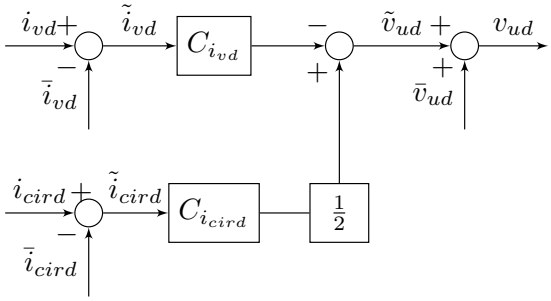

Source: Author

Figure 23 – Block diagram of control input v_{uq}.

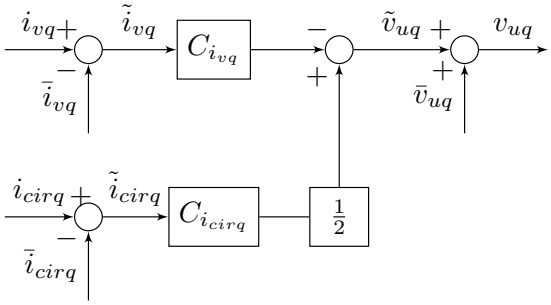

Source: Author

where v_{md} is v_{ud} and v_{ld}, and so on.

3.2.1 Tuning

The PI controllers were tuned to present a speed of convergence close to the controllers proposed in this thesis. By setting the desired time constant τ_i, the parameters k_p^x and k_i^x can be computed as presented in [88] at chapter 8.4. Considering the proportional-integral PI controller in (80), it enables states to track their references:

$$C_x = k_p^x + \frac{k_i^x}{s}$$

Figure 24 – Block diagram of control input v_{ld}.

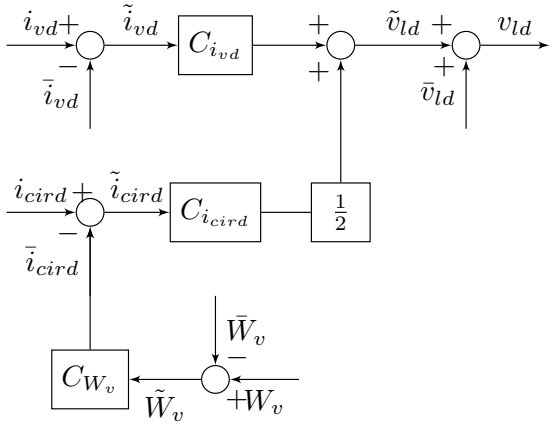

Source: Author

Figure 25 – Block diagram of control input v_{lq}.

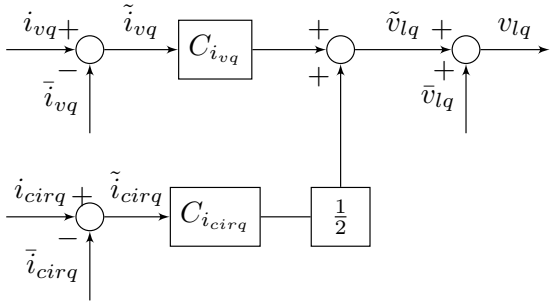

Source: Author

Figure 26 – Block diagram of control input v_{d0}.

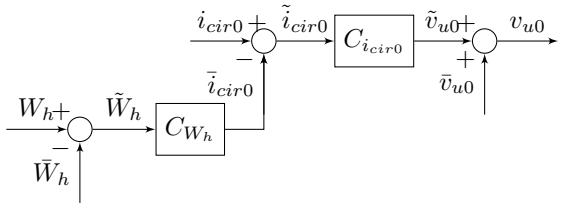

Source: Author

where k_p^x and k_i^x are the proportional and integral gains for state x. As described in [88], the power controller's gains can be obtained in term of the desired time constant for the closed-loop system τ_i, as shown in (98) and (99).

$$k_p^x = \frac{L_c}{\tau_i} \tag{98}$$

$$k_i^x = \frac{R_c}{\tau_i} \tag{99}$$

Figure 27 – Block diagram of firing pulses to m arms.

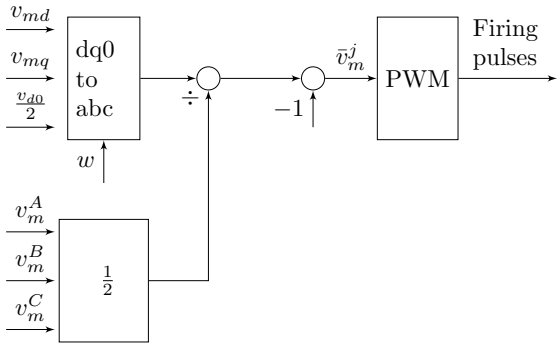

Source: Author

For smaller τ_i, the output current controllers track faster the references, which are obtained from the active and reactive power references. However, τ_i must be large enough to attain the system dynamic requirement, as to be ten times the converter's switching frequency. As [88] mentioned, τ_i uses to be selected in the range of $0.5\ ms$ to $5\ ms$. This choice is linked with the application's requirements and the converter's switching frequency.

The tuning of circulating currents' PIs is not much exploited on literature. In this thesis it is tuned considering the time constant as well as arm impedance, as shown in (100) and (101).

$$k_p^x = \frac{L}{\tau_i} \tag{100}$$

$$k_i^x = \frac{R}{\tau_i} \tag{101}$$

Moreover, gains drive the circulating currents to follow their respective reference values, given by the outer loop controllers, and maintain q component for the circulating current in its reference value, which is set to zero.

As a result of a limited literature available for the tuning of PIs used to control the energy on the MMC, this task is carried out by a trial and error approach. It is considered for the total energy and energy balance controllers, a slower response in comparison with currents. Such to avoid undesired interactions between inner and outer controllers.

First of all, the total energy controller is tuned; this controller sets the reference for the circulating current i_{cir0}. Finally, energy balancing controller is tuned and set the reference to i_{cird}.

The parameters for both controllers were set using Matlab - Simulink by adjusting the desired response.

3.3 Simulation test of MMC with the PI controller at switching-model and average-model

This section presents simulations for the MMC with 41 levels with the PI controller proposed in the previous section. First of all, it is presented simulations for a medium-voltage system described by an average arm model presented in section 2.2.3. In this case, a state-space simulation is carried out on Matlab/Simulink. Additionally, a switching model is also developed. The switching model is built using the Matlab Simscape Electrical environment. The model uses twenty half-bridge SMs per arm and a phase-shift PWM modulation. Finally, a high-voltage system is simulated by the switching model. Therefore, this section and the next comprise the following tests:

- ❏ Medium-voltage system
  - – average arm model
    - ∗ four-quadrant power operation
    - ∗ changes on converter energy
  - – switching model
    - ∗ four-quadrant power operation
    - ∗ changes on converter energy
- ❏ high-voltage
  - – Switching model
    - ∗ four-quadrant power operation
    - ∗ changes on converter energy

3.4 Medium-voltage system test with PI controller

In figure 28 a $50\ MVA$ HVDC connection is shown. The main AC grid is connected to symmetric monopole DC line/cable, by an AC-DC MMC converter. The MMC, highlighted by the red dashed line, is detailed in figure 10 for the switching model and in figure 19 for the reduced-order average model.

Figure 28 – Medium-voltage system test.

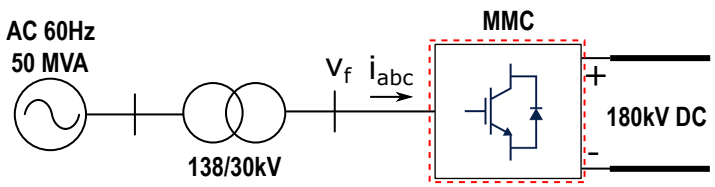

The detailed switching model of the three-phase MMC converter with 41 levels, with the proposed PI, is tested using the Matlab Simscape Electrical environment. The system test is adapted from [87]. The original DC voltage was changed to $180\ kV$ to amplify the capacity to inject reactive power. System's parameters are presented in Table 2, and the results are shown in the dq reference frame. The pulse generator used is a phase-shift PWM.

Table 2 – Parameters of simulated medium-voltage system and PI control gains.

Parameter	**Value**	**Parameter**	**Value**
S_{MMC}	$50\ MVA$	$k_p^{i_{vdq}}$	50
V_{AC}	$30\ kV$	$k_i^{i_{vdq}}$	1120
V_{DC}	$180\ kV$	$k_p^{i_{cirdq}}$	28
L_c	$5\ mH$	$k_i^{i_{cirdq}}$	1000
L	$14\ mH$	$k_p^{i_{cir0}}$	300
R_c	$0.03\ \Omega$	$k_i^{i_{cir0}}$	1000
C_{SM}	$3\ mF$	$k_p^{W_h}$	-0.5
Freq	$60\ Hz$	$k_i^{W_h}$	-25
R	$0.5\ \Omega$	$k_p^{W_v}$	0.8
N	20	$k_p^{W_v}$	0.1

Figure 29, figure 33, and figure 38 comprehend eight graphics each. At each figure, the first graphic depicts the active and reactive power demand, and the seven states follow it $x = [i_{vd}\ i_{vq}\ i_{cird}\ i_{cirq}\ i_{cir0}\ W_h\ W_v]$ and their desired value $\bar{x}$ denoted by (Ref.). All that three figures shows the simulation of the MMC average model in the medium-voltage level with the PI controller presented above. The step changes on active and reactive power (P_e and Q_e) shown at 1^{st} graphic comprehend the four-quadrant operation with the maximum power injection, 70% of nominal power, respecting the capability curve.

Figure 29 – Four-quadrant operation of MMC average model with PI controller.

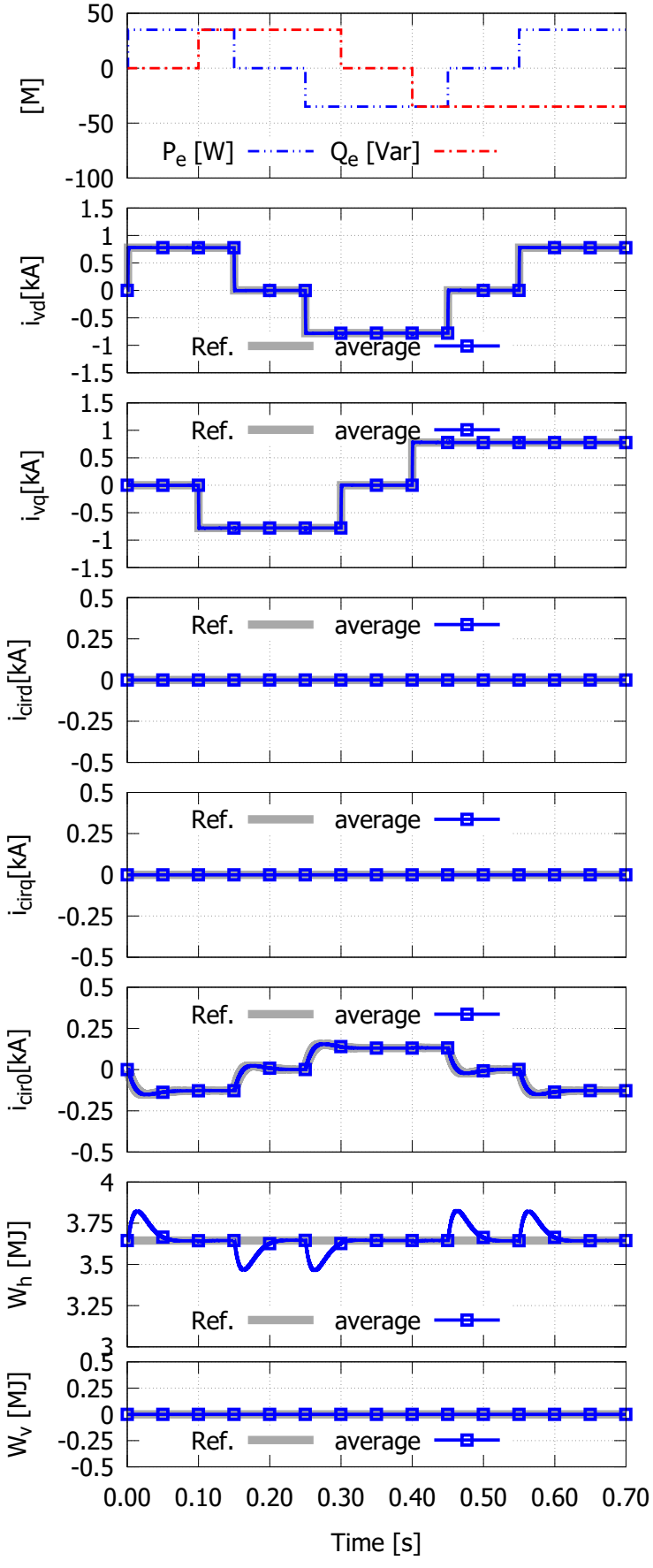

Four-quadrants operation average-model medium-voltage

At $t = 0.05\ s$ P_e turns to $35\ MW$, which is followed by the related states: i_{vd} (2^{nd} graphic) and i_{cir0} (6^{th} graphic). State i_{vq} in 3^{rd} graphic, faces a small transient which is shown in detail in figure 30. State W_h (7^{th} graphic) is affected and presents a transient of $50\ ms$. The same behaviour is observed in all the active power changes, at $t = 0.15\ 0.20\ 0.35\ 0.40s$.

Meanwhile, Q_e turns to $35\ MW$ at $t = 0.10\ s$, where the directly linked state, i_{vq} in the 3^{rd} graphic, follows the new reference in $1\ ms$. The direct component of AC current, i_{vd}, faces a fast transient associated with reactive power changes, see detail at figure 31. The same pattern is seen at all change of reactive power.

Furthermore, circulating currents i_{cirdq} remain on their references during all changes (4^{th} and 5^{th} graphic). However, total energy W_h deal with transients linked with changes in i_{cir0}, which can be explained because this current manages the DC output power, which affects the stored energy.

Figure 30 is a detail from figure 29. It shows states i_{vd} and i_{vq} under the active power step at $t = 0.05\ s$. State i_{vd} needs less than $1\ ms$ to track its reference, and presents no overshoot. As a consequence, i_{vq} presents a transient, and returns to its reference when $i_{vd} = \bar{i}_{vd}$.

Figure 30 – Detail of step on active power, from figure 29.

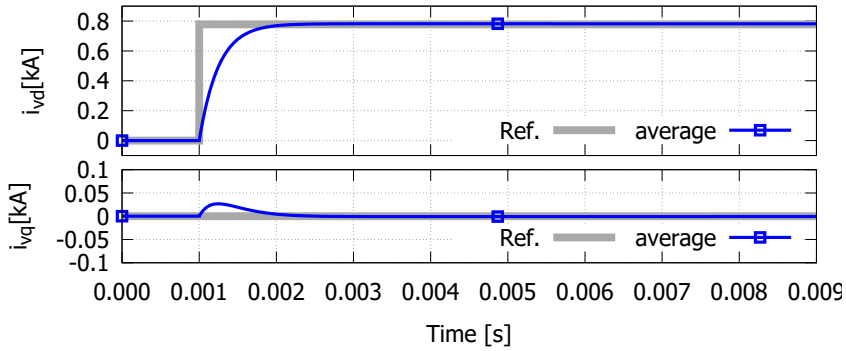

Source: Author

Figure 31 – Detail of step on reactive power, from figure 29.

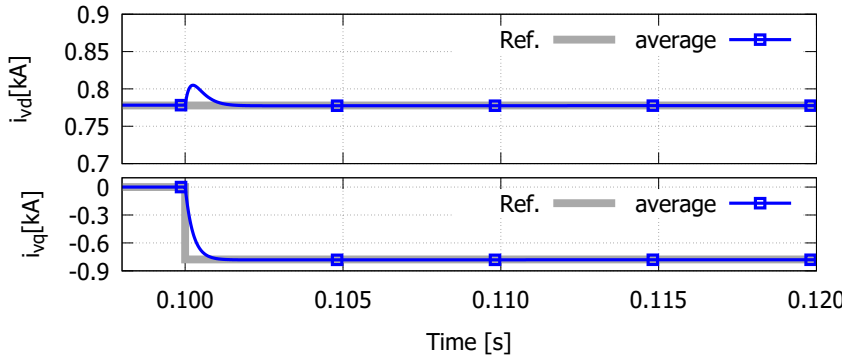

Source: Author

It is clear that the PI can drive the states of the MMC average-model to track their references. In figure 32, i_{cir0} is shown in detail and it is possible to see the state tracking its reference without delays.

Figure 32 – Detail of state i_{cir0} while a step on active power, from figure 29.

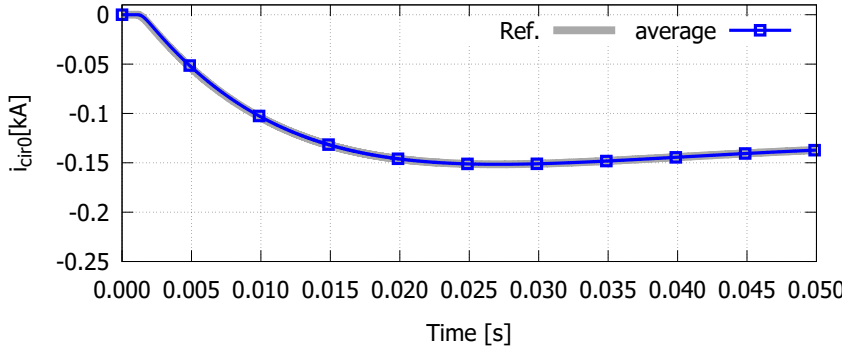

Source: Author

Figure 33 – Four-quadrant operation of MMC switching-model with PI controller.

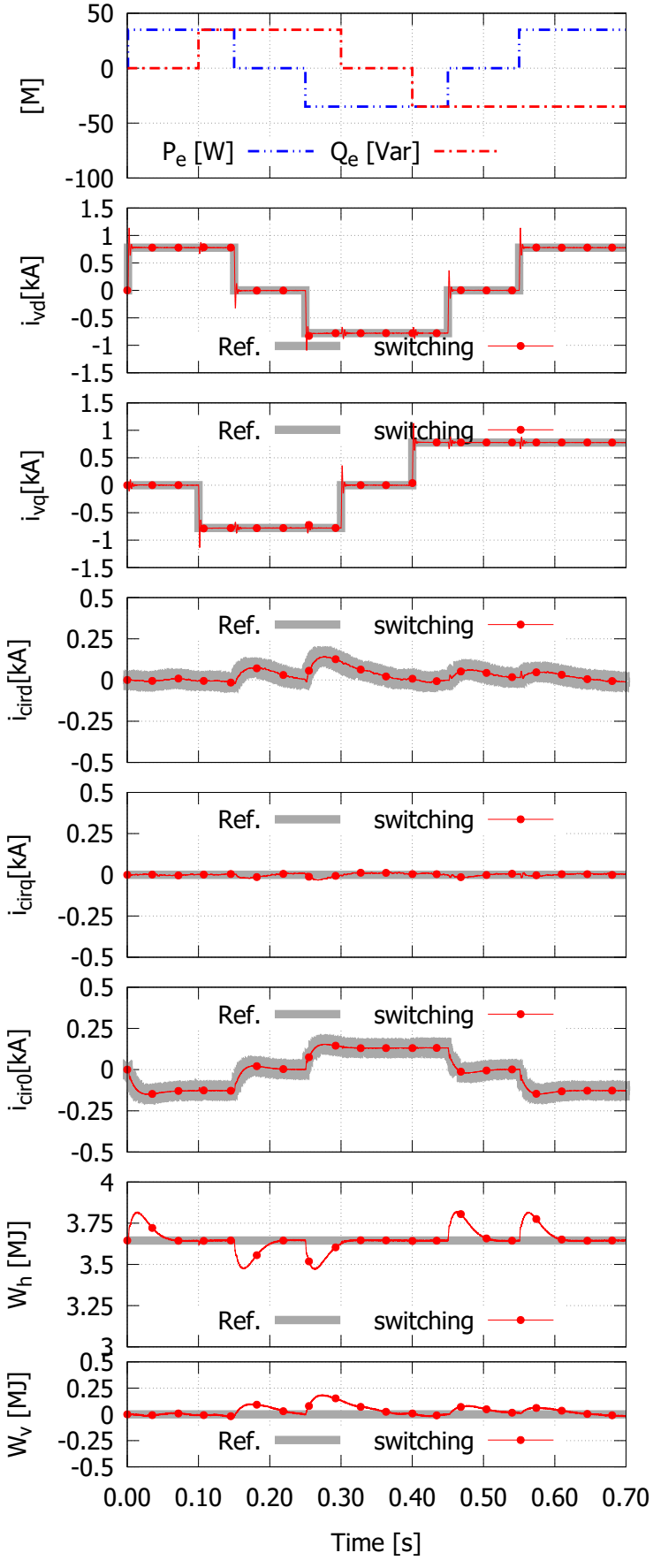

Four-quadrants operation switching-model medium-voltage

In figure 33, a switching model is simulated with the proposed PI controller. It is possible to see that states follow their references (Ref.).

In the same way as presented in the average model (figure 29), there are coupling effects between i_{vd} and i_{vq} (2^{nd} and 3^{rd} graphic). However the effects here were larger, and are detailed in figure 34 and figure 35. There it may be seen that, at each active power step ($t = 0.05\ 0.15\ 0.20\ 0.35\ 0.40\ s$) while i_{vd} reacts to track the new reference, i_{vq} oscillates around its reference. Similarly, when there are changes on i_{vq}, i_{vd} also oscillates around its reference, as for example, following reactive power steps, i_{vd} oscillates around its reference.

If compared with the average model at figure 29, it is possible to see that reference of direct component of circulating current (i_{cird} Ref.) and circulating current reference (i_{cir0} Ref.) present small oscillations which came from SMs switching, at 4^{th} and 6^{th} graphics.

Still on figure 33, the dq component of circulating currents (i_{cirdq}) present an overshoot at the inversion of the power-flow direction at $t = 0.20\ s$, to $P_e = -35\ MW$ and $Q_e = 35\ MVar$ where they react more powerfully even causing an unbalancing between upper and lower arms energy (W_v at 8^{th} graphic). Finally, W_h (7^{th} graphic) shows a stronger reaction for each change of active power in comparison with the average-model.

Figure 34 is a detail from figure 33. Show state i_{vd} and i_{vq} under the active power step at $t = 0.05\ s$. State i_{vd} need $10\ ms$ to track their references, and present an overshoot. In comparison with the average-model in figure 29, i_{vd} switching response is ten times slower and there is overshoot. Figure 34 also shows that i_{vq} deals with a slow transient, and takes $50\ ms$ to re-track the reference, substantially large than average-model.

It is important to highlight that PI controllers' gains were set the same for both the average-model and switching-model, aiming to have suitable performance in both models and fair comparison between them. However, the gains' adjust may improve the speed of convergence of the response on the switching-model.

Figure 34 – Detail of step on active power, from figure 33.

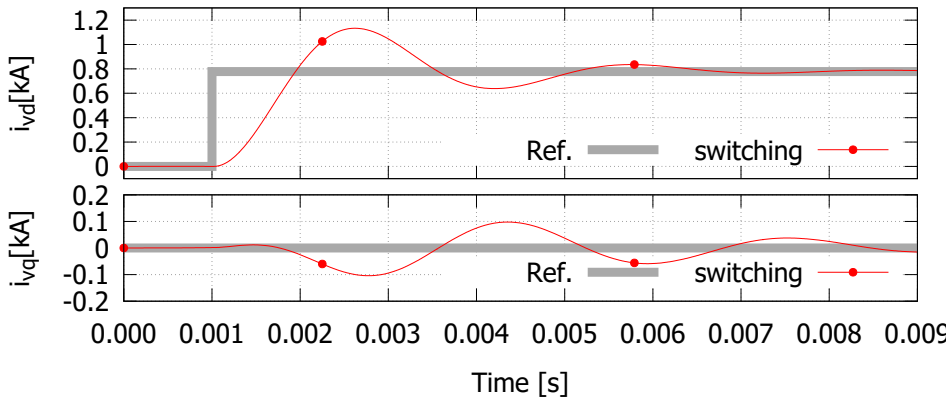

Source: Author

Figure 35 presents the detail of the reactive step from figure 33. States i_{vd} and i_{vq} are displayed. For the reactive step, i_{vd} faces a transient and takes longer than $50\ ms$ to re-track the reference. Quadrature-component, directly linked with reactive power, needs around $10\ ms$ to follow its reference. As mentioned before, it presents a slower dynamic in comparison with the average-model.

It is clear that PI can drive well the states of the MMC average-model to track their references. In figure 36, i_{cir0} is shown in detail and it is possible to see that state following its reference without delays. In addition, small oscillation can be seen in the reference and, as a consequence, in the state i_{cir0}.

Figure 37 presents state W_v, where a fluctuation around the reference is noticed. Once again, switching-model presents a slower dynamic in comparison with average-model.

Figure 35 – Detail of step on reactive power, from figure 33.

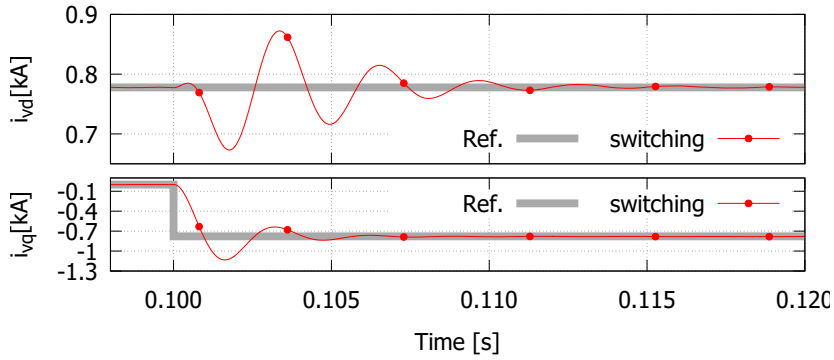

Source: Author

Figure 36 – Detail of state i_{cir0} while a step on active power, from figure 33.

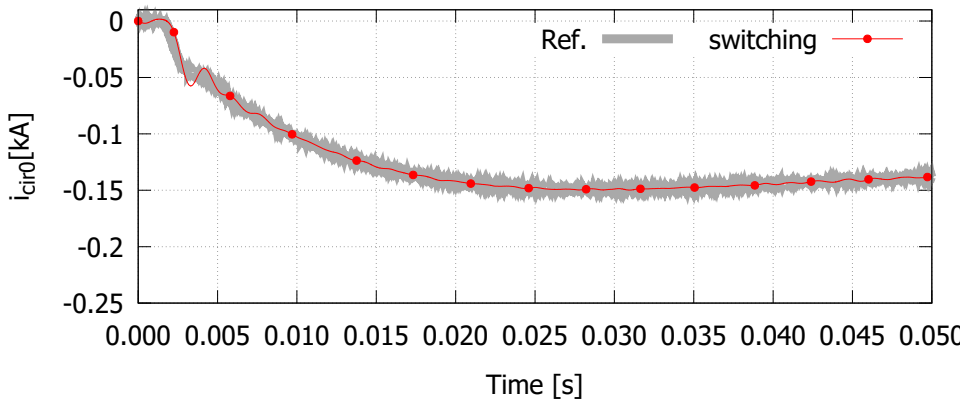

Source: Author

Figure 37 – Detail of state W_v.

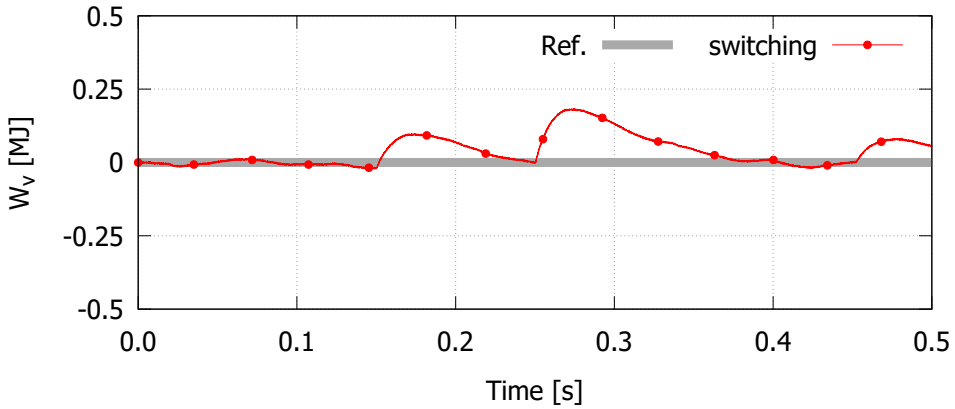

Source: Author

Figure 38 – Switching-model and average-model comparison.

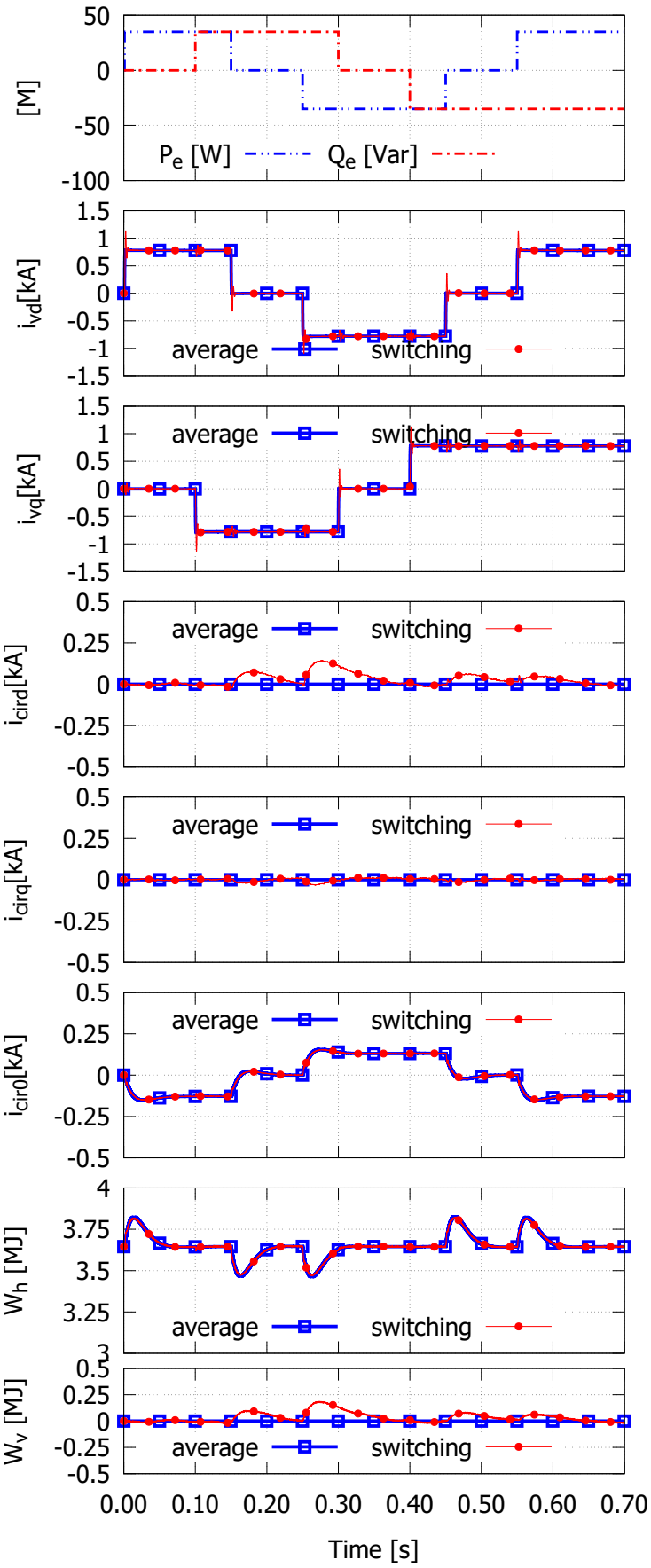

Four-quadrants operation of average-model and switching-model for comparison

Figure 38 shows the states' response from average-model (figure 29) and switching-model (figure 33) without their references (Ref.).

At figure 29 and 33 PI control states, are at their desired values, however present distinct references for each models, on states i_{cird} and i_{cir0}. This is a result of the additional dynamics from SMs switching, in which affect equations on (96) and (97) directly linked to above mentioned states.

At i_{cird} and i_{cir0} (4^{th} and 6^{th} graphic) it is possible to see the difference between responses for average and switching models.

Total energy W_h in the switching model presents larger overshoot compared with average model.

At energy balancing W_v at 8^{th} graphic, unbalance caused by oscillations at $t = 0.20\ s$ can be seen on the switching model. However, this can't be seen at the average model.

Figure 39 – Energy change at MMC average-model with PI controller.

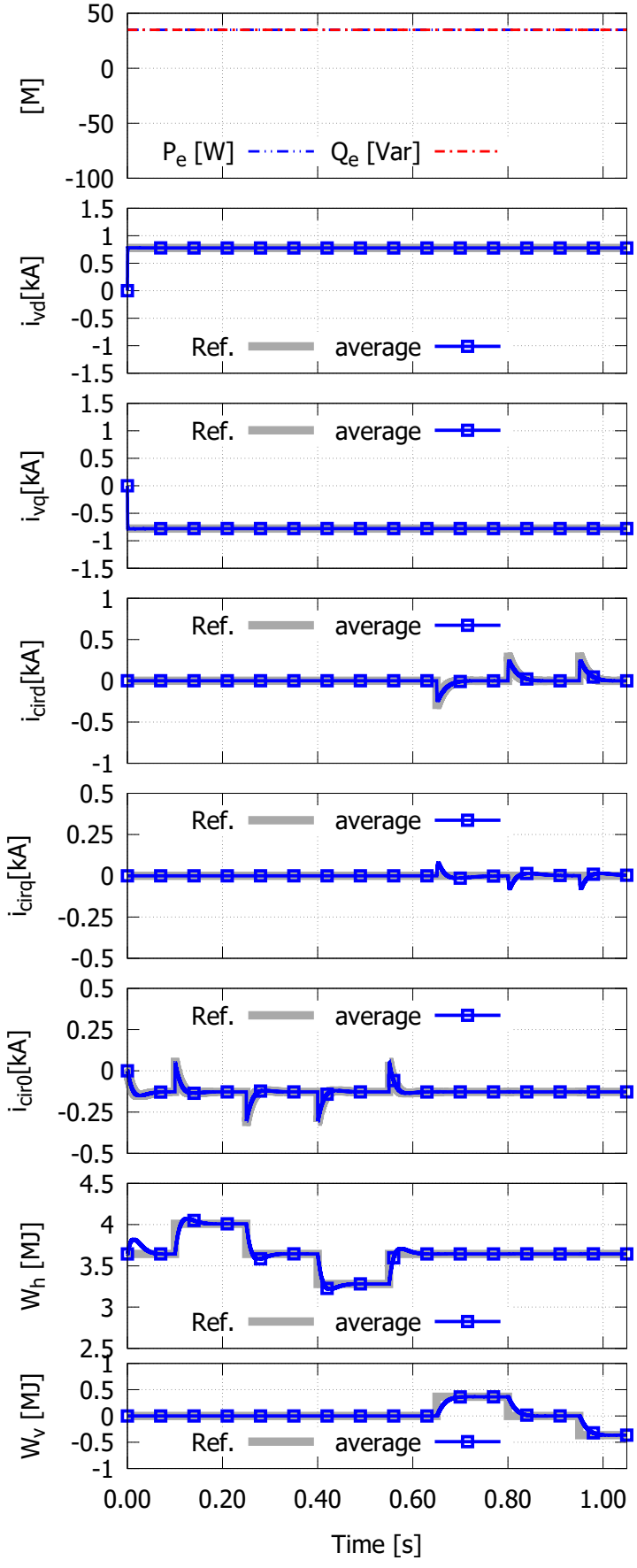

Change on converter energy W_h and W_v average-model medium-voltage

Figure 39, figure 42 and figure 43 also comprehend the eight graphics containing power and states' response. However, in these tests the PI control response for energy steps were analyzed. Power is set to 70 % of nominal power at $t = 0.01\ s$, and step changes in total energy are applied at $t = [0.1\ 0.2\ 0.25\ 0.35\ s]$, while balancing energy is changed at $t = [0.4\ 0.50\ 0.55\ s]$.

In figure 39 the performance of the average-model MMC with PI controller is evaluated for a change in converter energy. The operation point is changed at $t = 0.01\ s$, where $P_e = 35\ MW$ and $Q_e = 35\ MVar$. The designed PI control tested here allows the decoupling between DC voltage produced by the converter and the voltage imposed by the DC bus. As a result, it is possible to set the reference to converter energy without compromising system operation.

In this way, an increase in total energy is defined at $t = 0.10\ s$ at W_h (7^{th} graphic). To attain energy's desired reference, i_{cir0} increases momentarily around the reference at $t = [0.10\ 0.35\ s]$ and decreases to accomplish energy discharge at $t = [0.20\ 0.25\ s]$, as a result of control designed in (96).

An change is imposed for W_v (8^{th} graphic) at $t = 0.65\ s$. State variables i_{cird} and i_{cirq} swing until the energy balancing (W_v) track the new reference.

It is important to highlight that the tests done at figure 39 are not a conventional converter operating point (as delivery active and reactive power) and consists on a additional achievement where set point of converter energy can be modified to achieve grid requirements, as ancillary services.

Figure 40 presents a zoom from figure 39. It is possible to see that the speed of convergence of W_h is around $200\ ms$, with a minor overshoot. Meanwhile $\bar{i}_{cir0}$ momentarily changes to attain the new energy demand.

In figure 41 it is shown the detail of W_v increase. In this case, $\bar{i}_{cird}$ temporally changes to drive W_v to $\bar{W}_v$. Also, i_{cirq} is affected and re-tracks the reference in $10\ ms$. This agrees with the assumption of states i_{cirdq} to be used to manage the energy distribution between legs.

Figure 40 – Detail from figure 39 of increase in energy W_h.

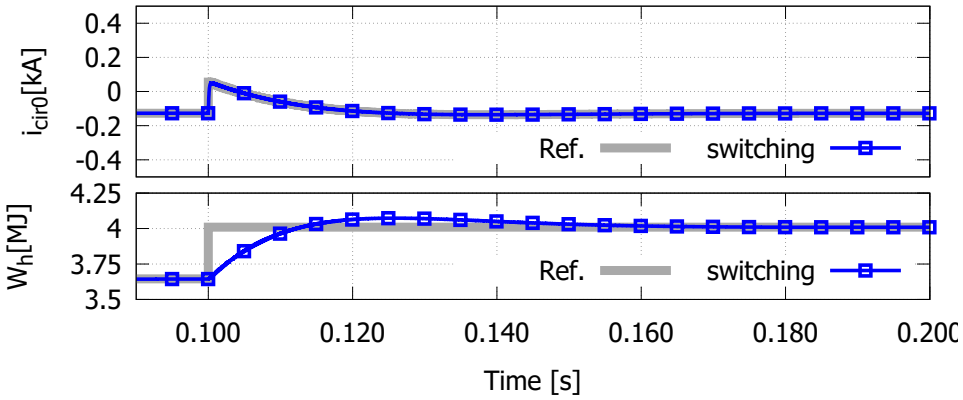

Source: Author

Figure 41 – Detail from figure 39 of increase in energy balancing W_v.

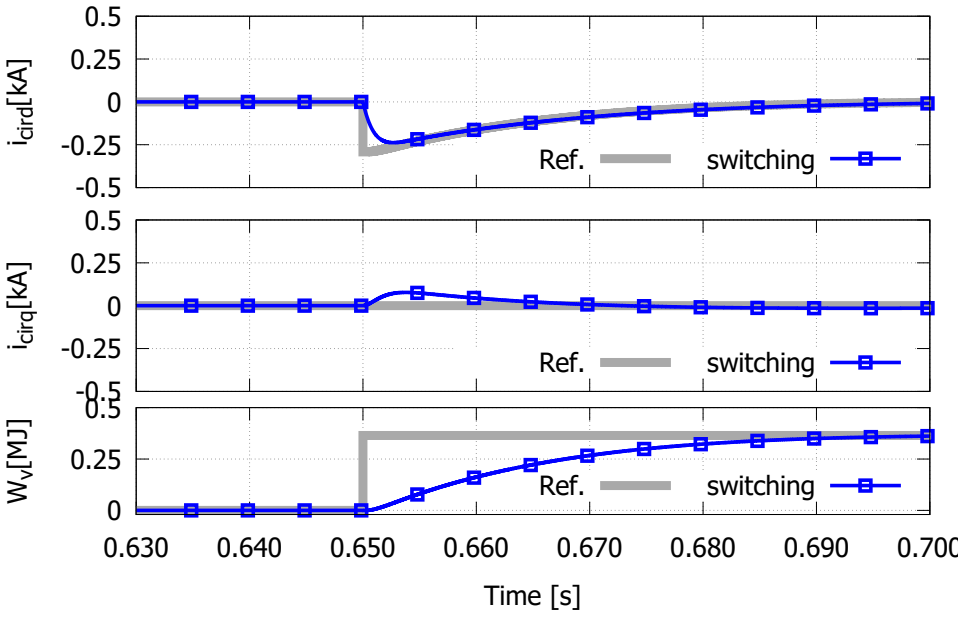

Source: Author

Figure 42 – Energy change at MMC switching-model with PI controller.

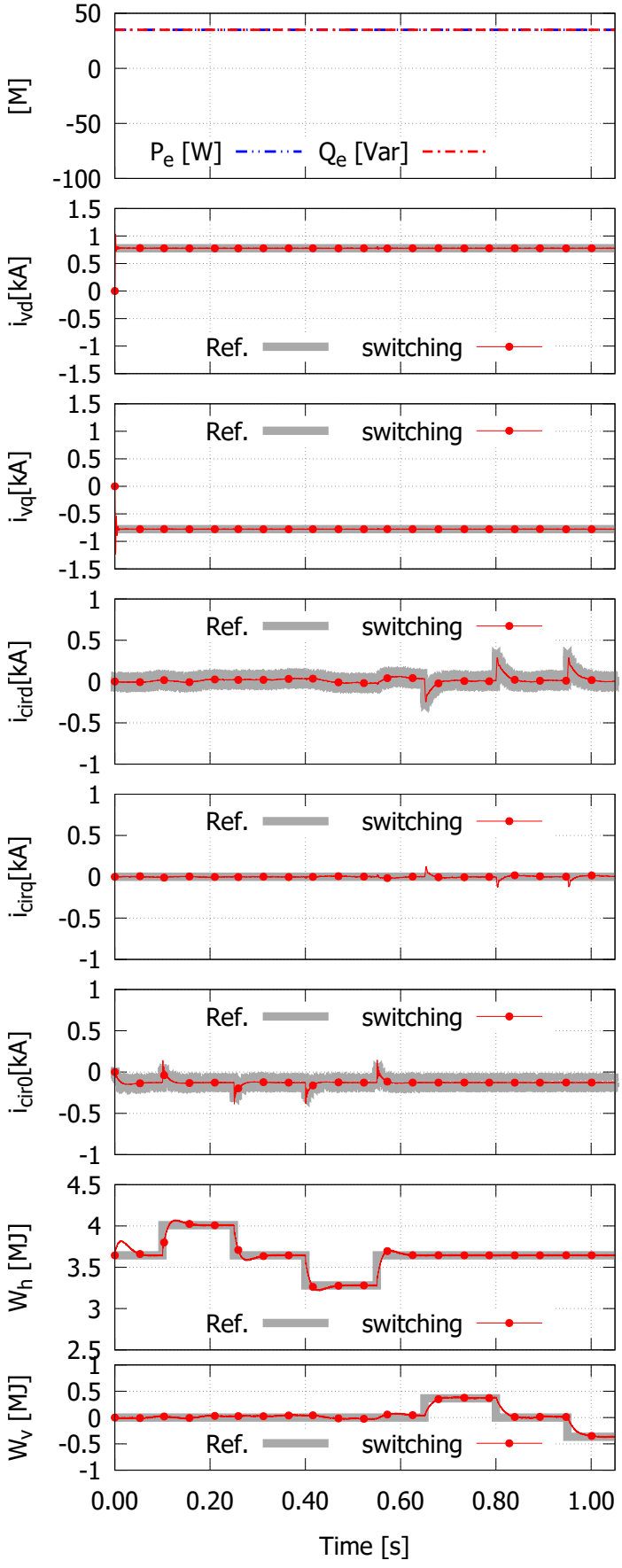

Change on converter energy W_h and W_v switching-model medium-voltage

In figure 42, the switching-model is simulated under changes on converter energy. The increase in total energy at $t = 0.10\ s$ at W_h (7^{th} graphic) is linked with the changes on i_{cir0}. The same behaviour can be seen at $t = [0.25\ 0.40\ 0.55\ s]$ where W_h decreases.

State i_{cird} on 4^{th} graphic has its reference changed to reach the desired value of W_v, as designed in equation (97). Also, i_{cirq} lightly swings around its reference at each change on W_v, indicating the share of responsibility to i_{cirdq} to promote energy balancing.

State i_{cir0} and state W_h are not affected by changes on energy balancing W_v.

The speed of convergence for all changes is close to the one presented by the average model.

The reference of i_{cir0} presents a small oscillation here. This may come from the switching devices effect.

Figure 43 – Average-model and switching-model comparison.

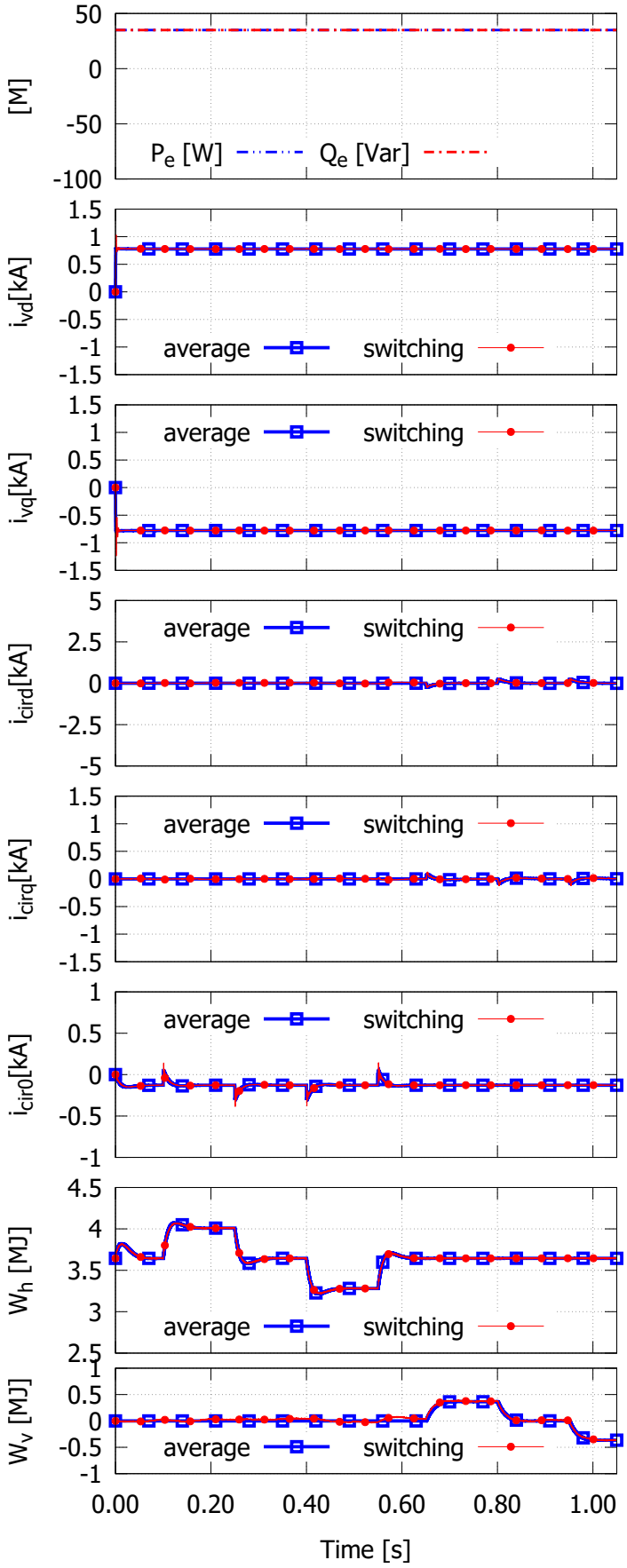

Energy changes for average-model and switching-model

Figure 43 merges responses from figures 39 and 42. In both previous results for energy change, states track their reference. As it is possible to see on the 6^{th} graphic of figure 43, there are distinct references for i_{cir0} at each model. Concerning the reaction of i_{cir0} for each energy change, states' response for each model, match in duration and range.

The difference noticed at i_{cir0} references comes from the divergence between real switching resistance and the equivalent value of SMs resistance at an arm (R), considered in the average model, also, the additional dynamic from switching SMs.

3.4.1 Control Effort

The chosen gains directly affect the control effort, which can be measured by the overshoots in transients on the control output. Figures 44 and 45 present average and switching model comparison, however they have similar performances, except in few moments where switching model presents a minor opposite overshoot which will be emphasized in the next comment. So, the following comments are suitable for both models.

In figure 44 and figure 45 are presented the control output signals (v_{ud}, v_{uq}, v_{ld}, v_{lq} and v_{d0}) for the two above presented tests. In figure 44, changes in active and reactive power produce a transient on control inputs which are not larger than three times of the desired value of v_{ud} and v_{uq}. Meanwhile, v_{ld} and v_{lq} present overshoots around thirteen times of the desired values. In the other hand, v_{d0} did not presented pronounced transients.

In figure 45, the changes in total energy ($t = [0.10\ 0.25\ 0.40\ 0.55]s$) have a major effect on v_{d0} because it drives the DC power output. For balancing energy changes at $t = [0.65\ 0.80\ 0.95]s$ the control inputs v_{ud}, v_{uq}, v_{ld} and v_{lq} overshoots are not larger than twice their respective desired values.

Figure 44 – Control inputs of average and switching model for the operating points presented in figure 38.

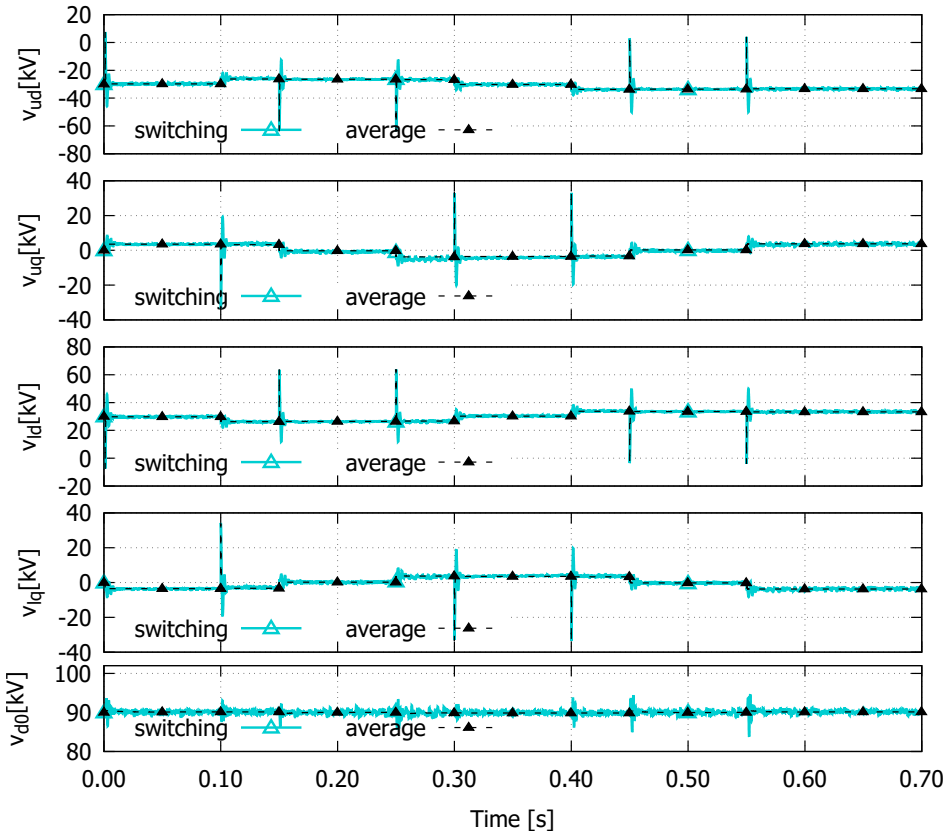

Source: Author

The results presented before aim to compare the performance of the average-model and switching-model. Furthermore, the switching-model will be further analyzed because of the

Figure 45 – Control inputs of average and switching model for the operating points presented in figure 43.

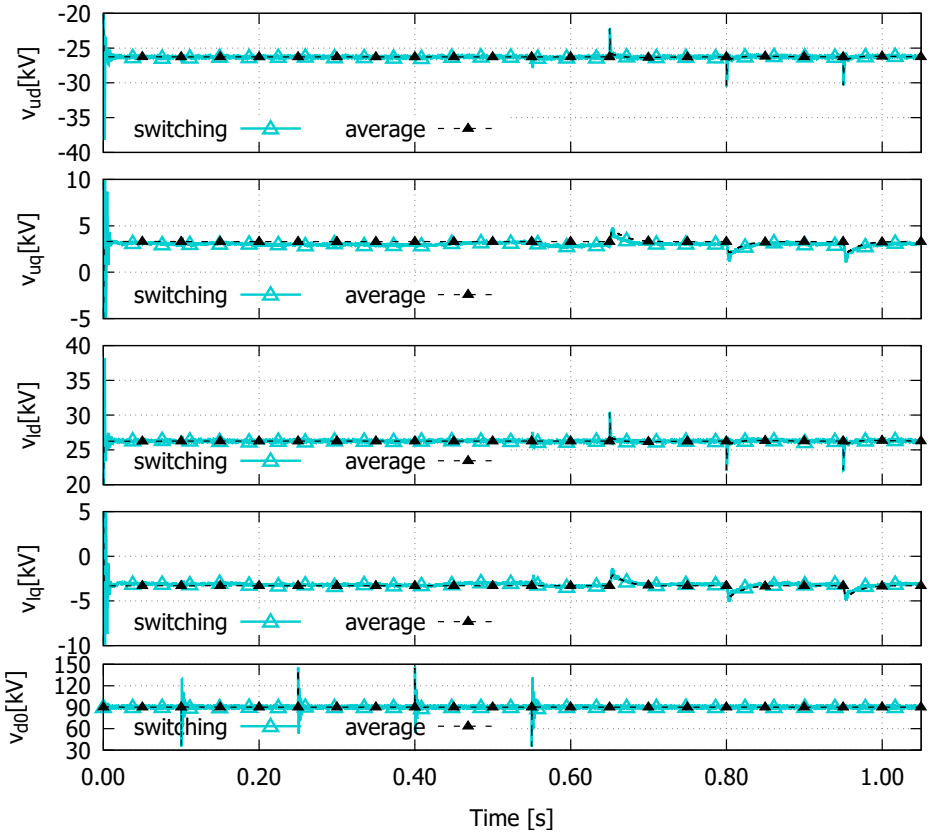

Source: Author

additional dynamics that come from SMs switching.

Figure 47 shows the voltage at each SM and figure 46 shows $dq0$ component of circulating currents for the operating point of P_e and Q_e equal to 70% of nominal power.

At the switching-model simulated here, it is not designed a controller to stabilize the double-fundamental frequency component of circulating currents. However it is possible to see in figure 46 that components dq are controlled around references, zero. They are amplified at each operating point change, however become smaller in steady state. Meanwhile component zero has small oscillation and follows the fundamental component.

Because of the sorting algorithm implemented, it is possible to notice a suitable balancing between each SM voltage. At the right part of the figure is presented a zoom in time from $0.32\ s$ to $0.38\ s$. By this, it is clear that the voltage range in one SM changes for each period and even when they are bypassed, keeping a constant value of voltage.

Figure 46 – Double-fundamental frequency component of circulating currents at medium-voltage switching model with PI controller.

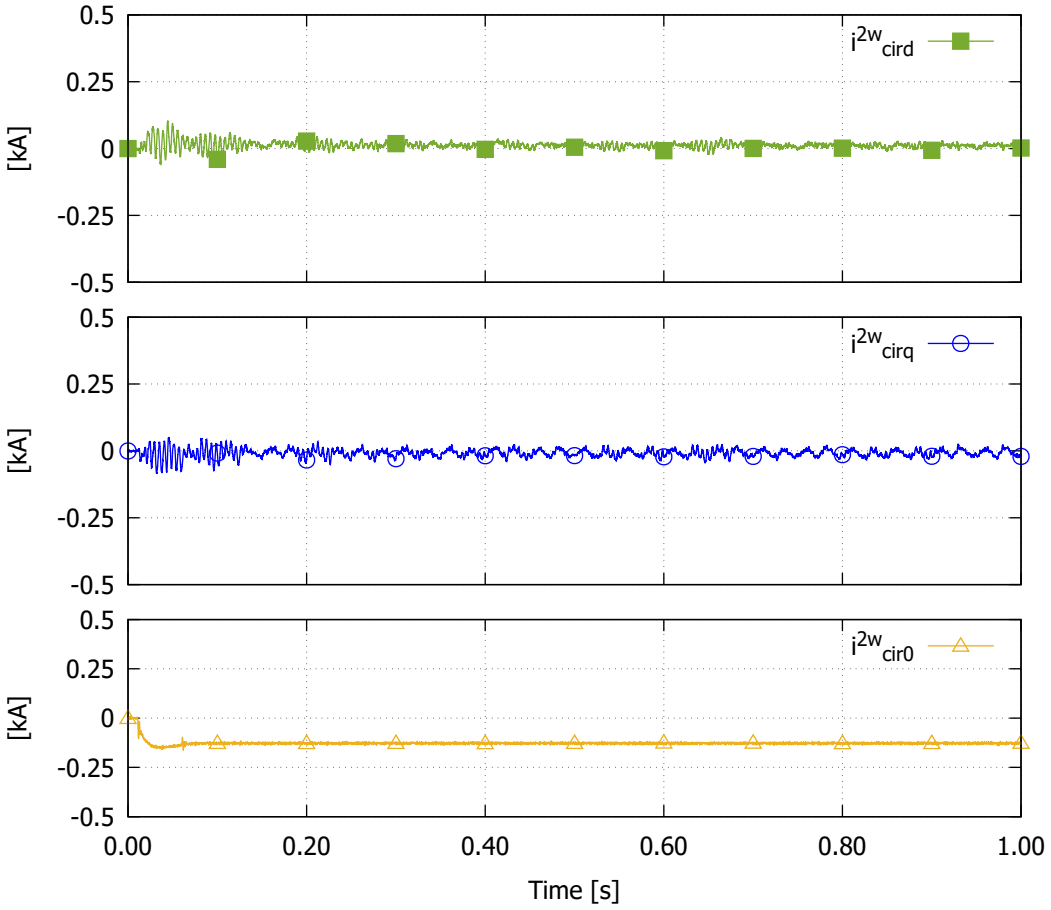

Source: Author

Figure 47 – Voltage of each SM per arm of medium-voltage system with PI controller.

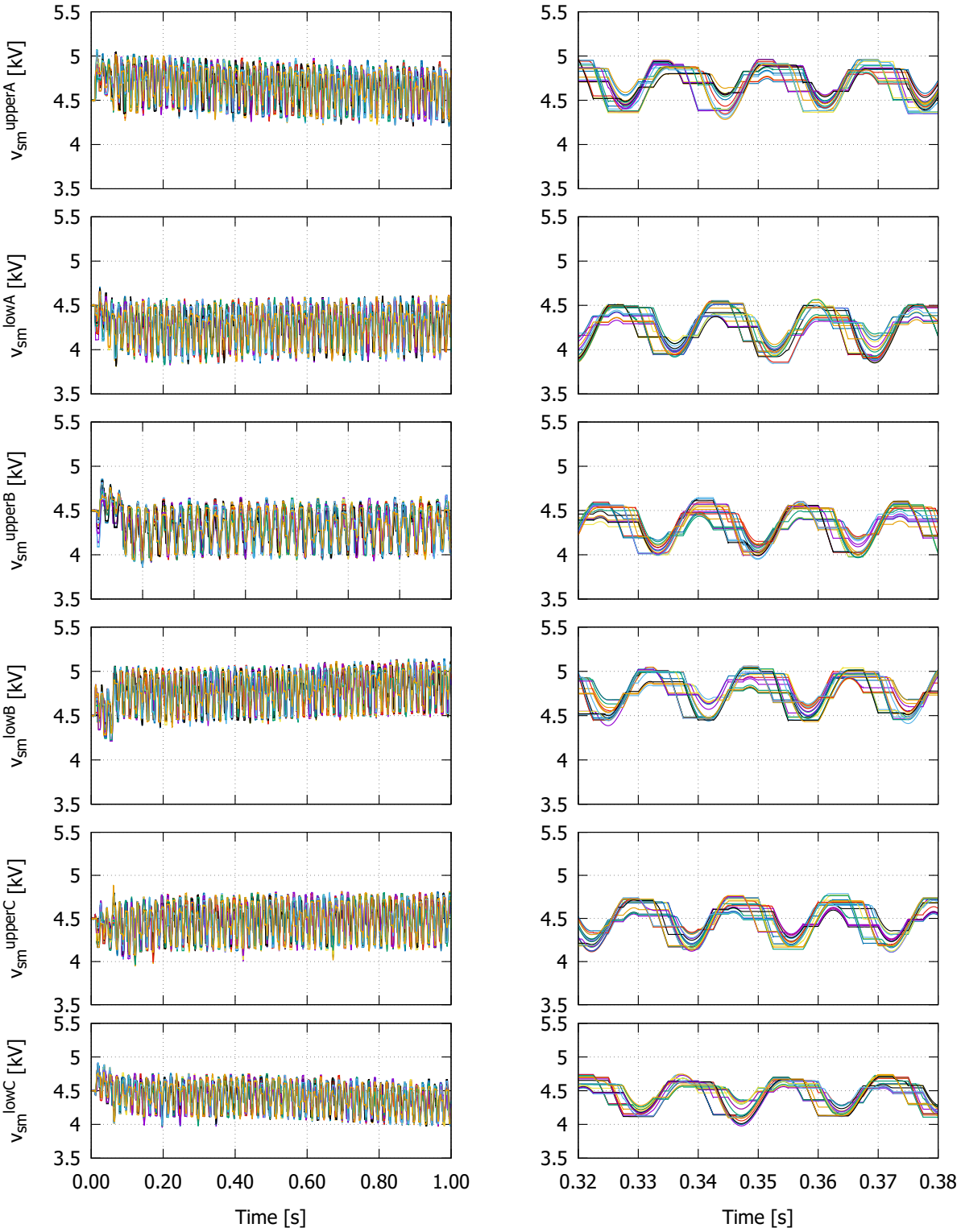

Source: Author

3.4.2 Robustness over parameters' uncertainties and voltage fluctuation on medium-voltage system with PI controller

Robustness

The robustness test considers the control's sensitivity over parameter uncertainties. This section shows different scenarios with parameter uncertainties considered.

It is essential to highlight that the manufacture of power electronics provides devices from low to high tolerance errors, directly affecting costs. Practical lower tolerances are 10%, and can be increased to a tolerance of less than 0.1%. The literature points to SMs capacitance tolerance error as the key to a proper MMC design, as mentioned by [89].

In this section's test, the simulations go beyond practical tolerance error, aiming to overstress the control performance. For each one, the parameters R, R_c, L, L_c and C_{SM} change (one at a time) in $\pm 10\%$ and $\pm 20\%$ from their nominal values. Meanwhile, the control remains the same, i.e., as designed using nominal values. At $t = 0.005\ s$ a change in active power is performed, while at $t = 0.01\ s$ a change in reactive power.

Figure 48 shows the state variables with $\pm 10\%$ and $\pm 20\%$ of arm resistance (R). This test PI controller drives all state variables to the desired value even with the arm resistance error. Additionally, for changes in R_c figure 49 shows that PI performs the state reference. However, i_{cird} and W_v present a small deviation in the test where R_C is equal to -20% of nominal value.

In figure 50 there is a response for changes in arm inductance L. Once again, there are light overshoot for state i_{cird} and W_v, but they can be neglected. The other state variables are well controlled by PI. Meanwhile, changes of $+20\% L_c$ result in a response of i_{cird} and W_v, which differ from the other scenarios.

For SM, capacitor uncertainties presented in figure 52 state variables face distinct response in transients. However, it tracks the reference in stead-state. Most of the transient comes from the initial value of W_h, which is linked with SM capacitance value; there is a high speed of convergence to the desired value. Also, $\pm 20\%\ C$ affect the speed of W_v, and consequently i_{cird}.

Voltage fluctuation

The voltage fluctuation is also analyzed in this section. This test consider (1) a over (under) AC voltage from nominal value at the PCC; (2) a over (under) from nominal DC voltage. The $\pm 10\%$ and $\pm 5\%$ from nominal value are considered.

- ❏ Fluctuation in AC voltage result over-signal in state variables i_{vd} and i_{vq}. The other state variables are not affected by the voltage change (see figure 53);
- ❏ Fluctuation in DC voltage has a similar effect of change in SM capacitors. This is a result of the desired value for W_h in equation (69) where V_{DC} play a crucial role.

Figure 48 – The system state over variation of parameter R of medium-voltage system with PI controller.

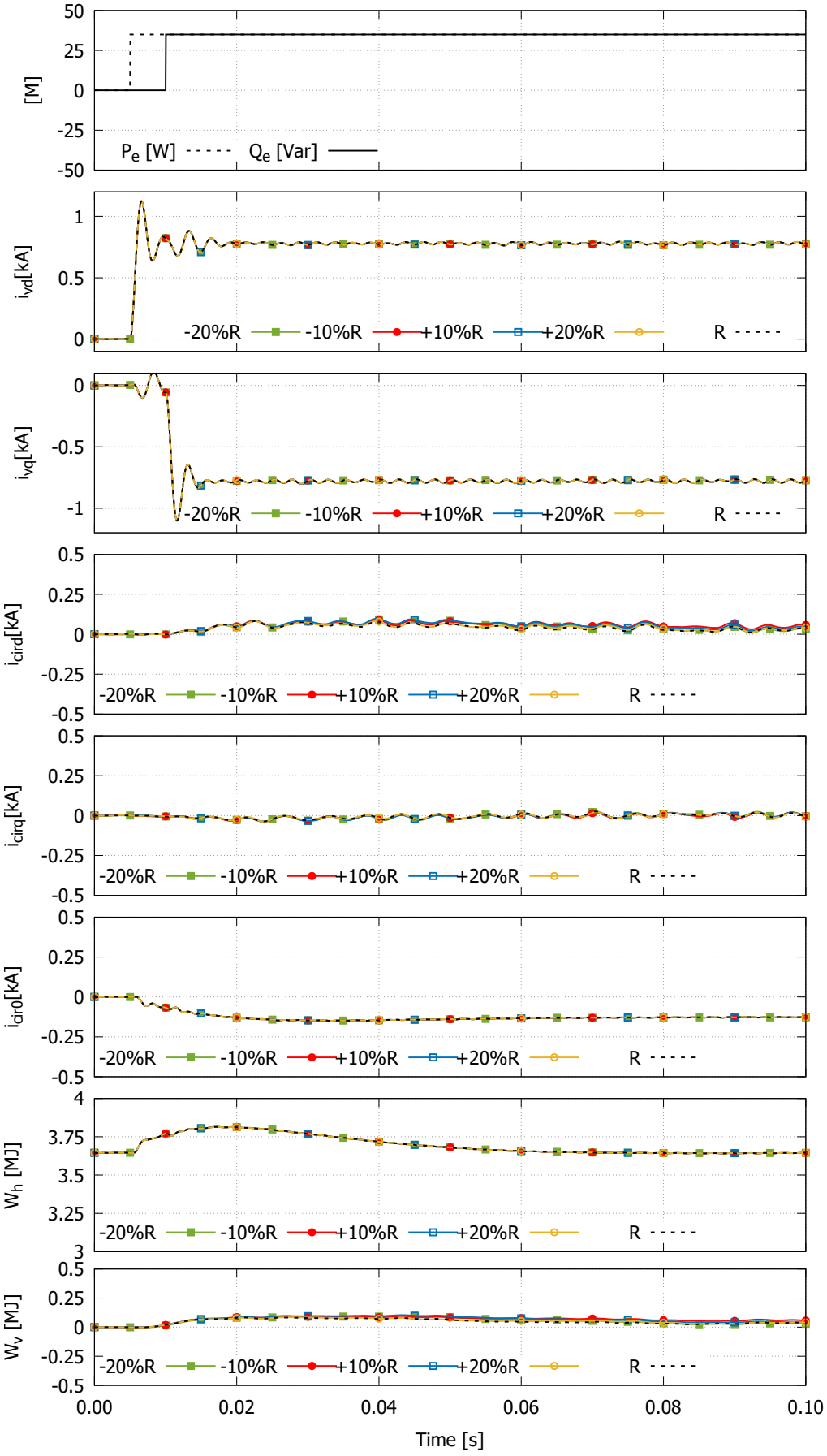

Source: Author

Figure 49 – The system state over variation of parameter R_c of medium-voltage system with PI controller.

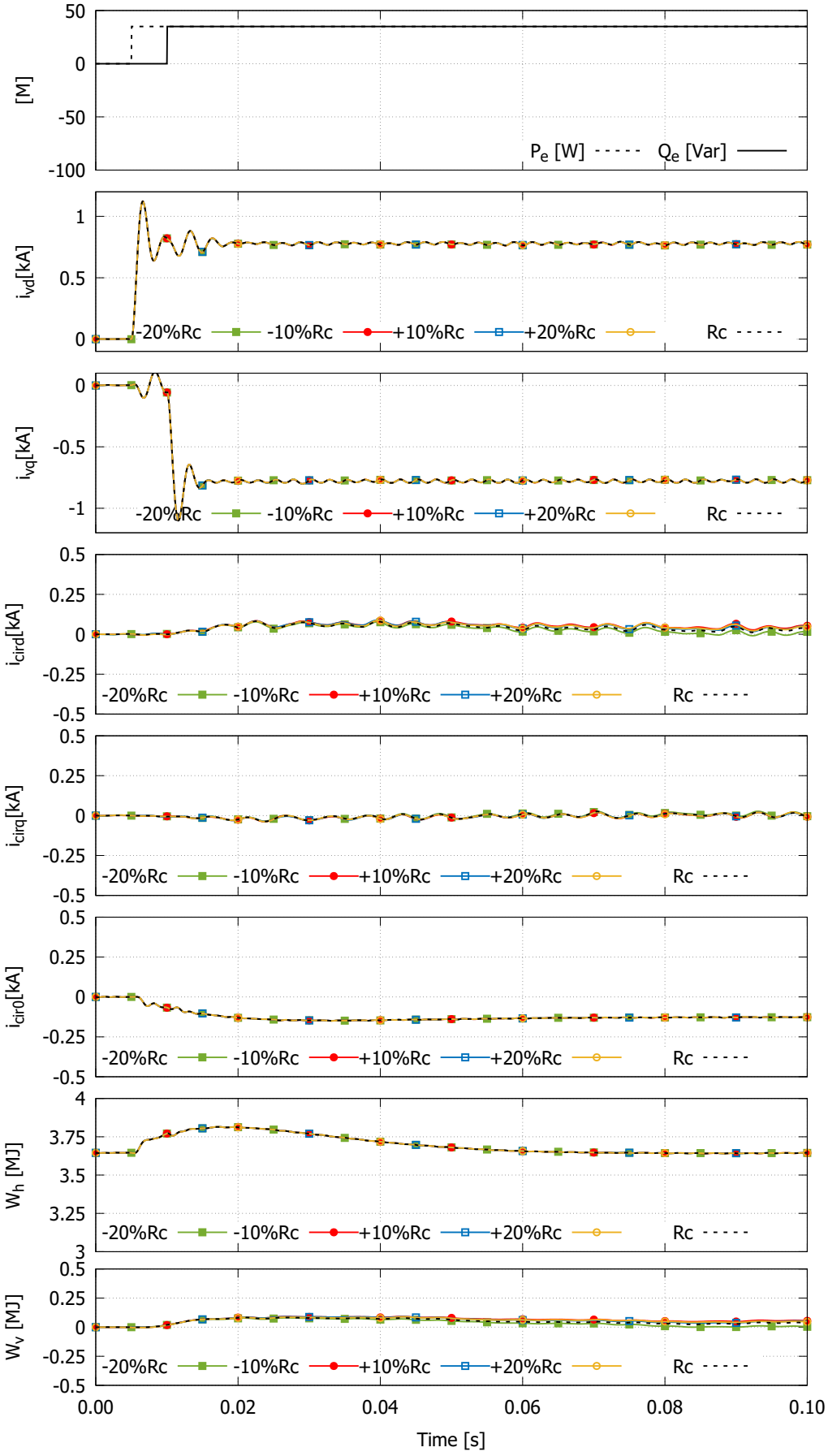

Source: Author

Figure 50 – The system state over variation of parameter L of medium-voltage system with PI controller.

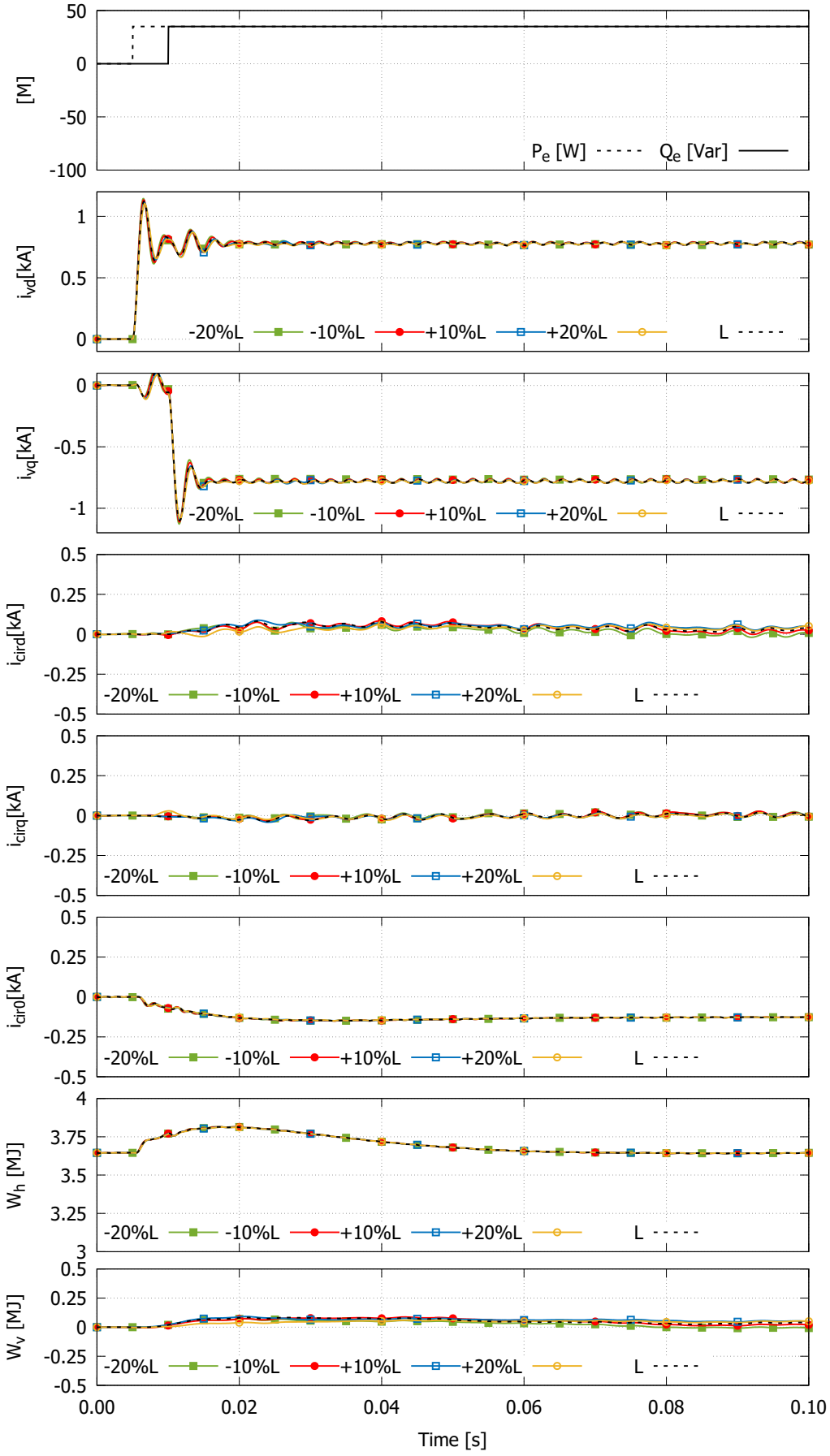

Source: Author

Figure 51 – The system state over variation of parameter L_c of medium-voltage system with PI controller.

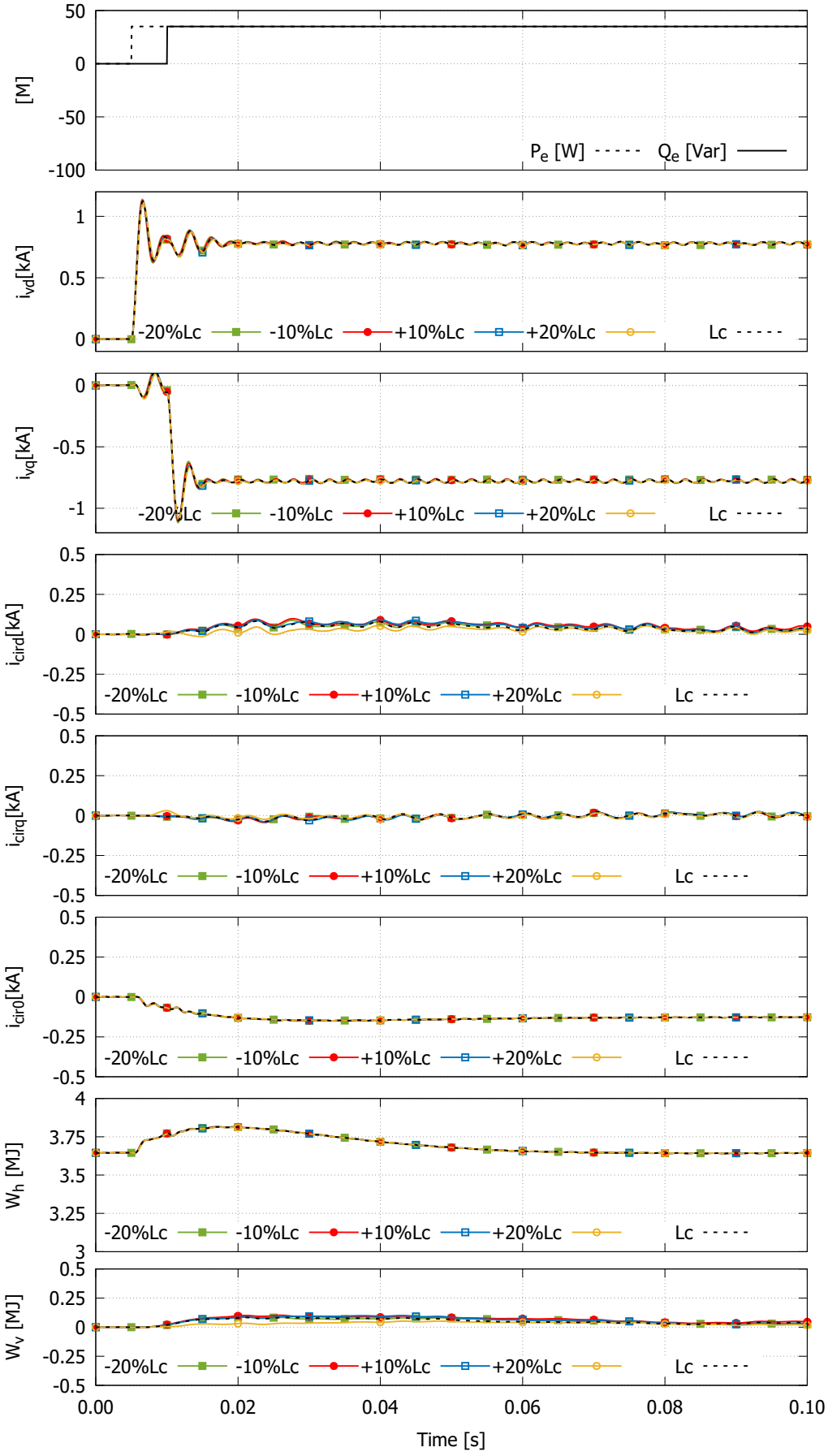

Source: Author

Figure 52 – The system state over variation of parameter C of medium-voltage system with PI controller.

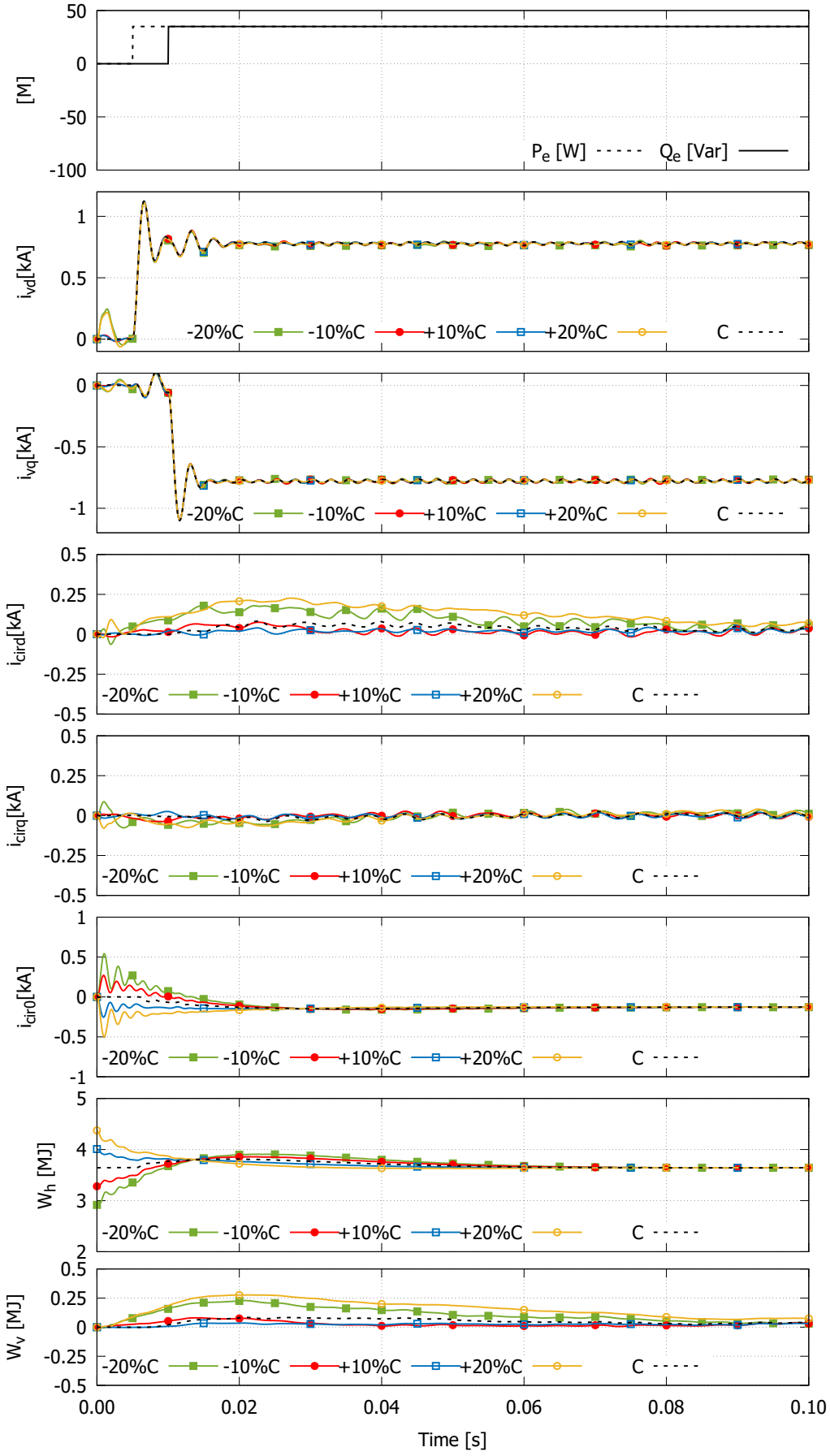

Source: Author

Figure 53 – The system state over variation in the voltage at the PCC of medium-voltage system with PI controller.

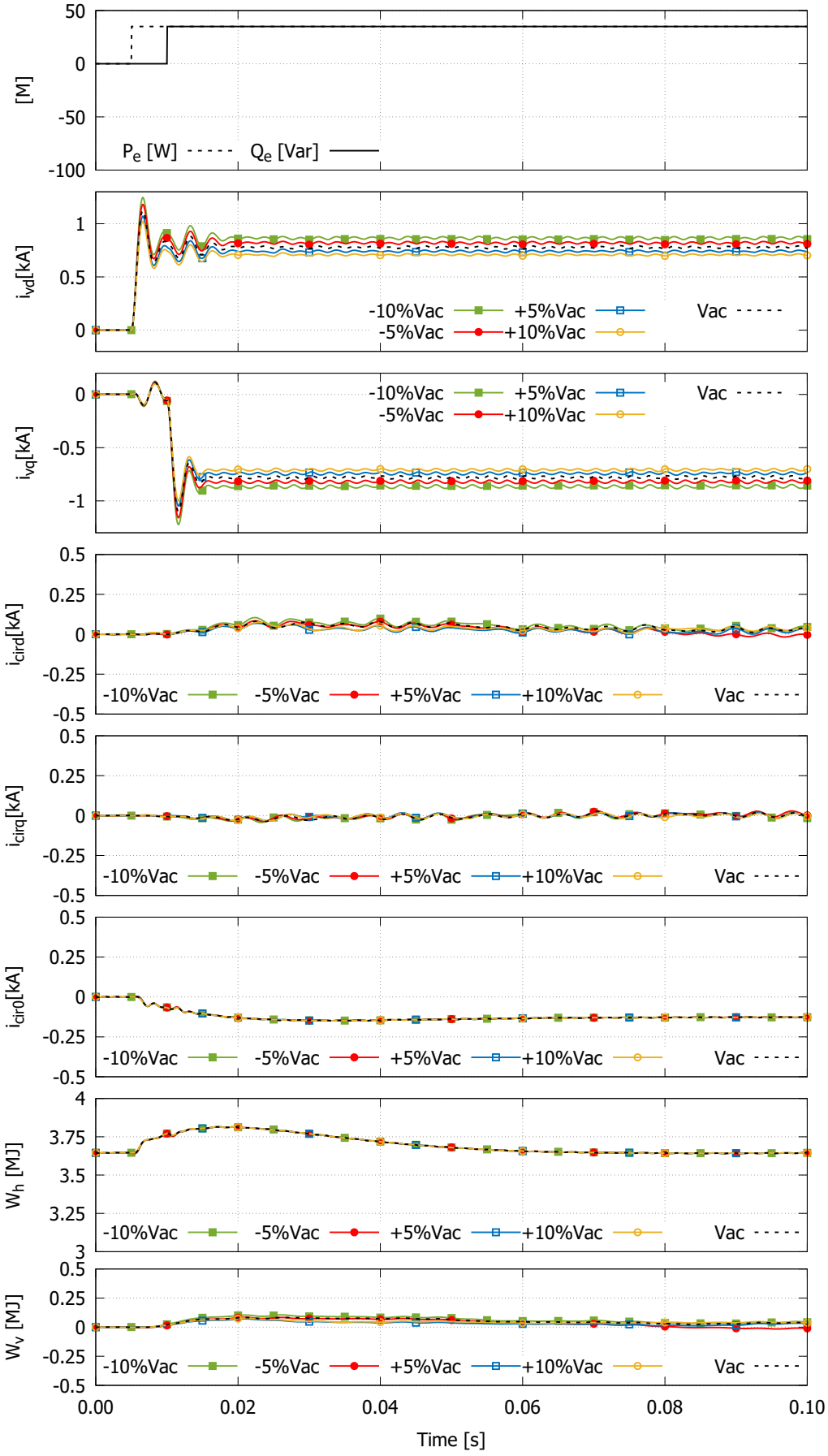

Source: Author

Figure 54 – The system state over variation in DC voltage of medium-voltage system with PI controller.

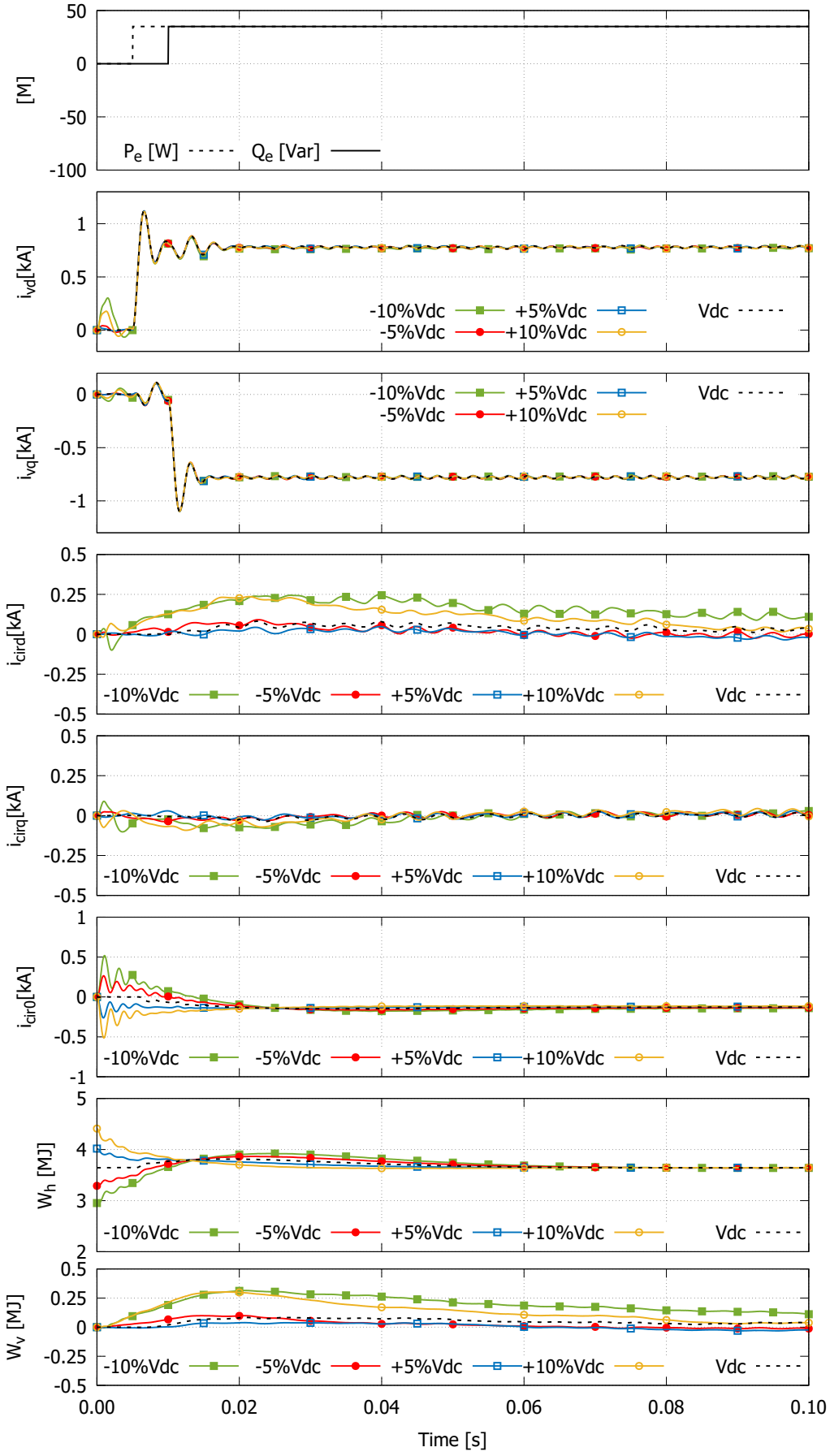

Source: Author

3.5 High-voltage system test with PI controller

A high-voltage system is also analysed, aiming to verify controllers' characteristics concerning these systems. In figure 55 a $450\ MVA$ HVDC connection is shown. The main AC grid is connected to symmetric monopole DC line/cable, by an AC-DC MMC converter.

Figure 55 – System diagram of $400\ kV$ system.

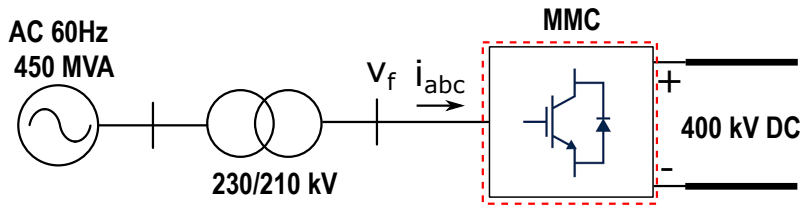

Source: Author

A detailed switching model of the three-phase MMC converter with twenty SMs per arm, with the PI controller proposed in this chapter, is tested using the Matlab Simscape Electrical environment. The system test is originally proposed in [87]. The pulse generator used is a phase-shift PWM with a sorting algorithm, and system's parameters are presented in Table 3.

For the tuning process, the gains for state variables i_{vdq} and i_{cirdq} are obtained such as to have the same time constant of medium-voltage system. $k_p^{W_h}$ becomes smaller because the response with (-0.5) has a high overshoot, and $k_i^{W_v}$ becomes larger once the previous gain (0.1) presents steady state error for state W_v.

Table 3 – Parameters of simulated high-voltage system and PI controller gains.

Parameter	Value	Parameter	Value
S_{MMC}	$450\ MVA$	$k_p^{i_{vdq}}$	120
V_{DC}	$400\ kV$	$k_i^{i_{vdq}}$	37453
V_{AC}	$210\ kV$	$k_p^{i_{cirdq}}$	80
C_{SM}	$3\ mF$	$k_i^{i_{cirdq}}$	1000
L	$40\ mH$	$k_p^{i_{cir0}}$	300
L_c	$12\ mH$	$k_i^{i_{cir0}}$	1000
R_c	$1\ \Omega$	$k_p^{W_h}$	-0.3
R	$0.5\ \Omega$	$k_i^{W_h}$	-25
N	20	$k_p^{W_v}$	0.8
Freq	$60\ Hz$	$k_i^{W_v}$	20

Figure 56 presents the four-quadrants operation for the high-voltage system with PI controller. A set of steps in active and reactive power is reproduced in the 1^{st} graphic. Previous section uses $70\ \%$ of active and reactive power for this test. Here this operation condition will be maintained, which for this system implies the limits of $P_e = \pm 315\ MW$ and $Q_e = \pm 315\ MVar$. It means, the voltage is ten times bigger than medium-voltage system.

This test presents larger overshoot and oscillation when compared with the medium-voltage system. Furthermore, the author would like to highlight that the process of tuning was harder than for the medium-voltage system, and it was not possible to define a set of gains in which all operating points performed well. As a result, for the five first operating point (until $0.40\ s$), all states variables present a smooth response. On the other hand, when the power flow has changed its direction (for the following three operating points), state variables present large oscillations.

The performance variation concerning operating points for PI controllers is as expected. An important feature to be addressed is the fact that the PI may need to re-adjust the control gains and parameters to keep following a new grid reference and to correctly perform stability, while controllers based on nonlinear theory gains can work in a broader region and consequently need less tuning.

Figure 56 – Four-quadrants operation of high-voltage system with proposed PI controller.

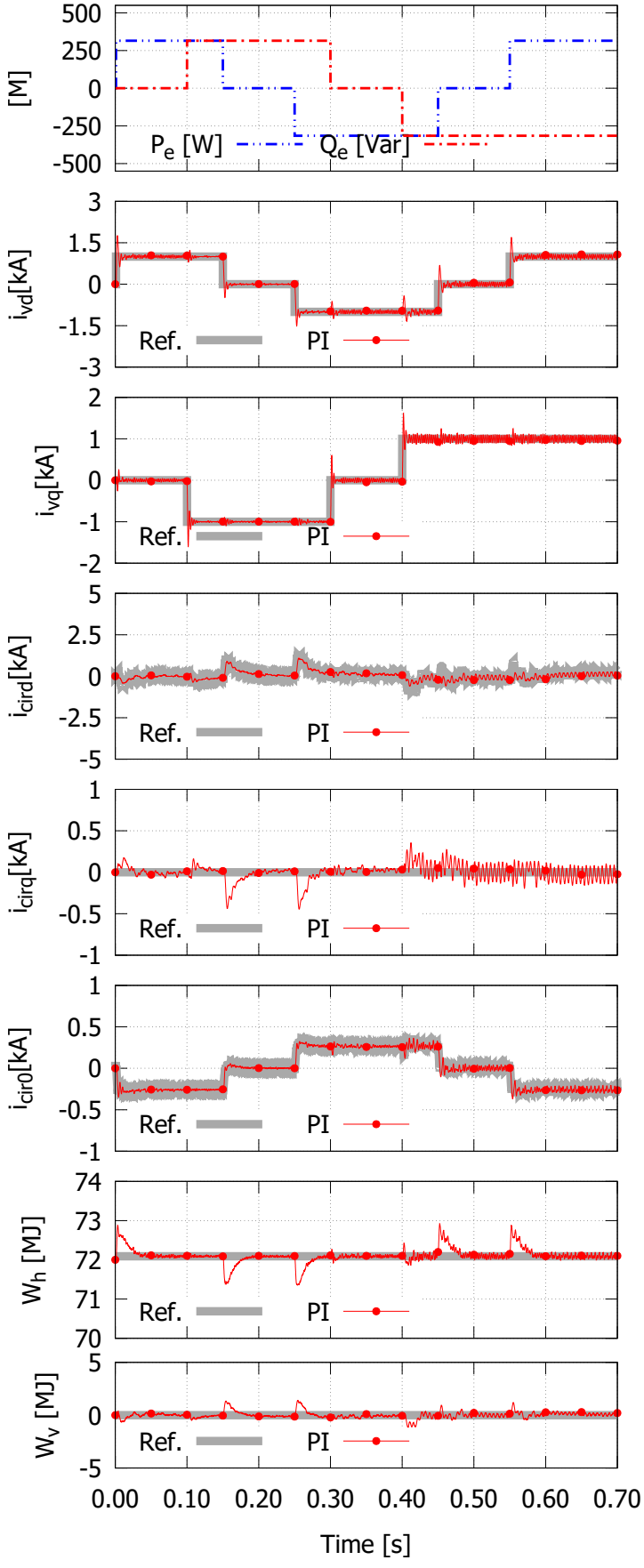

Four-quadrants operation of high-voltage system with PI controller

State variables i_{vdq} (2^{nd} and 3^{rd} graphics) track all the new references in less than $10\ ms$ and present a small overshoot. State variable i_{cird} follows well its reference.

At 4^{th} graphic the state variable i_{cirq} performs different operating points. As mentioned above, it is possible to see two different behaviours: first smooth, and then noisily response, what points out the need for a tuning improvement.

The i_{cir0} tracks well its reference, related with active power changes. Meanwhile, total energy and energy balance face transients for each P_e step.

Even though the controller deal with oscillation response for the operating point after $t = 0.40\ s$, PI can drives all state variables to their desired value (Ref.).

Figure 58 shows the control effort for this test. Steps in active and reactive power produce a proportional control effort. This will be further discussed in this section.

Figure 57 – Energy steps for high-voltage system with proposed PI controller.

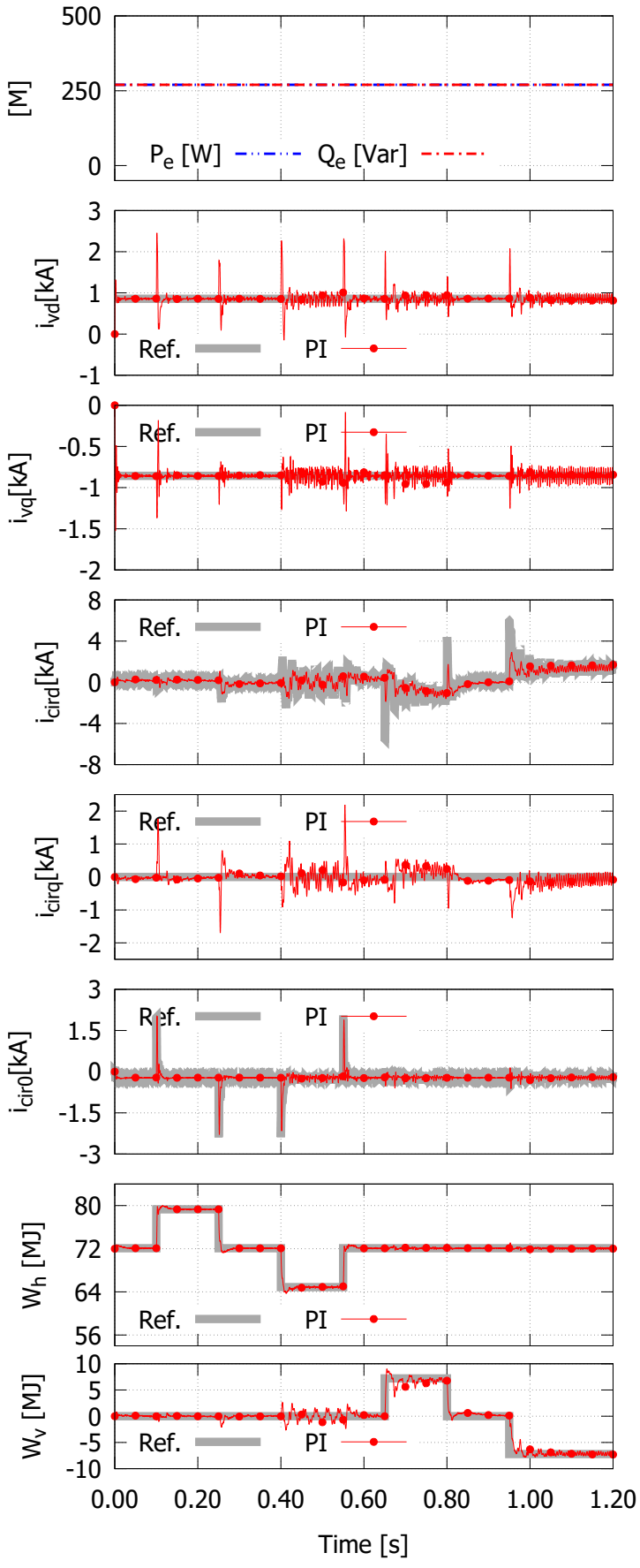

Energy changes of high-voltage system with PI controller.

In figure 57, steps in total energy of $\pm 10\%$ are defined at $0.10\ s$ and $0.40\ s$. During the total energy increase (from $0.10\ s$ to $0.25\ s$) most state variables present overshoots, however they also present a high speed of convergence to re-track their references. Otherwise for the total energy decrease, state variables have an oscillating response.

During the imbalances of W_v (overloading upper/lower arms), PI controller can drive states to their new reference value.

Figure 59 shows the control effort resulting from this test. Changes in the total energy and energy balancing are distributed among control inputs. Furthermore v_{d0} participates most on the changes of total energy than those of energy balancing. This is a direct result of the energy model in equation (32) and equation (33).

Additionally from figure 58, the effort linked with each change in active power is distributed among inputs, most for v_{ud} and v_{ld} (e.g. $0.15\ s$). Likewise, change on reactive power result in a more pronounced overshoot at v_{uq} and v_{lq} (e.g. $0.10\ s$). Also, v_{d0} react for each i_{cir0} change, which is linked with active power changes. These behaviors is result of the model, respectively described in equation (30) and equation (31).

Figure 58 – Control effort of four-quadrant operation of PI controller.

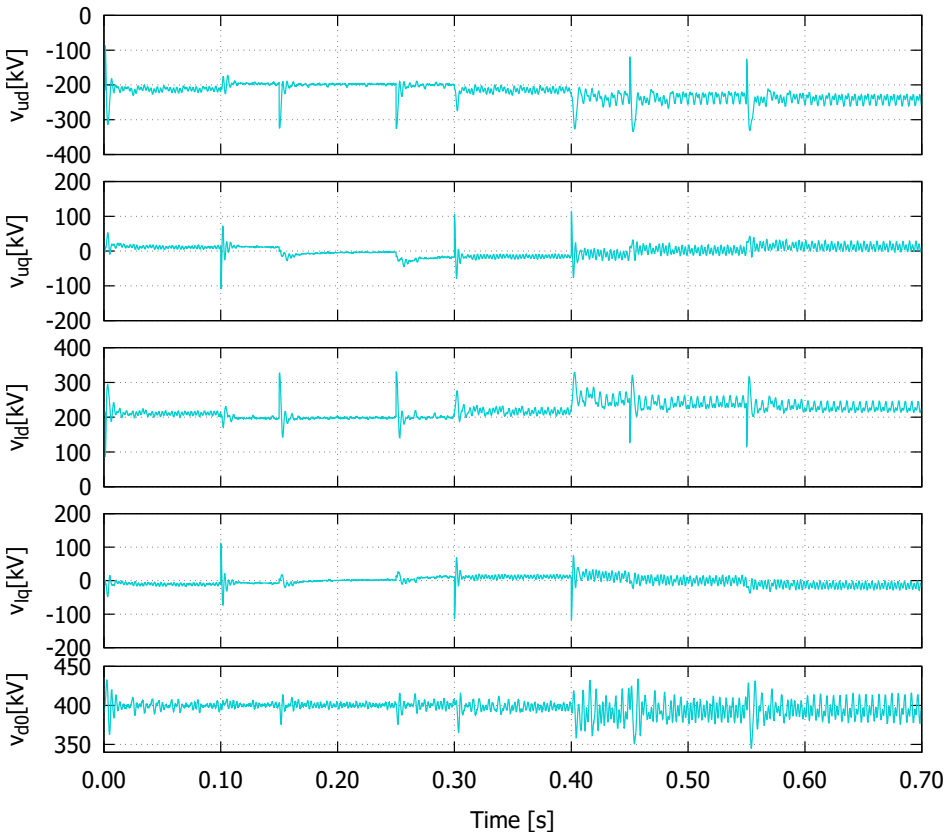

Source: Author

There are compromises to be considered while choosing an MMC model. Some of then are directly related to internal dynamics. The model used in this research considers the control of the energy summation at all upper arms to be equal to lower arms energy summation, which is called energy balancing W_v. However, an ideal balancing condition is to have the energy balanced individually per arm. So, figure 60 demonstrates how energy performed per arm. For this test, the operating point was set as $P_e = 315\ MW$ and $Q_e = 315\ MVar$ at $0.05\ s$. There it is possible to see the share of energy in the arms. After the transient caused by power injection, arms are well balanced in $450\ ms$. Furthermore total energy in upper (lower) arms are presented in figure 61. The summation of energy in upper (lower) arms (W_u and W_l) is controlled on the desired value and are balanced just after the transient caused by the power injection.

For the same operation point, double-fundamental frequency components of circulating currents are presented in figure 62. It is possible to verify that during the transient the three components present large oscillations, however, they become small and close to zero for components dq (i^{2w}_{cirdq}) and around reference of the fundamental for zero component (i^{2w}_{cir0}).

Figure 59 – Control effort of changes in energy of PI controller.

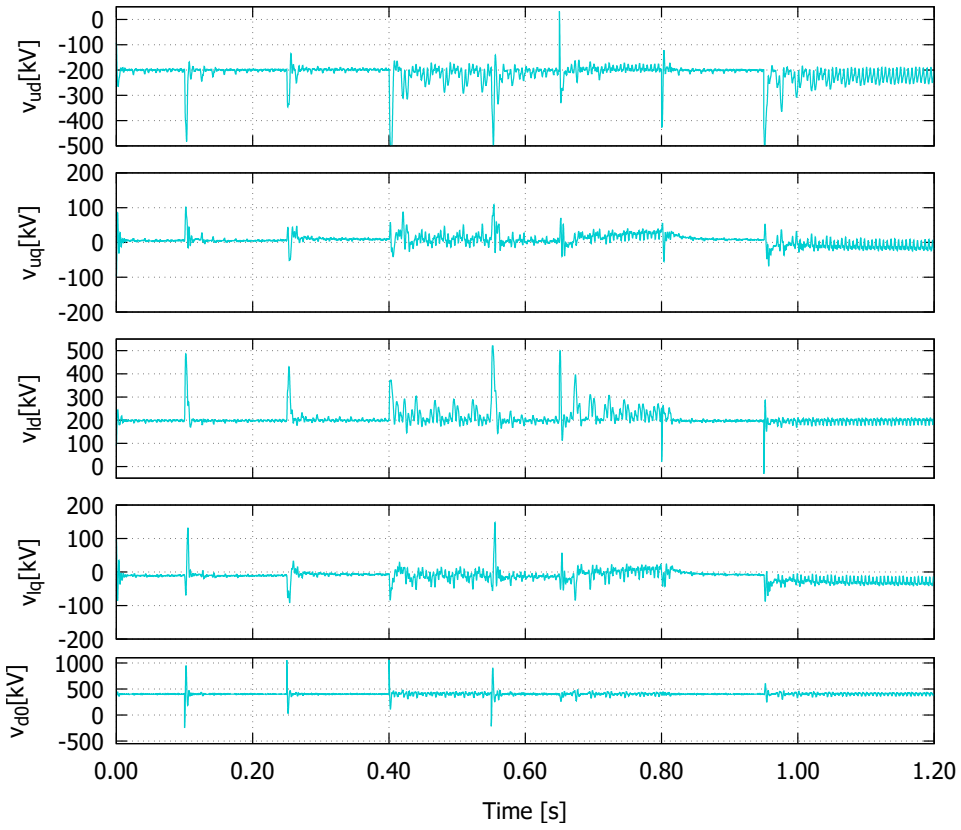

Source: Author

Figure 60 – Share of energy among arms with PI controller.

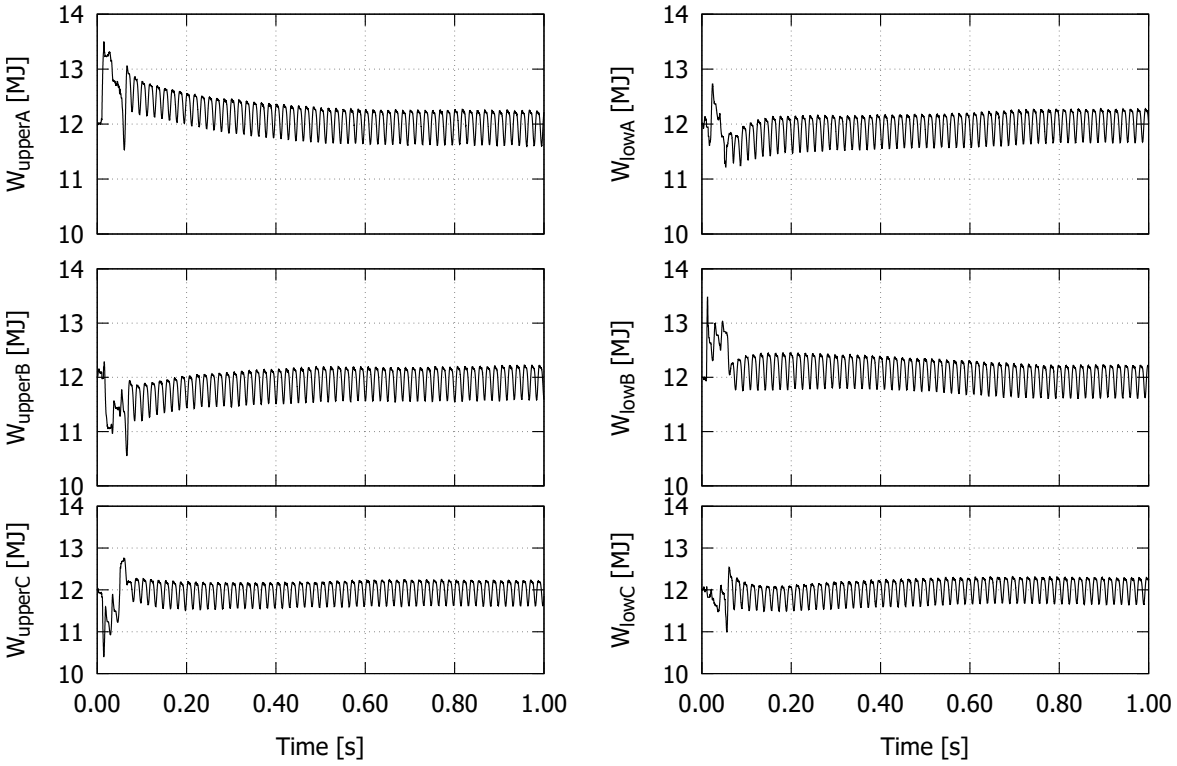

Source: Author

Figure 61 – Total energy in the three upper arms (W_u) and the three lower arms (W_l) with PI controller.

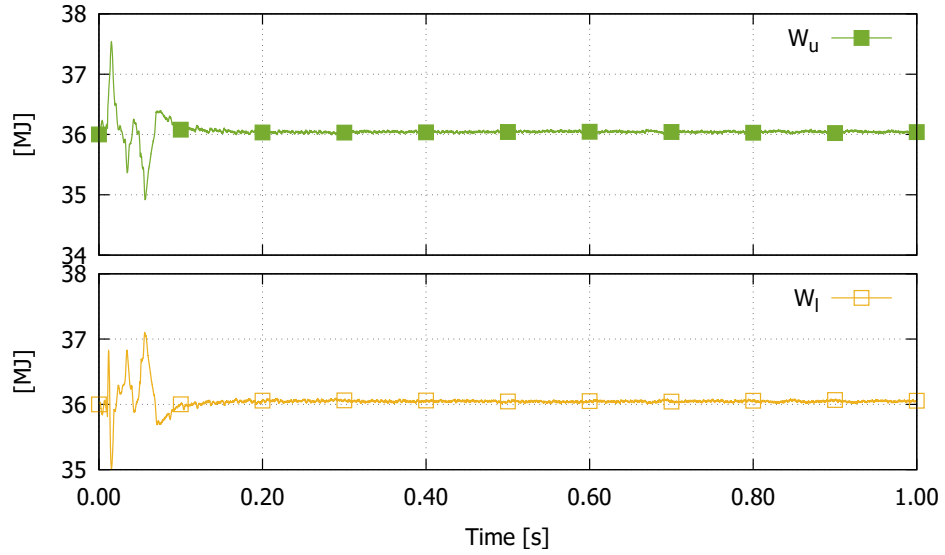

Source: Author

Figure 62 – Double-fundamental frequency component of circulating currents at high-voltage switching model with PI controller.

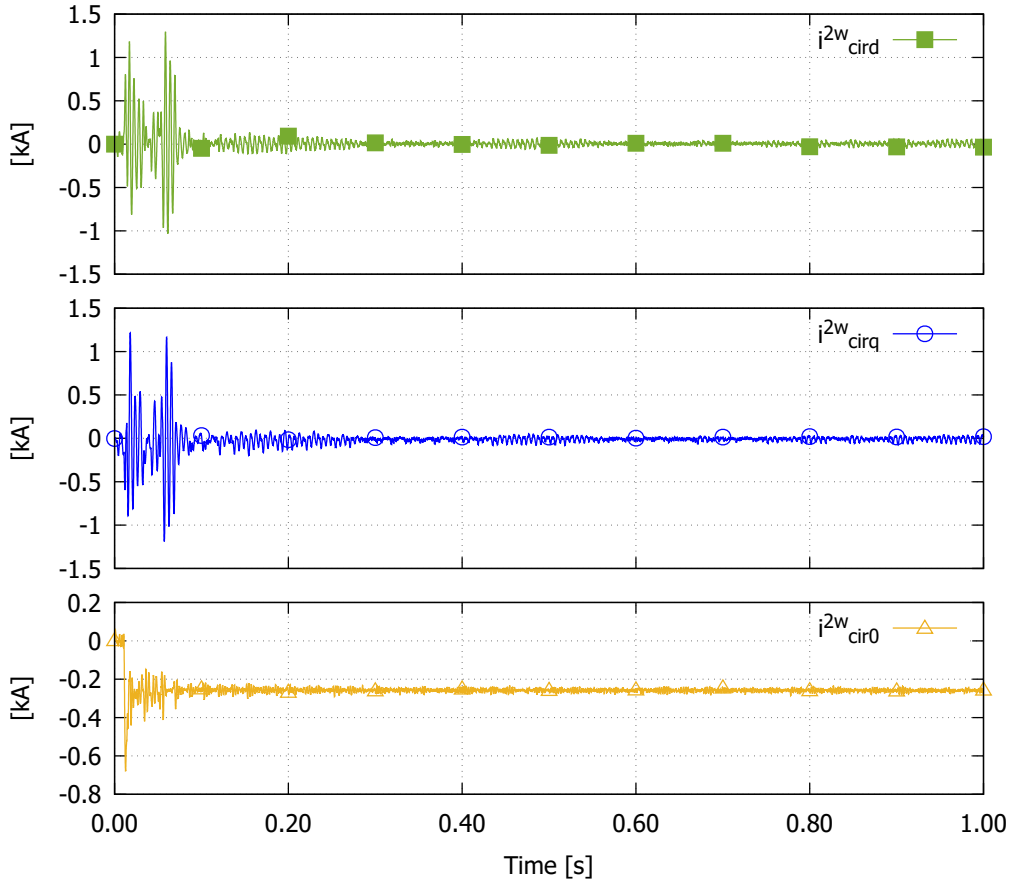

Source: Author

At last, figure 63 shows SMs capacitors voltages per arm, in the left graphics and a detail at right graphics (zoom on time from right graphics). It is verified that voltages are well balanced

by the implemented sorting algorithm.

Figure 63 – SMs capacitor voltage per arm and equivalent detail from PI controller.

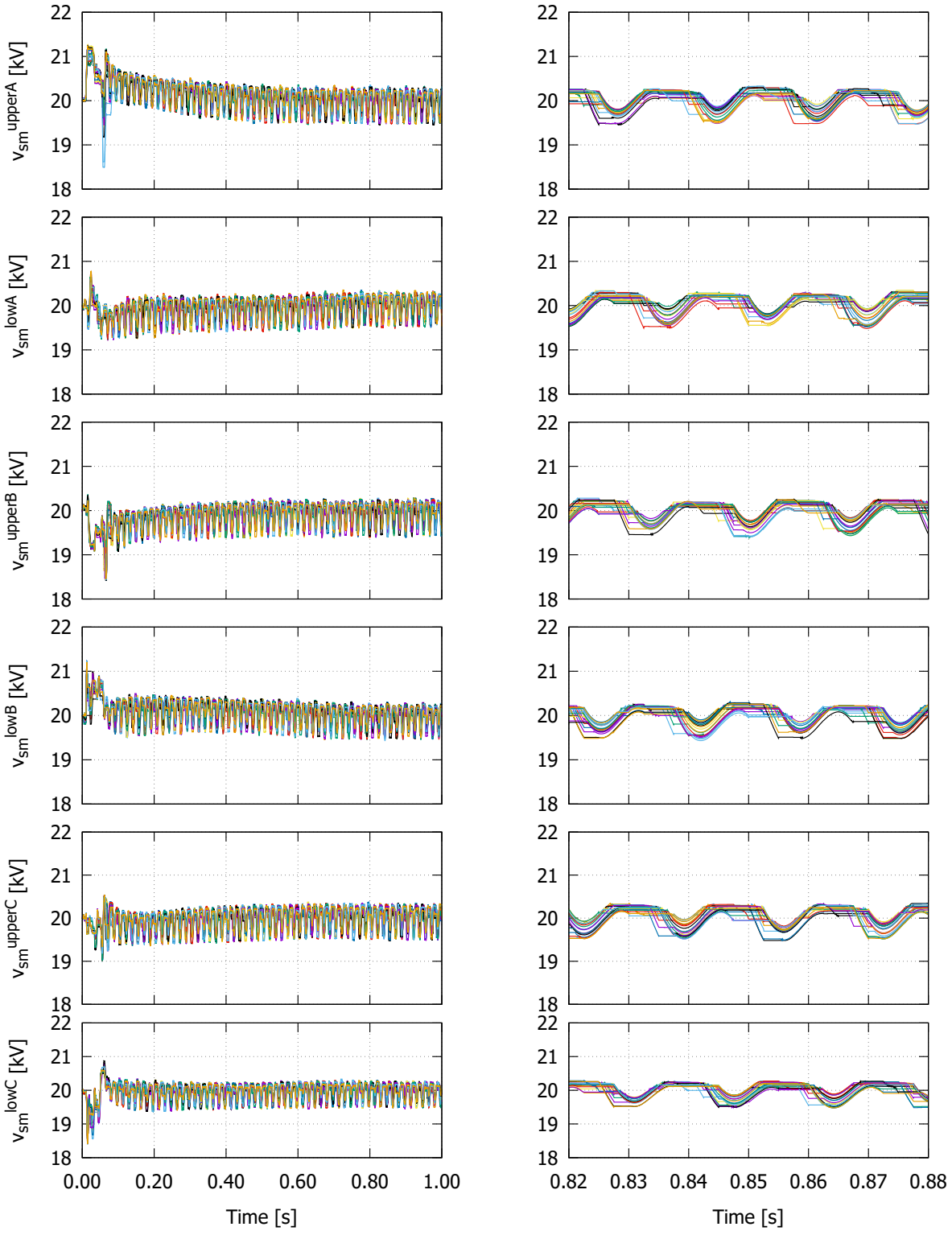

Source: Author

3.5.1 Robustness over parameters' uncertainties and voltage fluctuation on high-voltage system with PI controller

Robustness

The test presented in section 3.4.2 is performed here, considering the high-voltage system.

The R, L, R_c and L_c parameters' uncertainties are kept as $\pm 10\%$ and $\pm 20\%$ from the nominal values, however changes in SM capacitors is reduced to $\pm 10\%$ and $\pm 5\%$. The reduction is proposed here, once state variables' response becomes oscillatory during the transient, prejudicing the analyses.

Variations of $\pm 10\%$ and $\pm 20\%$ in arm resistance (R) is proposed and state variables response presented in figure 64. This test shows that the PI controller can drive all state variables to the desired value, even with the arm resistance error.

In figure 65, there are state variables over variation in R_c. As in the medium-voltage system, PI drive state to their reference. However, in this test, variables i_{cird} present a small deviation, but it can be neglected.

Figure 66 there is a response for changes in arm inductance L. As the medium-voltage, there are light deviations for state i_{cird} and W_v. They can be neglected once they are too small. PI well controls the other state variables.

Changes in L_c are well performed by the PI controller. This case differs from medium-voltage, where i_{cird} and W_v present deviation from the desired value in transients.

Finally, for the changes in SMs capacitor, the state variables response has a larger overshoot in comparison with medium-voltage, as shown in figure 68. The states are most affected by the increase of $+10\%C$, when, even in stead-state, they present oscillatory response for most state variables.

Voltage fluctuation

Voltage fluctuations are performed at the PCC. It is tested $\pm 10\% V_{ac}$ and $\pm 5\% V_{ac}$, and figure 69 shows the result. State variables i_{vd} and i_{vq} present over-signal and oscillatory response for the increase in V_{ac}. On the other hand, the decrease in V_{ac} result in a response just with over-signal.

State variables i_{cirdq0} has a oscillatory response during transient however track the reference in stead-state. At last, W_v is light affected.

State variables response over changes in V_{dc} are presented in figure 70. System states deal with over-shoot during transients, and PI drive states to their references in stead-state. However for the increase of $+10\% V_{dc}$, state variables i_{cirdq0} and W_v has a large oscillatory response which may affect MMC operation.

Figure 64 – The system state over variation of parameter R of high-voltage system with PI controller.

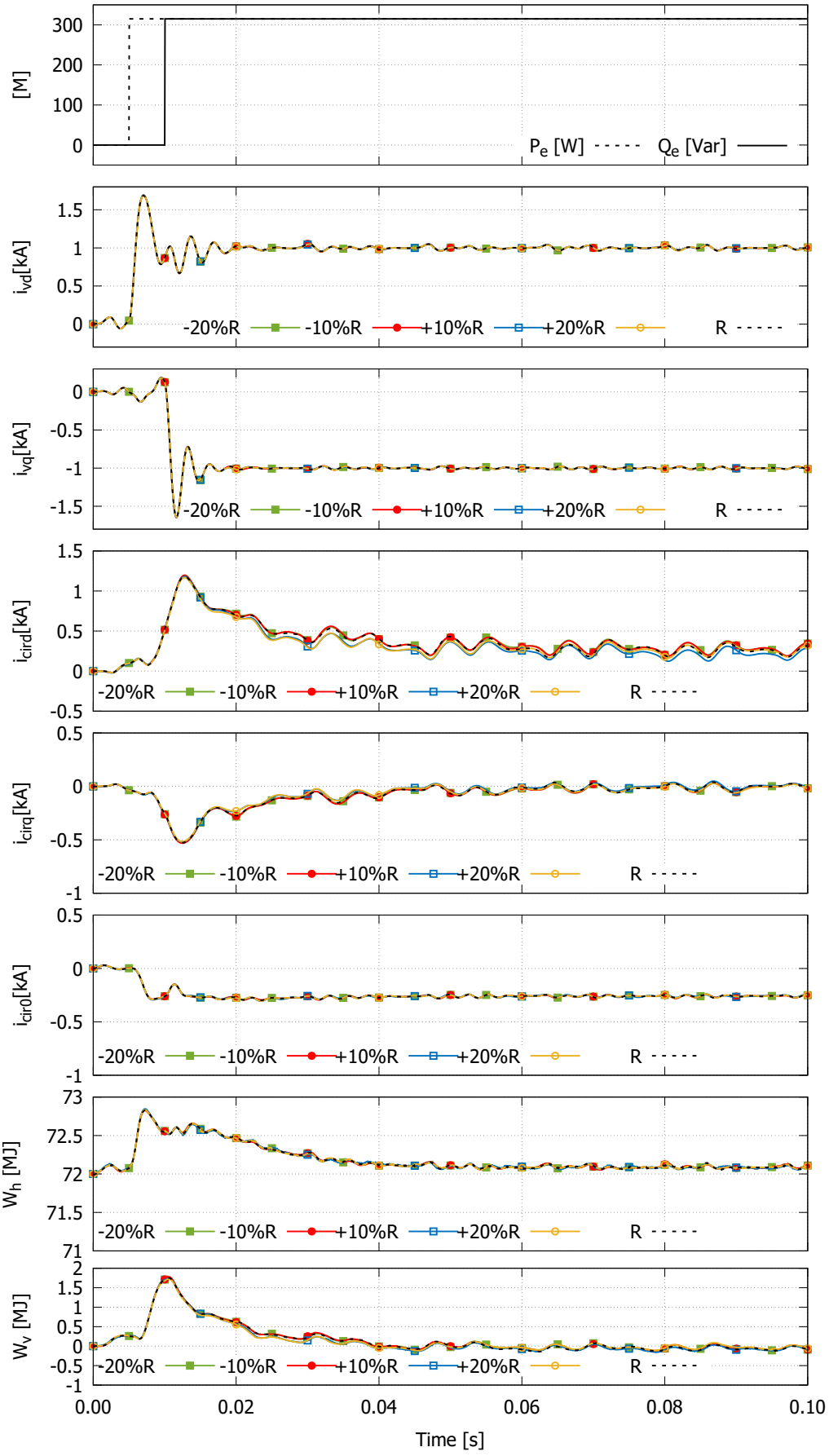

Source: Author

Figure 65 – The system state over variation of parameter R_c of high-voltage system with PI controller.

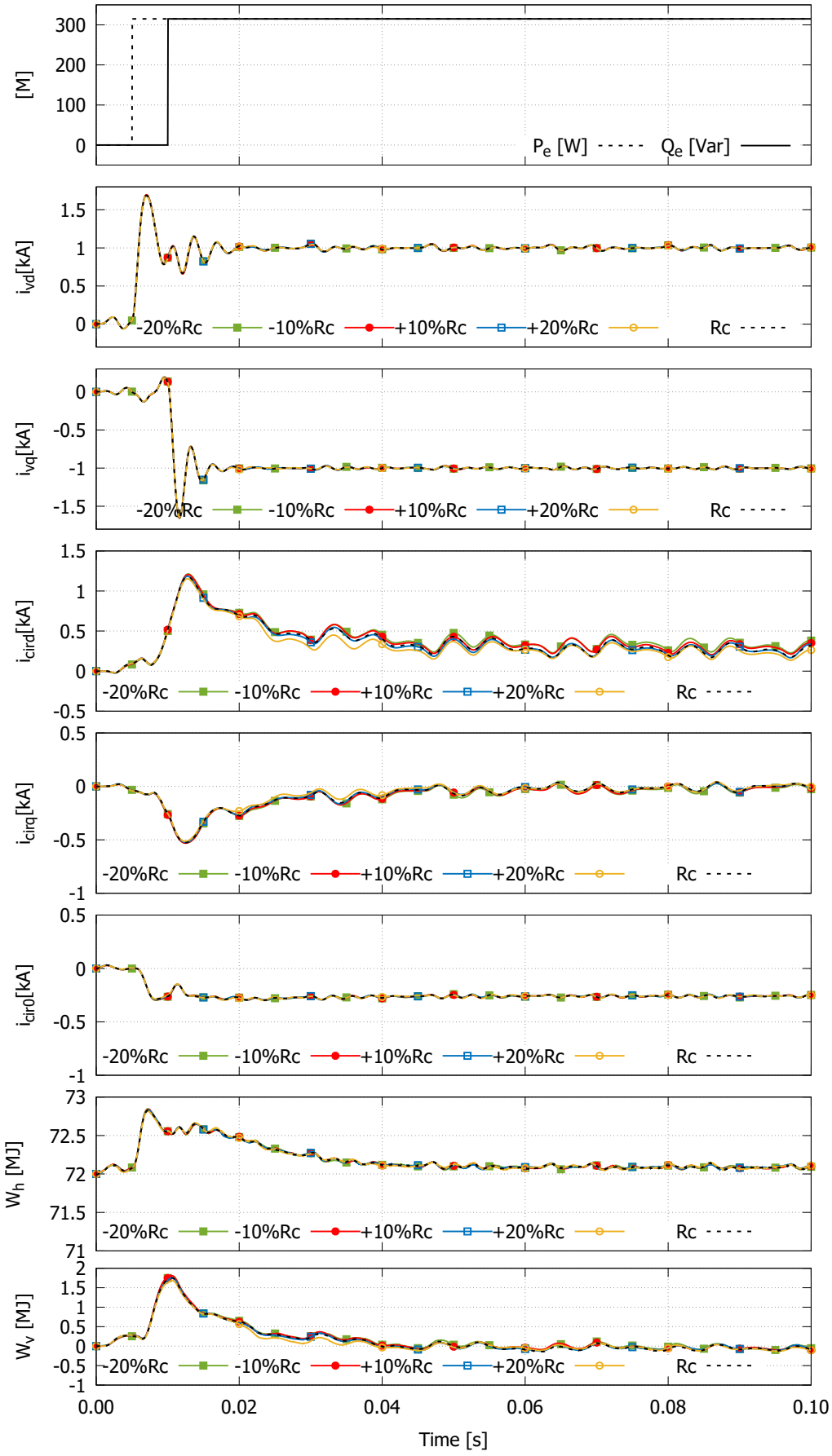

Source: Author

Figure 66 – The system state over variation of parameter L of high-voltage system with PI controller.

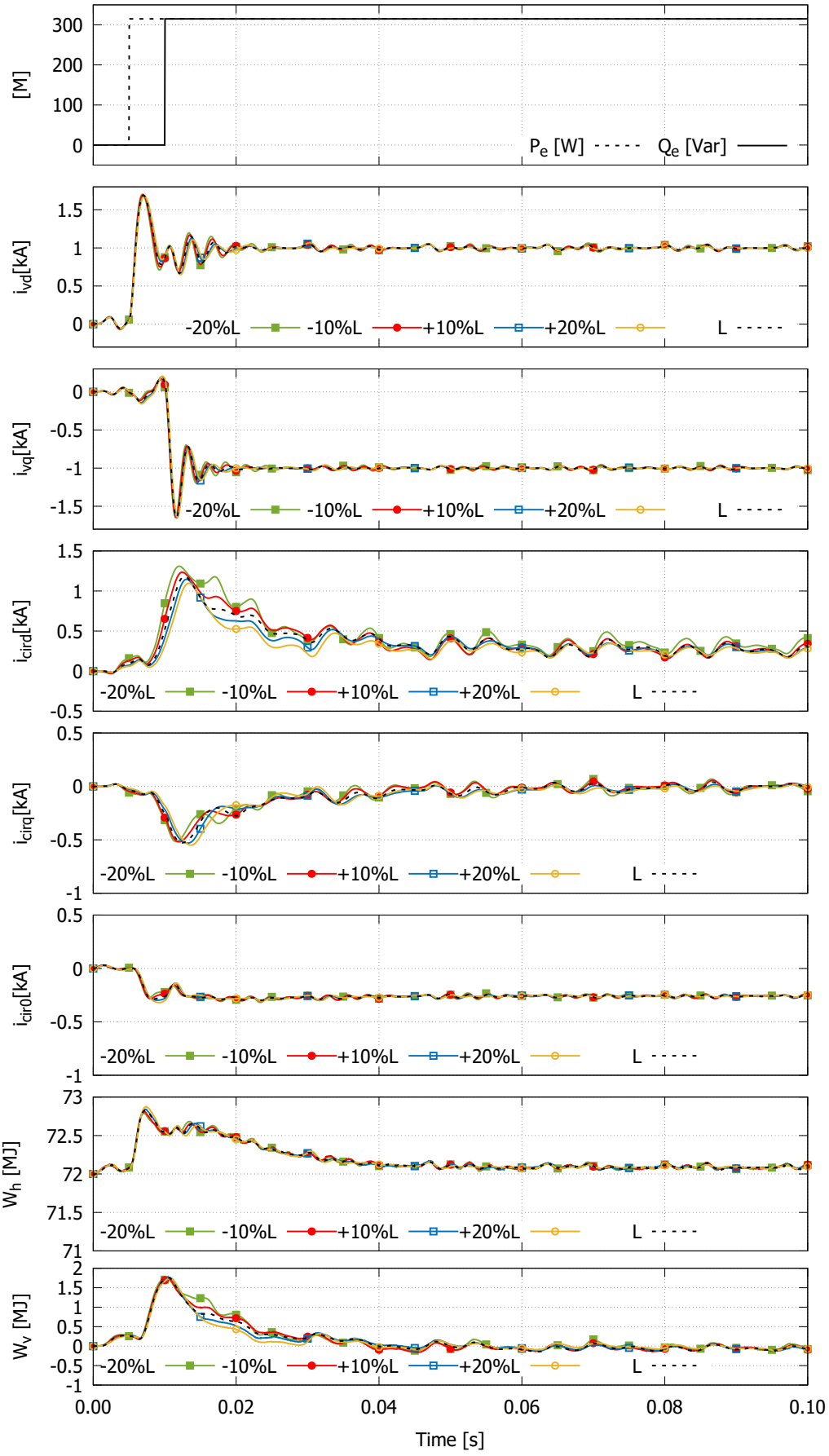

Source: Author

Figure 67 – The system state over variation of parameter L_c of high-voltage system with PI controller.

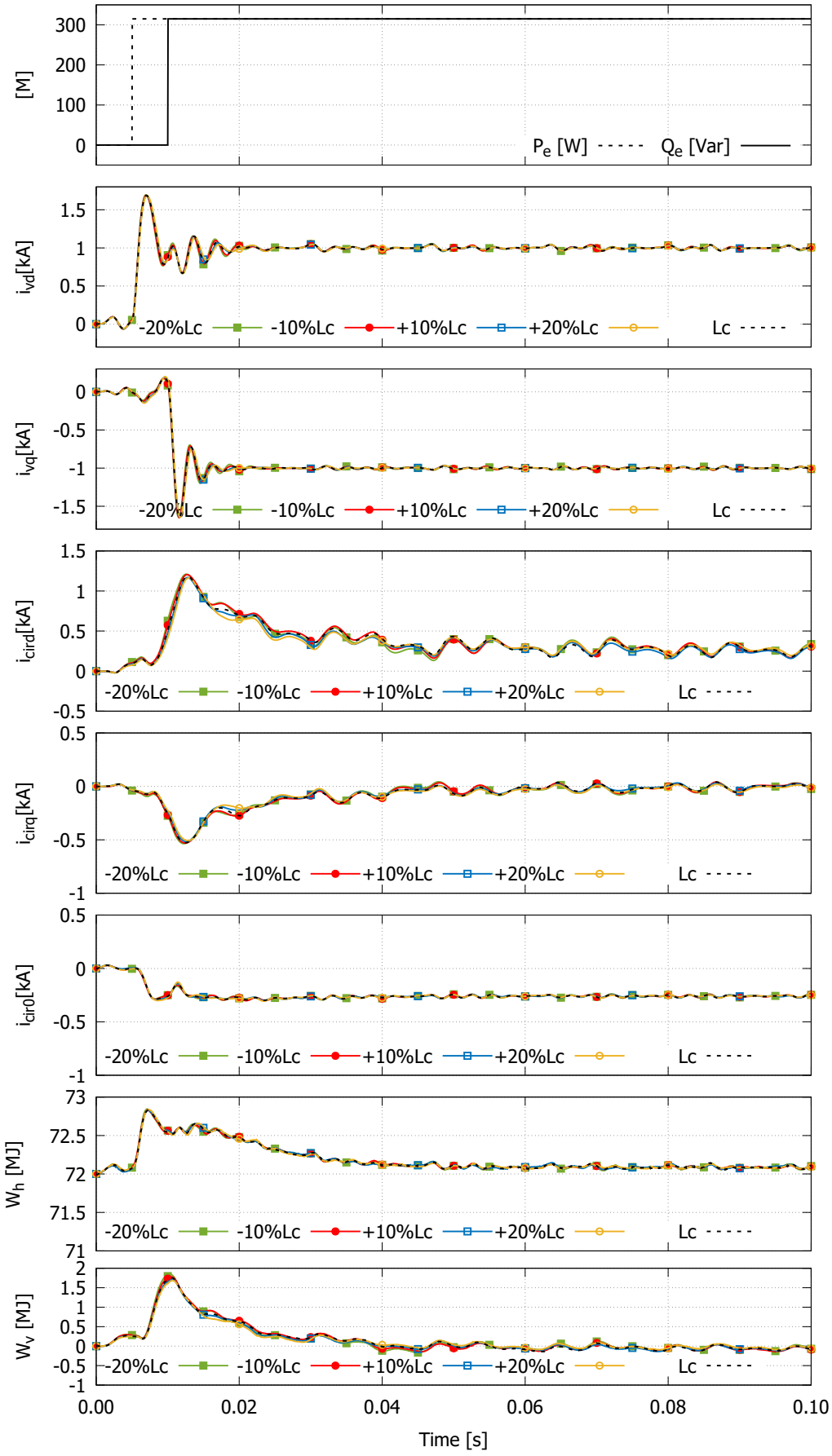

Source: Author

Figure 68 – The system state over variation of parameter C of high-voltage system with PI controller.

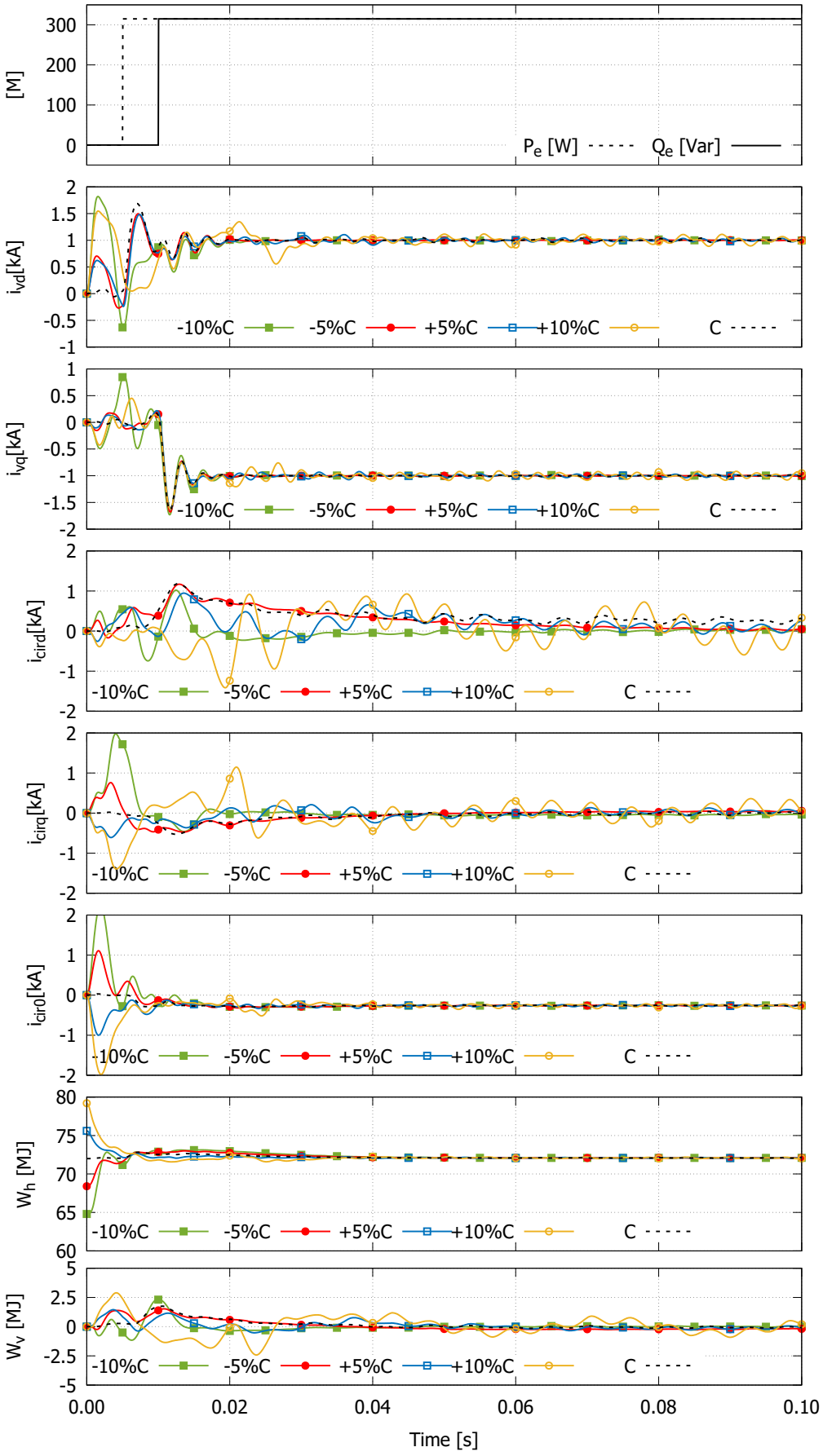

Source: Author

Figure 69 – The system state over variation in the voltage at the PCC of high-voltage system with PI controller.

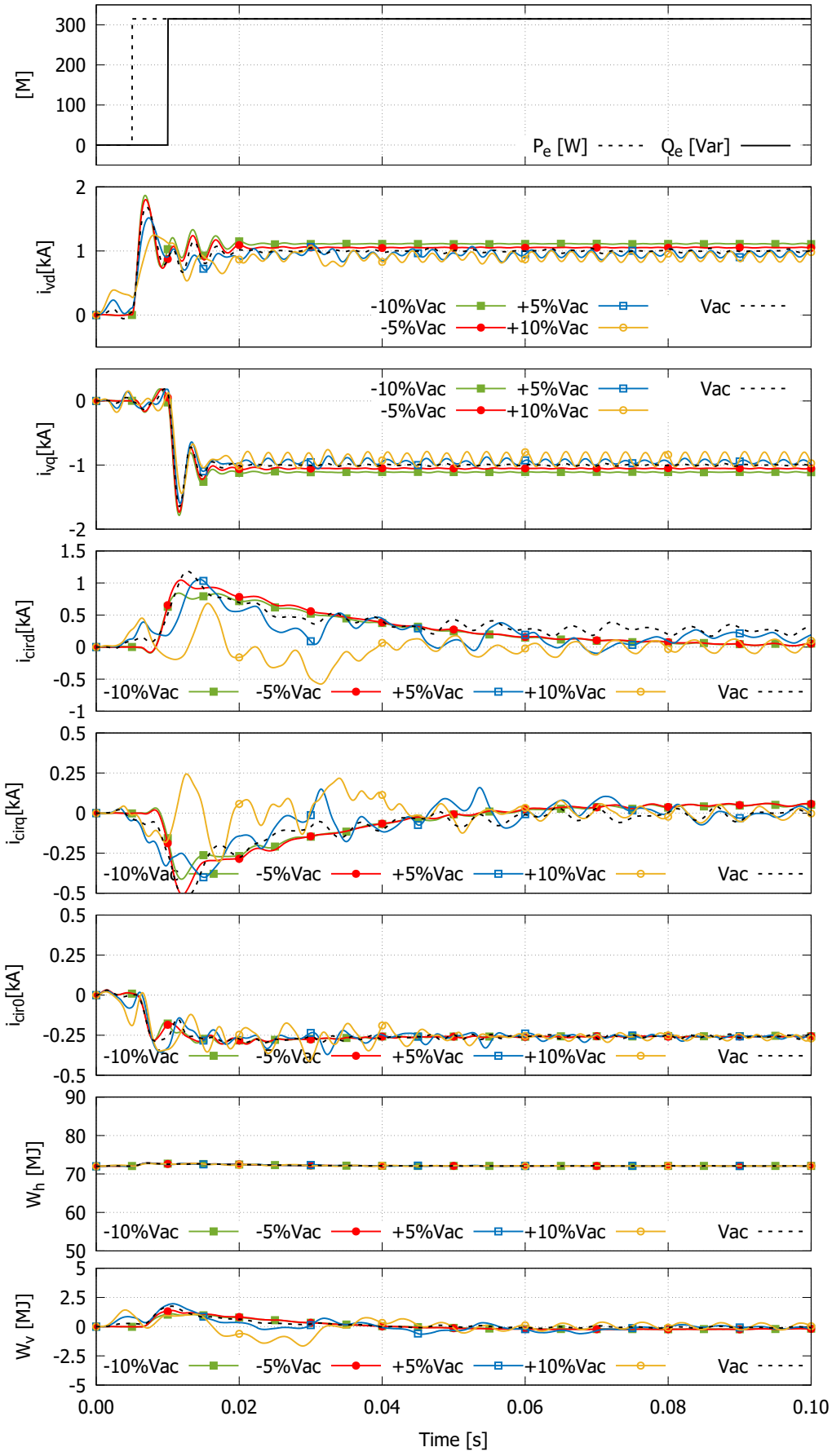

Source: Author

Figure 70 – The system state over variation in DC voltage of high-voltage system with PI controller.

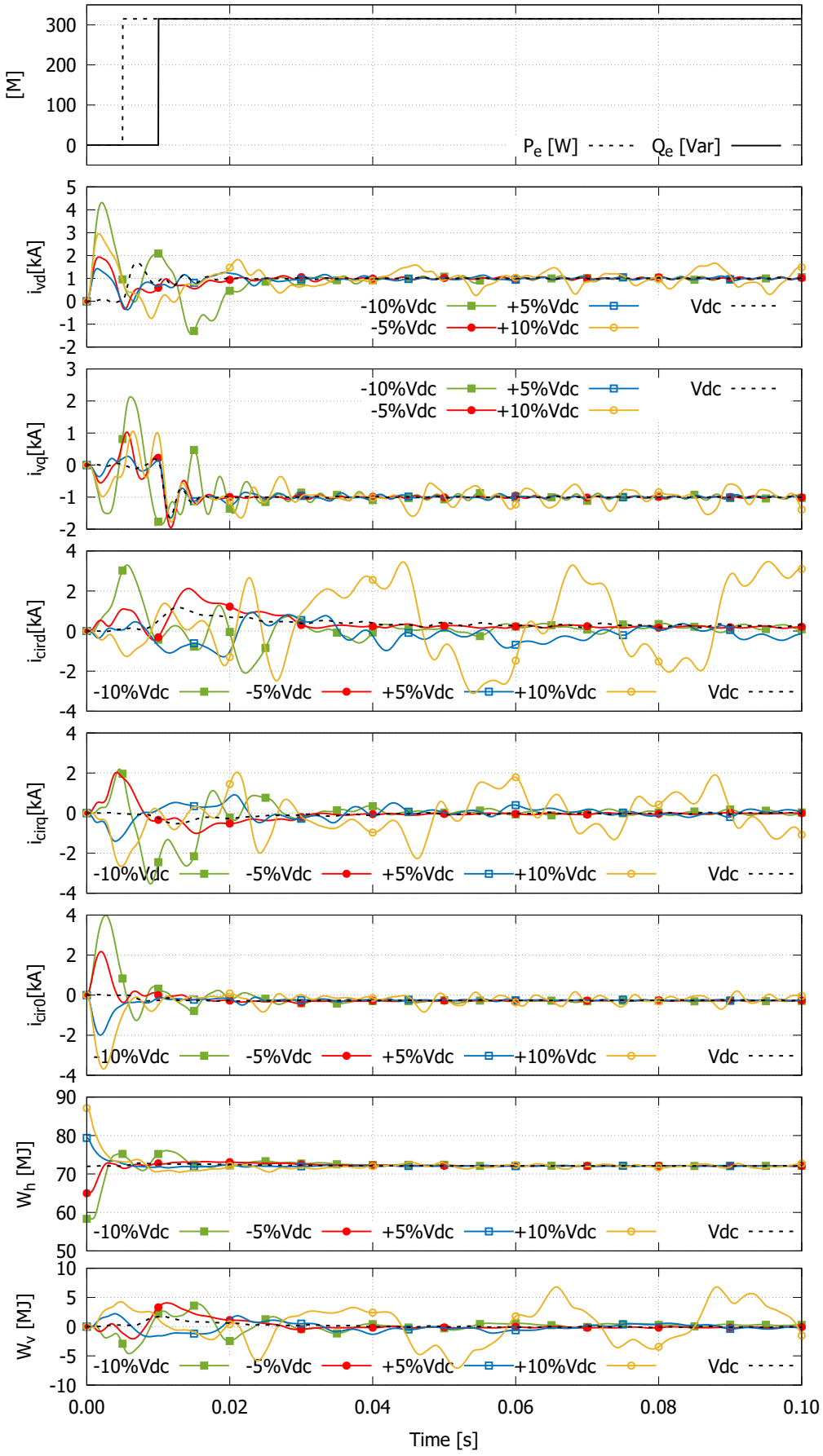

Source: Author

3.6 Chapter conclusion

This chapter presented the design of the PI controller, adapted from [25]. This chapter defines the state desired values and control inputs references. In addition, there is a description of the tuning procedure.

An average and a switching MMC models in medium-voltage were simulated using the PI controller. They present suitable performance for a set of operating points and energy steps, where states have a high speed of convergence and light overshoots. The tests also show the associated control efforts. Average and switching models present equivalent performance which allows the use of the average model if a more simple model is required.

It is essential to highlight that the PI controller's gains were set to have the same responses for the average-model and switching-model aiming to have suitable performance in both models and fair comparison. However, the controller gains adjust may improve the response on the state variables i_{cird} and W_v from the switching-model.

Although both models present similar performance, the focus will be on the switching model when analyzing the internal dynamics.

Additionally, a high-voltage model is simulated with the PI controller, with a set of operating points and energy steps. Concerning internal dynamics, PI accomplish the balancing between submodule capacitors' voltage and the balancing between W_u and W_l.

The robustness over parameter uncertainties shows that the PI controller can drive state variables even for changes of $\pm 20\%$ in R, R_c, L, and L_c. Additionally, uncertainties in the SMs capacitor are harmful to the state variables, especially for the high-voltage system.

Voltage fluctuation of V_{ac} and V_{dc} has a moderate effect over the medium-voltage system, however more harmfully for the high-voltage system. The desired value for the zero component of the circulating current ($\bar{i}_{cir0}$) comes from the equilibrium point at steady-state of equation (18), where ($\dot{\bar{x}} = 0$). In (18) replacing (60) and (62) and collecting terms to obtain (65).

CHAPTER 4

Nonlinear control

This chapter presents the nonlinear control design with formal stability proof for an MMC, which is critical for interaction between AC and DC grids. Lyapunov theory is used to develop the proposed controller, which is based on Backstepping and Feedback Linearization techniques, and to perform the stability analysis. The proposed controller allows to asymptotically stabilize the MMC system. The proposed algorithm allows to manage the converter in a wide range of operation points, by means of arbitrary tuning assignment. Robustness and performances of proposed control are verified by means of Matlab Simscape Electrical simulations, including active and reactive power reference variations and grid imbalance conditions. A detailed MMC switching model, of $450MVA$ is considered on Matlab validation. A phase-shift PWM is considered with a sorting algorithm. In addition, MMC's internal energy is also controlled, what can contribute to help in the high-speed frequency control by using of this energy for synthetic inertia.

In this chapter, the control design is firstly presented, followed by the main mathematical results. Then, the control is implemented on a switched model. The performance over power flow changes, energy unbalance conditions, robustness over parameter uncertainties, and robustness over DC and AC voltage fluctuation are analyzed. Management of circulating current and the voltage balancing are shown on abc referential. To conclude, the tuning procedure and control effort are discussed.

4.1 Nonlinear controller in the context of MMC

Most of the existing results on the control strategy for MMCs consist of linear controllers, as vector control (nested Proportional Integral - PI - controllers), without formal proof of stability. This because only one point of operation is considered in its design, and because the system's nonlinearities are disregarded [28; 29; 30].

In this point of view, one may cite works as [31], where the nonlinear MMC model is first linearized, and then linear controllers are designed for it. In a different way, [27] proposes a discrete-time bilinear model of an MMC, controlled by a sum-of-squares decomposition method,

following a nonlinear analysis. These studies are motivated by the relevance of designing nonlinear controllers that can assure stability throughout large electrical grid operation regions, including rigorous stability analysis [32; 33].

This chapter presents a nonlinear controller for an MMC based on Lyapunov theory. The resulting nonlinear scheme is independent of the operation point since it uses the full nonlinear model. The controller compensates several nonlinear components and imposes desired closed loop dynamics. For this reason, there is a decoupling on resulting closed loop system, and tuning becomes effortless, because its parameters represent these desired dynamics. The proposed controller is also robust, what can be seen by the fact that it was developed using the averaged model but simulations were carried out using a more complex switched model. Finally, the fact that the system is underactuated is clearly exploited such that the controller steers the actuated states, that are on their turn used to drive the underactuated states to desired values. This backstepping procedure creates a clear structure on which states are driven by individual control inputs or other states. The resulting closed loop system can then provide fast ancillary services (sub second) that will be capital for future power grids, like fast frequency response and synthetic inertia, for a wide range of operation points.

4.2 Mathematical model - Recalling main definitions

Here again we consider the circuit shown in figure (19) with the average model of the MMC in the *dq0* reference frame presented by system (35).

The system states are the AC currents in the d and q axis ($i_{v,d}$ $i_{v,q}$), circulating currents in the d, q and 0 axis ($i_{cir,d}$ $i_{cir,q}$ $i_{cir,0}$), total energy (W_h) and energy balancing (W_v) and are summarised as

$$x = [i_{v,d}\ i_{v,q}\ i_{cir,d}\ i_{cir,q}\ i_{cir,0}\ W_h\ W_v]$$

The controller inputs are the equivalent voltage produced per arm. $v_{u,d}$ is the direct component of equivalent voltage of the upper arm, $v_{u,q}$ is the quadrature component of equivalent voltage of the upper arm, $v_{l,d}$ is the direct component of equivalent voltage of the lower arm, $v_{l,q}$ is the quadrature component of equivalent voltage of the lower arm, and v_{d0} is the zero component of equivalent voltage in upper an lower arm. In $dq0$ reference that will be

$$u = [v_{u,d}\ v_{u,q}\ v_{l,d}\ v_{l,q}\ v_{d0}]$$

At the switching model, the controller inputs are the voltage waveforms to be sent to the modulation scheme. The modulation scheme is responsible for generating the gating signals to the SMs IGBTS to produce the desired output voltage at the converter terminals. In this chapter we use phase-shift PWM modulation.

4.3 Control Objective

The control objective is to stabilize the MMC system. In order to achieve this objective it is used a backstepping procedure where states $i_{v_{dq}}$ and $i_{cir_{dq0}}$ are directly controlled to steer states W_h and W_v. Therefore, an important characteristic of the MMC presented in the model above is that there are seven states and just five control inputs. So, the system is under-actuated with five actuated states and two free-dynamic states. In this chapter the actuated states were selected as $[i_{v,d}\ i_{v,q}\ i_{cir,d}\ i_{cir,q}\ i_{cir,0}]$ and therefore the behaviour of $[W_h\ W_v]$ are considered as free-dynamic states. To tackle this problem, it is used a combination of input-output feedback linearization and backstepping.

4.3.1 The Actuated States

Next, the error from a state $x_i \quad \forall i \in \{1 \cdots 7\}$ and its reference $\bar{x}_i$ is represented by $\tilde{x}_i$, as shows (102):

$$\tilde{x}_i \triangleq x_i - \bar{x}_i \quad \forall i \in \{1 \cdots 7\} \tag{102}$$

First, it is considered the control design for state $i_{v,d}$. So, it is proposed a first Lyapunov function (103):

$$V_{i_{v,d}} = \frac{1}{2}(i_{v,d} - \bar{i}_{v,d})^2 + \beta_{v,d}\xi_{v,d}^2 \tag{103}$$

with $\xi_{v,d}$ given by:

$$\dot{\xi}_{v,d} = \tilde{i}_{v,d}$$

Its time derivative is:

$$\begin{aligned}\dot{V}_{i_{v,d}} =& \tilde{i}_{v,d} \cdot \left(-\frac{R_{eq}}{L_{eq}}\tilde{i}_{v,d} - \frac{R_{eq}}{L_{eq}}\bar{i}_{v,d} + \omega\tilde{i}_{v,q} + \omega\bar{i}_{v,q} + \frac{v_{u,d}}{L_{eq}} - \frac{v_{l,d}}{L_{eq}} + \frac{2v_{f,d}}{L_{eq}} \right) + \\ &+ \beta_{v,d}\xi_{v,d}\tilde{i}_{v,d}\end{aligned} \tag{104}$$

The time derivative of Lyapunov function must be smaller than zero to assure asymptotic stabilization for state $i_{v,d}$, the following equation is defined:

$$-\alpha_{i_{v,d}} \cdot \tilde{i}_{v,d} = -\frac{R_{eq}}{L_{eq}}\tilde{i}_{v,d} - \frac{R_{eq}}{L_{eq}}\bar{i}_{v,d} + \omega\tilde{i}_{v,q} + \omega\bar{i}_{v,q} + \frac{v_{u,d}}{L_{eq}} - \frac{v_{l,d}}{L_{eq}} + \frac{2v_{f,d}}{L_{eq}} + \beta_{v,d}\xi_{v,d} \tag{105}$$

with constants $\alpha_{i_{v,d}},\ \beta_{i_{v,d}} \in \mathbb{R}_+^*$.

Collecting terms from (105), the following expression for $v_{u,d}$ is obtained in (106). The control input $v_{l,d}$, which was not designed yet, needs to be considered in a future step to finally establish the control law $v_{u,d}$.

$$\begin{aligned} v_{u,d} =& R_{eq}\bar{i}_{v,d} + R_{eq}\tilde{i}_{v,d} - L_{eq}\omega\tilde{i}_{v,q} - L_{eq}\omega\cdot\bar{i}_{v,q} + \\ & - 2v_{f,d} - L_{eq}\alpha_{i_{v,d}}\tilde{i}_{v,d} - L_{eq}\beta_{i_{v,d}}\xi_{v,d} + v_{l,d} \end{aligned} \tag{106}$$

Thus, a Lyapunov function for state $i_{cir,d}$ is proposed in (107), and its time derivative shown in (108).

$$V_{i_{cir,d}} = \frac{1}{2}(i_{cir,d} - \bar{i}_{cir,d})^2 \tag{107}$$

$$\dot{V}_{i_{cir,d}} = \tilde{i}_{cir,d}\left(-\frac{R}{L}\tilde{i}_{cir,d} - \frac{R}{L}\bar{i}_{cir,d} + \omega\tilde{i}_{cir,q} + \omega\bar{i}_{cir,q} - \frac{v_{u,d}}{2L} - \frac{v_{l,d}}{2L}\right) \tag{108}$$

In order to obtain a suitable Lyapunov function's derivative, one may define the control law $v_{l,d}$ as:

$$\begin{aligned} v_{l,d} =& -\frac{R_{eq}}{2}\cdot(\bar{i}_{v,d} + \tilde{i}_{v,d}) + \frac{L_{eq}\omega}{2}\cdot(\tilde{i}_{v,q} + \bar{i}_{v,q}) + v_{f,d} + \frac{L_{eq}\alpha_{i_{v,d}}}{2}\cdot\tilde{i}_{v,d} + \\ & + \frac{L_{eq}}{2}\beta_{i_{v,d}}\xi_{v,d} + Lw\cdot(\tilde{i}_{cir,q} + \bar{i}_{cir,q}) + L\alpha_{i_{cir,d}}\tilde{i}_{cir,d} - R\cdot(\tilde{i}_{cir,d} + \bar{i}_{cir,d}) \end{aligned} \tag{109}$$

such that the time derivative of the Lyapunov function becomes:

$$\dot{V}_{i_{cir,d}} = -\alpha_{i_{cir,d}}\cdot\tilde{i}^2_{cir,d} \tag{110}$$

where we define the constant $\alpha_{i_{cir,d}} \in \mathbb{R}^*_+$. By (107) and (110), one can assure exponential stability for state $i_{cir,d}$ towards its reference.

Replacing (109) in (106), the control law $v_{u,d}$ is defined as:

$$\begin{aligned} v_{u,d} =& \frac{R_{eq}}{2}\cdot(\bar{i}_{v,d} + \tilde{i}_{v,d}) - \frac{L_{eq}\omega}{2}\cdot(\tilde{i}_{v,q} + \bar{i}_{v,q}) - v_{f,d} - \frac{L_{eq}\alpha_{i_{v,d}}}{2}\cdot\tilde{i}_{v,d} + \\ & - \frac{L_{eq}}{2}\beta_{i_{v,d}}\xi_{v,d} + Lw\cdot(\tilde{i}_{cir,q} + \bar{i}_{cir,q}) + L\alpha_{i_{cir,d}}\tilde{i}_{cir,d} - R\cdot(\tilde{i}_{cir,d} + \bar{i}_{cir,d}) \end{aligned} \tag{111}$$

Applying these control laws, (109) and (111) in (104), the time derivative of the Lyapunov function becomes:

$$\dot{V}_{i_{v,d}} = -\alpha_{i_{v,d}}\cdot\tilde{i}^2_{v,d} \tag{112}$$

By (103) and (112), and calling upon La Salle's theorem one can assure asymptotic stability for the state $i_{v,d}$ towards its reference. In addition, calling upon theorem 4.6 in [79], it is possible

to show that this stability is indeed exponential for states $i_{v,d}$ and $\xi_{v,d}$. The same procedure presented above is considered for states $i_{v,q}$ and $i_{cir,q}$. The following Lyapunov functions are considered:

$$V_{i_{v,q}} = (i_{v,q} - \bar{i}_{v,q})^2 + \frac{1}{2}\beta_{v,q}\xi_{v,q}^2 \tag{113}$$

$$V_{i_{cir,q}} = (i_{cir,q} - \bar{i}_{cir,q})^2 + \frac{1}{2}\beta_{cir,q}\xi_{cir,q}^2 \tag{114}$$

with $\xi_{v,q}$ and $\xi_{cir,q}$ given by:

$$\dot{\xi}_{v,q} = i_{v,q} - \bar{i}_{v,q}$$

$$\dot{\xi}_{cir,q} = i_{cir,q} - \bar{i}_{cir,q}$$

Considering the time derivative of the Lyapunov functions from (113) and (114), the control laws $v_{l,q}$ and $v_{u,q}$ can be obtained as:

$$\begin{aligned} v_{l,q} = &- R \cdot (\tilde{i}_{cir,q} + \bar{i}_{cir,q}) - L\omega \cdot (\tilde{i}_{cir,d} + \bar{i}_{cir,d}) - \frac{R_{eq}}{2} \cdot (\bar{i}_{v,q} + \tilde{i}_{v,q}) + \\ &+ L\beta_{i_{cir,q}}\xi_{cir,q} - \frac{L_{eq}\omega}{2} \cdot (\tilde{i}_{v,d} + \bar{i}_{v,d}) + v_{f,q} + \\ &+ \frac{L_{eq}\alpha_{i_{v,q}}}{2} \cdot \tilde{i}_{v,q} + \frac{L_{eq}\beta_{i_{v,q}}}{2} \cdot \xi_{v,q} + L\alpha_{i_{cir,q}}\tilde{i}_{cir,q} \end{aligned} \tag{115}$$

$$\begin{aligned} v_{u,q} = &- R \cdot (\tilde{i}_{cir,q} + \bar{i}_{cir,q}) - L\omega \cdot (\tilde{i}_{cir,d} + \bar{i}_{cir,d}) + \frac{R_{eq}}{2} \cdot (\bar{i}_{v,q} + \tilde{i}_{v,q}) + \\ &+ L\beta_{i_{cir,q}}\xi_{cir,q} + \frac{L_{eq}\omega}{2} \cdot (\tilde{i}_{v,d} + \bar{i}_{v,d}) - v_{f,q} + \\ &- \frac{L_{eq}\alpha_{i_{v,q}}}{2} \cdot \tilde{i}_{v,q} - \frac{L_{eq}\beta_{i_{v,q}}}{2} \cdot \xi_{v,q} + L\alpha_{i_{cir,q}}\tilde{i}_{cir,q} \end{aligned} \tag{116}$$

Control laws (115) and (116), with $\alpha_{i_{cir,q}}$, $\alpha_{i_{v,q}}$, $\beta_{i_{cir,q}}$ and $\beta_{i_{v,q}}$ positive constants, leads to the Lyapunov functions' time derivatives:

$$\dot{V}_{i_{cir,q}} = -\alpha_{i_{cir,q}} \cdot \tilde{i}_{cir,q}^2 \tag{117}$$

$$\dot{V}_{i_{v,q}} = -\alpha_{iv,q} \cdot \tilde{i}_{v,q}^2 \tag{118}$$

As before, (113), (114), (117) and (118) with La Salle's theorem assure asymptotic stabilization of states $i_{cir,q}$ and $i_{v,q}$ towards their references. Again, it is possible to show that stabilization of states $i_{v,q}$, $\xi_{v,q}$, $i_{cir,q}$ and $\xi_{cir,q}$ are exponential.

At last, concerning state $i_{cir,0}$, a Lyapunov function is proposed in (119) with time derivative (120).

$$V_{i_{cir,0}} = \frac{1}{2}(i_{cir,0} - \bar{i}_{cir,0})^2 \tag{119}$$

$$\dot{V}_{i_{cir,0}} = \tilde{i}_{cir,0} \cdot \left(-\frac{R}{L}\tilde{i}_{cir,0} - \frac{R}{L}\bar{i}_{cir,0} - \frac{v_{d0}}{2L} + \frac{V_{DC}}{2L} \right) \tag{120}$$

Rearranging (120), the control law $v_{d,0}$ is obtained in (121), which leads to (122).

$$v_{d0} = 2L\tilde{i}_{cir0}\alpha_{icir0} - 2R \cdot (\bar{i}_{cir0} + \tilde{i}_{cir0}) + V_{DC} \tag{121}$$

$$\dot{V}_{i_{cir,0}} = -\alpha_{icir,0} \cdot \tilde{i}^2_{cir,0} \tag{122}$$

Again, it is possible to show that $\tilde{i}_{cir,0}$ exponentially converges to zero. By the procedure described above, the five available control inputs ($v_{u,d}$, $v_{u,q}$, $v_{l,d}$, $v_{l,q}$ and v_{d0}) were defined respectively in (111), (116), (109), (115) and (121). Moreover, exponential stabilization was obtained by design for all actuated states ($i_{v,d}$, $i_{v,q}$, $i_{cir,d}$, $i_{cir,q}$ and $i_{cir,0}$).

4.3.2 Free-dynamic States

The total converter's energy W_h and balance energy W_v do not have a exclusive control input as the other states. So a backstepping procedure was used in their cases. For this reason, virtual inputs are proposed as $i^*_{cir,0}$ and $i^*_{cir,d}$.

The variable $i^*_{cir,0}$ is used as a reference for $i_{cir,0}$, and will be applied to steer W_h to its desired equilibrium. Thus, it is now defined the state error $\tilde{i}_{cir,0}$ in (123), where $\widetilde{W}_h$ is the error from total converter's energy W_h and its equilibrium value $\bar{W}_h$. In a similar way, because $i_{cir,dq}$ represent the flow inside the converter, it is possible to transfer energy between converters' arms. So, $i^*_{cir,d}$, is chosen to be used as a control signal for W_v. It is then defined the error between the state and its reference as in (124).

$$\begin{cases} \tilde{i}_{cir,0} = i_{cir,0} - i^*_{cir,0} \\ i^*_{cir,0} = \bar{i}_{cir,0} + \alpha_W \widetilde{W}_h + \beta_{W_h}\xi_{W_h} \end{cases} \tag{123}$$

$$\begin{cases} \tilde{i}_{cir,d} = i_{cir,d} + i^*_{cir,d} \\ i^*_{cir,d} = \bar{i}_{cir,d} + \alpha_{W_v} \cdot W_v + \beta_{W_v} \cdot \xi_{W_v} \end{cases} \tag{124}$$

where α_{W_h}, α_{W_v}, β_{W_h} and β_{W_v} are positive constants, and ξ_W and ξ_{W_v} will be defined latter.

Therefore, the total converter energy (W_h) dynamic is rewritten considering the predefined control inputs introduced in (109), (111), (115), (116) and (121) and the virtual input (123).

It is important to emphasize that the remaining states do not rely on the two energy states. For this reason, these two are considered as zero dynamics (similarly could be seen as a cascaded system) of the feedback linearization of the remaining states [79]. To analyze these zero dynamics, it is now considered $\tilde{i}_{v,d} = 0$, $\tilde{i}_{v,q} = 0$, $\tilde{i}_{cir,d} = 0$, $\tilde{i}_{cir,q} = 0$ and $\tilde{i}_{cir,0} = 0$. Based on this, it is now defined the state ξ_{W_v} and we rewrite $\dot{\tilde{W}}_h$ as (125).

$$\begin{aligned}\dot{\xi}_{W_h} =& W_h - \bar{W_h} \triangleq \tilde{W}_h \\ \dot{\tilde{W}}_h =& \boxed{\frac{3}{2} i_{v,d} v_{f,d}} \boxed{+\frac{3}{2} i_{v,q} v_{f,q}} \boxed{-\frac{3}{4} R_{eq} i_{v,d}^2} \boxed{-\frac{3}{4} R_{eq} i_{v,q}^2} \boxed{+3\bar{i}_{cir,0} v_{DC}} \boxed{-3R\bar{i}_{cir,d}^2} + \\ & \boxed{-3R\bar{i}_{cir,q}^2} \boxed{-3R\bar{i}_{cir,0}^2} + 12R\bar{i}_{cir,0}\alpha_{W_h}\tilde{W}_h - 3v_{DC}\alpha_{W_h}\tilde{W}_h - 6R\alpha_{W_h}^2\tilde{W}_h^2\end{aligned} \tag{125}$$

the sum of highlighted terms is zero because they represent the elements of the converter's power balance, so (125) becomes (126). Highlighted terms indeed constitute AC power, DC power, losses in AC elements, and losses in DC elements. Their sum is always zero for physical reasons.

$$\dot{\tilde{W}}_h = 12R\bar{i}_{cir,0}\alpha_{W_h}\tilde{W}_h - 3v_{DC}\alpha_{W_h}\tilde{W}_h - 6R\alpha_{W_h}^2\tilde{W}_h^2 \tag{126}$$

One may now consider the Lyapunov function candidate:

$$V_{W_h} = \frac{1}{2}\left(W_h - \bar{W_h}\right)^2 + \frac{1}{2}\cdot\xi_{W_h}^2 \tag{127}$$

and compute its derivative:

$$\dot{V}_{W_h} = 12R\bar{i}_{cir,0}\alpha_{W_h}\widetilde{W}_h^2 - 3v_{DC}\alpha_{W_h}\tilde{W}_h^2 - 6R\alpha_{W_h}^2\tilde{W}_h^3 \tag{128}$$

For physical reasons, $12R\bar{i}_{cir,0} << 3v_{DC}$, then, inside a region

$$||\widetilde{W}_h|| < \frac{(3v_{DC} - 12R\bar{i}_{cir,0})}{6R\alpha_{W_h}} \tag{129}$$

Lyapunov function's derivative (128) is negative, and as a consequence for a given operation region around the equilibrium point $\xi_{W_h} = 0$ and $\tilde{W}_h = 0$, this Lyapunov function assures asymptotic stability towards this point. Furthermore, the size of this operation region is given by the tuning parameter of α_{W_h}.

Following the same procedure, the zero dynamics represented by W_v are considered with the predefined control inputs (109), (111), (115), (116), and (121) as:

$$\dot{W}_v = i_{cir,d}^*\left(-3v_{fd} + R_{eq2}\bar{i}_{v,d} + 3\omega L_c\bar{i}_{v,q}\right) \tag{130}$$

where $R_{eq2} = \frac{3(R+R_{eq})}{2}$. Then, using $i^*_{cir,d}$ as an virtual input defined by (124) and setting $\bar{i}_{cir,d} = 0$:

$$\dot{W}_v = -\alpha_{W_v} W_v \left(3v_{fd} - R_{eq2}\bar{i}_{v,d} - 3\omega L_c \bar{i}_{v,q}\right) - \beta_{W_v}\xi_{W_v}\left(3v_{fd} - R_{eq2}\bar{i}_{v,d} - 3\omega L_c \bar{i}_{v,q}\right) \quad (131)$$

with $\dot{\xi}_{W_v} = W_v$. In the HVDC system, v_{fd} represents a large quantity, while voltage drop across resistance and inductance of PCC are small in comparison to v_{fd}. For physical reasons, the term inside the box is always positive, and it is concluded exponential stability for zero dynamics given by states W_v and ξ_{W_v}, because it is a linear Hurwitz system.

4.4 Main result

One can now state the constructive result built in the previous sections in the form of a theorem.

Theorem 1. *The MMC represented by the system in (35), with control inputs given by (109), (111), (115), (116) and (121) with tuning parameters* $\alpha_{i_{vd}}$, $\alpha_{i_{vq}}$, $\alpha_{i_{cird}}$, $\alpha_{i_{cirq}}$, $\alpha_{i_{cir,0}}$, α_{W_h} *and* $\alpha_{W_v} \in \mathbb{R}^*_+$*, is split into an actuated subsystem including states* $[\, i_{v,d} \;\; i_{v,q} \;\; i_{cir,d} \;\; i_{cir,q} \;\; i_{cir,0} \,]$*, extended by the integral of their dynamics, represented by states* $[\, \xi_{v,d} \;\; \xi_{v,q} \;\; \xi_{cir,q} \,]$*. This first subsystem has an exponential stable equilibrium point, represented by (47), (48), (124), (50) and (123). In addition, the remaining non-actuated subsystem including states* $[\, W_h \;\; W_v \,]$ *and their extended integral terms* $[\, \xi_{W_h} \;\; \xi_{W_v} \,]$ *have asymptotically stable equilibrium points (69) and (70) inside the domain:*

$$\mathcal{D} = \left\{ W_v \in \mathbb{R}^*_+, \;\; \xi_{W_h}, \xi_{W_v} \in \mathbb{R}, \;\; \|W_h - \bar{W}_h\| < \frac{(3v_{DC} - 12R\bar{i}_{cir,0})}{6R\alpha_{Wh}} \right\}$$

As a consequence the full system is asymptotic stable inside a domain, which size is given by a tuning parameter.

Proof. The proof is based on the composite Lyapunov function:

$$\begin{aligned} V &= V_{i_{v,d}} + V_{i_{v,q}} + V_{i_{cir,d}} + V_{i_{cir,q}} + V_{i_{cir,0}} + V_{W_h} + V_{W_v} \\ &= \frac{1}{2}(i_{v,d} - \bar{i}_{v,d})^2 + \frac{1}{2}(i_{v,q} - \bar{i}_{v,q})^2 + \frac{1}{2}(i_{cir,d} - \bar{i}_{cir,d})^2 + \\ &\quad + \frac{1}{2}(i_{cir,q} - \bar{i}_{cir,q})^2 + \frac{1}{2}(i_{cir,0} - \bar{i}_{cir,0})^2 + \frac{1}{2}\left(W_h - \bar{W}_h\right)^2 + \\ &\quad + \frac{1}{2}\left(W_v - \bar{W}_v\right)^2 \end{aligned}$$

in which derivative $\dot{V} \leq 0$ by virtue of (112), (117), (110), (118) and (122), provide $\alpha_{i_{cird}}$, α_{icirq}, $\alpha_{i_{vd}}$, $\alpha_{i_{vq}}$, $\alpha_{i_{cir,0}}$, α_{W_h} and $\alpha_{W_v} \in \mathbb{R}^*_+$. Then, applying theorem 4.6 in 79, it is shown that the

actuated states are exponentially stable. Furthermore, the zero dynamics are asymptotically stable inside an operation region given by condition (129). Then it is possible to conclude that the whole system is asymptotically stable inside a domain, that will increase its size by reducing design parameter α_{Wh}. □

Figure 71 summarize the simulation implementation of nonlinear controller.

Figure 71 – Diagram of nonlinear control.

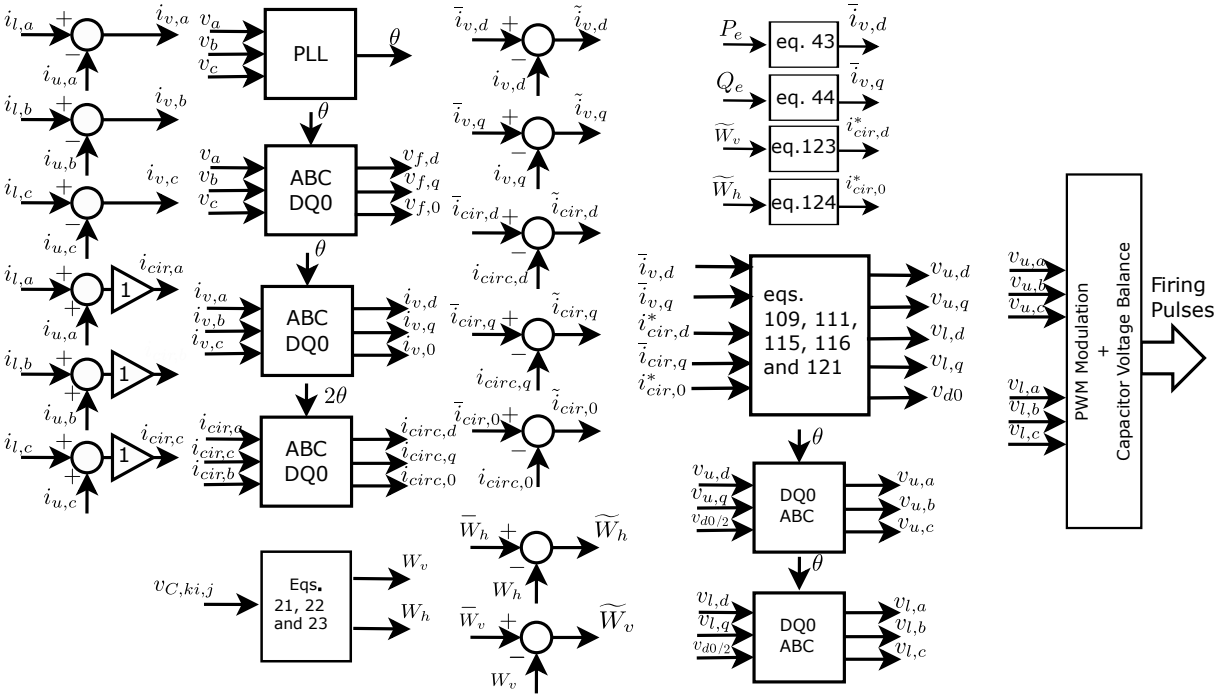

Source: Author

4.5 Medium-voltage system test with the nonlinear controller

The system presented in figure 28 is simulated using the nonlinear control for the switching and average models. The nonlinear control gains are tuned using the switching model, because its extra dynamics may turn the system more sensitive to tuning.

Nonlinear control tuning for medium-voltage system test

Control gains imply in system performance. The tuning procedure provides the control gains shown in Table (4). These gains are directly linked to the control effort, which is possible to see on the figure of control inputs. The tuning process shown in this section considers a balancing between the speed of convergence and the overshoots. Indeed, each pair of αs and βs place the corresponding poles.

Tuning βs while αs are equal to zero, enable to set the speed of convergence of the related state variables, i.e. place the poles' modulus:

$$\tau_{i_{vd}} = \frac{1}{\beta_{i_{vd}}}; \quad \beta_{i_{vd}} = 1000 \tag{132}$$

$$\tau_{i_{vq}} = \frac{1}{\beta_{i_{vq}}}; \quad \beta_{i_{vq}} = 1000 \tag{133}$$

$$\tau_{i_{cirq}} = \frac{1}{\beta_{i_{cirq}}}; \quad \beta_{i_{cirq}} = 1000 \tag{134}$$

$$\tau_{W_h} = \frac{1}{\beta_{W_h}}; \quad \beta_{W_h} = 50 \tag{135}$$

$$\tau_{W_v} = \frac{1}{\beta_{W_v}}; \quad \beta_{W_v} = 50 \tag{136}$$

Adjusting α_s, one obtains the damping ratio, and as consequence, the response of state variables i_{vd} and i_{vq} are improved as shows figure 72. It is possibles to verify i_{vd} and i_{vq} convergence for $\alpha_{i_{vd}}$ $\alpha_{i_{vq}}$ equal to 100, 500 and 1000. The speed of convergence is improved by the tuning, however it results in a overshoot in the case of $\alpha = 1000$. The intermediate value (500) is chosen for $\alpha_{i_{vd}}$ and $\alpha_{i_{vq}}$.

Figure 72 – Response of state i_{vd} and i_{vq} over tuning of αs.

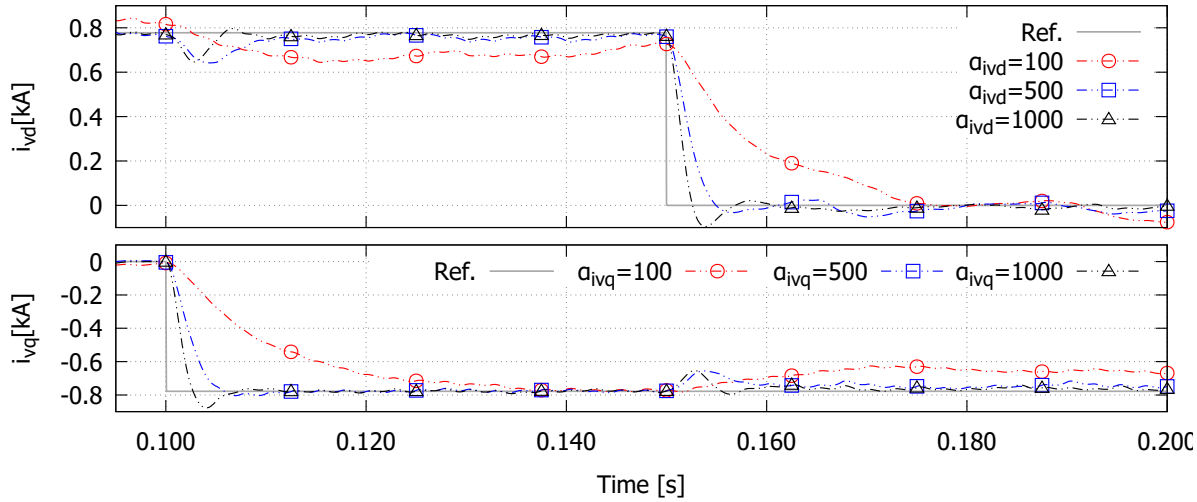

Source: Author

State variable i_{cirq} track their reference just by the adjust of $\beta_{i_{cirq}}$. Furthermore, it presents a reduction of noise when $\alpha_{i_{cirq}}$ increases.

State variables i_{cird} and i_{cir0}, which are used as virtual inputs, are directly tuned by their αs. For $\alpha_{i_{cird}}$ and $\alpha_{i_{cir0}}$ equals to 1000, there is no steady-state error for these states.

The β_{W_v} and β_{W_h} are tuned to have a slower response compared to the other state variables. They are set to 50, and both W_h and W_v present no steady-state error and have high speed of convergence. As a consequence, their respective αs are set to be equal to 1.

Remark 1. *It is clear that other methods of pole placement could be used, in particular robust techniques as LQR. These possibilities will be tested in future works.*

The following results for the medium-voltage system, consider the parameters summarised in table 4.

Table 4 – Parameters of simulated medium-voltage system and nonlinear control gains.

Parameter	**Value**	**Parameter**	**Value**
S_{MMC}	$50\ MVA$	$\beta_{i_{vdq}}$	1000
V_{AC}	$30\ kV$	$\beta_{i_{cirq}}$	1000
V_{DC}	$180\ kV$	β_{W_h}	50
L_c	$5\ mH$	β_{W_v}	50
L	$14\ mH$	$\alpha_{i_{vdq}}$	500
R_c	$0.03\ \Omega$	$\alpha_{i_{cird}}$	1000
C_{SM}	$3\ mF$	$\alpha_{i_{cirq}}$	500
Freq	$60\ Hz$	$\alpha_{i_{cir0}}$	1000
R	$0.5\ \Omega$	α_{W_h}	1
N	20	α_{W_v}	1

Figure 73 and figure 74 present the performance of the MMC over the proposed nonlinear controller. A four-quadrant operation is presented and also an energy step change. Both average-model (avm) and switching-model (swit) are presented.

Figure 73 – Four-quadrant operation of the medium-voltage system with the nonlinear controller.

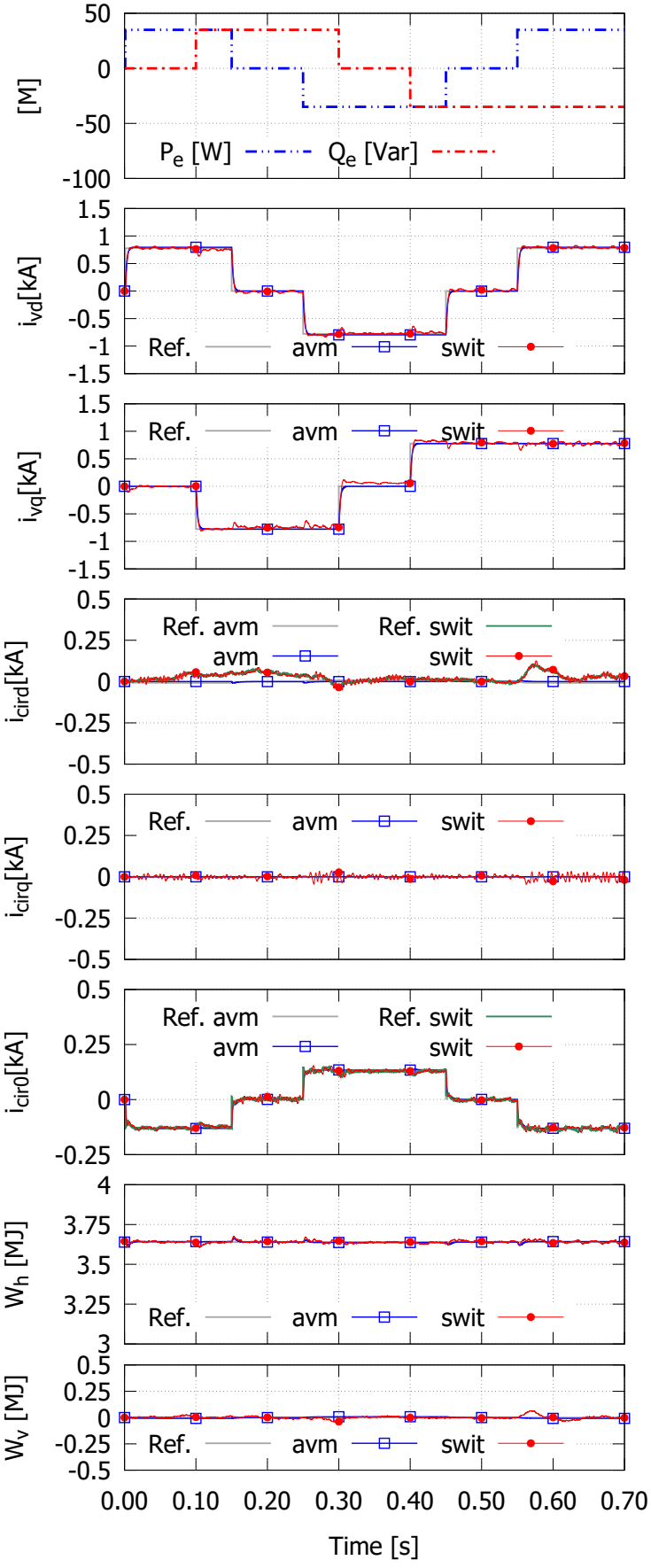

Four-quadrant operation of average and switching models of the medium-voltage system with the nonlinear controller.

In figure 73 a set of active and reactive power steps are performed. Both average-model and switching-model perform well using nonlinear controller. They present the same speed of convergence and no overshoot.

The switching-model present small oscillations if compared to average-model.

The state variables i_{cird} and i_{cir0} present different reference values (Ref.) between average-model and switching-model. Thus, they are distinguished at the figure.

At 4^{th} graphic, i_{cird} shows a different behaviour for each model, for some operating points. However nonlinear control drives the state variable for the respective desired value. The other state variables present close performance between MMC models.

Figure 74 – Energy changes of the medium-voltage system with the nonlinear controller.

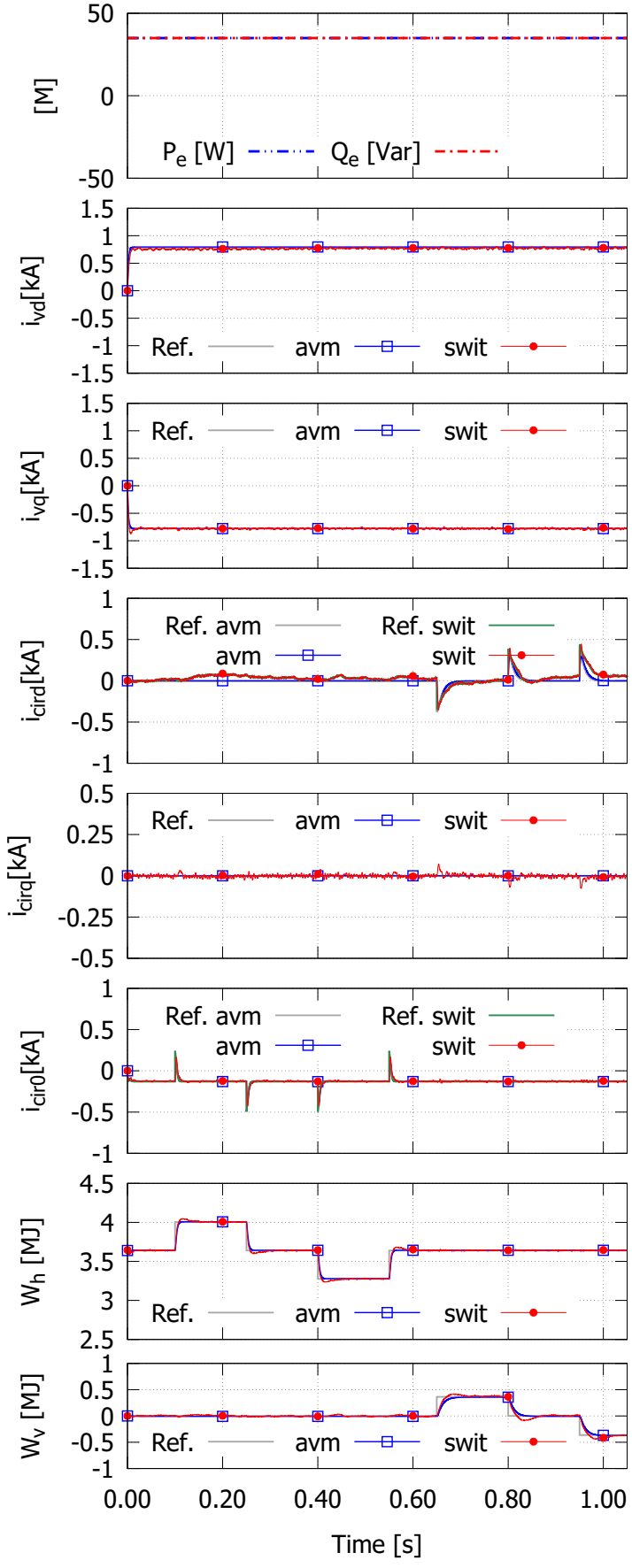

Energy changes of average and switching models for medium-voltage system with the nonlinear controller.

Concerning energy changes, figure 74 presents average and switching models' performance with the the nonlinear controller.

Both models achieve their desired values, however switching-model presents a tiny overshoot.

The models' performance has a solid equivalence which allows the use of the average model if a more simple simulation is required.

4.5.1 Robustness over parameters uncertainties and voltage fluctuation for medium-voltage system with nonlinear controller

Robustness

Robustness analysis is performed for nonlinear control's sensitivity performance. The parameter uncertainties are considered in this chapter: R, R_c, L, L_c and C_{SM} change (one at a time) in $\pm 10\%$ and $\pm 20\%$ from their nominal values. Real valuers are used in the control. The operating point is set to 70% of nominal active and reactive power.

Figure 75 shows a variation in the arm equivalent resistance R. The state variables present no overshoot neither deviation in steady-state. Additionally, the system's states are also not affected by the deviation on AC side resistance R_c (see figure 76).

Figure 77 and figure 78 point out stead-state error when arms inductance L and AC side inductance L_c are far from the nominal values. That error appears in the AC currents i_{vd} and i_{vq}.

Figure 79 shows system's states for changes in SM capacitance. It is possible to see in 7^{th} graphic that the initial value of total energy W_h comes from equation (69) which is linked with SM capacitance. However, the nonlinear controller can drive the state variable to the desired reference. Also, the convergence's speed of i_{cird} is large.

Therefore, the nonlinear controller proposed in this thesis presented steady-state error when arm inductance L and AC side inductance L_c changes. The state variables most affected were $i_{v,d}$ and $i_{v,q}$. However, these errors can be minimized by the increase of controller gains.

Voltage fluctuation

- ❏ Variation in the AC voltage at the PCC result in i_{vd} and i_{vq} with over-signal. The same problem was faced by PI controller, in the test from section 3.4.2. The other state variables are well drive to their reference for all value of V_{ac};
- ❏ Fluctuation in DC voltage result in slow speed of convergence to i_{cird} and W_v. However faster than PI convergence through the same test.

Figure 75 – The system state over variation of parameter R with nonlinear controller.

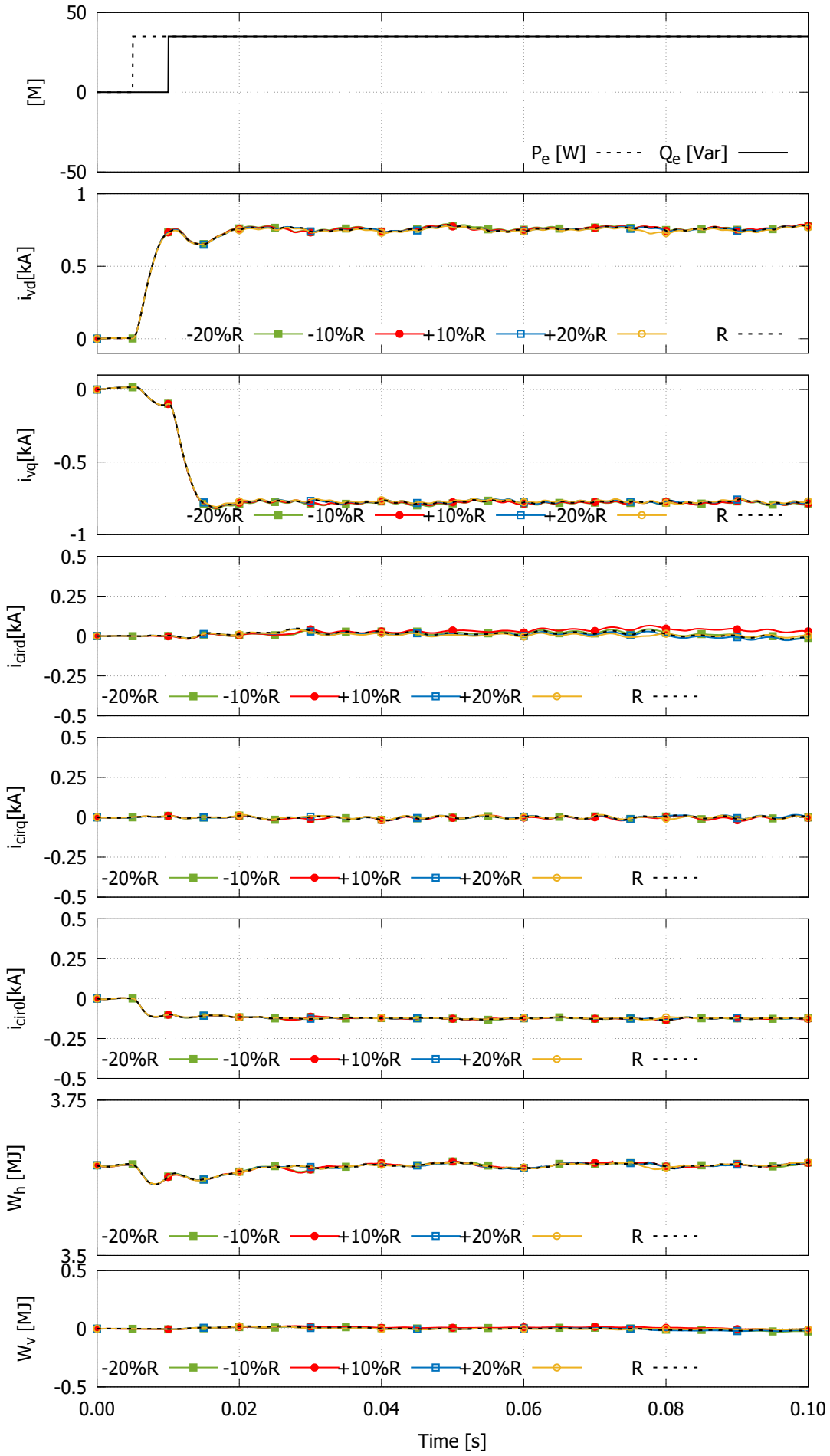

Figure 76 – States over variation of parameter R_c with nonlinear controller.

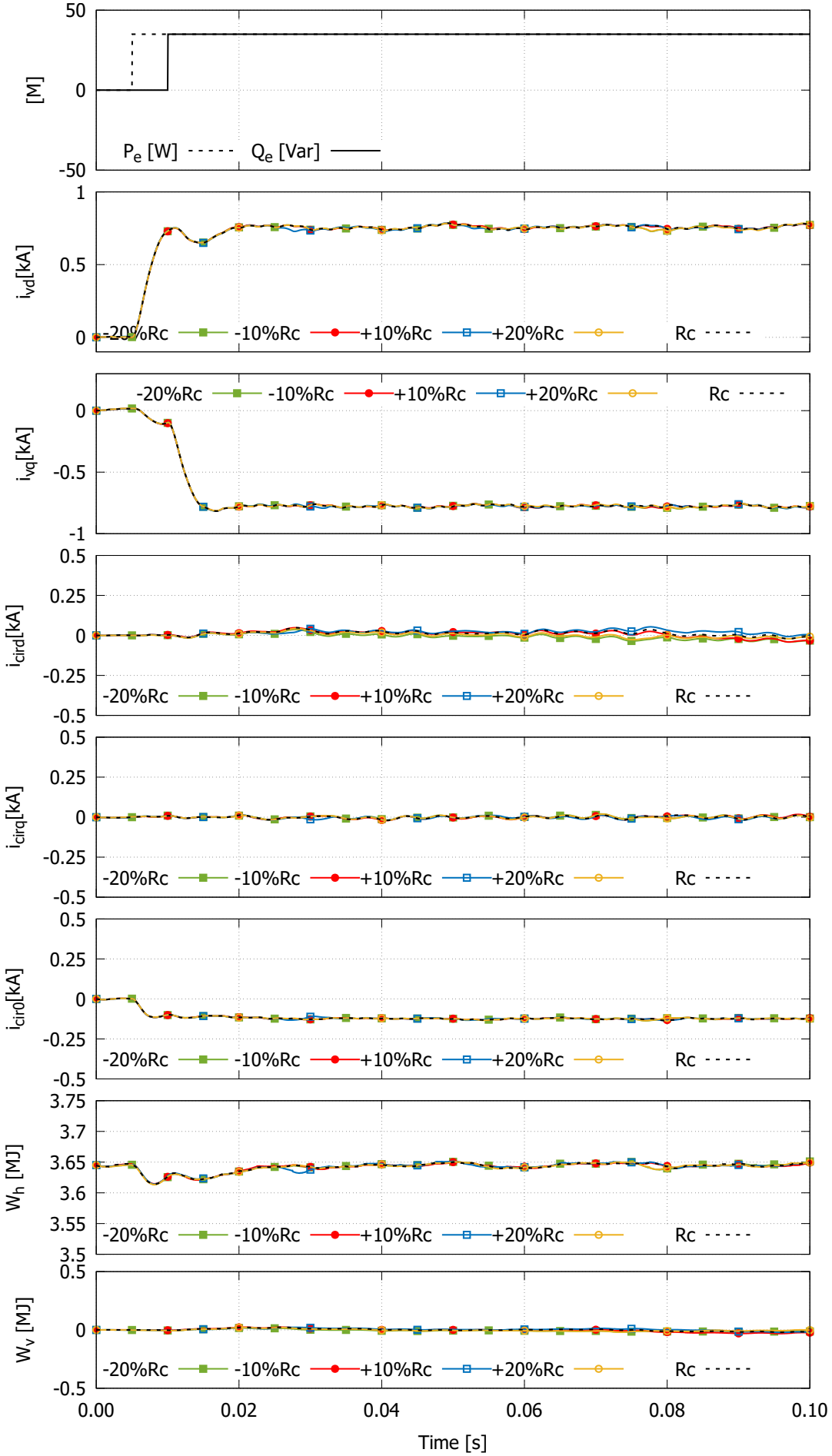

Figure 77 – States over variation of parameter L with nonlinear controller.

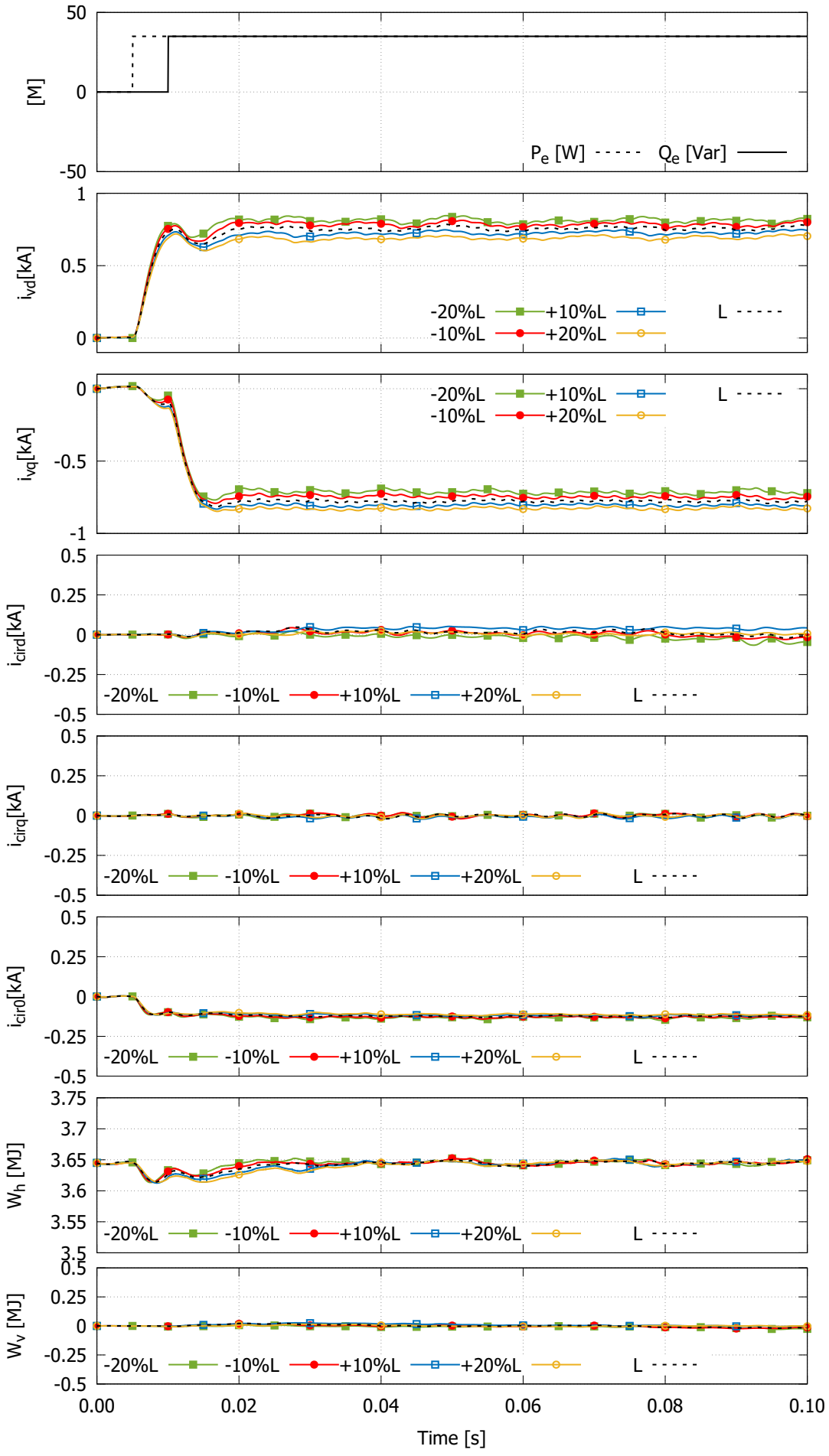

Figure 78 – States over variation of parameter L_c with nonlinear controller.

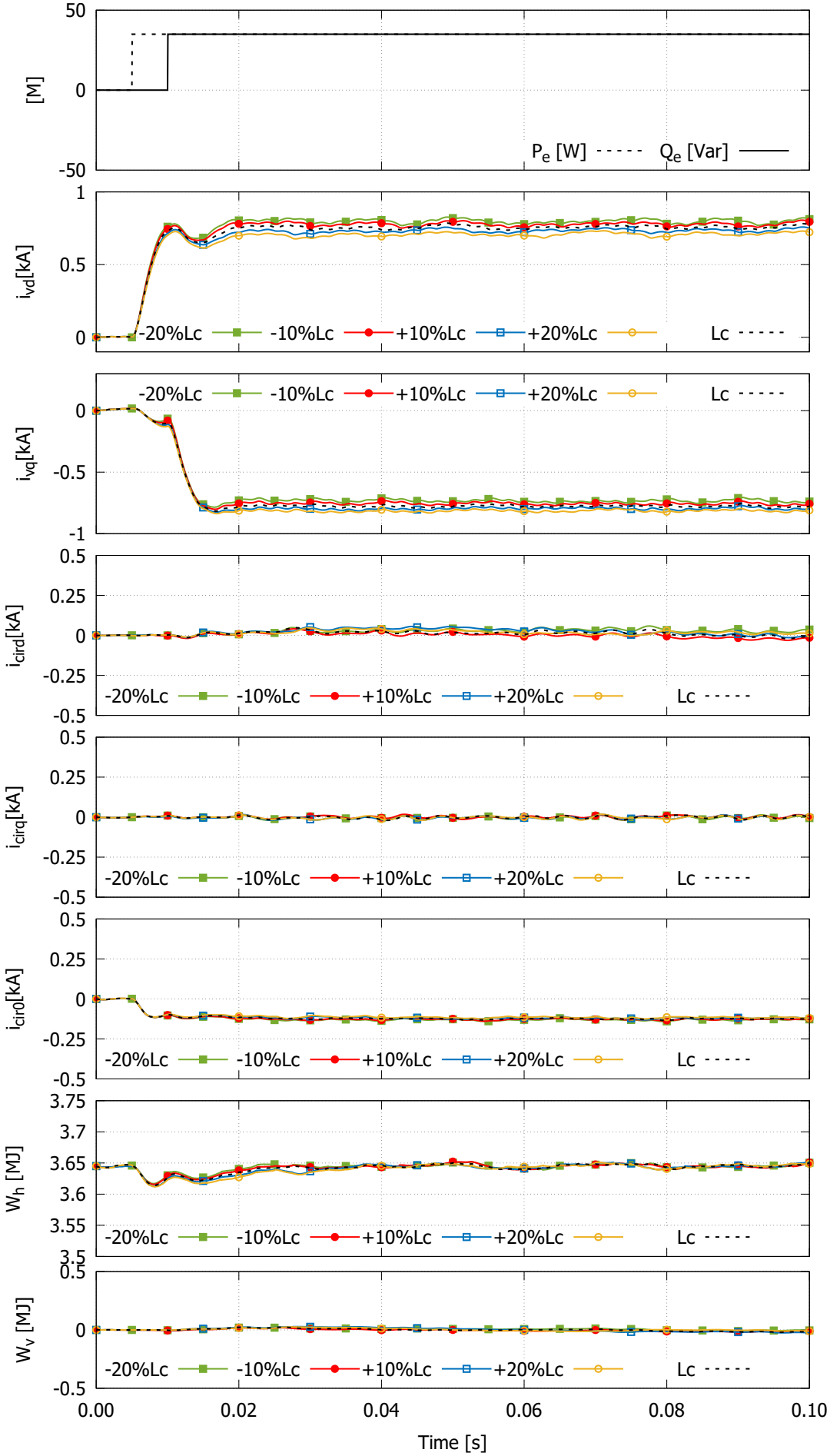

Figure 79 – States over variation of parameter C with nonlinear controller.

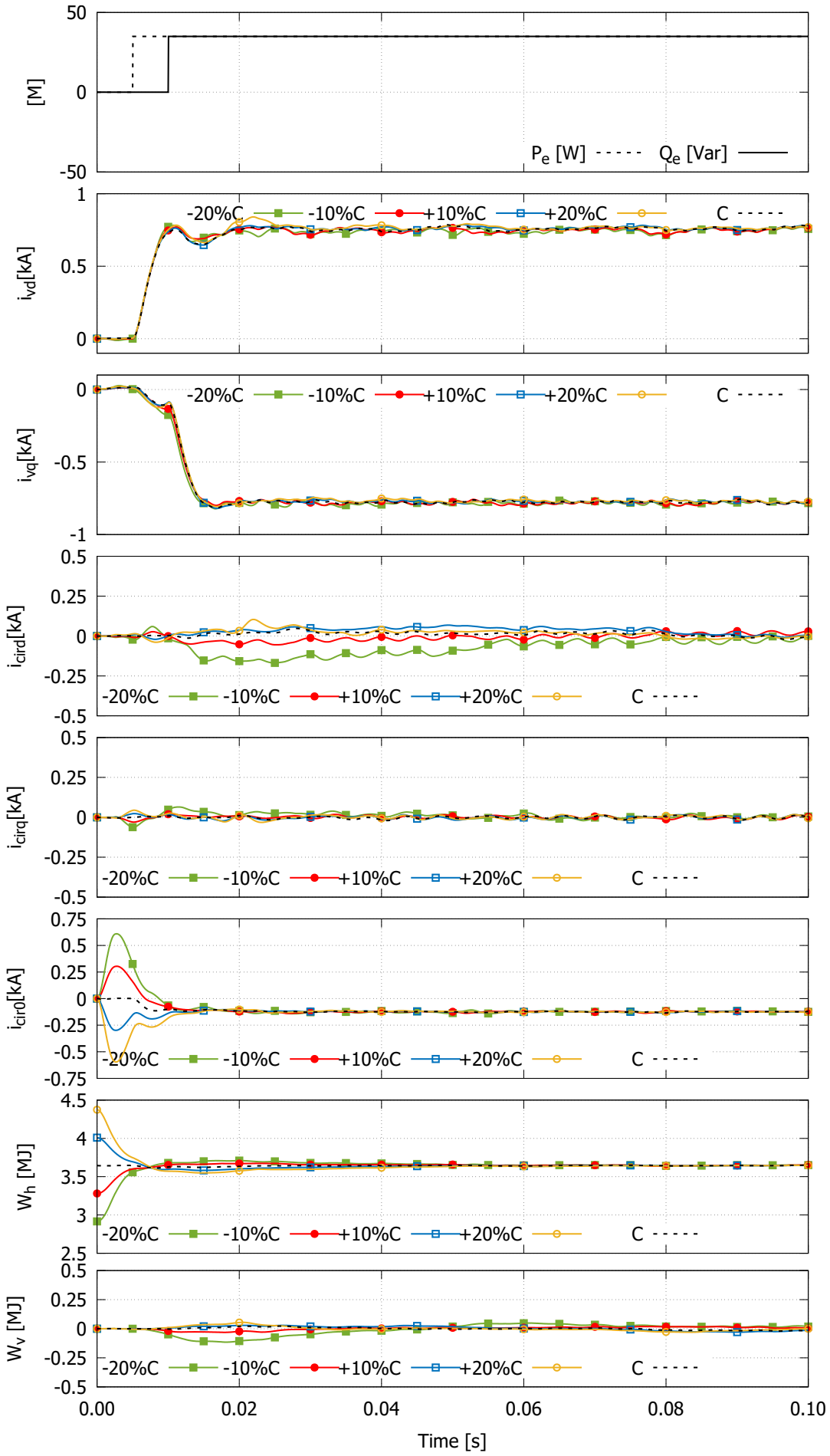

Figure 80 – Fluctuation of AC voltage at the PCC with nonlinear controller.

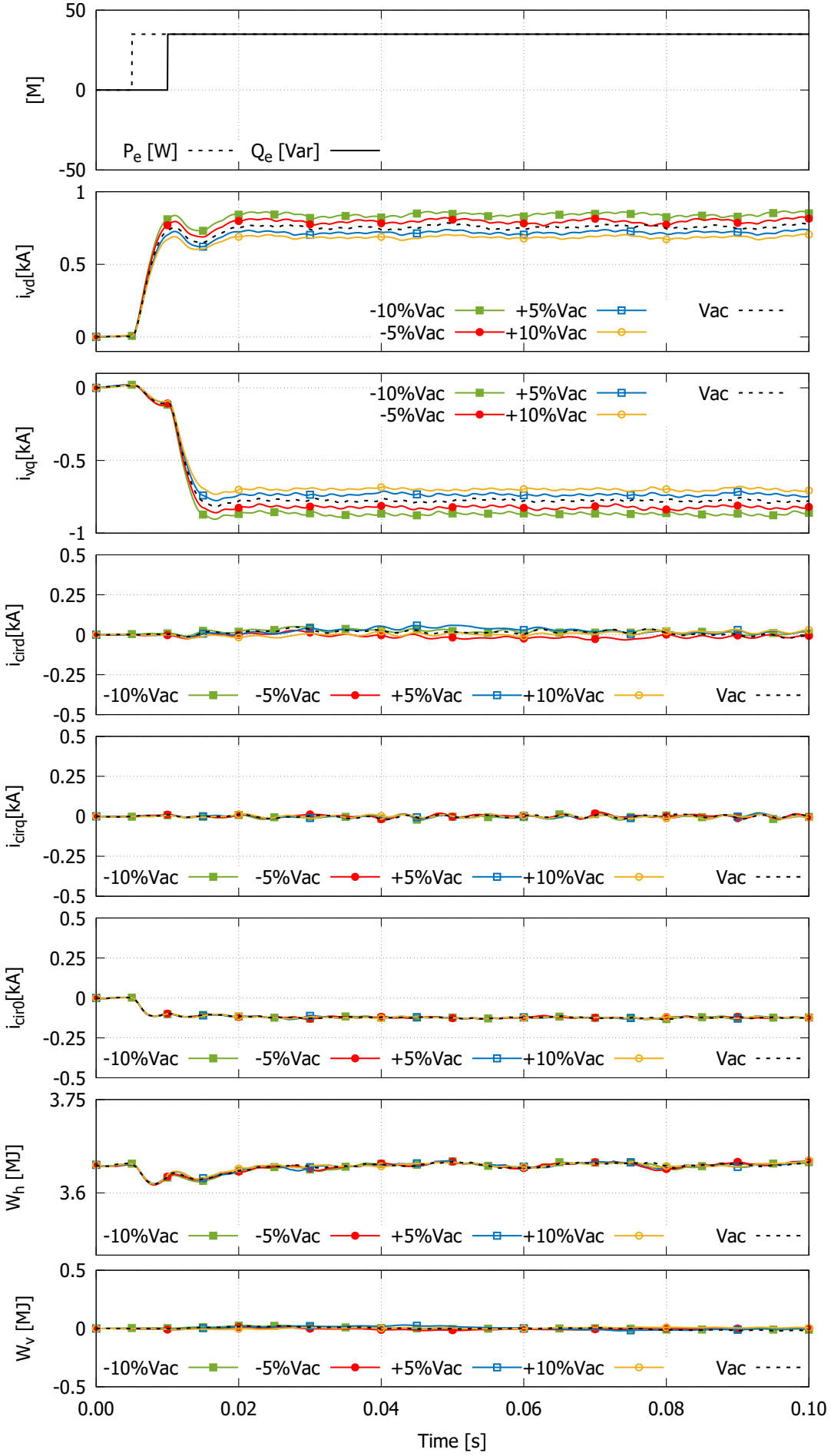

Figure 81 – DC voltage fluctuation with nonlinear controller.

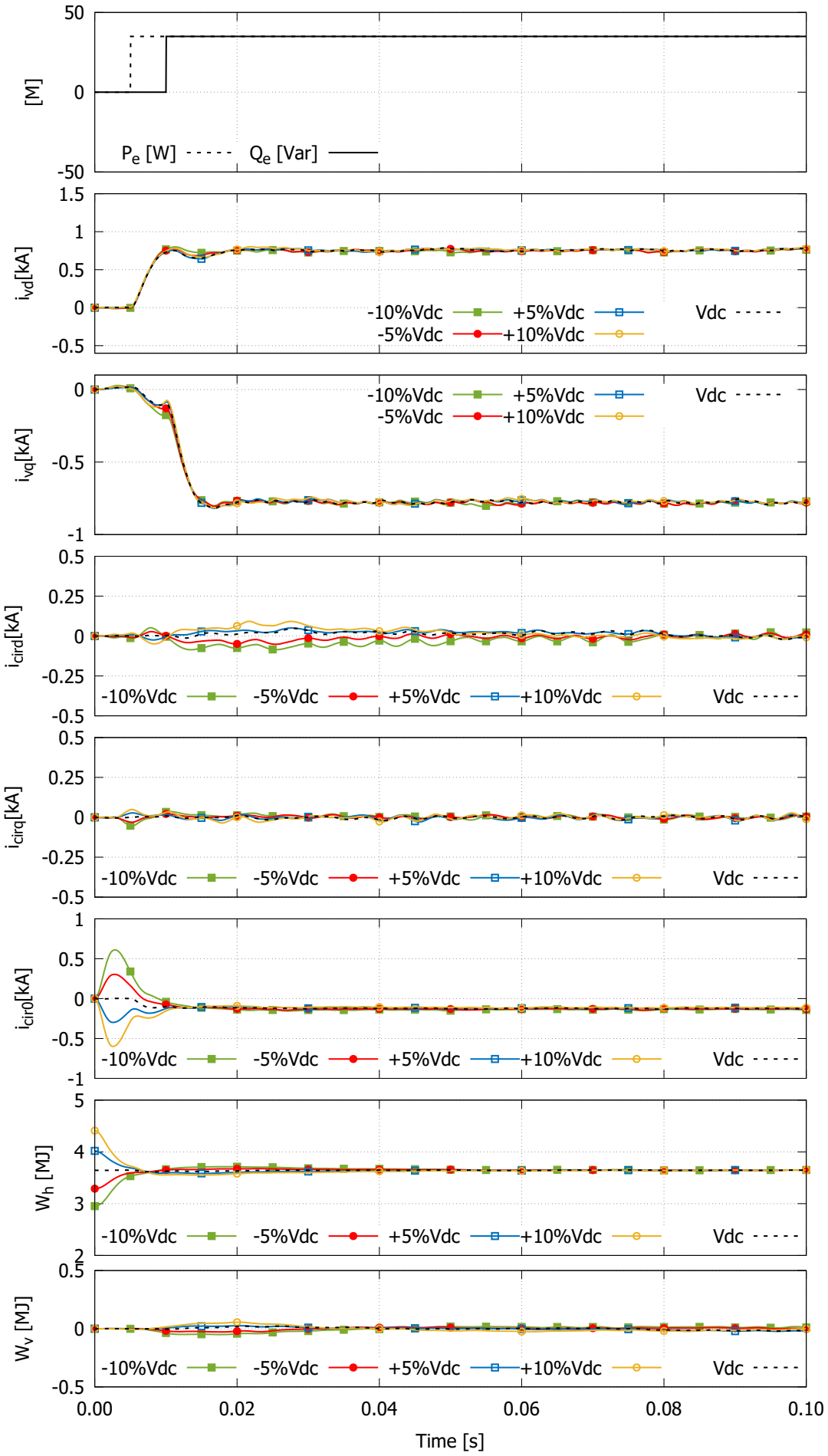

4.6 High Voltage system test with nonlinear controller

The system presented in figure 55 is simulated with the nonlinear controller. In these simulations it is used the switching model. Furthermore, a comparison with the PI controller is carry out.

Nonlinear control tuning for High Voltage system test

The same procedure as presented in section 4.5 is accomplished here. Tuning βs while αs are equal to zero, enable to set the speed of convergence of the related state variables. The $\beta_{i_{vd}}$, $\beta_{i_{vq}}$ and $\beta_{i_{cirq}}$ needed to be set ten times bigger than medium-voltage system, once a smaller gain result in a large overshoot with slow state convergence. The βs related to energy are kept the same as medium-voltage system.

$$\tau_{i_{vd}} = \frac{1}{\beta_{i_{vd}}}; \;\; \beta_{i_{vd}} = 10000 \tag{137}$$

$$\tau_{i_{vq}} = \frac{1}{\beta_{i_{vq}}}; \;\; \beta_{i_{vq}} = 10000 \tag{138}$$

$$\tau_{i_{cirq}} = \frac{1}{\beta_{i_{cirq}}}; \;\; \beta_{i_{cirq}} = 10000 \tag{139}$$

$$\tau_{W_h} = \frac{1}{\beta_{W_h}}; \;\; \beta_{W_h} = 50 \tag{140}$$

$$\tau_{W_v} = \frac{1}{\beta_{W_v}}; \;\; \beta_{W_v} = 50 \tag{141}$$

Adjusting αs, response of state variables i_{vd} and i_{vq} are improved as shows figure 82. It is possible to verify i_{vd} and i_{vq} convergence for $\alpha_{i_{vd}}$ $\alpha_{i_{vq}}$ equal to 500, 1000 and 2000. The speed of convergence is improved by the tuning. The intermediate value (1000) is chosen for $\alpha_{i_{vd}}$ and $\alpha_{i_{vq}}$ in the high voltage system test.

As in the medium-voltage, in the high voltage system the state variable i_{cirq} track its reference just by the tuning of $\beta_{i_{cirq}}$, and there is a reduction of noise when $\alpha_{i_{cirq}}$ increase. Also, state variables i_{cird} and i_{cir0}, are directly tuned by their αs. For $\alpha_{i_{cird}}$ equals to 1000 and $\alpha_{i_{cir0}}$ equals to 2000, there is no steady-state error for these states. The β_{W_v} and β_{W_h} are both tuned to 50, and both W_h and W_v present no steady-state error and high speed of convergence. Their respective αs are set to be equal to 0.2 reducing the signals' noise.

The following results of high voltage system, use the parameters summarised in table 5.

Figure 82 – Response of state i_{vd} and i_{vq} over tuning of αs.

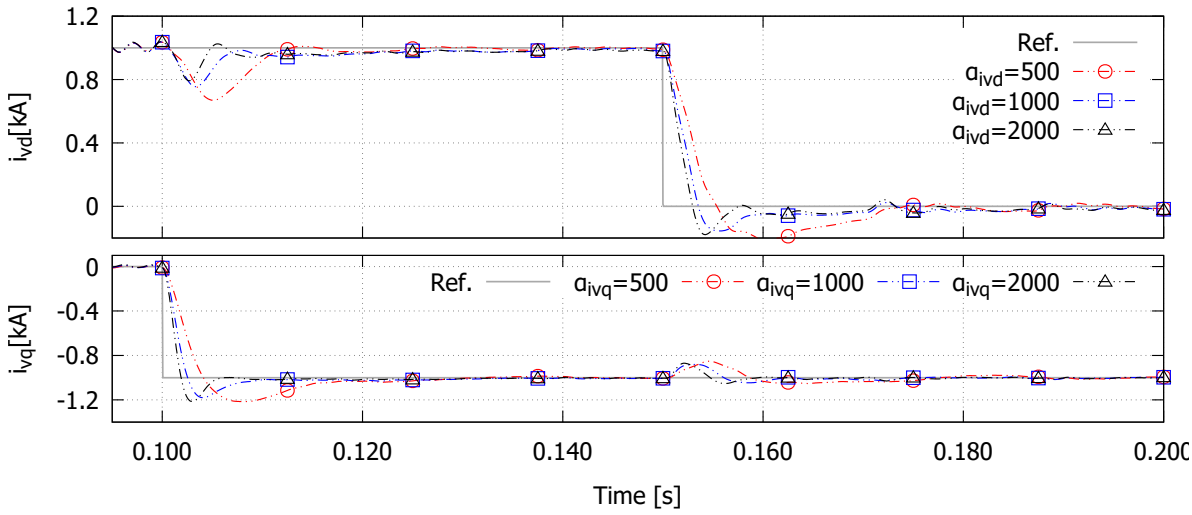

Source: Author

Table 5 – Parameters of simulated high-voltage system and nonlinear control gains.

Parameter	Value	Parameter	Value
S_{MMC}	$450\ MVA$	$\beta_{i_{vdq}}$	$1E4$
V_{DC}	$400\ kV$	$\beta_{i_{cirq}}$	$1E4$
V_{AC}	$210\ kV$	β_{Wh}	50
C_{SM}	$3\ mF$	β_{Wv}	50
L	$40\ mH$	$\alpha_{i_{vdq}}$	$1E3$
L_c	$12\ mH$	$\alpha_{i_{cird}}$	$1E3$
R_c	$1\ \Omega$	$\alpha_{i_{cirq}}$	$1E3$
R	$0.5\ \Omega$	$\alpha_{i_{cir0}}$	$2E4$
N	20	α_{W_h}	0.2
Freq	$60\ Hz$	α_{W_v}	0.2

4.6.1 Comparison of nonlinear and PI controllers

A detailed switching model of the three-phase MMC converter with 41 levels, depicted in figure 10 with the proposed nonlinear control and the PI, is tested using the Matlab Simscape Electrical environment. The system's parameters are presented in table 3 and table 5, and the results are shown in the dq reference frame.

The performance of the proposed nonlinear control strategy for the MMC was first evaluated through step changes of active and reactive power (P_e and Q_e). All state variables are shown in Figure (83), over the power steps. The system is initialized, transmitting zero power.

The considered controllers, nonlinear and PI, provide to the states i_{cird} and i_{cir0} different references. So, for those two states it is written *Ref. Non* to indicate Nonlinear controller's reference and *Ref. PI* to identify the PI's references. Remaining states have same references, indicated as *Ref.*.

At $t = 0.01\ s$, there is an active power step of 70% of the nominal power, see first graphic. It is possible to see a fast response for both controllers, on either output P_e and state i_{vd} on second graphic. The active power step generates an overshoot on state i_{vq} (third graphic). In the same moment, i_{cir0} (reference and state together) react to transmit the equivalent DC power. For the nonlinear controller, the transient unbalance between AC and DC power (directly related to i_{vd} and i_{cir0}) causes less than 1% of increase in the total energy (W_h at the 7^{th} graphic) until the system regulates the input and output power, which takes $20ms$.

Concerning PI controller, the increase in the total energy is slightly larger in comparison with the nonlinear one. However there is a clear compromise between time response and control gains.

Each change in P_e or Q_e implies in a new operating point. On these operating points, PI and nonlinear perform similarly. Then, at $t = 0.40\ s$, reactive power become negative, followed by active power, which became positive at $t = 0.45\ s$. As a result of the change in the power flow directions, both controllers present oscillations on state variables, PI larger than nonlinear.

At $t = 0.10\ s$ there is a reactive power step. The directly related state i_{vq} sets to the new reference in less than $10\ ms$. Remaining states are not affected, and the system can provide the required reactive power.

In figure 84 the control performance over free-dynamic state variables is illustrated. The control of converter's energy opens some possibilities concerning very fast ancillary grid services, that will be focused on future research.

Figure 84 shows the system performance over converter energy changes. An operating point was set at $t = 0.01\ s$, where the active and the reactive power supply $70\ \%$ of the nominal power, respecting the capability curve (see 1^{st} graphic). At 8^{th} graphic, on $t = 0.1\ s$, the reference for the total energy is increased by 10% of the nominal value. One can see that control drives the concerned states, in order to track the new reference in less than $20ms$. It is important to remark that the reference $i^*_{cir,0}$ controls W_h, and at the 5^{th} graph it can be seen that the reference value is accurately tracked by the circulating current.

It is possible to identify a deviation at i_{cir0} related to changes on W_h. Additionally, an overshoot on i_{cird} and i_{cirq}, which match the steps on balancing energy. That overshoot is necessary to redistribute the energy between the SMs.

At $t = 0.40\ s$ total energy is reduced by 10%. It is possible to verify that this condition compromises the entire converter operation once state variables start to oscillate around their references. Decrease total energy may imply in the SM capacitor's voltage, which has a crucial role in the entire converter operations. These conditions may need to be further analyzed to be useful for ancillary services.

Finally, step changes of $\pm 10\%$ of the nominal total stored energy is applied to the reference of W_v (energy difference between the upper and lower arms), respectively at $t = 0.65\ s$ and $t = 0.95\ s$. It can be seen that the controller is able to track the reference, presenting damped oscillations that settle in $70ms$.

Comparing with the PI, the proposed nonlinear controller presented a similar response regarding the performed step tests for total energy and energy difference.

It is important to remark that the desired energy difference between upper and lower arms in normal operation is zero. This step test is used to demonstrate that the proposed controller has the capability of accurately controlling the energy difference independent of the prescribed value, what can be important in unbalanced conditions.

Figure 85 shows the controller inputs for the scenario presented on figure 83. Each change on power (P_e or Q_e) results on a overshoot at the controller inputs, PI larger than nonlinear. They are considered acceptable.

Figure 86 shows the controller inputs for the scenario presented on figure 84. These results were produced for W_h and W_v step scenario presented above. Both controllers presenting a suitable control effort.

Figure 83 – Four-quadrant operation of the high voltage system with the nonlinear and PI controller.

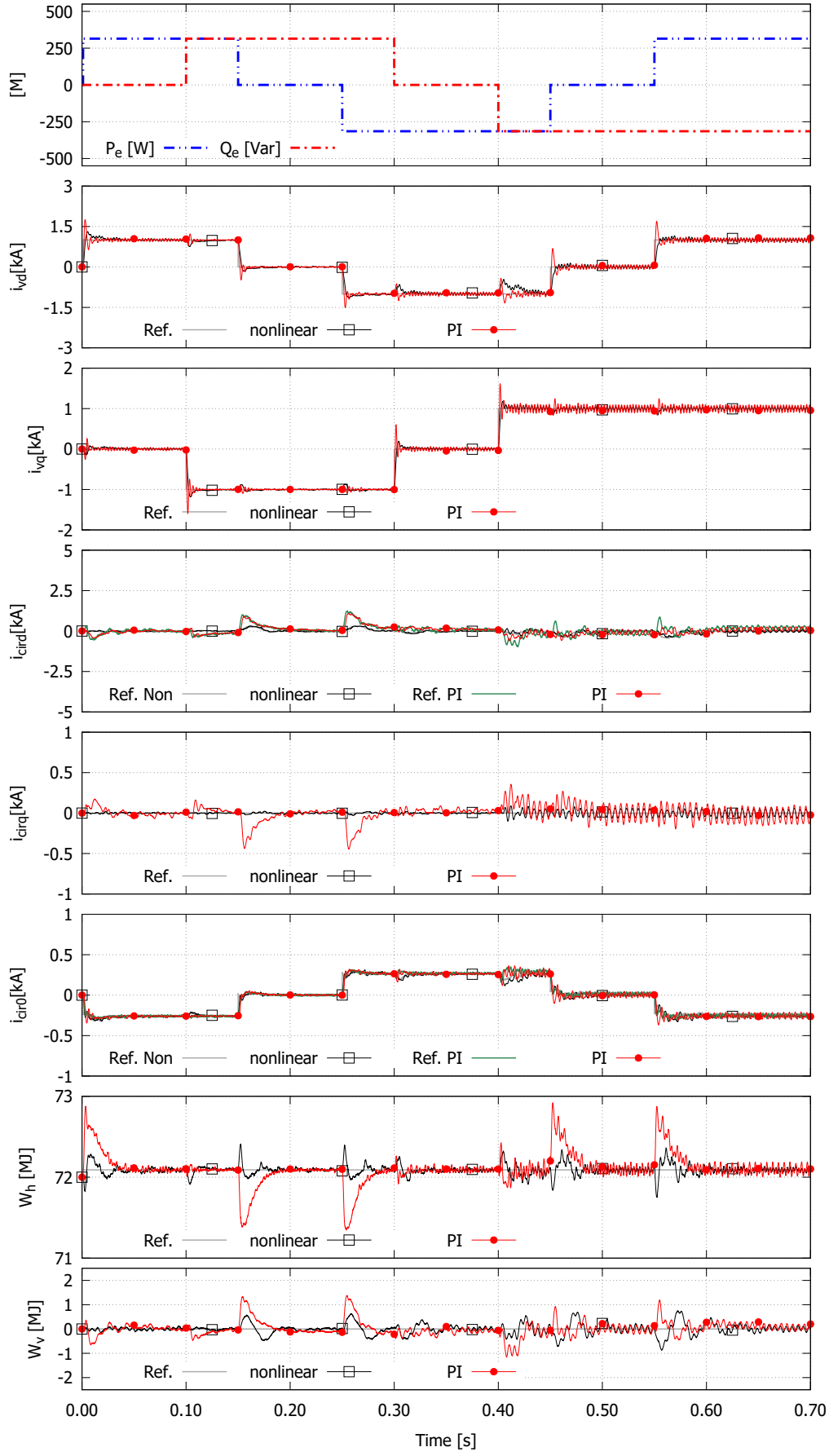

Figure 84 – State variables response over changes on energy.

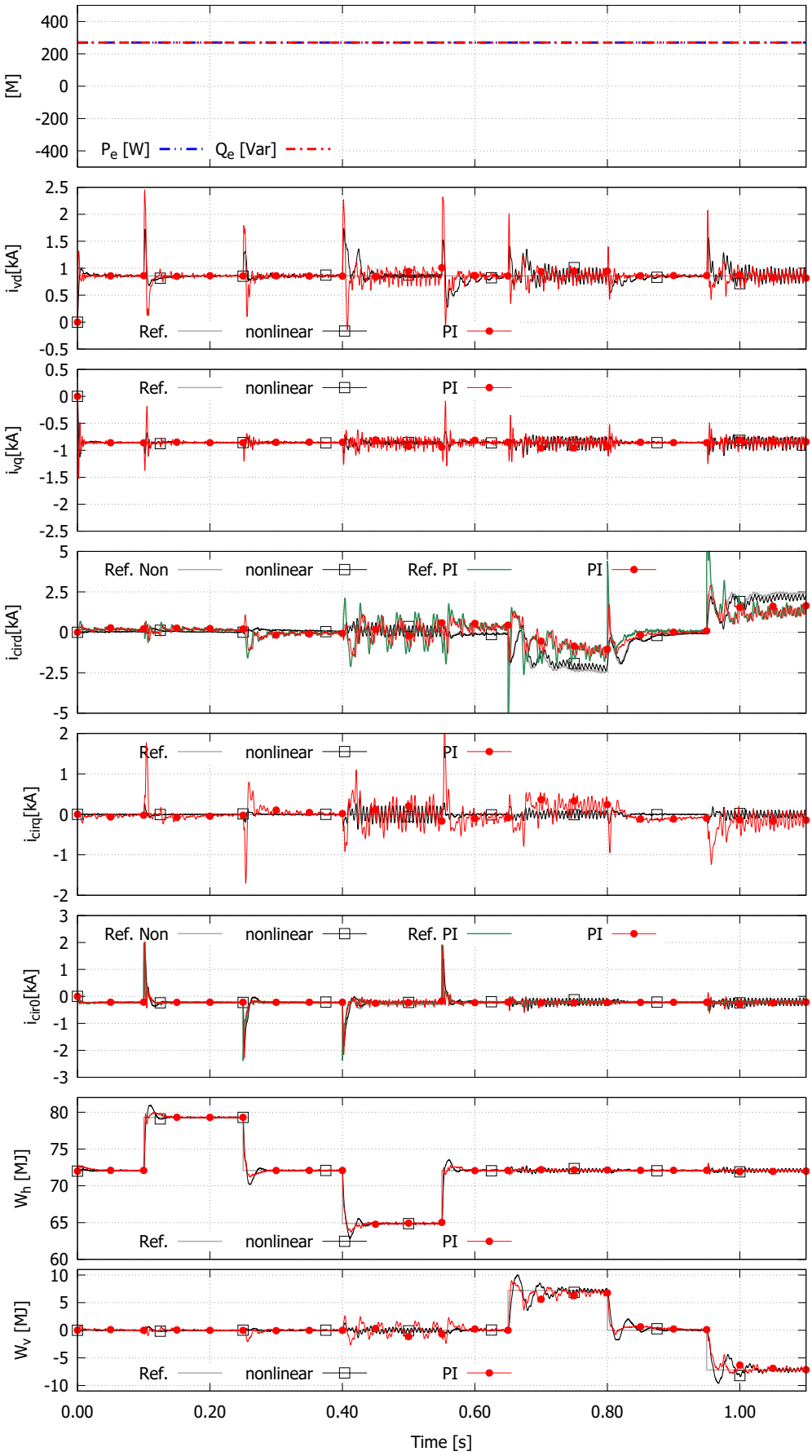

Figure 85 – Control efforts over power changes.

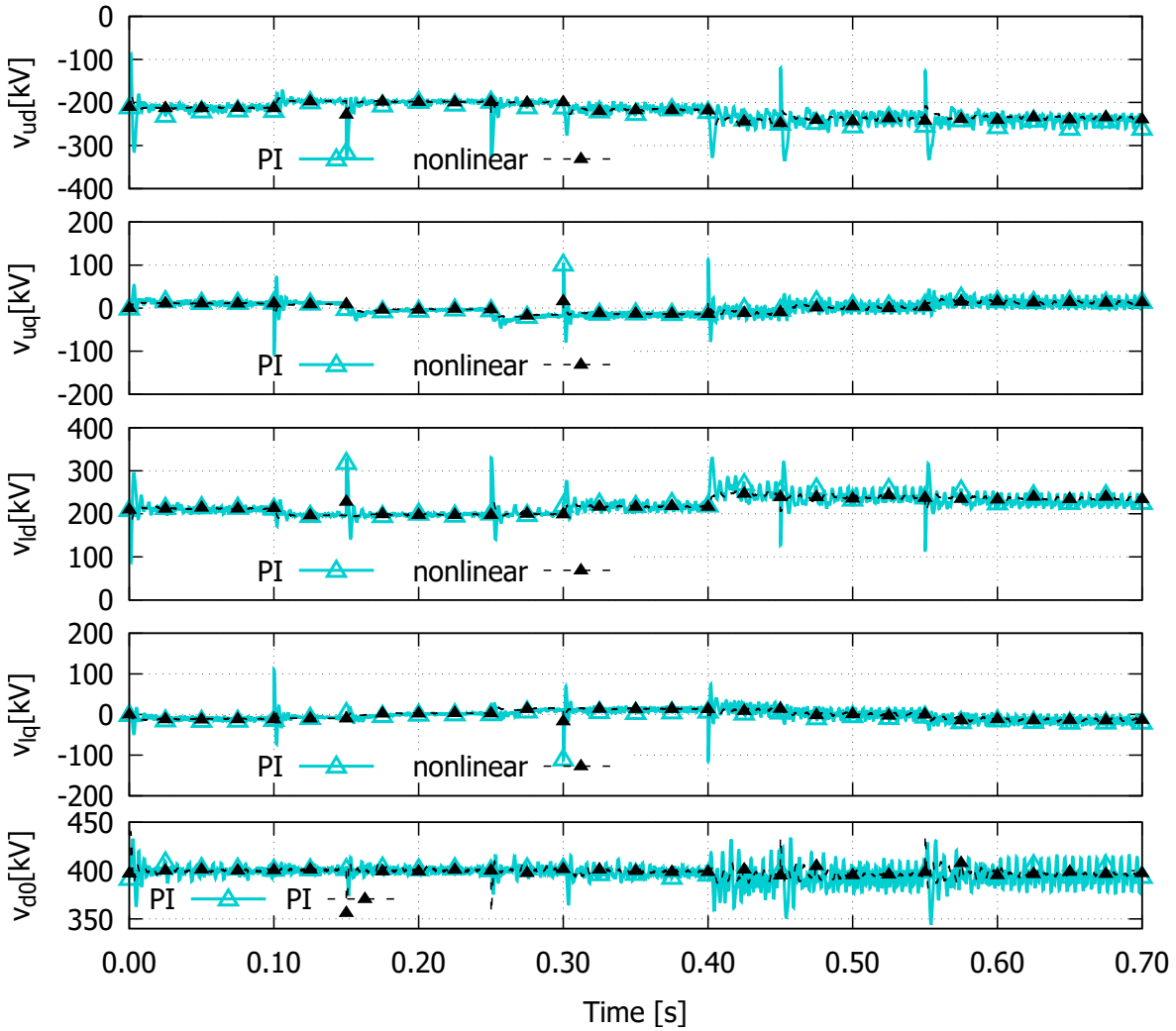

Source: Author

Figure 86 – Control efforts over energy changes.

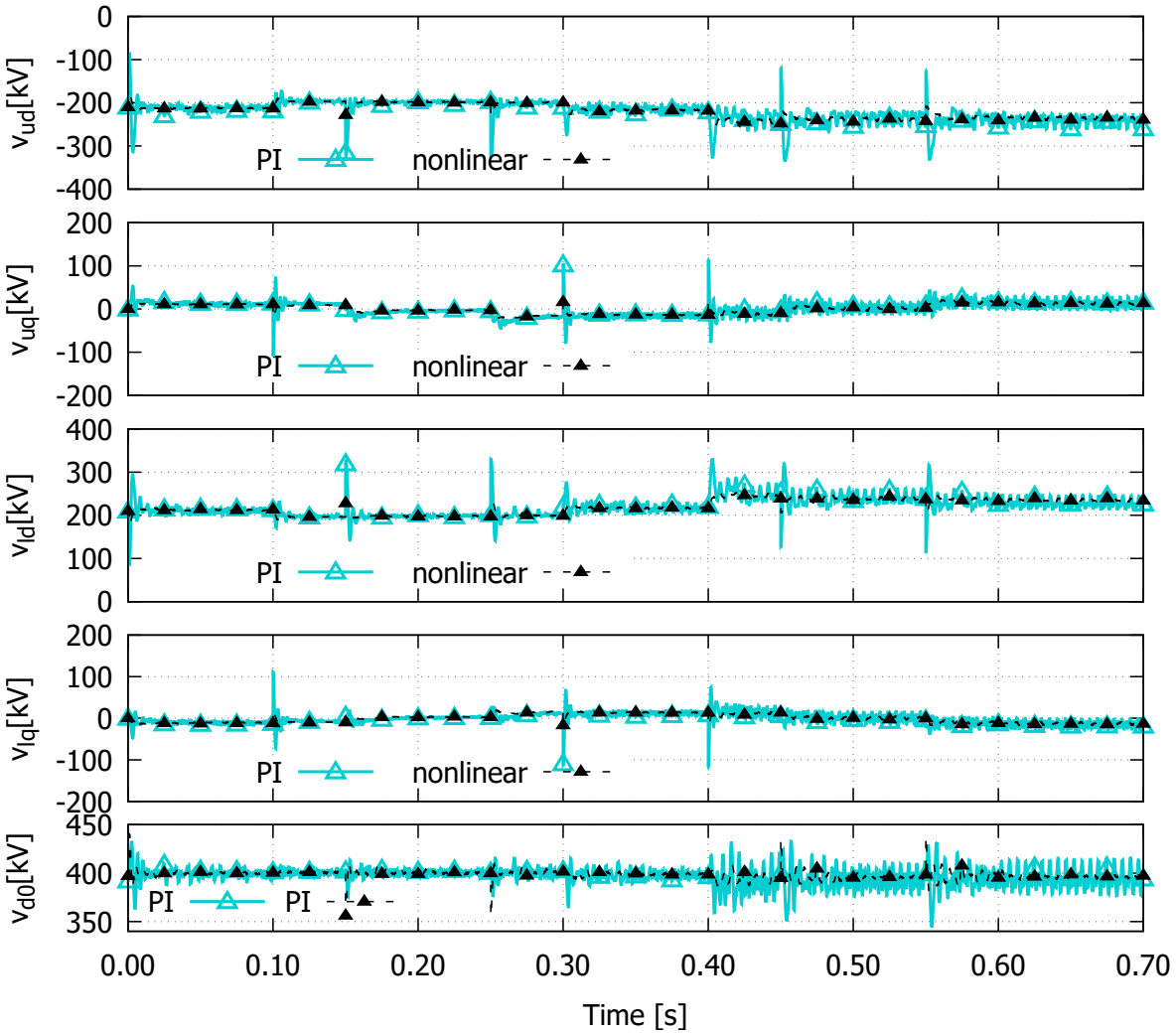

Source: Author

Nonlinear control management of internal dynamics

As mentioned in chapter 1, there are two main challenges concerning control MMC converters: circulating current management and voltage balancing between arm's capacitors. This section shows how nonlinear controller performs over these challenges.

An operating point is set as $P_e = 315\ MW$ and $Q_e = 315\ MVar$ at $0.05\ s$, and an equal share of energy in the arms is obtained at around $t = 450\ ms$, as shown in figure 87. It is the same convergence speed accomplished by PI controller showed in the previous chapter, figure 87.

In figure 88, nonlinear controller accomplished the control of total energy in upper (lower) arms. In comparison with PI controller performance (see figure 61), the overshoot during the power transient is lower for nonlinear with same convergence speed.

Concerning circulating currents, their performance in dq0 reference frame with the nonlinear controller is presented in figure 89. By this result it is possible to conclude that nonlinear controller performs well over the circulating currents, even during changes on the operating point, and have negligible overshoot in comparison with PI controller in figure 46.

Figure 90 displays the capacitors' voltage attained by nonlinear controller, i.e. the voltage of the twenty SMs in each arm. The figure shows that capacitors' voltages are well balanced and the detail in time between 0.82 s to 0.88 s displays that the sorting algorithm properly switch the SMs. They change the voltage level once per cycle, and are bypassed (keep the voltage for a while). Finally, it is possible to conclude that the nonlinear controller proposed in this thesis can properly balance capacitor's voltage.

Figure 87 – Share of energy in each arm with the nonlinear controller.

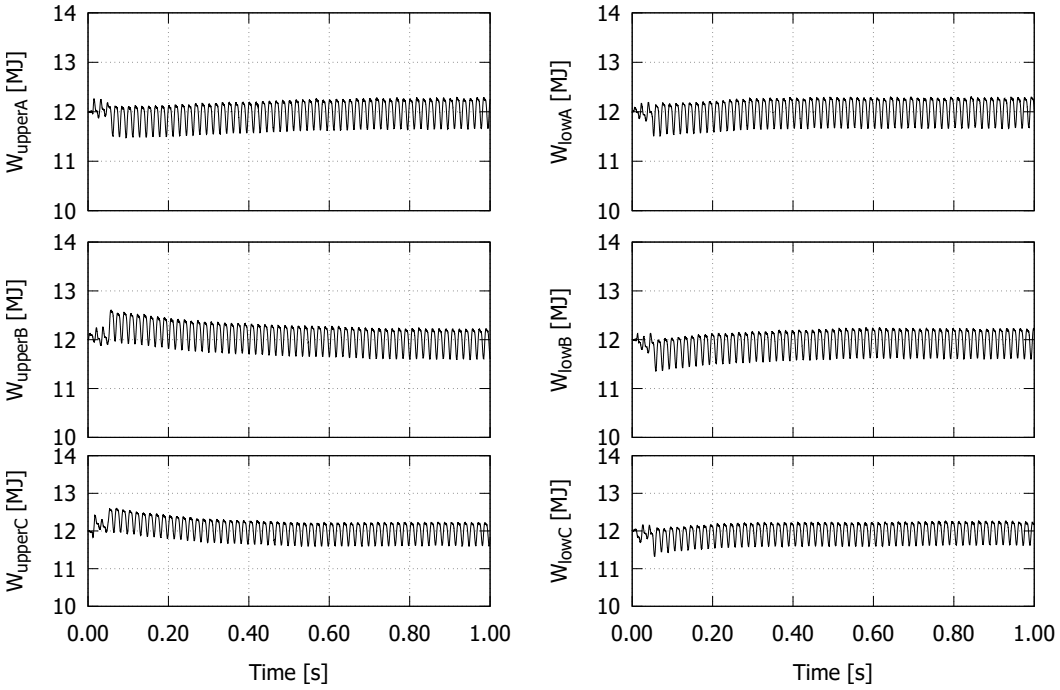

Figure 88 – Total energy in the three upper arms (W_u) and at the three lower arms (W_l).

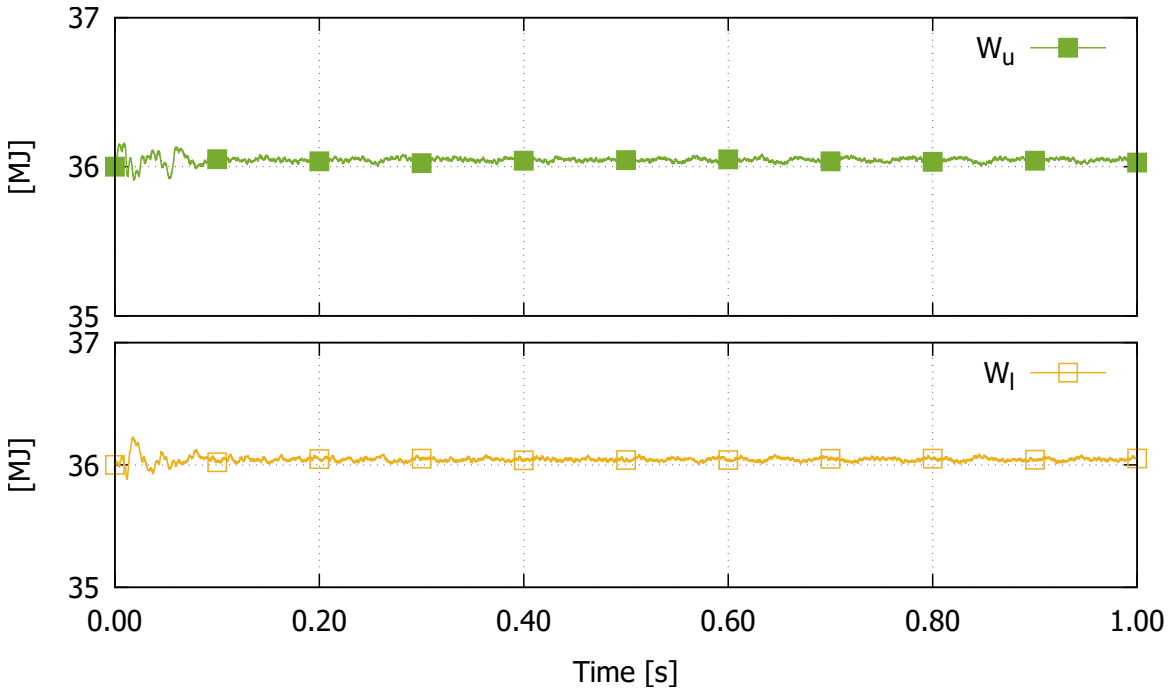

Figure 89 – Double-fundamental frequency component of circulating currents at high voltage switching model with the nonlinear controller.

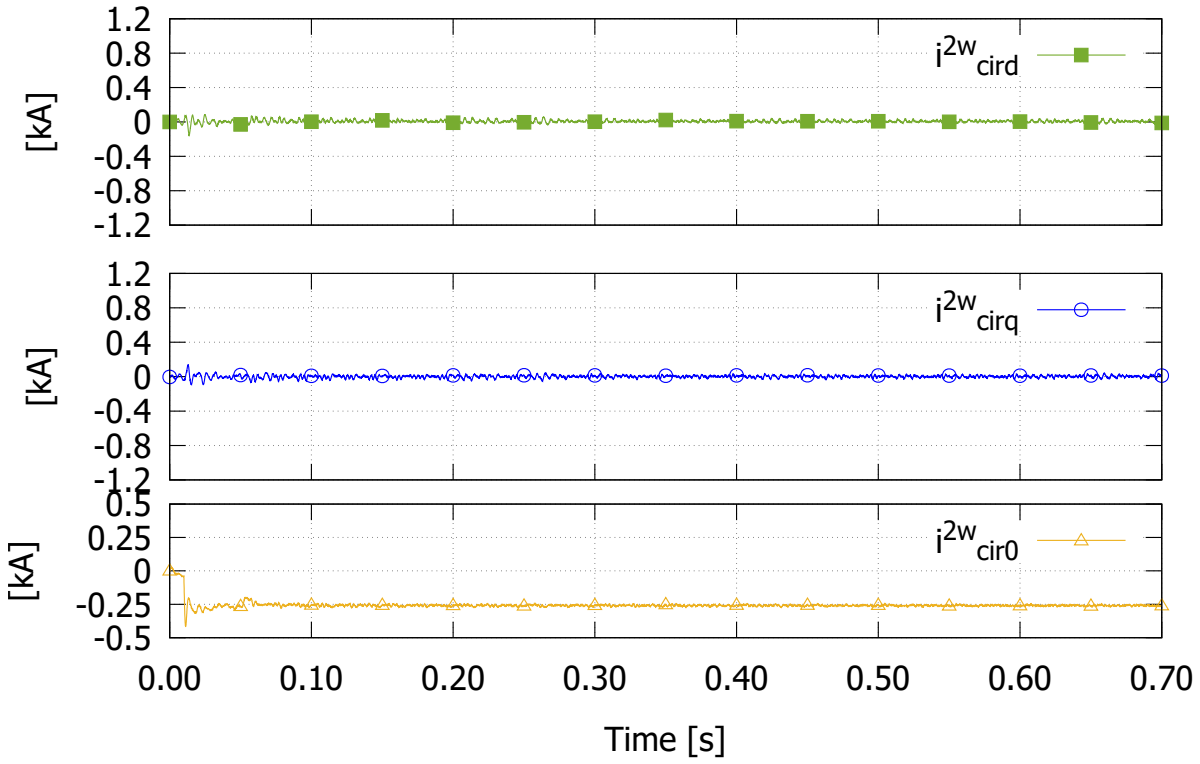

Figure 90 – SMs' capacitor voltage per arm and equivalent detail in time, accomplished by nonlinear controller.

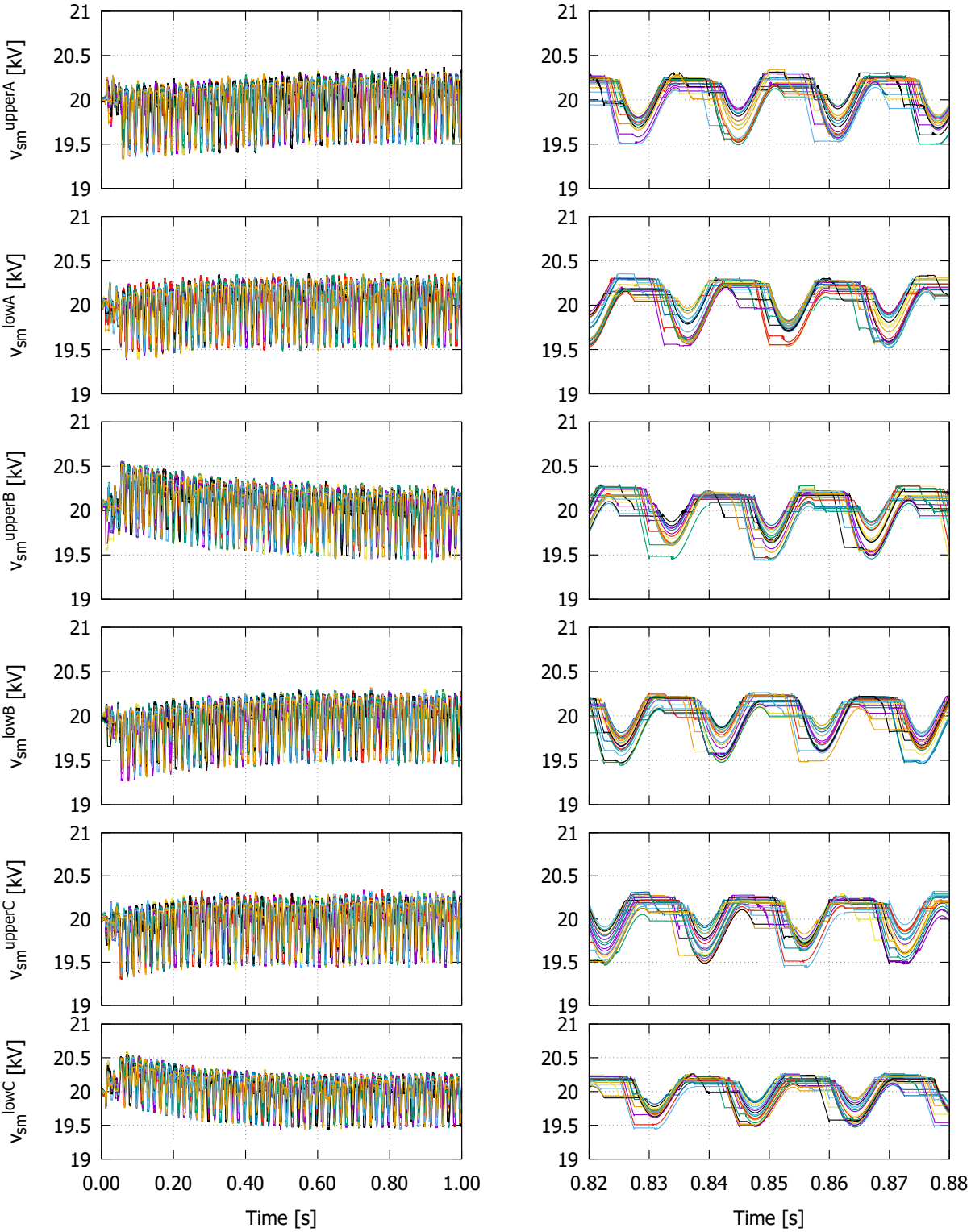

Source: Author

4.6.2 Robustness over parameters' uncertainties and voltage fluctuation for high-voltage system with nonlinear controller

Robustness

This section analyses the control performance under parameters' uncertainties, as first presented in section 3.4.2. In the present simulation scenarios, parameters (R, R_c, L, L_c and C_{SM}) change one at a time from their nominal value to $\pm 10\%$ and $\pm 20\%$. The active and reactive power changes at $t = 0.005\ s$ and $t = 0.01\ s$, respectively.

In figure 91 is presented a variation in the arm equivalent resistance R, and in figure 92 is presented a variation in AC side resistance. In both cases, the controller is robust over parameter variations. In comparison with the test showed in section 3.5.1, it is possible to see that both PI and nonlinear performs well under parameters' uncertainties.

In figure 93 and figure 94 there are variations on arms' inductance L and AC side inductance L_c. Both results show tiny deviations during step transients, however it shows high convergence speed for all state variables.

Finally, the controller was more sensitive to changes in SM capacitance, as shown in Figure 95. The variations in C were $pm10$ and $pm5$. The state variable i_{vd}, $2^n d$ graphic, has a lower speed of convergence and a larger overshoot. State variables i_{cird} and i_{cirq} have an oscillating response for an increase C of $+5\%$ and $+10\%$, and slower response for the cases of decreasing C of -5% and -10%. As well, the total energy (W_v) presents the same performance. On the other hand, i_{cir0} and W_h are well controlled to their desired references.

Voltage fluctuation

The performance of the control for voltage's fluctuation is analyzed in this section. P_e and Q_e were settled to 70% of the nominal power, respectively at $t = 0.005\ s$ and $t = 0.01\ s$.

Figure 96 shows system's response when voltage at the PCC assumes $\pm 10\%$ and $\pm 5\%$ one at a time. The convergence speed of state variables decreases for the increase in voltage $+10\%$ and $+5\%$. However, they track their reference in a steady-state. On the other hand, circulating currents dq, followed by an energy balancing W_h, present an oscillatory response.

In figure 97 states are affected by changes in V_{DC}. States have overshoot and a high speed of convergence.

Moreover, a fluctuation in the AC and DC nominal voltages was performed, and nonlinear control drives, in most cases, the states to their desired value.

Figure 91 – The system state over variation of parameter R.

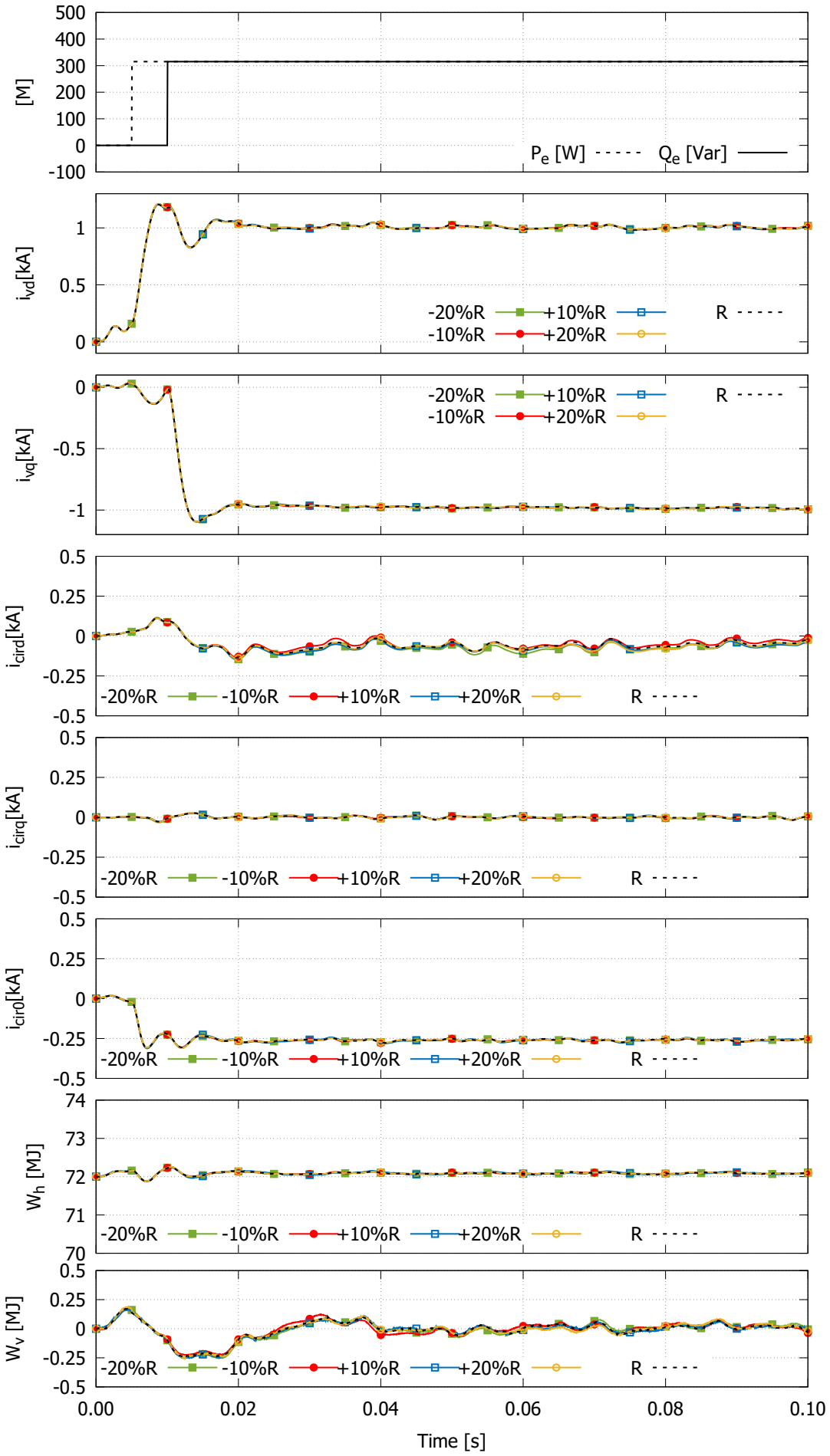

Figure 92 – States over variation of parameter R_c.

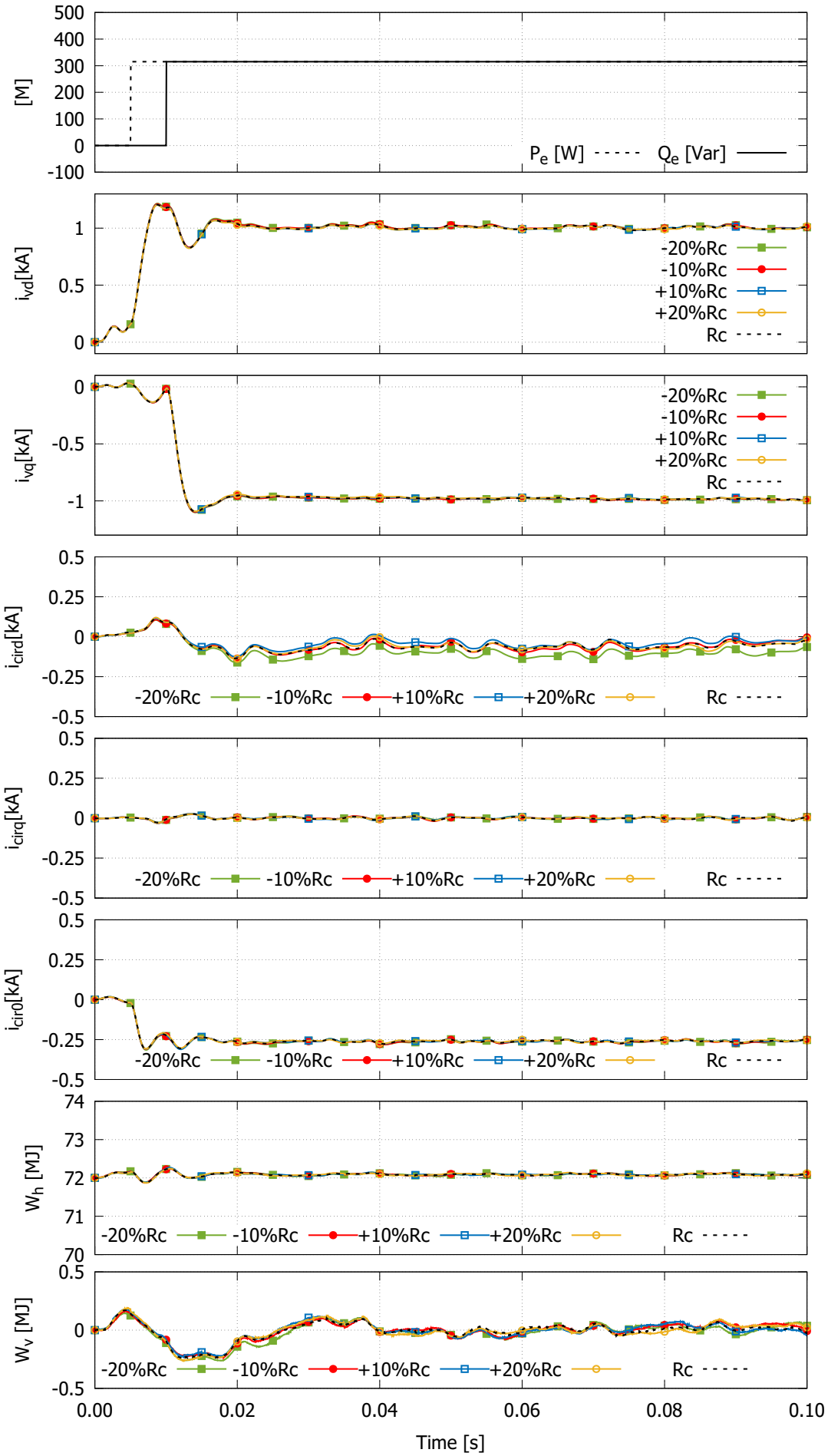

Figure 93 – States over variation of parameter L.

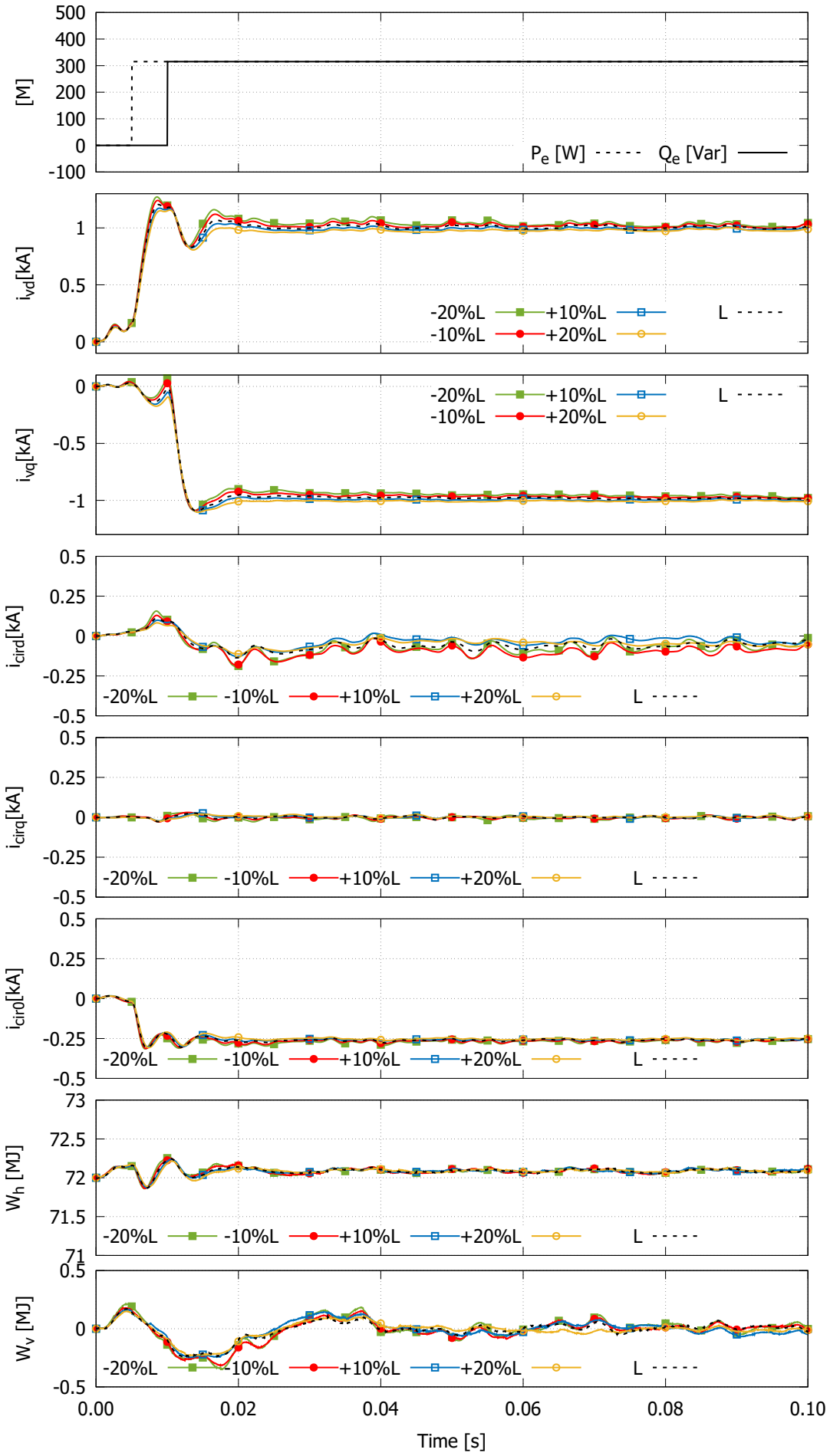

Figure 94 – States over variation of parameter L_c.

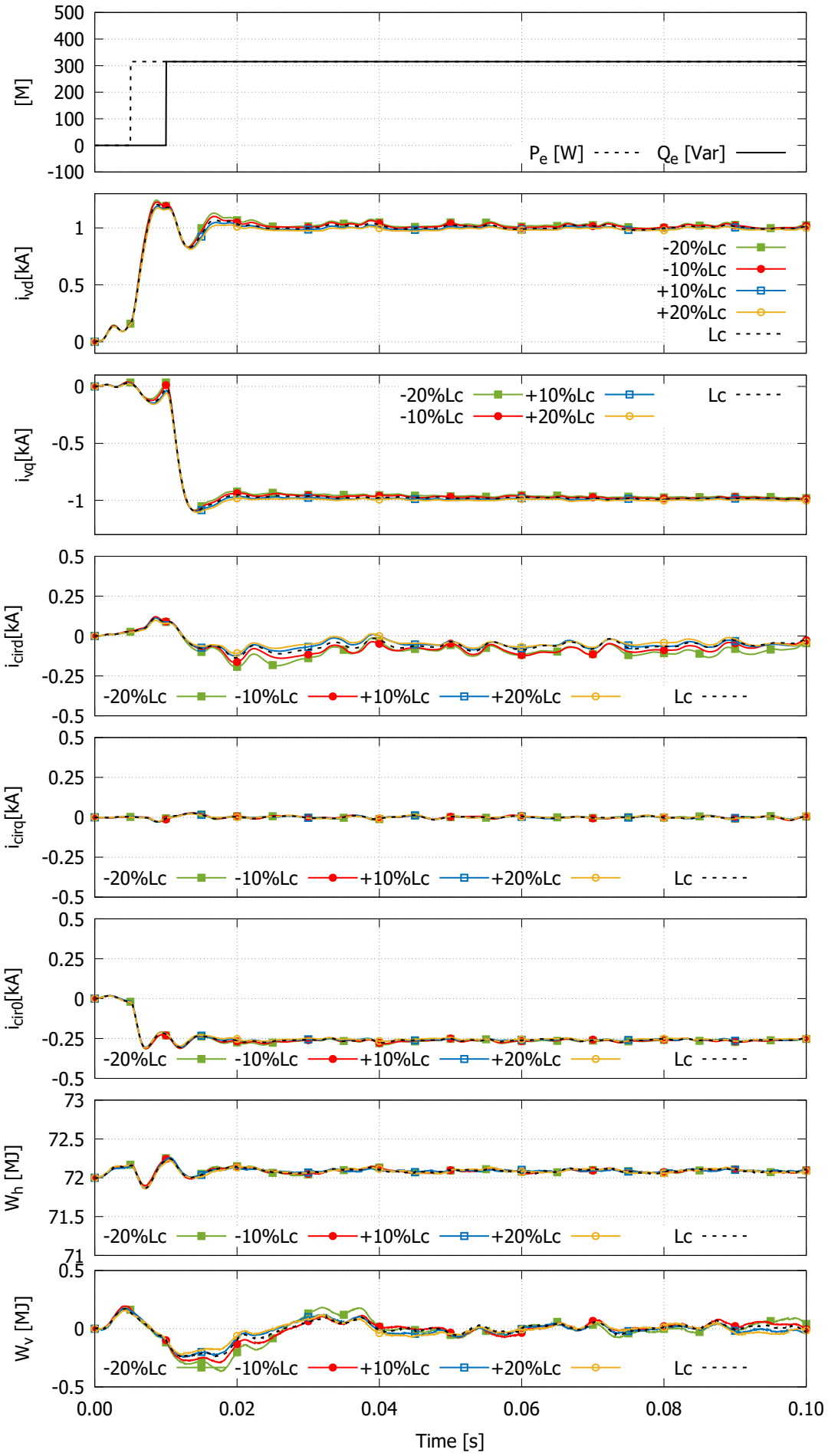

Figure 95 – States over variation of parameter C.

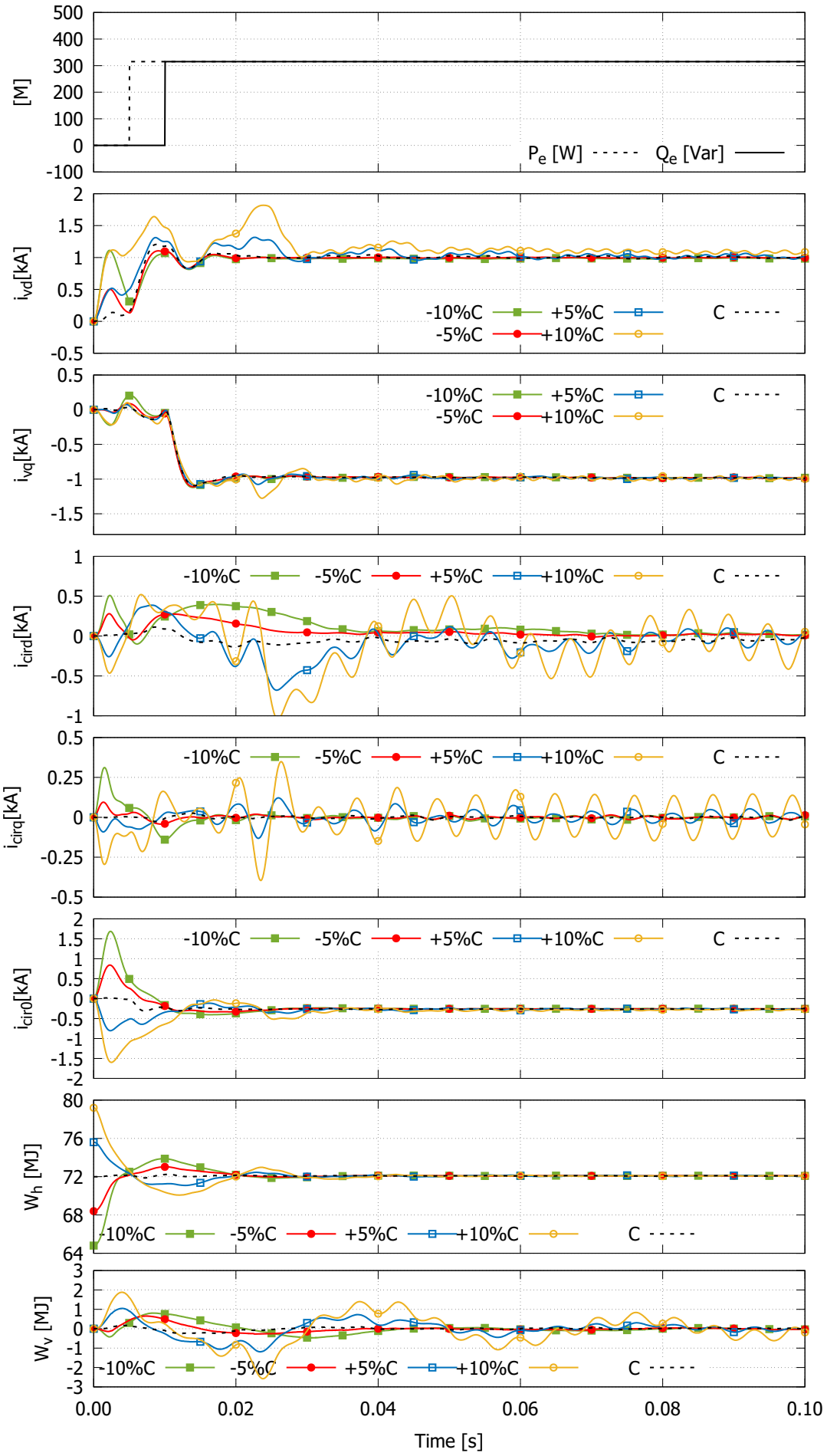

Figure 96 – Voltage in the PCC changes $\pm 10\%$ and $\pm 5\%$ from the nominal value.

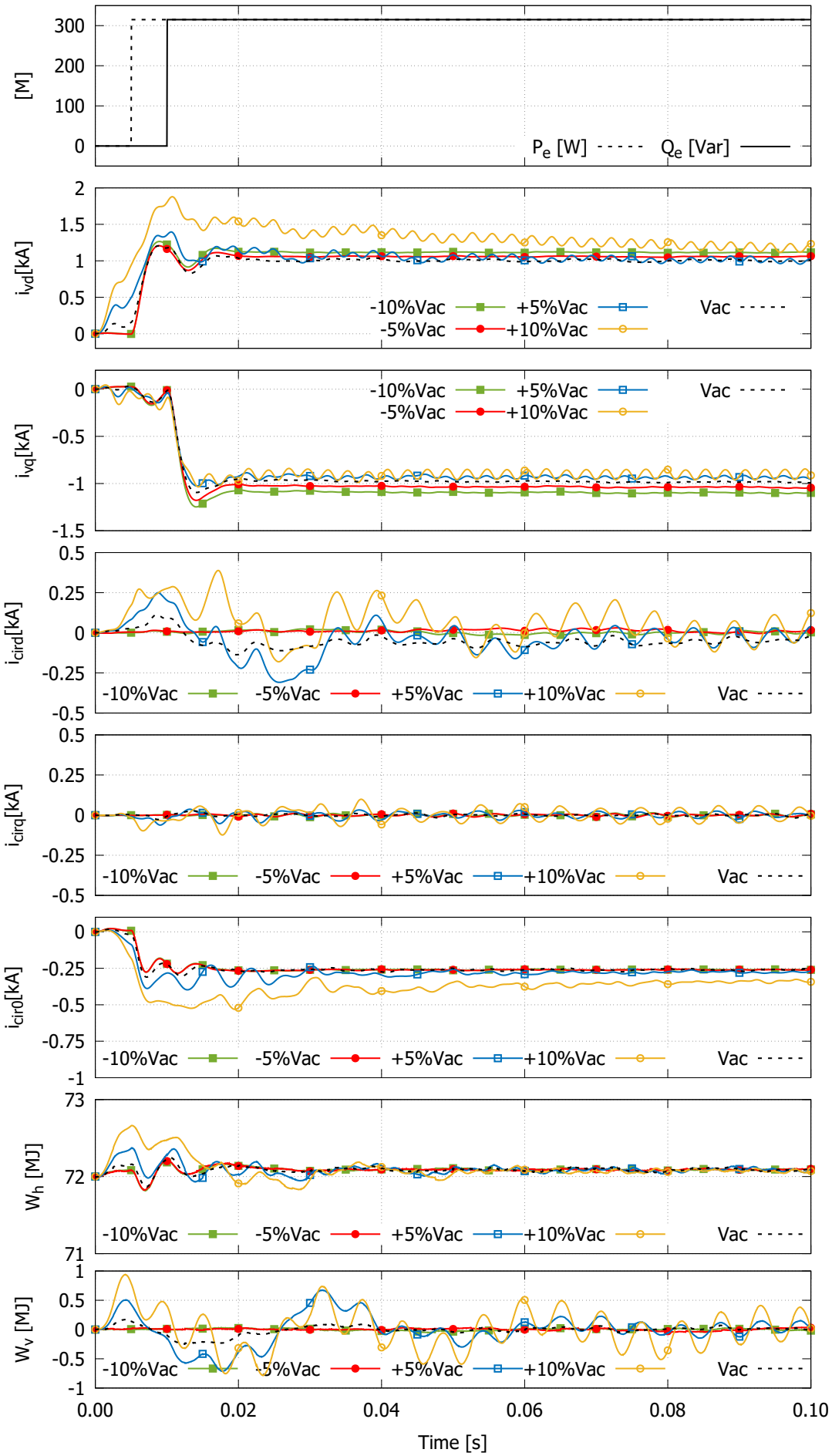

Figure 97 – DC voltage changes $\pm 10\%$ and $\pm 5\%$ from the nominal value.

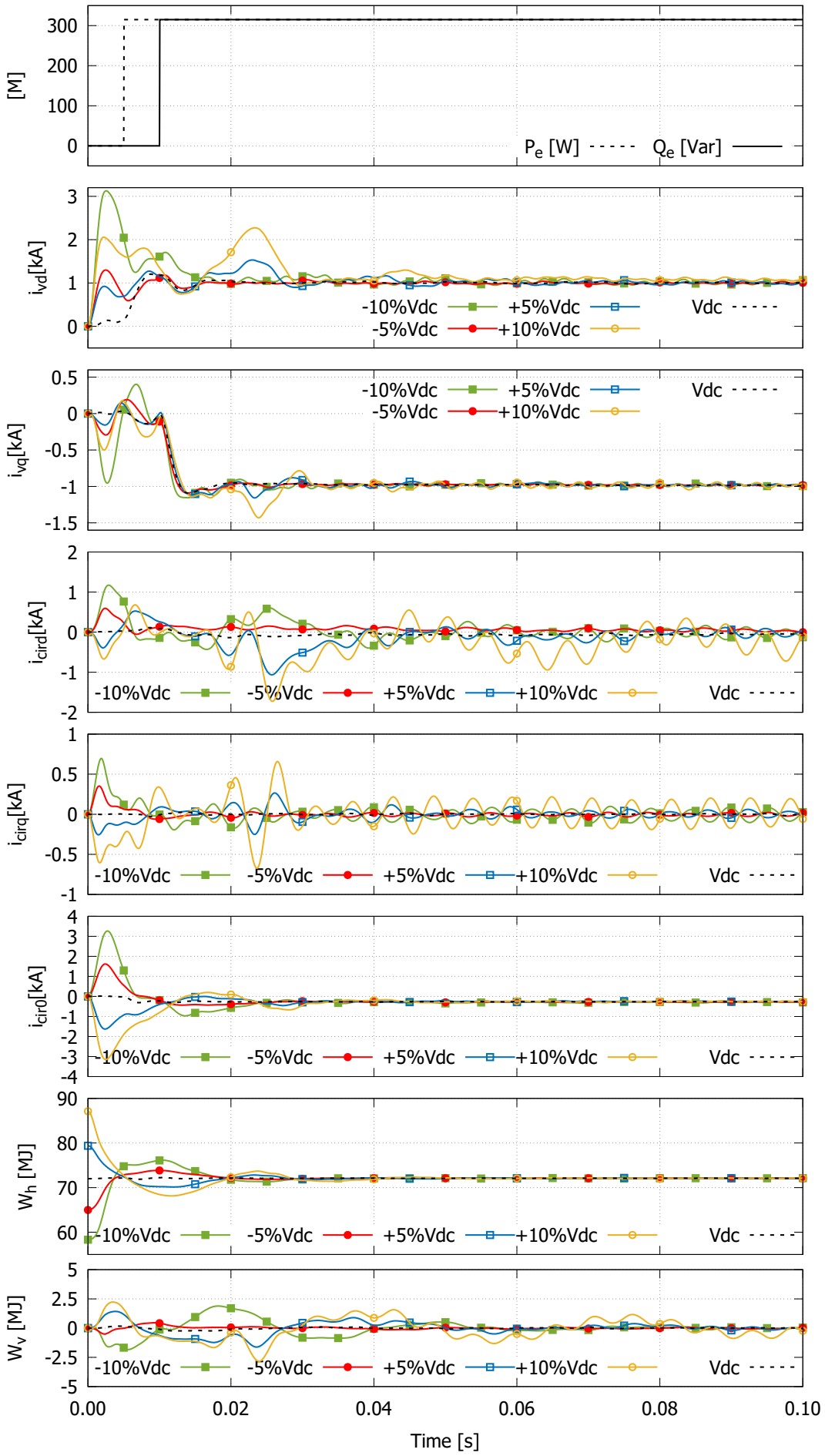

4.7 Chapter conclusion

This chapter presented a nonlinear controller for an MMC converter applied for HVDC transmission purposes. The control strategy is designed to control alternating and circulating currents, as well as the converter's stored energy and energy balance. Lyapunov theory is the base to develop the nonlinear control presented in this research, where a rigorous stability analysis is performed to assure proper operation of the grid.

The proposed control performance is tested in a detailed switching MMC model and in average model on the Matlab Simscape Electrical platform. For the proposed control, it is noteworthy that gains are based on the desired state's performances and are straightforward to tune. Moreover, the nonlinear controller has good behavior considering a vast region of operation for the MMC restricted by the system's physical limitations.

Simulations show that the nonlinear controller presents appropriated performance, with small over-signal in transients. The nonlinear control successfully drives the controlled variables to their references, as well as the energy states. The latter being free-dynamics controlled by the designed virtual inputs.

The test of robustness show that nonlinear has a similar performance of PI controller, except for changes in L and L_c at the medium-voltage system with the nonlinear controller. In this case, there is a stationary error in state variables i_{vd} and i_{vq}. This may be solved by tuning nonlinear controller gains.

CHAPTER 5

Bilinear Quadratic Feedback Control

The present chapter develops a model-based control algorithm for MMCs, including the interesting case of internal energy stabilization. The proposed algorithm is designed following bilinear theory based on quadratic feedback control. The stability of the proposed controller is analyzed through a rigorous procedure based on Lyapunov theory.

Lyapunov's theory is used to formally prove and verify the asymptotic stability for the proposed control, considering the MMC system. This proof is valid for the whole validity region of Lyapunov's function, which has the advantage of allowing an explicit computation of the operation region for the proposed controller [90; 82].

The theoretical results are then evaluated through computer simulations using an MMC average-model and a switching-model in *Simscape Electrical* environment. Furthermore, the chapter accomplishes a comparison with the PI controller presented in chapter 3.

The proposed controller has then shown to control both the converter's currents (circulating and AC) and MMCs' internal energy. The MMC internal dynamics are analysed, as energy per arm, SMs voltage and the double-fundamental frequency component of circulating currents. At last, robustness tests over parameter uncertainties and voltage fluctuation is carried out for the proposed bilinear controller.

The system used in this chapter is the one shown in the system of equations 36, and the equilibrium points for state variables and control inputs comes from section 3.1. The system can be summarized as follows:

State vector

$$x = [i_{vd}\ i_{vq}\ i_{cird}\ i_{cirq}\ i_{cir0}\ W_h\ W_v]^T$$

Control input

$$u = \left[v_{ud}\ v_{uq}\ v_{ld}\ v_{lq}\ v_{d0}\ \right]^T$$

Bilinear form

The MMC system, with state and input vectors defined above, can be re-written in the standard bilinear form:

where, considering $\rho = 5$ for the 5 inputs, to represent a three phase MMC:

$$A = \begin{bmatrix} -\frac{R_{eq}}{L_{eq}} & \omega & 0 & 0 & 0 & 0 & 0 \\ -\omega & -\frac{R_{eq}}{L_{eq}} & 0 & 0 & 0 & 0 & 0 \\ 0 & 0 & -\frac{R}{L} & \omega & 0 & 0 & 0 \\ 0 & 0 & -\omega & -\frac{R}{L} & 0 & 0 & 0 \\ 0 & 0 & 0 & 0 & -\frac{R}{L} & 0 & 0 \\ 0 & 0 & 0 & 0 & 0 & 0 & 0 \\ 0 & 0 & 0 & 0 & 0 & 0 & 0 \end{bmatrix}$$

$$B_1 = \begin{bmatrix} 0 & 0 & 0 & 0 & \cdots & 0 \\ \vdots & \vdots & \vdots & \vdots & \iddots & \vdots \\ 0 & 0 & 0 & 0 & \cdots & 0 \\ -\frac{3}{4} & 0 & \frac{3}{2} & 0 & \cdots & 0 \\ -\frac{3}{4} & 0 & \frac{3}{2} & 0 & \cdots & 0 \end{bmatrix}$$

$$B_2 = \begin{bmatrix} 0 & 0 & 0 & 0 & 0 & \cdots & 0 \\ \vdots & \vdots & \vdots & \vdots & \vdots & \iddots & \vdots \\ 0 & 0 & 0 & 0 & 0 & 0 & 0 \\ 0 & -\frac{3}{4} & 0 & \frac{3}{2} & 0 & 0 & 0 \\ 0 & -\frac{3}{4} & 0 & \frac{3}{2} & 0 & 0 & 0 \end{bmatrix}$$

$$B_3 = \begin{bmatrix} 0 & 0 & 0 & 0 & \cdots & 0 \\ \vdots & \vdots & \vdots & \vdots & \iddots & \vdots \\ 0 & 0 & 0 & 0 & \cdots & 0 \\ \frac{3}{4} & 0 & \frac{3}{2} & 0 & \cdots & 0 \\ -\frac{3}{4} & 0 & -\frac{3}{2} & 0 & \cdots & 0 \end{bmatrix}$$

$$B_4 = \begin{bmatrix} 0 & 0 & 0 & 0 & 0 & \cdots & 0 \\ \vdots & \vdots & \vdots & \vdots & \vdots & \iddots & \vdots \\ 0 & 0 & 0 & 0 & 0 & 0 & 0 \\ 0 & \frac{3}{4} & 0 & \frac{3}{2} & 0 & 0 & 0 \\ 0 & -\frac{3}{4} & 0 & -\frac{3}{2} & 0 & 0 & 0 \end{bmatrix}$$

$$B_5 = \begin{bmatrix} 0 & \cdots & 0 & 0 & 0 & 0 \\ \vdots & \ddots & \vdots & \vdots & 0 & 0 \\ 0 & \cdots & 0 & 0 & 0 & 0 \\ 0 & \cdots & 0 & 3 & 0 & 0 \\ 0 & \cdots & 0 & 0 & 0 & 0 \end{bmatrix}$$

$$b_1 = \begin{bmatrix} \frac{1}{L_{eq}} & 0 & -\frac{1}{2L} & 0 & 0 & 0 & 0 \end{bmatrix}^T$$

$$b_2 = \begin{bmatrix} 0 & \frac{1}{L_{eq}} & 0 & -\frac{1}{2L} & 0 & 0 & 0 \end{bmatrix}^T$$

$$b_3 = \begin{bmatrix} -\frac{1}{L_{eq}} & 0 & -\frac{1}{2L} & 0 & 0 & 0 & 0 \end{bmatrix}^T$$

$$b_4 = \begin{bmatrix} 0 & -\frac{1}{L_{eq}} & 0 & -\frac{1}{2L} & 0 & 0 & 0 \end{bmatrix}^T$$

$$b_5 = \begin{bmatrix} 0 & 0 & 0 & 0 & -\frac{1}{2L} & 0 & 0 \end{bmatrix}^T$$

$$z = \begin{bmatrix} \frac{2v_{f,d}}{L_{eq}} & \frac{2v_{f,q}}{L_{eq}} & 0 & 0 & \frac{V_{DC}}{2L} & 0 & 0 \end{bmatrix}^T$$

5.1 Bilinear Control Theory

The MMCs, as the majority of power electronic converters, can be represented by a bilinear model [91]. The control inputs are multiplied by the states as shows equation (36). Considering a bilinear system in which the state variables are $x \in \mathbb{R}^n$, and the input variables are $u \in \mathbb{R}^\rho$.

5.1.1 Bilinear System Stability - a general case

There are several ways to study the stability of bilinear systems [83]. However, a direct way to prove stability is to apply standard Lyapunov theory [92; 80].

The goal is to find a positive definite Lyapunov function candidate V_g, whose time derivative will be negative definite. Therefore, the candidate $V_g : \mathbb{R}^n \to \mathbb{R} > 0$ could be defined as a quadratic function as:

$$V_g(x) = x^T P_e x \tag{142}$$

Firstly, in a general case, it is sufficient to obtain a positive definite matrix $P_e \in \mathbb{R}^{n \times n}$, in order to prove the first condition for the candidate function. Next, the proof of stability is

obtained by the derivation of the Lyapunov function:

$$\begin{aligned}\dot{V}_g(x) =&\dot{x}^T P_e x + x^T P_e \dot{x} \\ =&(Ax + \sum_{k=1}^{\rho} B_k u_k x + b_k u_k)^T P_e x + x^T P_e (Ax + \sum_{k=1}^{\rho} B_k u_k x + b_k u_k) \\ =&x^T [A^T P_e + P_e A] x + 2x^T P_e \sum_{k=1}^{\rho} u_k (B_k x + b_k)\end{aligned} \tag{143}$$

where $(B_k u_k x + b_k u_k)^T P_e x = x^T P_e (B_k u_k x + b_k u_k)$.

Now, we use the control law $u_k = -\alpha [B_k x + b_k]^T P_e x$, and the further assumptions that for $k = 1, ..., \rho$, it is true that $(B_k x + b_k)^T P_e x \neq 0 \ \ \forall x \neq 0$ and that $x^T [A^T P_e + P_e A] x \leq 0$, see [82]. So, equation (143) in closed loop will be:

$$\begin{aligned}\dot{V}_g(x) \leq& -\Phi ||x||^2 - 2\alpha \sum_{k=1}^{\rho} (x^T P_e (B_k x + b_k))^2 \\ \dot{V}_g(x) <& 0\end{aligned} \tag{144}$$

where the constant $-\Phi = \lambda_{min}(A^T P_e + P_e A)$ is smaller or equal than zero.

Considering $\alpha > 0$, Lyapunov's theory assures that if the derivative of Lyapunov's function is always strictly negative (negative definite), then the full system is asymptotically stable.

5.1.2 Bilinear System Stability: studied case

Following [90], with the purpose of maintaining the state variable x on a desired operation point $\bar{x}$, it is performed a change of variables:

$$x \triangleq \tilde{x} + \bar{x}$$

$$u \triangleq \tilde{u} + \bar{u}$$

Changing the variables in equation (36), one obtains (145).

$$\dot{\tilde{x}} + \dot{\bar{x}} = A(\tilde{x} + \bar{x}) + \sum_{k=1}^{\rho} \{(\tilde{u}_k + \bar{u}_k)(B_k(\tilde{x} + \bar{x}) + b_k)\} + z \tag{145}$$

As in the equilibrium point the error between state and their reference is zero ($\tilde{x} = 0$), equation (145) can be rewritten into two parts: 1) terms with only the equilibrium states and inputs, that are regrouped in equation (146), and 2) remainder terms shown in equation (147).

$$\dot{\bar{x}} = A\bar{x} + \sum_{k=1}^{\rho} \bar{u}_k (B_k \bar{x} + b_k) + z = 0 \tag{146}$$

and then:

$$\dot{\tilde{x}} = A\tilde{x} + \sum_{k=1}^{\rho} \bar{u}_k B_k \tilde{x} + \sum_{k=1}^{\rho} (B_k \tilde{x} + B_k \bar{x} + b_k)\tilde{u}_k. \tag{147}$$

The evolution of the error states is analysed by the Lyapunov function and its derivative:

$$V(\tilde{x}) = \tilde{x}^T P_e \tilde{x} \tag{148}$$

$$\dot{V}(\tilde{x}) = \underbrace{\tilde{x}^T(\tilde{A}^T P_e + P_e \tilde{A})\tilde{x}}_{1^{st}\ Term} + \underbrace{2[\sum_{k=1}^{m} \tilde{u}_k(B_k\tilde{x} + B_k\bar{x} + b_k)]^T P\tilde{x}}_{2^{nd}\ Term} \tag{149}$$

where: $\tilde{A} = A + \sum_{k=1}^{\rho} \bar{u}_k B_k$. Now we propose the control law:

$$\tilde{u}_k = -\alpha_k[B_k\tilde{x} + B_k\bar{x} + b_k]^T P_e \tilde{x} \tag{150}$$

$$u_k = \tilde{u}_k + \bar{u}_k \tag{151}$$

Remark 2. *Due to the MMC model characteristics (shape of A matrix), not all state variables are present in the first part of equation (149). In this way, this part of the Lyapunov's function derivative would only be negative semi-definite. Consequently, its second part will provide the convergence of the remaining states.*

Acknowledging these facts, the following procedure based on Lemma 1 of [93] is necessary to design the controller, and access the stability properties of the closed-loop system.

Matrix $\tilde{A} \in \mathbb{R}^{n\times n}$ has two zero eigenvalues: $\lambda_{n-1}(\tilde{A}) = 0$ and $\lambda_n(\tilde{A}) = 0$, such that $\tilde{A}$ admits the Jordan decomposition: $\tilde{A} = U\Lambda U^{-1}$, where $U \in \mathbb{C}^n$ is non-singular and Λ is a diagonal Jordan matrix of $\tilde{A}$. Considering $\Lambda_R := diag(\Re e(\Lambda_i))$ for all $i \in [1, n-2]$, then since $\Re e(\lambda_i) < 0\ \forall\ i \in [1, n-2]$, there exists a matrix $\Gamma_R \in \mathbb{R}^{n-2\times n-2}$, symmetric and positive definite, such that $\Gamma_R\Lambda_R + \Lambda_R^T\Gamma_R = -\Phi$, where the diagonal matrices $\Phi \in \mathbb{R}^{n-2\times n-2}$ and $\Gamma \in \mathbb{R}^{n\times n}$ are positive definite, and constants $\Gamma_1, \Gamma_2 > 0$ as follows:

$$\Phi := \begin{bmatrix} \Phi_1 & 0 & 0 \\ 0 & \ddots & 0 \\ 0 & 0 & \Phi_{n-2} \end{bmatrix} \tag{152}$$

$$\Gamma := \begin{bmatrix} 1 & 0 & 0 & 0 & 0 \\ 0 & \ddots & 0 & 0 & 0 \\ 0 & 0 & 1 & 0 & 0 \\ 0 & 0 & 0 & \Gamma_1 & 0 \\ 0 & 0 & 0 & 0 & \Gamma_2 \end{bmatrix} \tag{153}$$

Solving the equation $\Gamma\Lambda + \Lambda^*\Gamma = -Q$, where:

$$Q := \begin{bmatrix} \Phi_1 & 0 & 0 & 0 & 0 \\ 0 & \ddots & 0 & 0 & 0 \\ 0 & 0 & \Phi_{n-2} & 0 & 0 \\ 0 & 0 & 0 & 0 & 0 \\ 0 & 0 & 0 & 0 & 0 \end{bmatrix} \tag{154}$$

Then, $P_e = U\Gamma U^{-1}$ is Hermitian positive definite since Γ is symmetric positive definite and U^{-1} has full rank, as presented in [93]. It implies that $V(x)$ is a real positive definite function. Next, the derivative of the Lyapunov function, $\dot{V}(\tilde{x})$ is evaluated as:

$$\dot{V}(\tilde{x}) = -\sum_{c=1}^{n-2} \Phi_c ||\tilde{x}_c||^2 - 2(\sum_{k=1}^{\rho} \alpha_k ((B_k\tilde{x} + B_k\bar{x} + b_k)^T P_e \tilde{x})^2) \tag{155}$$

where we can show that $\dot{V}(\tilde{x}) < 0,\ \forall \tilde{x} \neq 0$.

Theorem 1. *The MMC converter described by the system of equations (36), with the bilinear control law described in equation (150), and with desired equilibrium point satisfying equation (146) and the assumption that for $k = 1, ..., \rho$, it is truth that $(B_k\tilde{x} + b_k)^T P_e \tilde{x} \neq 0 \ \ \forall\ \tilde{x} \neq 0$, will be asymptotically stabilized towards this equilibrium point, inside the whole domain where the assumption is valid.*

Proof. The proof is standard and is obtained under the positive definite Lyapunov function (148) of the error system, in which closed-loop derivative (155) is negative definite. Then, by Lyapunov theory, the considered equilibrium point is asymptotically stable. □

In order to use the bilinear control defined above, the references for the state variables (see previous chapter) and the steady state inputs must be derived from the desired outputs. Consequently, equation (146) is solved to obtain the input reference values ($\bar{u}_k$) on the equilibrium as equation (156), for $c \in [1, n-2]$.

$$\begin{bmatrix} \bar{u}_1 \\ \bar{u}_2 \\ \bar{u}_3 \\ \bar{u}_4 \\ \bar{u}_5 \end{bmatrix} = \begin{bmatrix} \frac{R_{eq}}{2} & -\omega\frac{L_{eq}}{2} & -R & w & 0 \\ \omega\frac{L+L_c}{2} & \frac{R_{eq}}{2} & -wL & -R & 0 \\ -\frac{R_{eq}}{2} & \omega\frac{L+L_c}{2} & -R & \omega & 0 \\ -\omega\frac{L+L_c}{2} & -\frac{R_{eq}}{2} & -\omega L & -R & 0 \\ 0 & 0 & 0 & 0 & -2R \end{bmatrix} \begin{bmatrix} \bar{x}_1 \\ \bar{x}_2 \\ \bar{x}_3 \\ \bar{x}_4 \\ \bar{x}_5 \end{bmatrix} + \begin{bmatrix} -v_{fd} \\ -v_{fq} \\ v_{fd} \\ v_{fq} \\ v_{DC} \end{bmatrix} \tag{156}$$

Figure 98 summarize by a block diagram the implemented bilinear controller.

The dynamic performance of the proposed bilinear control strategy applied to an MMC average model is verified by computer simulations using the *Matlab/Simulink* environment. The

Figure 98 – Diagram of bilinear controller.

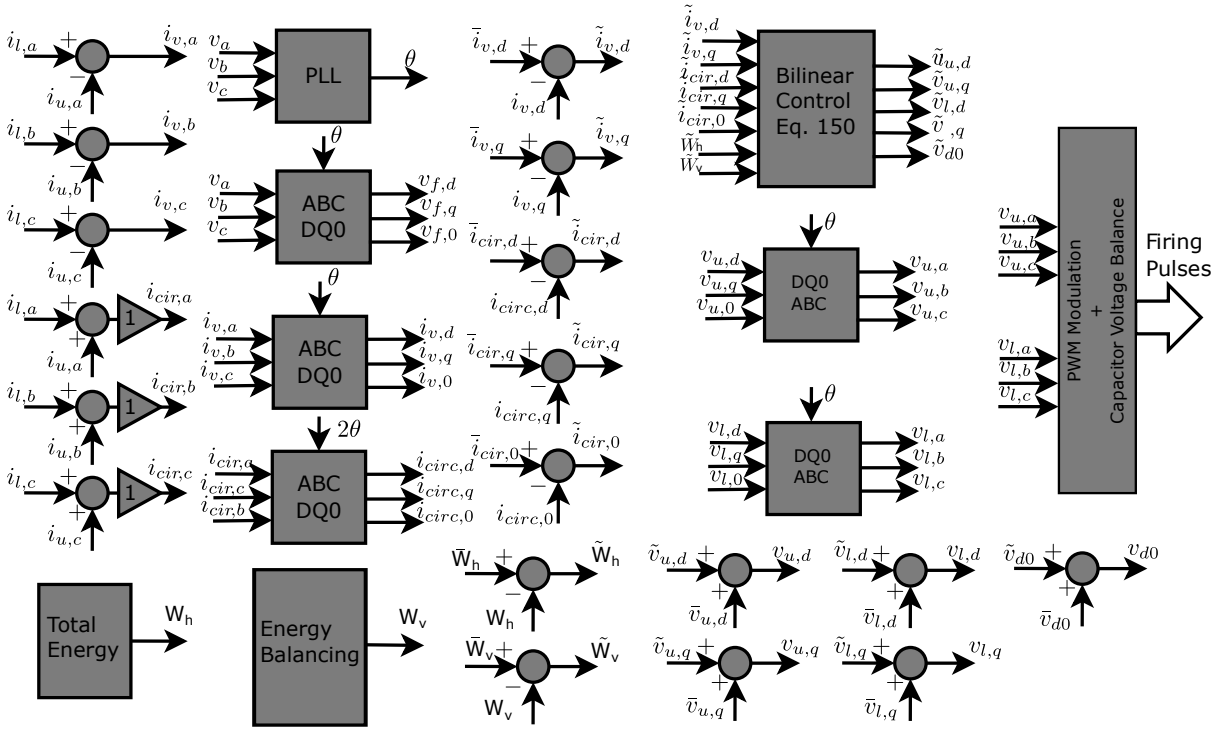

Source: Author

medium-voltage system is used and the controller gains are presented in Table 6. The suitable feedback gains were elected by a trade-off between speed of convergence and overshoot.

Table 6 – Parameters of simulated system and bilinear control's gains.

Parameter	Value	Parameter	Value
S_{MMC}	$50\ MVA$	α_1	0.5
V_{AC}	$30\ kV$	α_2	0.5
V_{DC}	$180\ kV$	α_3	0.5
L_c	$5\ mH$	α_4	0.5
L	$14\ mH$	α_5	0.5
R_c	$0.03\ \Omega$	Γ_1	1
C_{SM}	$3\ mF$	Γ_2	1
Freq	$60\ Hz$	Φ_c	1
R	$0.5\ \Omega$		
N	20		

Figure 99 – Four-quadrant operation for medium-voltage system with bilinear controller.

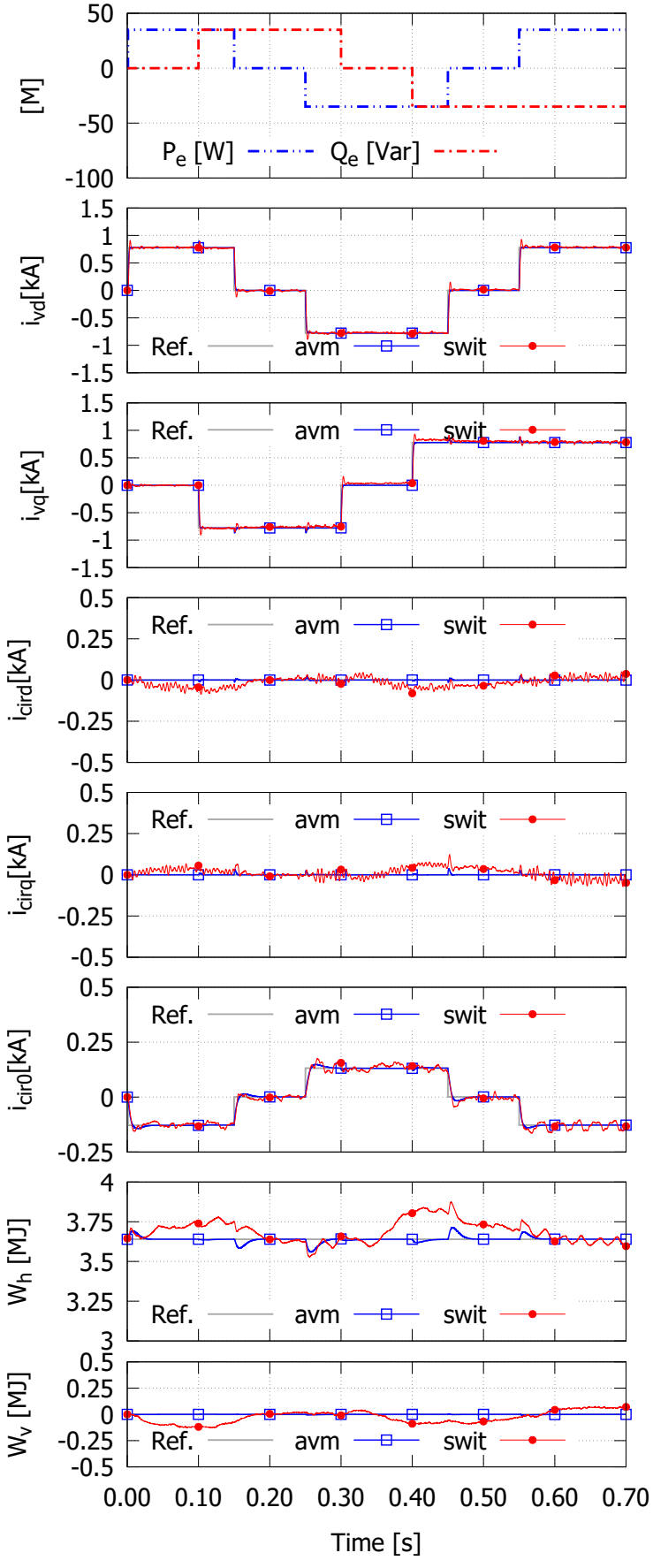

Four-quadrant operation of the medium-voltage system with bilinear controller.

In figure 99 eight operating points are performed. A detailed switching-model and an average-model are simulated with bilinear controller.

Bilinear performs well for each new operation point in both models. AC current i_{vd} and i_{vq} (2^{nd} and 3^{rd} graphic) present overshoot for switching-model while average-model doesn't.

The dq components of circulating current present a low speed of convergence by the switching-model. This is the result of a slow dynamic of the energy control. In total energy W_h and energy balancing W_v (7^{th} and 8^{th} graphics).

Figure 100 – Energy change for medium-voltage system with bilinear controller.

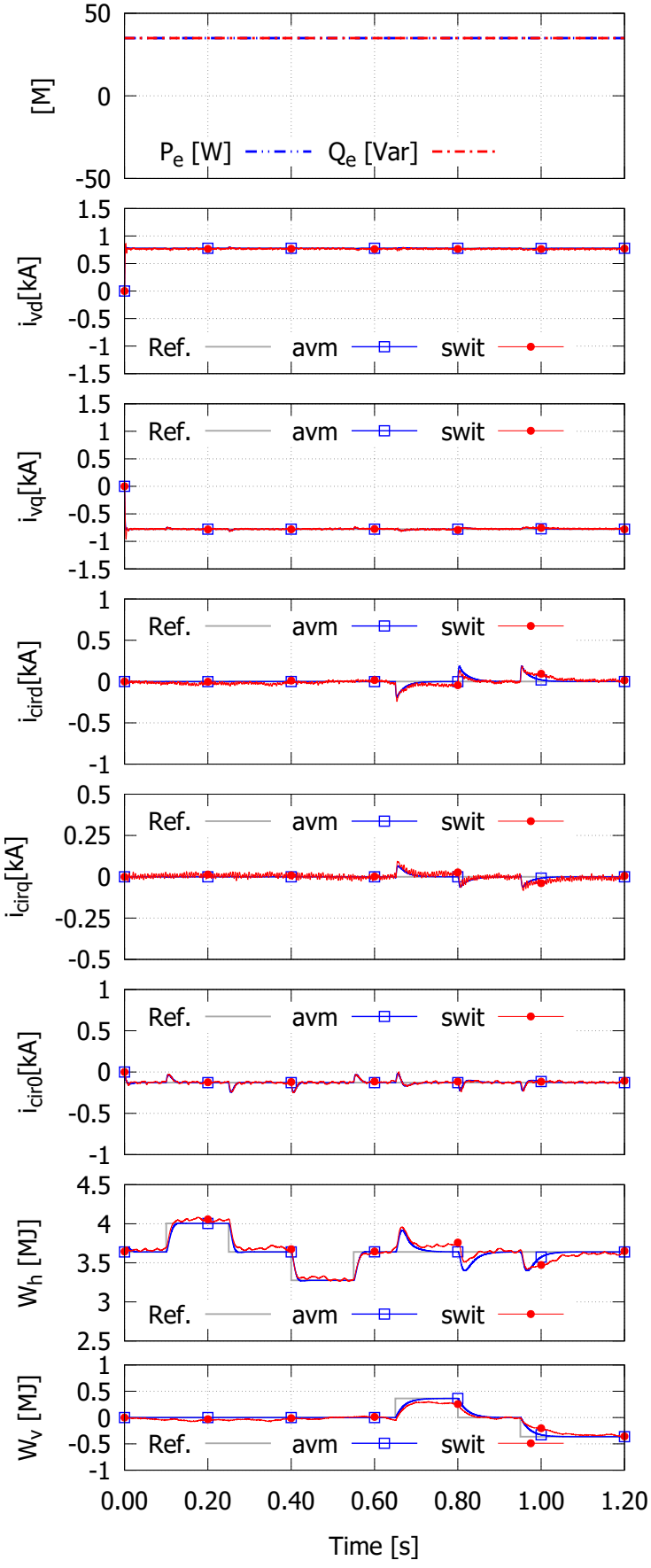

Energy change for medium-voltage system with average-model and switching-model with bilinear controller.

In figure 100 P_e and Q_e are set to 70% of nominal power. Average and switching-model are simulated.

A change in total energy is performed at $0.10\ s$. Concerning state variable W_h there is no overshoot to track the new reference for both models, however a slow speed of convergence for switching-model is observed. Only state variable i_{cir0} momentarily left its reference to steer total energy to the new reference. The same behaviour is seen for all changes in W_h.

It is possible to observe that the i_{cir0} reference ($\bar{i}_{cir0}$) comes from equation (65). It is different from PI and nonlinear controllers, where the desired value of i_{cir0} consider the error on total energy W_h. However, the bilinear control illustrates that this behaviour comes from the fact that input and output power (which are directly linked to W_h) are managed by i_{cir0}, what justify the control strategy used on PI and nonlinear control design.

Figure 101 shows the voltage balancing attained by the MMC with bilinear control. It is possible to observe that balancing is achieved in $1.5\ s$. In comparison with PI and nonlinear, the bilinear control has a slower response. However, this is directly linked with the slower convergence of energy W_v. The energy per arm, shown in figure 102 is also affected and result in a slower convergence, in comparison with the PI and nonlinear.

Figure 101 – SMs voltage balancing per arm with the bilinear control.

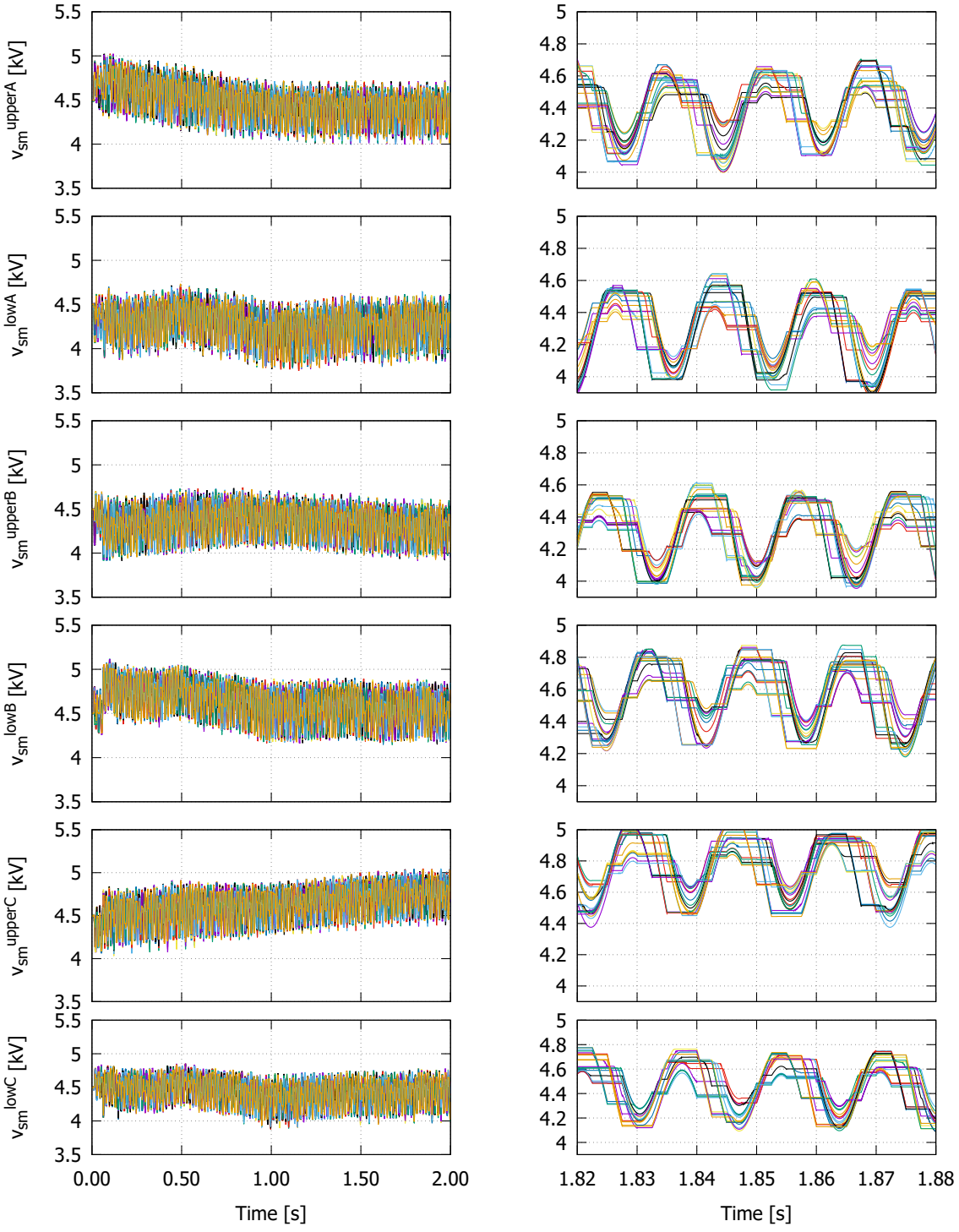

Source: Author

Figure 102 – Energy per arm of MMC with the bilinear.

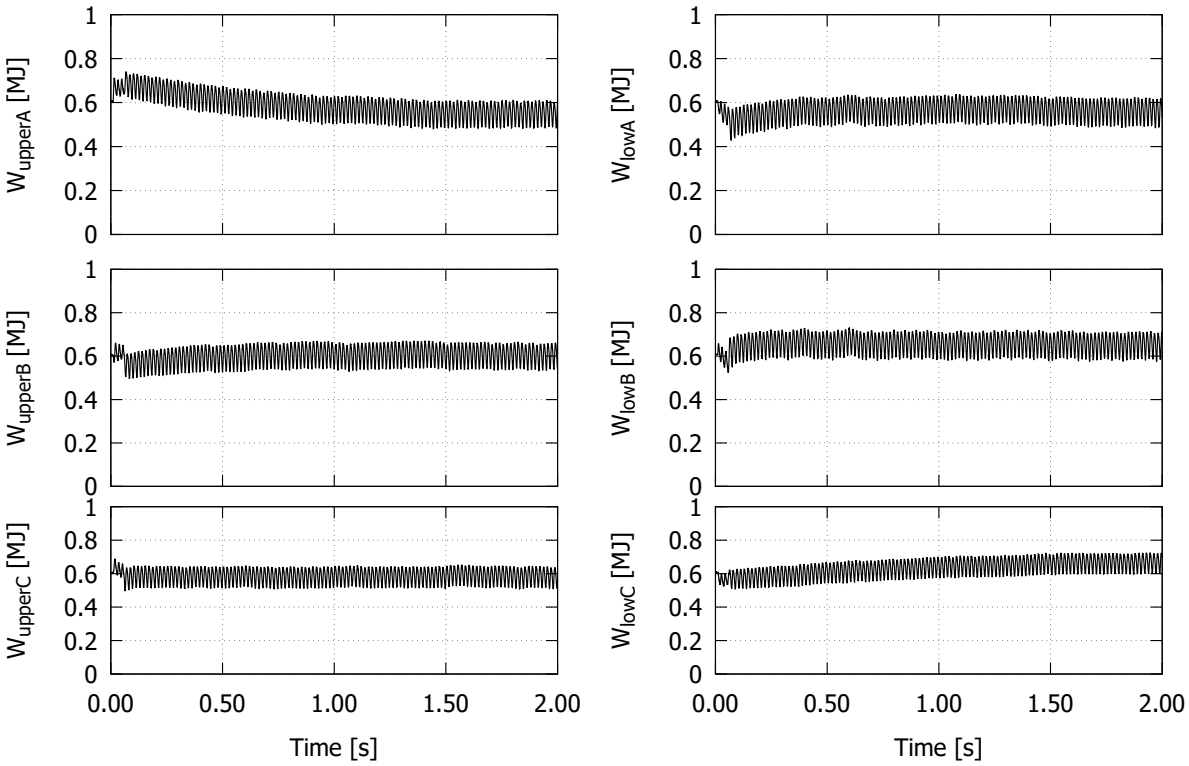

Figure 103 shows the total energy in upper (lower) arms, using bilinear control. The result achieved differs from the previous controllers once it has an oscillating and slower response.

Figure 103 – Total energy in upper (lower) arms using bilinear controller.

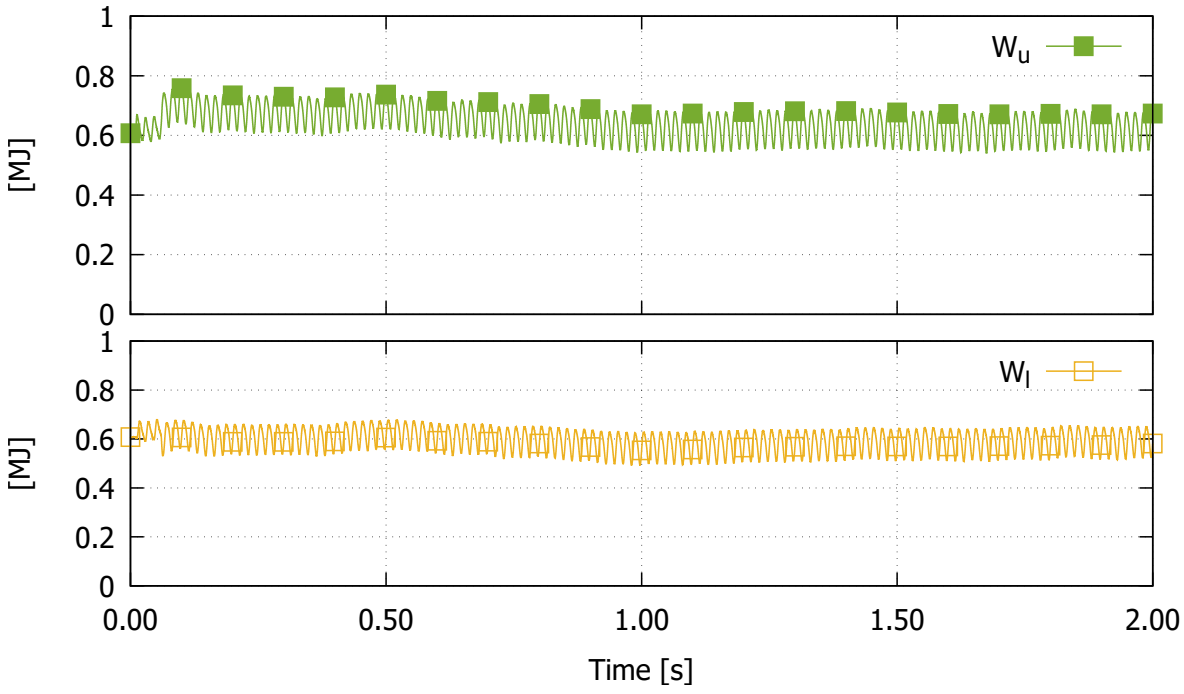

Bilinear controller is able to manage the double-fundamental frequency of circulating currents, as shown at figure 104.

Figure 104 – Double-fundamental frequency of circulating current with bilinear controller.

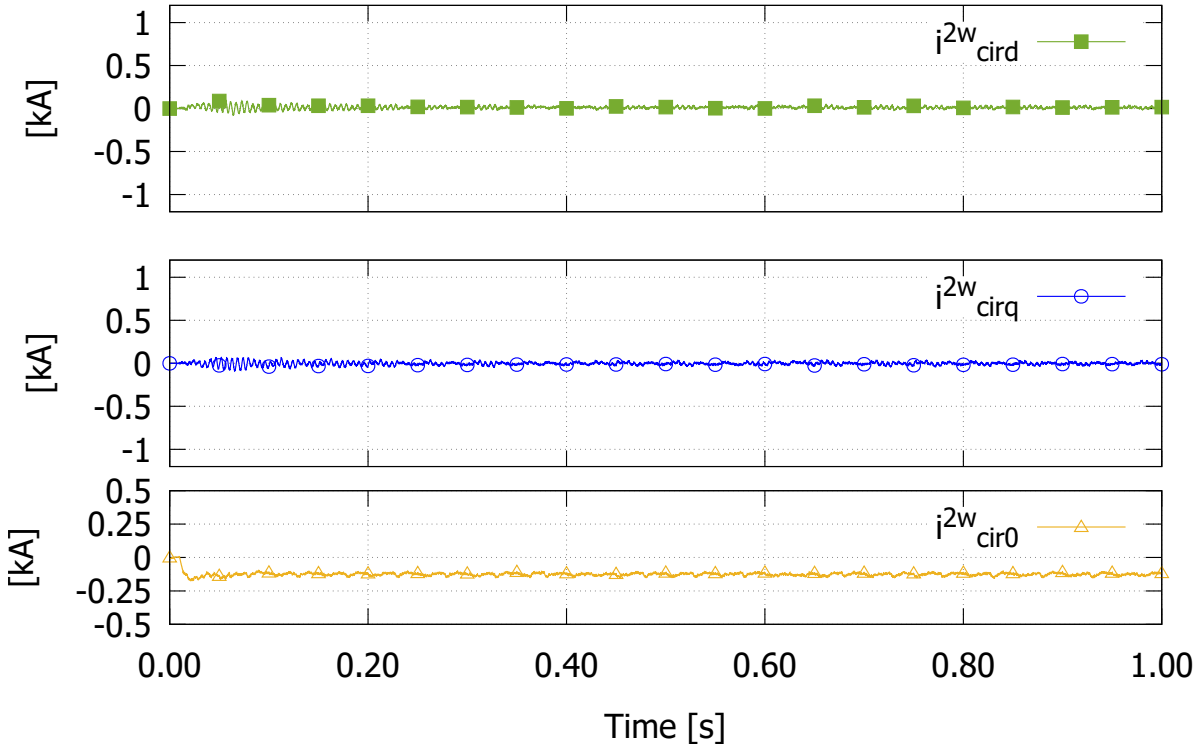

Figure 105 shows PI and bilinear controllers with four-quadrants operation. The convergence speed for AC currents (i_{vd} and i_{vq}) is high for both controllers, and they present low over-shoot. At 4^{th} graphic, PI follow their reference, and bilinear experienced a slow convergence. In the same way, PI has a higher convergence speed than bilinear for state variable i_{cirq}. Regarding i_{cir0}, both controllers drive the state variable to its desired value. 7^{th} graph shows the total energy of the MMC . As previously mentioned, the convergence speed of state variable W_h with the bilinear controller is linked with gains Γ and Φ. Additionally, state variables are strongly linked, if Γ and Φ are large, larger over-shoot is seen in the other state variables. As a result, changes in P_e and Q_e hinder W_h to reach its reference.

However, the outcome mentioned above does not imply in the speed of convergence for energy changes, as presented in figure 106, at the 7^{th} graphic. Here bilinear and PI have similar convergence for total energy changes W_h and energy balancing W_v. Additionally, state variable W_v deals with over-shoot (at $0.65\ s$, $0.80\ s$ and $0.95\ s$) for changes in energy balancing.

Figure 105 – A performance comparison between PI and bilinear controller through four-quadrants operation.

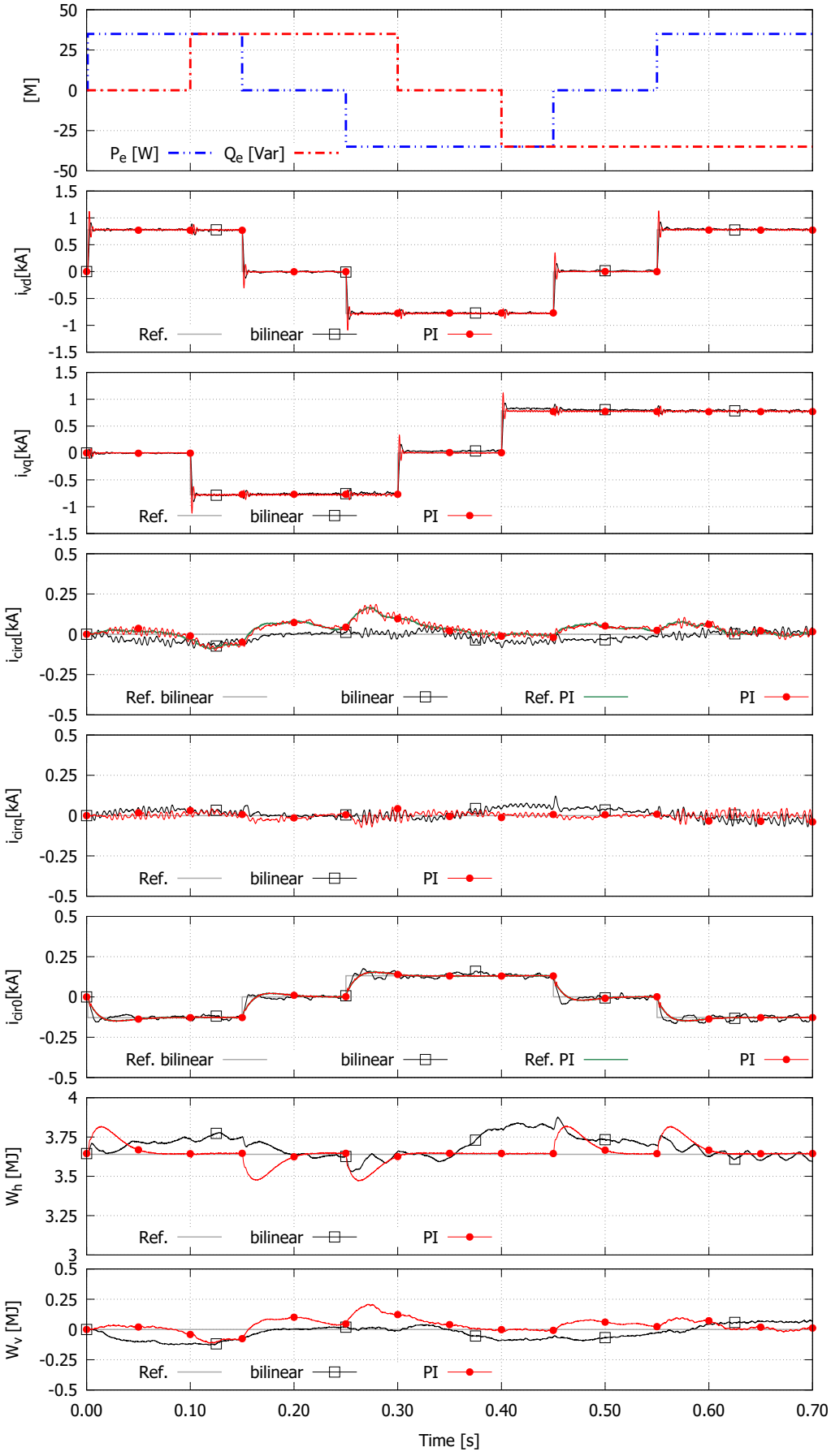

Source: Author

Figure 106 – A performance comparison between PI and bilinear controller through energy change.

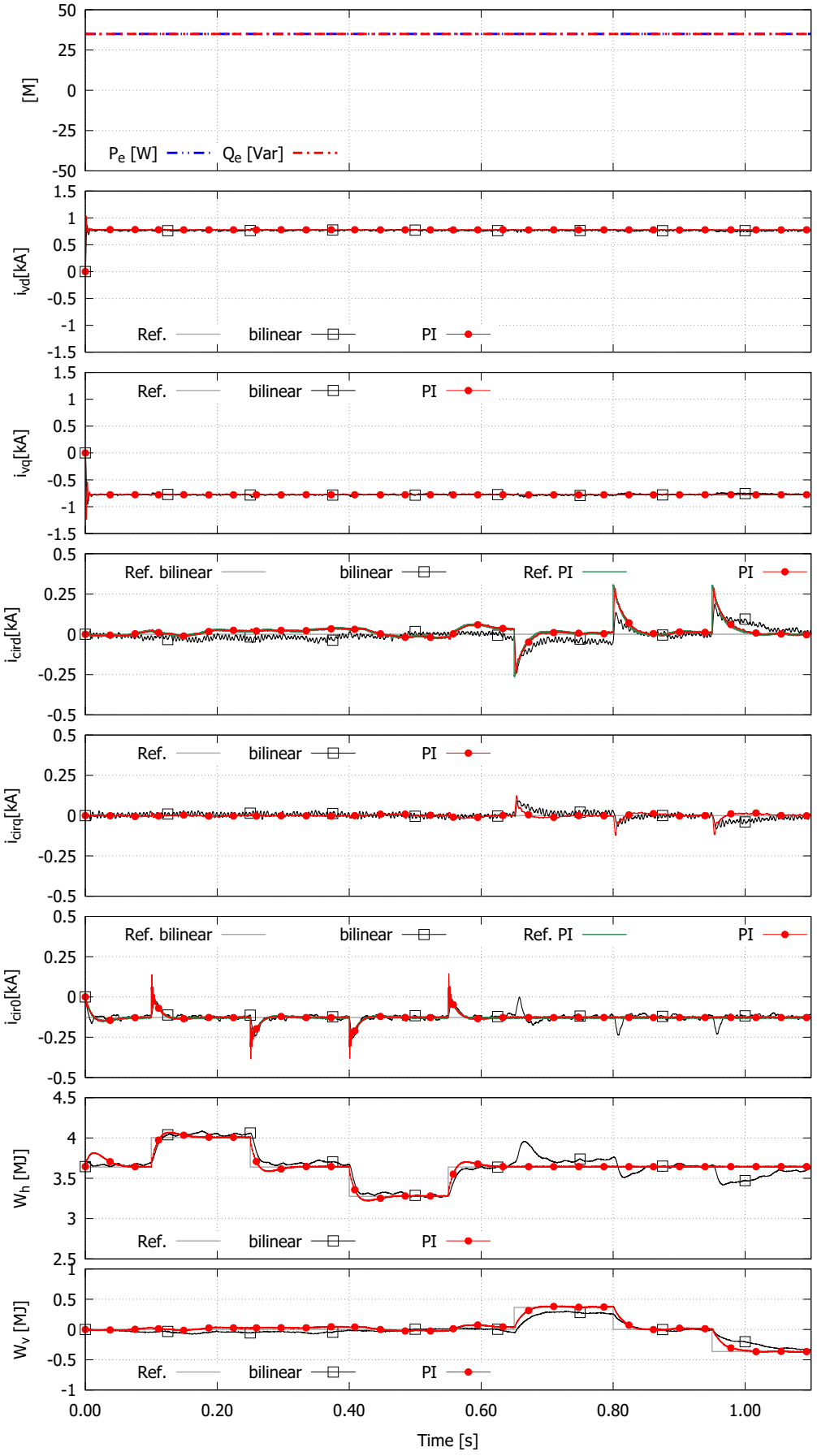

Source: Author

5.2 Robustness over parameters' uncertainties and voltage fluctuation for medium-voltage system with bilinear controller

This section analyses the sensitivity of the bilinear controller over parameter uncertainties. A set of scenarios are created, where parameter uncertainties are considered. For each scenario, one parameter (R, R_c, L, L_c or C_{SM}) assume $\pm 10\%$ or $\pm 20\%$ from their nominal values. Meanwhile, the bilinear controller is computed using the parameters' nominal values. At $t = 0.01\ s$ the operating point is changed.

In the scenarios with uncertainties in arm resistance (R), bilinear controls well the MMC state variables. In comparison with PI and nonlinear controllers, the bilinear deal with a slower convergence response for total energy W_h, see figure 107. Furthermore, in figure 108 the bilinear performance is analysed for uncertainties in R_c. Bilinear has suitable performance, similar to PI and nonlinear.

Figure 109 and 110 consider uncertainties in arm inductance L and AC side inductance L_c. This result in i_{vd} with stationary error; meanwhile, i_{vq} is perfectly driven to its reference for all proposed scenarios. This result differs from PI and nonlinear. Another set of gains was chosen to deal with the stationary error problem, where $\alpha_{1,\dots,4} = 1.5$.

Figure 111 and figure 112 present state variables i_{vd} and i_{vq} through the robustness test with bilinear controller using a larger gain $\alpha_{1,\dots,4}$. A further investigation needs to be accomplished to improve the total energy W_h response. The state variable W_h is directly linked with gains of Γ and Q. However, a larger Γ and Q result in a high coupling response between state variables. This will be further investigated in futures researches.

For C uncertainties, bilinear achieved similar result of PI (section 3.4.2) and nonlinear (section 4.5.1). The state variables are presented in figure 113.

The previous analyses can ensure that the bilinear controller appropriately manages state variables to their desired value. Furthermore,the gains play a crucial role in the bilinear controller performance.

Finally, bilinear performs well face to AC voltage fluctuation, and DC voltage fluctuation. Simulations illustrate the control performance for higher and lower values of nominal voltage in the system's buses.

Figure 114 presents state variables with fluctuation in AC voltage. There is a time-varying response during transitory, with a fast convergence to the desired value; Figure 115 presents state variables for fluctuation in DC voltage. Bilinear presents similar performance to PI and nonlinear.

Figure 107 – The system state over variation of parameter R with bilinear controller.

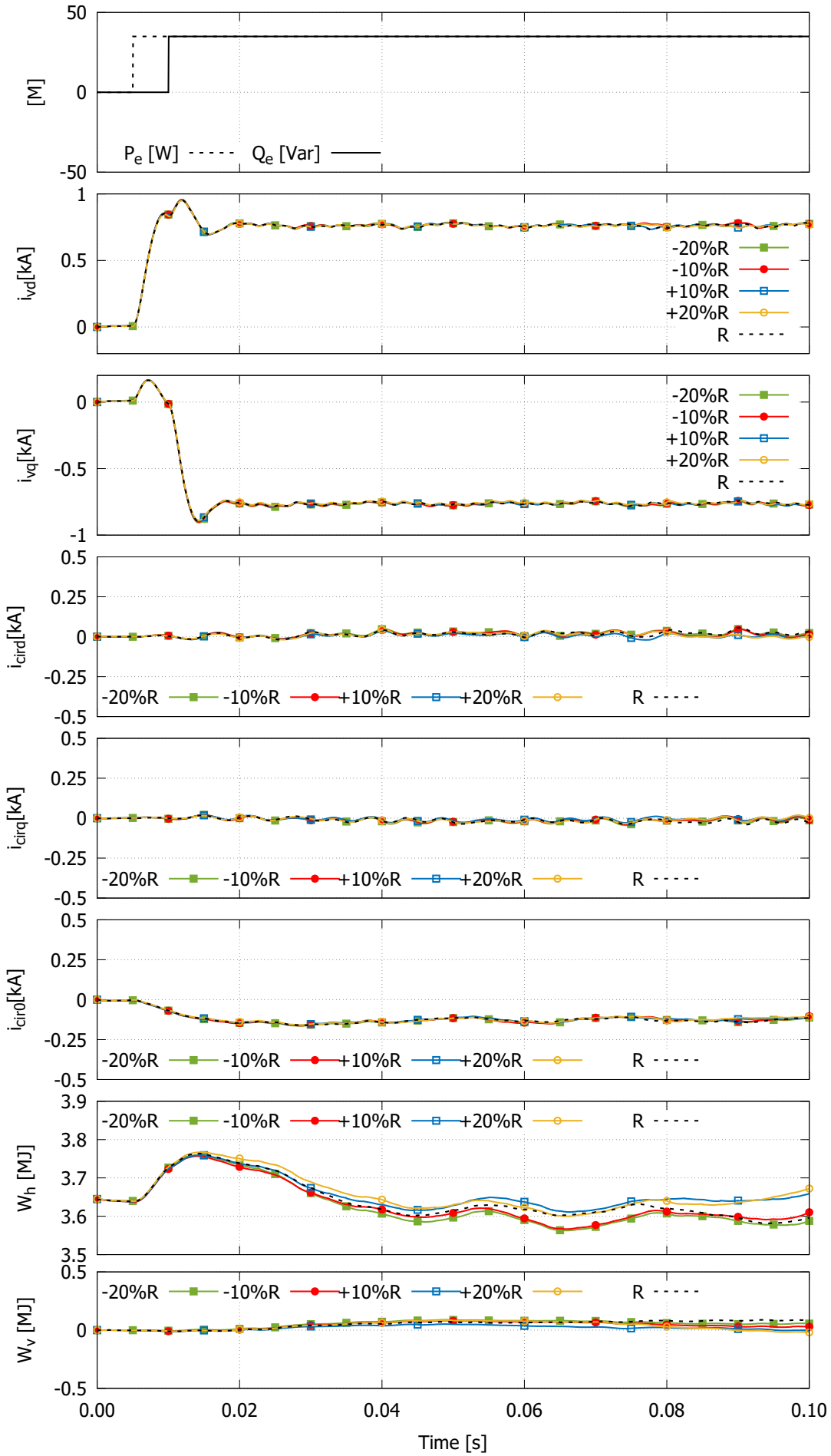

Source: Author

Figure 108 – States over variation of parameter R_c with bilinear controller.

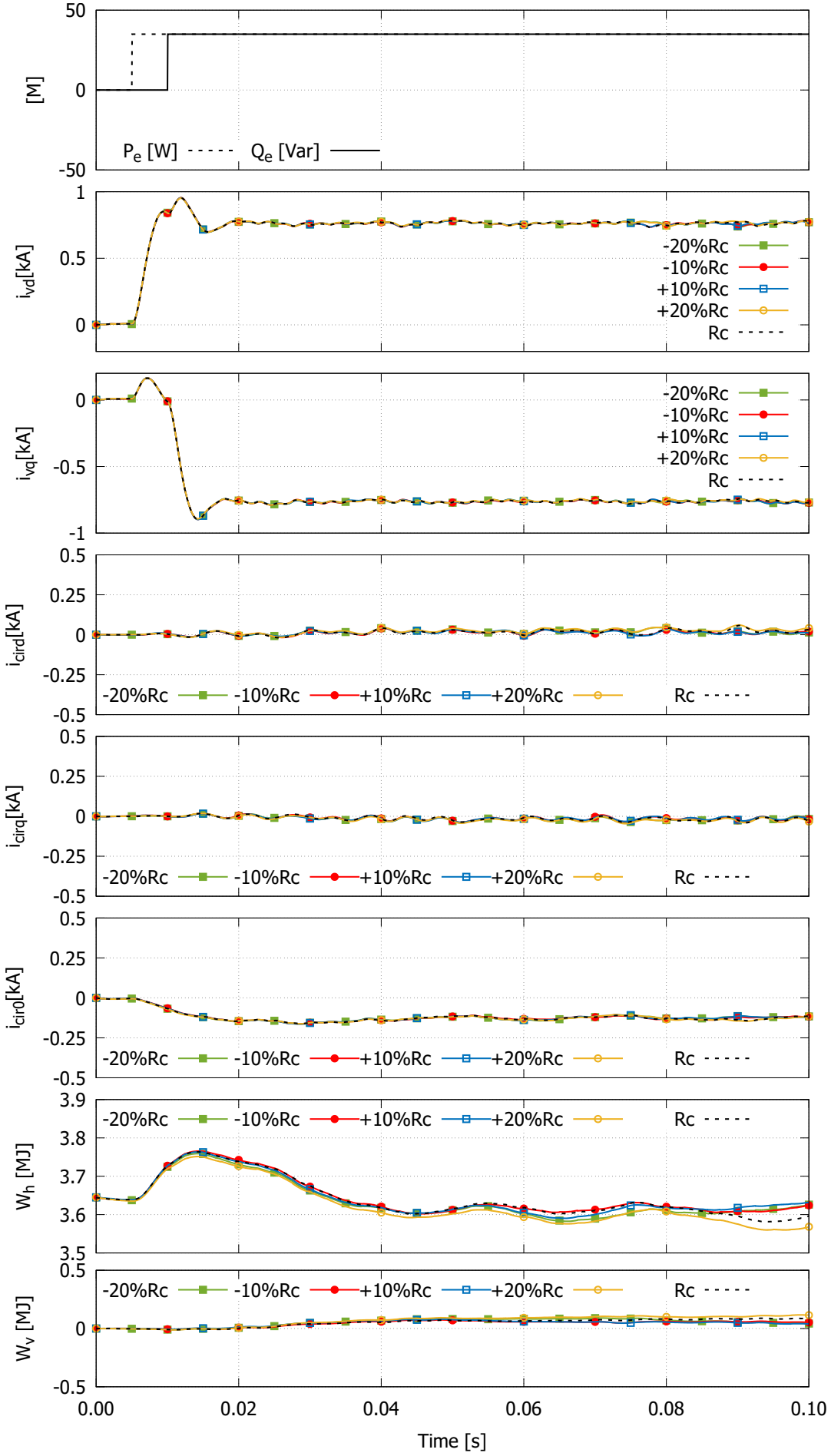

Source: Author

Figure 109 – States over variation of parameter L with bilinear controller.

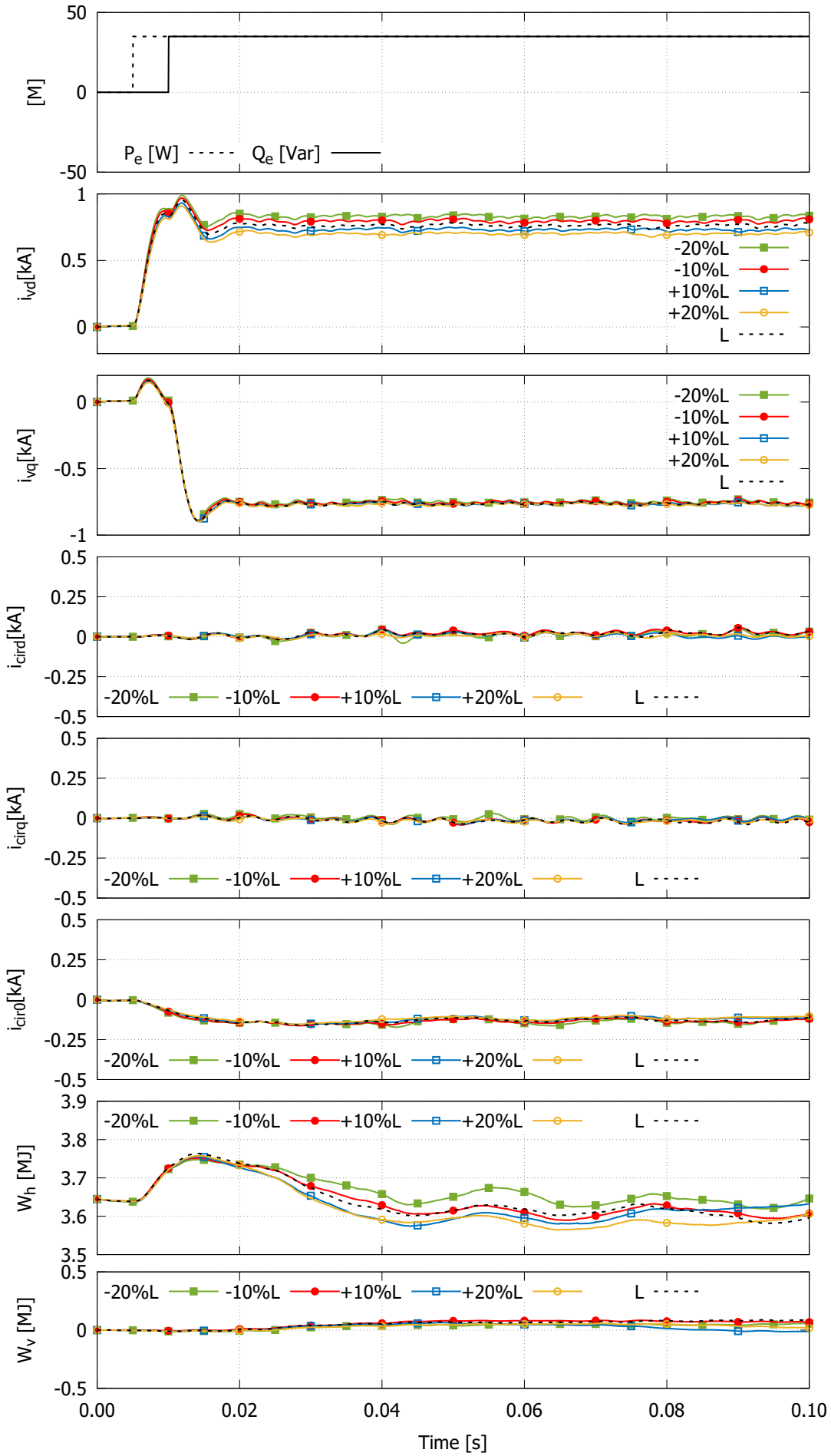

Source: Author

Figure 110 – States over variation of parameter L_c with bilinear controller.

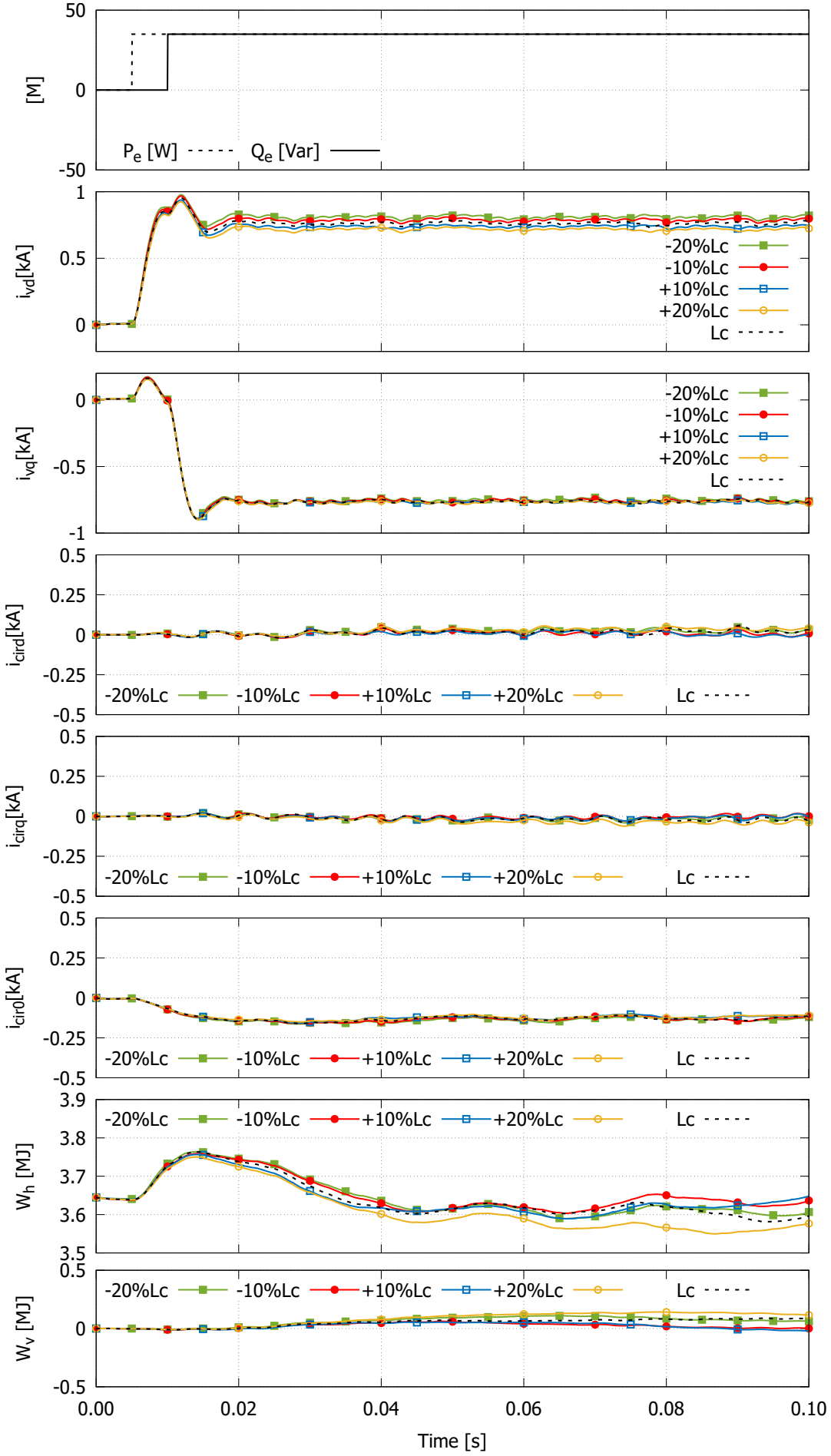

Source: Author

Figure 111 – Bilinear robustness over uncertainties in L with a larger gain.

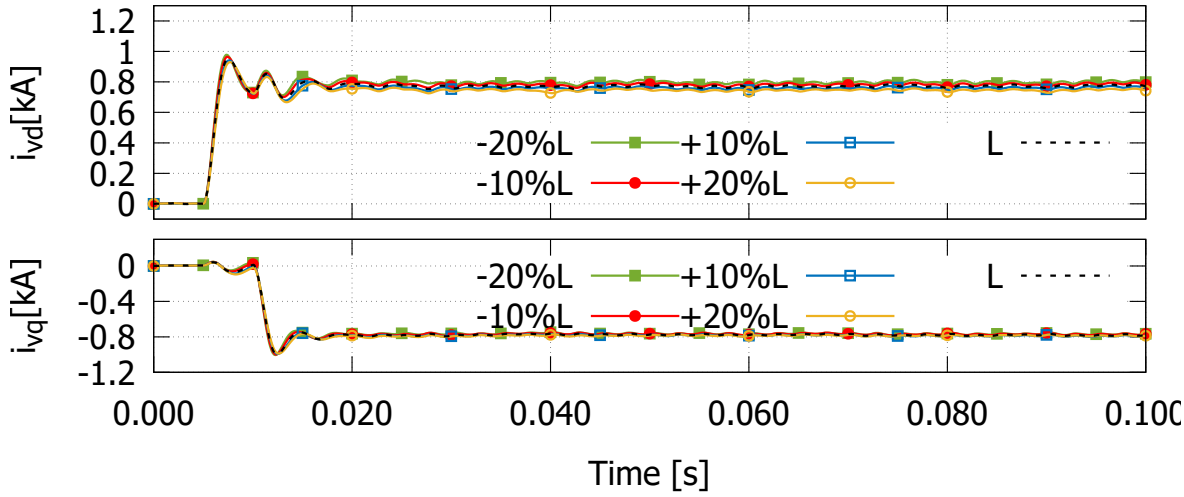

Figure 112 – Bilinear robustness over uncertainties in L_c with a larger gain.

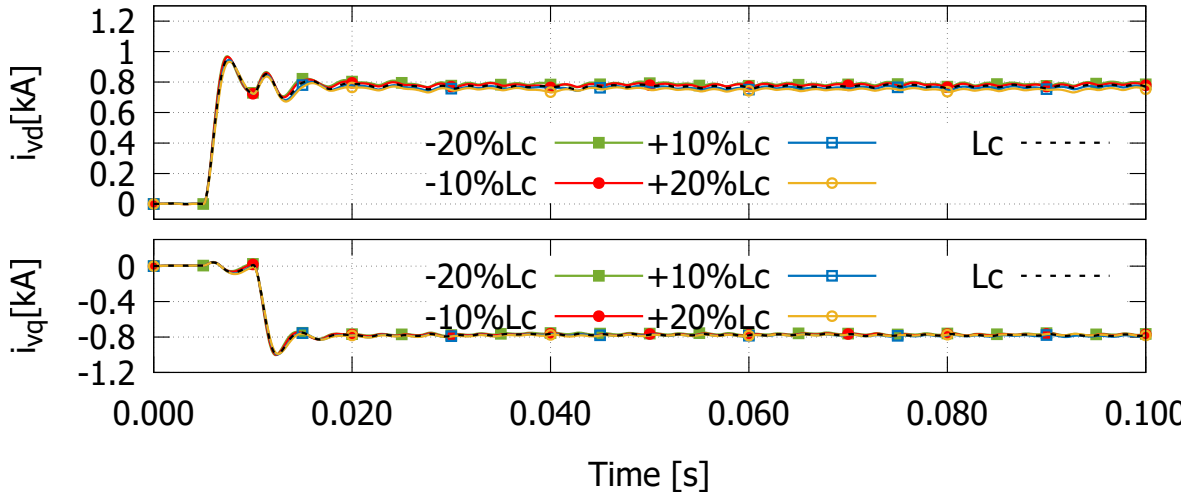

Figure 113 – States over variation of parameter C with bilinear controller.

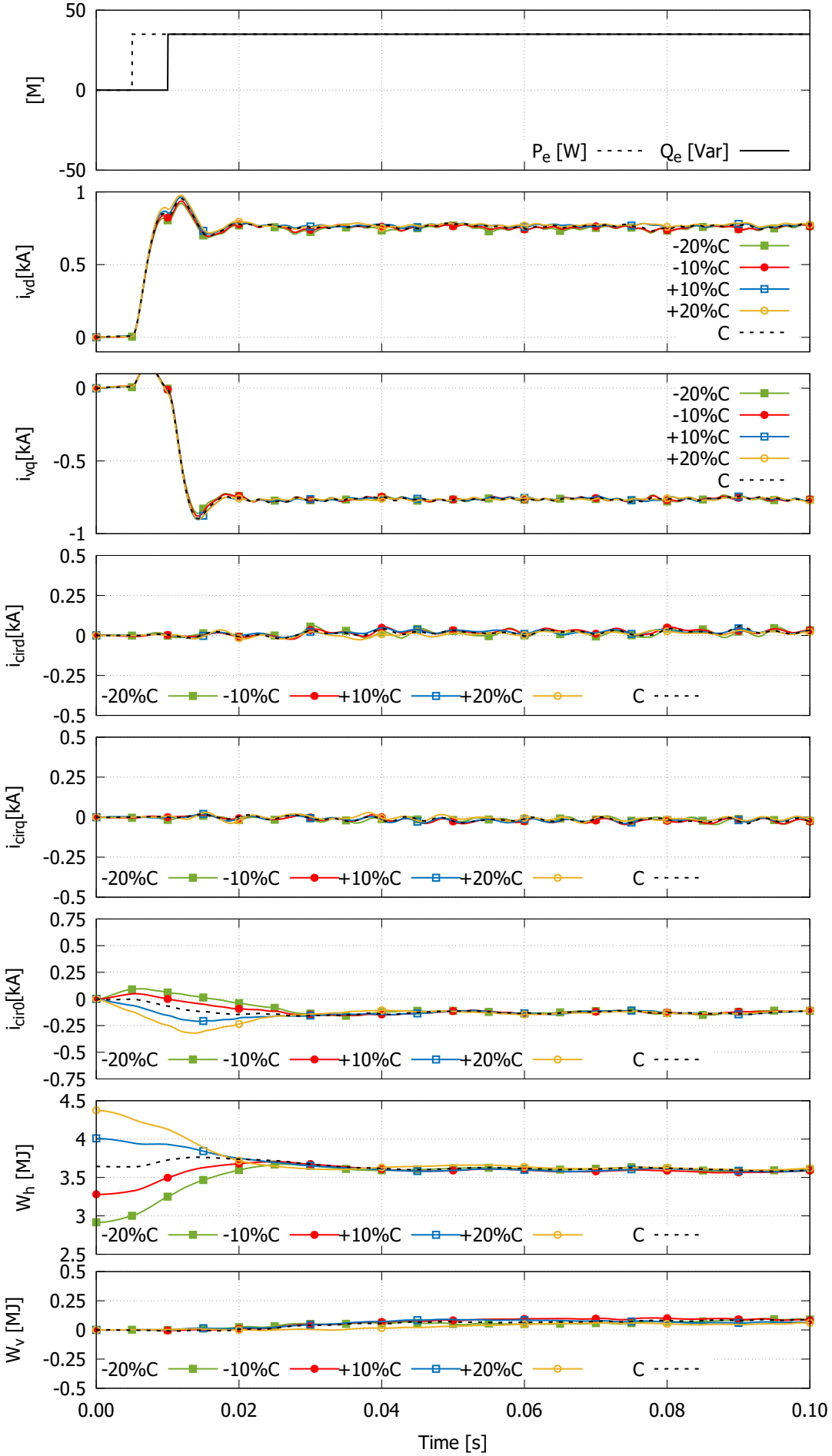

Source: Author

Figure 114 – Fluctuation of AC voltage with bilinear controller.

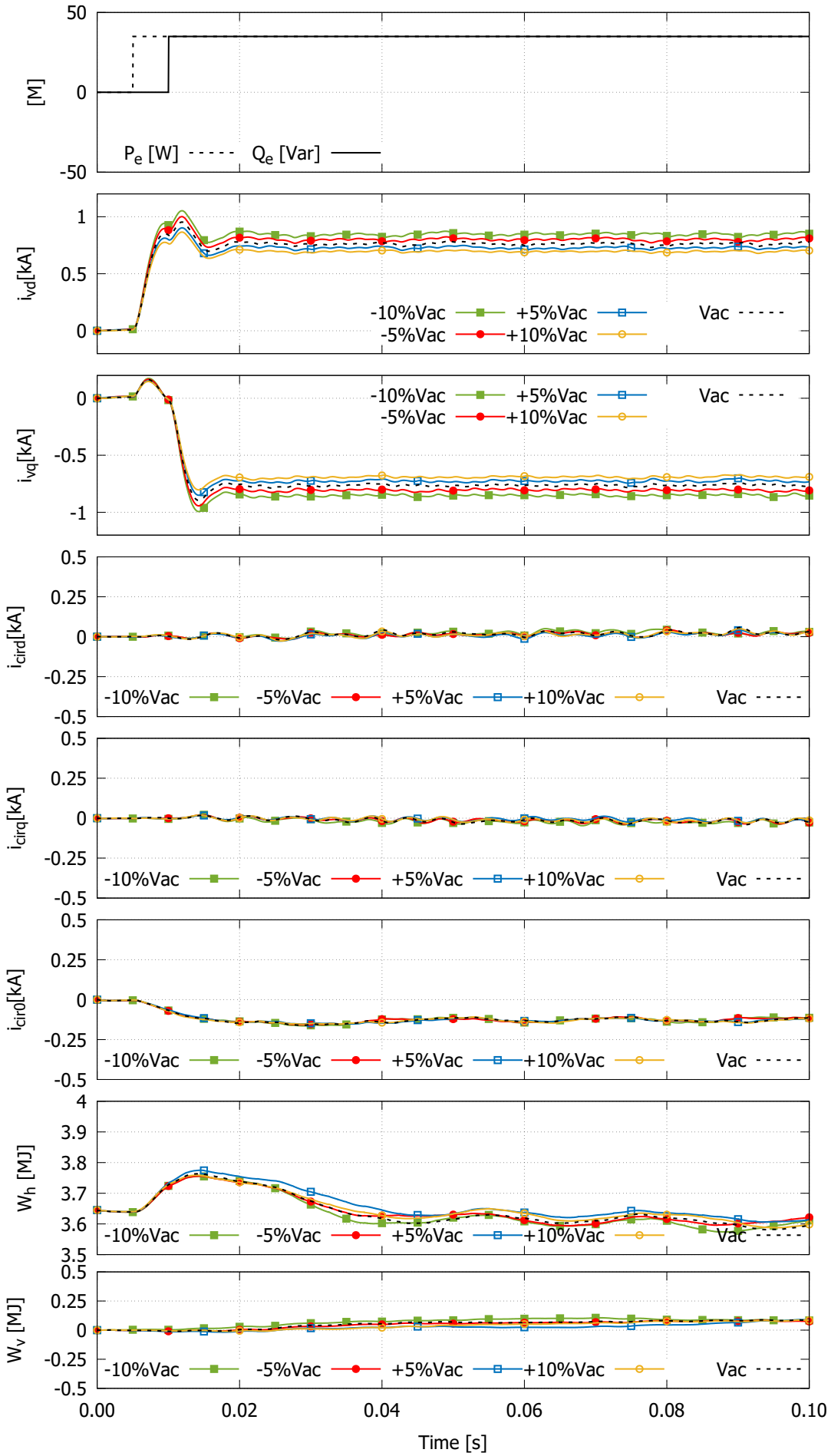

Source: Author

Figure 115 – Fluctuation of DC voltage with bilinear controller.

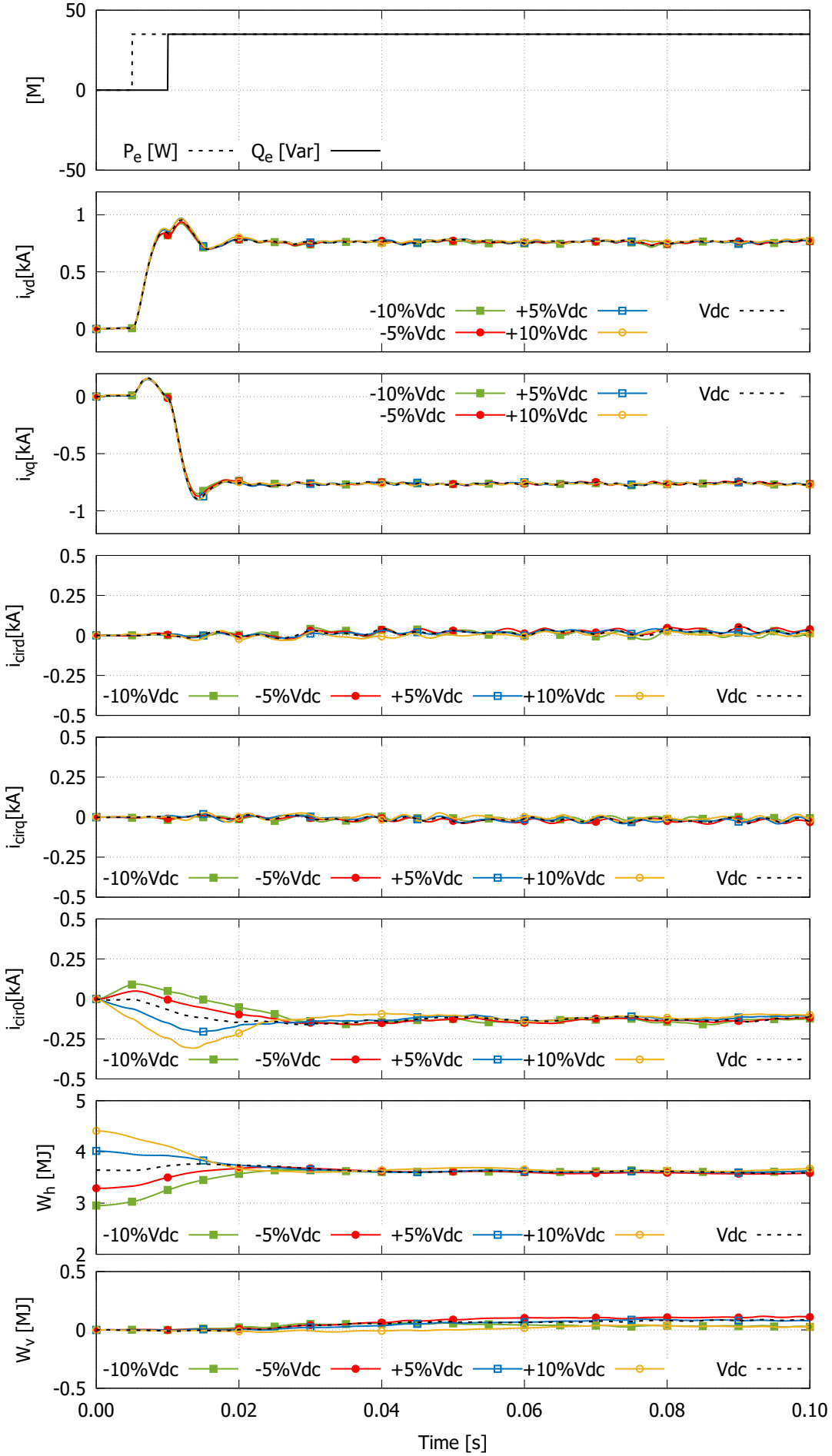

Source: Author

5.3 Chapter conclusions

This chapter presented a control algorithm design for MMC converters. An extensive set of operating points are evaluated. Additionally, changes in converter energy are performed. Furthermore, the performance comparison with the PI controller is proposed, where bilinear has a similar performance.

The results include a formal mathematical proof of stability, first for a class of bilinear systems, and then its application for the MMC converter, allowing to stabilize it in a larger operating region than linear controllers.

Furthermore, the proposed control strategy allows for the stabilization of all converter's state variables by a single control law.

Control's robustness over parameter uncertainties is accomplished, and bilinear performs well face to uncertainties. However, it is essential to highlight that the gain adjustment needs to consider the uncertainties to be adequately tuned.

Finally, the full state vector using the bilinear controller reaches its desired value for the four-quadrant operation. Additionally, it was accomplished changes in total energy and energy balancing.

CHAPTER 6

General Conclusion

The electrical grids are becoming more complex worldwide because of a diversity of power generation, more interconnected systems, and an intense energy market. The power generation which comes from renewable increases the number of weak bars in the system. A high number of weak buses can increase the risk of experiencing stability loss. In this way, the demand for ancillary services is growing, for example, increasing the need for systems with synthetic inertia. A solution might be the incorporate to power electronics devices for additional features through the control system. However, in the field of HVDC converters', control for supporting the transmission system's overall stability has yet much to be done. This is an essential issue in electrical grid planning, especially with the huge penetration of renewable connected to the main grid through HVDC. Therefore, this thesis delivers results that contribute to the field of control of MMC converters, that could allow further ancillary services.

Chapter 1 explains the current electrical grid features, as a result of the more interconnected system and the increase of renewable power production. Additionally, it introduces background about power electronics' development and an overview of the technical features attained by each kind of switching device. The chapter points out the last achievement in this field, as the upgrade of the VSC that produces the MMC. That upgrade brings advantages like scalability and lowers switching frequency at devices, in comparison with the VSC. Finally, a short control overview highlights the drawbacks of the MMCs controller and justify the thesis development.

Chapter 2 goes through the technical aspects of the MMC converter. This chapter also includes an overview of modeling and indicates the compromises on simulation speed while using full order models or reduced order models. Furthermore, the detailed overview in control design for MMC is presented, where the achievements obtained by developed nonlinear controllers are emphasized.

Chapter 3 shows the design of a linear control which is used for comparison purposes. The two tests systems are presented, one in medium-voltage and other in high-voltage. Moreover, a comparison between average-model and switching-model using the PI controller is performed. This comparison proves the faithfulness between models for the MMC state variables. Then a high-voltage system is simulated through switching-model and the internal dynamics are

analysed. From the internal dynamics, the upper and lower energy balancing is fast accomplished after transients. In spite of this fact, the fact that the controller does not allow to directly control the energy per arms, this is achieved in $400\ ms$. Finally, the capacitors voltage balancing is well achieved by the implemented sorting algorithm.

Chapter 4 presents a nonlinear controller for an MMC converter applied for HVDC transmission purposes. The control strategy is designed to control not only the alternating and circulating currents, but also the converter's stored energy and energy balance. Lyapunov theory is the base to develop the nonlinear control presented in this research, where a rigorous stability analysis is performed to assure proper operation of the grid.

The proposed control performance is tested in average model and in a detailed switching MMC model on the Matlab Simscape Electrical platform. For the proposed control, it is noteworthy that gains are based on the desired state's performances and are straightforward to tune. PI and nonlinear controls have similar performances. Moreover, the nonlinear controller has suitable behavior considering a vast region of operation for the MMC restricted by the system's physical limitations.

Robustness over parameters uncertainties are analysed. For changes in R, R_c, L and L_c the control drive state variables to their desired values in stead-state. However the increase on SM capacitors' value C, dq components of circulating cur rent (i_{cirdq}) and consequently energy balancing W_v present an oscillatory response.

DC and AC voltages fluctuation affect the speed of convergence for system's state. Meanwhile circulating current has large oscillation when V_{ac} increases, and also oscillates for changes in V_{dc}.

Simulations show that the nonlinear controller presents appropriat performance, with small over-signal in transients. The nonlinear control successfully drives the controlled variables to their references, as well as the energy states. The latter being free-dynamics are controlled by the designed virtual inputs.

Chapter 5 presents a bilinear control for an MMC converter, which directly controls AC and circulating currents and MMC energy. A rigorous mathematical proof is given for its stability, which is based on Lyapunov's theory. This result provides asymptotically stabilization for the three-phases MMC, and the use of a Lyapunov function implies in formal verification of stability and a specific region of attraction for the considered model. Moreover, tuning guidelines are also presented, considering the trade-off between speed of response, coupling effect, and control effort. A sensitivity analysis is also shown. It presents strong robustness properties for realistic parameter's errors.

The bilinear control technique is simulated using an average-model and a switching-model in Simscape Electrical environment. The theoretical and simulation results show that the proposed controller is suitable for the MMC requirements as time response and overshoot, and allows a useful trade-off between power and energy control in the converter. Furthermore, the bilinear control's energy management opens the path to new ancillary services for grid support, for both

AC and DC grids, as fast as frequency response or synthetic inertia.

The bilinear control presents rigorous stability proof, and has a well established operating region. In simulations, bilinear control performs well.

Finally, the proposed controllers, nonlinear and bilinear, stabilizes well the MMC state variables. Additionally, nonlinear implementation is simple once the relation between the performance of state variables and gains is clear. However, Bilinear has a straightforward solution by a single control law.

6.1 Main Results

- ❏ Two nonlinear control algorithms, based on a bilinear mathematical model, are designed for MMC converters;
- ❏ These algorithms are able to control AC and DC power flows, total converter's energy and converter energy's balancing at the switching MMC model;
- ❏ There are formal stability analysis by Lyapunov theory for both controllers;
- ❏ Once the proposed controls are not based on a linearized model, a vast operation region is reachable;
- ❏ For the bilinear, compared to other control techniques for MMCs, the proposed control strategy allows stabilizing all converter's state variables by a single control law. The fact that there is a single control law makes the controller much easier to tune than the industry's standard cascaded PI controllers.

6.2 Perspectives for future research

At this point, the thesis met some challenges related to the converter energy controller, and the future topics to be addressed are:

- ❏ To use the control in an MTDC grid, also controlling V_{DC};
- ❏ To expand to an MTDC grid fully controlled by bilinear;
- ❏ To use MMC control as a fault detector and protection;
- ❏ For certain MTDC operating points, it will be defined the distance until the voltage collapses in each bar;

- ❏ To use the SM energy storage to provide ancillary services, such as inertial, frequency and voltage support for the grid.

6.3 Publication

Main publication

- ❏ **Oliveira G.C.**, Damm G., Monaro R.M., Luís F. N. Lourenço, Carrizosa M.J., Françoise Lamnabhi-Lagarrigue *Nonlinear Control for Modular Multilevel Converters with Enhanced Stability Region and Arbitrary Closed Loop Dynamics*. International Journal of Electrical Power & Energy Systems. *October, 2020*

Other publications

- ❏ Prezotto G.C., Suzuki N.Y., **Oliveira G.C.**, Monaro R.M., Di Santo S.G. *Simulação de um Disjuntor de Corrente Contínua para Aplicações em Alta Tensão*. 12th Latin-American Congress on Electricity Generation and Transmission, Mar del Plata - Argentina, 2017

- ❏ Suzuki N.Y., Lacerda V.A., **Oliveira G.C.**, Monaro R.M., Coury D.V. *Comparação de Métodos para Seleção de Parâmetros de Conversores Modulares Multiníveis*. 12th Latin-American Congress on Electricity Generation and Transmission, Mar del Plata - Argentina, 2017

- ❏ Suzuki N.Y., Monaro R.M., **Oliveira G.C.**, Di Santo S.G. *Desenvolvimento de um Sistema Microcontrolado para Controle de um Conversor de um Sistema HVDC*. Simpósio Brasileiro de Sistemas Elétricos, Natal- RN - Brazil, 2016

- ❏ Funabashi V., Monaro R.M., **Oliveira G.C.**, Di Santo S.G. *Sistema Microcontrolado para o Controle em Tempo Real do Ângulo de Ataque das Pás de Turbinas Eólicas*. Simpósio Brasileiro de Sistemas Elétricos, Natal - RN - Brazil, 2016

References

[1] Akshat Rathi, "Two countries are the reason the EU is hitting its ambitious renewable energy targets," https://sandbag.org.uk/wp-content/uploads/2018/01/EU-power-sector-report-2017.pdf, 2018, online; accessed 18 May 2018.

[2] Eurostat. (2020) Share of energy from renewable sources. [Online]. Available: https://appsso.eurostat.ec.europa.eu/nui/submitViewTableAction.do

[3] E. Commission. (2020) 2030 climate energy framework. [Online]. Available: https://ec.europa.eu/clima/policies/strategies/2030_en

[4] Gerhard Seyrling, "Supercharge Me: The Case For The European Energy Supergrid," https://www.ge.com/reports/helping-europe-interconnected-supergrid-right-way-digital/, 2017, online; accessed 18 May 2018.

[5] European Commission, "Commission launches new electricity interconnection targets expert group," https://ec.europa.eu/energy/news/commission-launches-new-electricity-interconnection-targets-expert-group_en?redir=1, 2017, online; accessed 2 Sep 2020.

[6] P. L. Francos, S. S. Verdugo, H. F. Álvarez, S. Guyomarch, and J. Loncle, "Inelfe x2014; europe's first integrated onshore hvdc interconnection," in *2012 IEEE Power and Energy Society General Meeting*, July 2012, pp. 1–8.

[7] K. Meah and S. Ula, "Comparative evaluation of hvdc and hvac transmission systems," in *2007 IEEE Power Engineering Society General Meeting*, 2007, pp. 1–5.

[8] N. R. Watson and J. D. Watson, "An overview of hvdc technology," *Energies*, vol. 13, no. 17, p. 4342, Aug 2020. [Online]. Available: http://dx.doi.org/10.3390/en13174342

[9] Y. Chen, "Nonlinear control and stability analysis of multi-terminal high voltage direct current networks," Theses, Université Paris-Sud, Apr. 2015.

[10] G. C. de Oliveira, "Probabilistic short-circuit using monte carlo si- mulations in direct current transmission systems," Master's thesis, Escola de Engenharia de São Carlos, 2015.

[11] A. Lesnicar and R. Marquardt, "An innovative modular multilevel converter topology suitable for a wide power range," in *2003 IEEE Bologna Power Tech Conference Proceedings,*, vol. 3, June 2003, pp. 6 pp. Vol.3–.

[12] Siemens, "Inelfe, the france-spain hvdc plus interconnection is being realized as part of the european hvdc power freeways," 2014.

[13] B. C. Paucar, "Sistema HVDC baseado em conversores multinivel modulares," Ph.D. dissertation, Universidade Federal do Rio de Janeiro, 2014.

[14] G. B. Diaz, "Modular multilevel converter control for hvdc operation," Ph.D. dissertation, Norwegian University of Science and Technology, 2015.

[15] C. Ren, J. Wang, P. Yan, R. Xu, and T. Wang, "Polarity effect on corona discharge of needle-plane electrodes and audible noise under dc voltage," in *2015 IEEE 11th International Conference on the Properties and Applications of Dielectric Materials (ICPADM)*, 2015, pp. 784–787.

[16] E. Kontos, R. T. Pinto, S. Rodrigues, and P. Bauer, "Impact of hvdc transmission system topology on multiterminal dc network faults," *IEEE Transactions on Power Delivery*, vol. 30, no. 2, pp. 844–852, April 2015.

[17] T. Vrana, S. Dennetiere, Y. Yang, J. Jardini, D. Jovcic, and H. Saad, "The cigré b4 dc grid test system," *CIGRE Electra*, vol. 270, 10 2013.

[18] J. Arrillaga, Y. Liu, and N. Watson, *Flexible Power Transmission: The HVDC Options*. Wiley, 2007.

[19] R. Itiki, S. G. D. Santo, E. C. M. Costa, and R. M. Monaro, "Methodology for mapping operational zones of vsc-hvdc transmission system on offshore ports," *International Journal of Electrical Power & Energy Systems*, vol. 93, pp. 266 – 275, 2017.

[20] M. C.F.T., L. L.F.N., S. M.B.C., and M. R.M., "Dynamic performance analysis of distribution/sub-transmission networks with high penetration of pv generation," *World Academy of Science, Engineering and Technology, International Journal of Electrical, Computer, Energetic, Electronic and Communication Engineering*, vol. 10, no. 6, pp. 799–803, april 2016.

[21] C. Kang, Z. Chen, N. Zhang, O. Gomis-Bellmunt, M. Barnes, J. Yan, W. Hu, and K. Sun, "Guest editorial for the special section on enabling very high penetration renewable energy integration into future power systems," *IEEE Transactions on Power Systems*, vol. 33, no. 3, pp. 3223–3226, May 2018.

[22] A. S. Anees, "Grid integration of renewable energy sources: Challenges, issues and possible solutions," in *2012 IEEE 5th India International Conference on Power Electronics (IICPE)*, Dec 2012, pp. 1–6.

[23] G. M. Mufti, A. Basit, M. U. Rehman, S. Z. Hassan, and R. A. Khan, "Comparative analysis of the effects of renewable energy integration on the utility grid system," in *2018 International Conference on Computing, Mathematics and Engineering Technologies (iCoMET)*, March 2018, pp. 1–5.

[24] D. Jovcic and K. Ahmed, *High Voltage Direct Current Transmission: Converters, Systems and DC Grids*. Wiley, 2015.

[25] H. Saad, S. Dennetière, J. Mahseredjian, P. Delarue, X. Guillaud, J. Peralta, and S. Nguefeu, "Modular multilevel converter models for electromagnetic transients," *IEEE Transactions on Power Delivery*, vol. 29, no. 3, pp. 1481–1489, June 2014.

[26] A. Antonopoulos, L. Angquist, and H. Nee, "On dynamics and voltage control of the modular multilevel converter," in *2009 13th European Conference on Power Electronics and Applications*, 2009, pp. 1–10.

[27] M. Vatani, M. Hovd, and M. Saeedifard, "Control of the modular multilevel converter based on a discrete-time bilinear model using the sum of squares decomposition method," *IEEE Transactions on Power Delivery*, vol. 30, no. 5, pp. 2179–2188, Oct 2015.

[28] H. Saad, X. Guillaud, J. Mahseredjian, S. Dennetiere, and S. Nguefeu, "Mmc capacitor voltage decoupling and balancing controls," *IEEE Transactions on Power Delivery*, vol. 30, no. 2, pp. 704–712, 2014.

[29] G. Bergna, J. Vannier, P. Lefranc, A. Arzande, E. Berne, P. Egrot, and M. Molinas, "Modular multilevel converter leg-energy controller in rotating reference frame for voltage oscillations reduction," in *2012 3rd IEEE International Symposium on Power Electronics for Distributed Generation Systems (PEDG)*. IEEE, 2012, pp. 698–703.

[30] S. Samimi, F. Gruson, X. Guillaud, and P. Delarue, "Control of dc bus voltage with a modular multilevel converter," in *2015 IEEE Eindhoven PowerTech*. IEEE, 2015, pp. 1–6.

[31] S. Yang, P. Wang, and Y. Tang, "Feedback linearization-based current control strategy for modular multilevel converters," *IEEE Transactions on Power Electronics*, vol. 33, no. 1, pp. 161–174, 2018.

[32] Y. Chen, M. Jimenez Carrizosa, G. Damm, F. Lamnabhi-Lagarrigue, M. Li, and Y. Li, "Control induced time-scale separation for multi-terminal high voltage direct current systems using droop control," *IEEE Transactions on Control Systems Technology*, 2019.

[33] M. J. Carrizosa, F. D. Navas, G. Damm, and F. Lamnabhi-Lagarrigue, "Optimal power flow in multi-terminal hvdc grids with offshore wind farms and storage devices," *International Journal of Electrical Power & Energy Systems*, vol. 65, pp. 291 – 298, 2015.

[34] A. Antonopoulos, "Control, Modulation and Implementation of Modular Multilevel Converters," Theses, School of Electrical Engineering, KTH, 2011.

[35] M. Eremia, C. Liu, and A. Edris, *Advanced Solutions in Power Systems: HVDC, FACTS, and Artificial Intelligence*, ser. IEEE Press Series on Power Engineering. Wiley, 2016. [Online]. Available: https://books.google.com.br/books?id=LxjkDAAAQBAJ

[36] S. Khan and E. Tedeschi, "Modeling of mmc for fast and accurate simulation of electromagnetic transients: A review," *Energies*, vol. 10, no. 8, p. 1161, Aug 2017. [Online]. Available: http://dx.doi.org/10.3390/en10081161

[37] M. Abdelsalam, M. Marei, S. Tennakoon, and A. Griffiths, "Capacitor voltage balancing strategy based on sub-module capacitor voltage estimation for modular multilevel converters," *CSEE Journal of Power and Energy Systems*, vol. 2, pp. 65–73, 03 2016.

[38] X. Shi, Z. Wang, L. M. Tolbert, and F. Wang, "A comparison of phase disposition and phase shift pwm strategies for modular multilevel converters," in *2013 IEEE Energy Conversion Congress and Exposition*, 2013, pp. 4089–4096.

[39] M. Tayyab and A. Sarwar, "Submodule capacitor voltage balancing of modular multilevel converter," in *2019 International Conference on Electrical, Electronics and Computer Engineering (UPCON)*, Nov 2019, pp. 1–5.

[40] D. F. Baú, G. Sebastião da Silva, H. Pinheiro, and F. B. Grigoletto, "Pd modulation strategy for modular multilevel converters," in *2016 12th IEEE International Conference on Industry Applications (INDUSCON)*, 2016, pp. 1–6.

[41] G. Konstantinou, M. Ciobotaru, and V. Agelidis, "Selective harmonic elimination pulse-width modulation of modular multilevel converters," *IET Power Electronics*, vol. 6, no. 1, pp. 96–107, Jan 2013.

[42] S. Debnath, J. Qin, B. Bahrani, M. Saeedifard, and P. Barbosa, "Operation, control, and applications of the modular multilevel converter: A review," *IEEE Transactions on Power Electronics*, vol. 30, no. 1, pp. 37–53, Jan 2015.

[43] D. K. C. S. M. Venkatesh, "A literature survey on modular multilevel converter key challenges," *International Research Journal of Engineering and Technology*, vol. 5, no. 9, pp. 899 – 904, 2018.

[44] L. Qu, Z. Lu, C. Liu, and C. He, "A sort method of balancing capacitor voltage of mmc," in *2019 18th International Symposium on Distributed Computing and Applications for Business Engineering and Science (DCABES)*, Nov 2019, pp. 241–244.

[45] H. Behbahanifard, S. Abazari, and A. Sadoughi, "New scheme of she-pwm technique for cascaded multilevel inverters with regulation of dc voltage sources," *ISA Transactions*, vol. 97, pp. 44 – 52, 2020. [Online]. Available: http://www.sciencedirect.com/science/article/pii/S0019057819303039

[46] H. Torkaman, M. Fakhari, H. Karimi, and B. Taheri, "New frequency modulation strategy with she for h-bridge multilevel inverters," in *2018 4th International Conference on Electrical Energy Systems (ICEES)*, 2018, pp. 157–161.

[47] Y. Deng, K. H. Teo, C. Duan, T. G. Habetler, and R. G. Harley, "A fast and generalized space vector modulation scheme for multilevel inverters," *IEEE Transactions on Power Electronics*, vol. 29, no. 10, pp. 5204–5217, 2014.

[48] B. Li, R. Yang, D. Xu, G. Wang, W. Wang, and D. Xu, "Analysis of the phase-shifted carrier modulation for modular multilevel converters," *IEEE Transactions on Power Electronics*, vol. 30, no. 1, pp. 297–310, 2015.

[49] M. Saeedifard and R. Iravani, "Dynamic performance of a modular multilevel back-to-back hvdc system," *IEEE Transactions on Power Delivery*, vol. 25, no. 4, pp. 2903–2912, 2010.

[50] N. Geddada, A. Ukil, and Y. M. Yeap, "Circulating current controller in dq reference frame for mmc based hvdc system," *IECON 2016 42nd Annual Conference of the IEEE Industrial Electronics Society*, pp. 3288–3293, Oct 2016.

[51] P. Rodriguez, J. Pou, J. Bergas, J. I. Candela, R. P. Burgos, and D. Boroyevich, "Decoupled double synchronous reference frame pll for power converters control," *IEEE Transactions on Power Electronics*, vol. 22, no. 2, pp. 584–592, March 2007.

[52] M. Zama, "Modeling and Control of Modular Multilevel Converters (MMCs) for HVDC applications," Theses, COMMUNAUTE UNIVERSITE GRENOBLE ALPES, 2006.

[53] H. Saad, S. Dennetière, and J. Mahseredjian, "On modelling of mmc in emt-type program," in *2016 IEEE 17th Workshop on Control and Modeling for Power Electronics (COMPEL)*, June 2016, pp. 1–7.

[54] E. N. Abildgaard and M. Molinas, "Modelling and control of the modular multilevel converter (mmc)," *Energy Procedia*, vol. 20, pp. 227 – 236, 2012, technoport 2012 - Sharing Possibilities and 2nd Renewable Energy Research Conference (RERC2012). [Online]. Available: http://www.sciencedirect.com/science/article/pii/S1876610212007539

[55] Jun Wang, E. Farr, R. Burgos, D. Boroyevich, R. Feldman, A. Watson, J. Clare, and P. Wheeler, "State-space switching model of modular multilevel converters," in *2013 IEEE 14th Workshop on Control and Modeling for Power Electronics (COMPEL)*, June 2013, pp. 1–10.

[56] G. Bergna-Diaz, J. A. Suul, and S. D'Arco, "Energy-based state-space representation of modular multilevel converters with a constant equilibrium point in steady-state operation," *IEEE Transactions on Power Electronics*, vol. 33, no. 6, pp. 4832–4851, June 2018.

[57] J. Peralta, H. Saad, S. Dennetiere, J. Mahseredjian, and S. Nguefeu, "Detailed and averaged models for a 401-level mmc–hvdc system," *IEEE Transactions on Power Delivery*, vol. 27, no. 3, pp. 1501–1508, July 2012.

[58] J. Freytes, S. Akkari, J. Dai, F. Gruson, P. Rault, and X. Guillaud, "Small-signal state-space modeling of an hvdc link with modular multilevel converters," in *2016 IEEE 17th Workshop on Control and Modeling for Power Electronics (COMPEL)*, June 2016, pp. 1–8.

[59] S. Yang, J. Fang, Y. Tang, H. Qiu, C. Dong, and P. Wang, "Modular multilevel converter synthetic inertia-based frequency support for medium-voltage microgrids," *IEEE Transactions on Industrial Electronics*, vol. 66, no. 11, pp. 8992–9002, Nov 2019.

[60] F. She, L. Liu, X. Wang, X. Mou, J. Cui, and H. Xiong, "A novel coordinated control strategy for vsc-mtdc system," in *2018 2nd IEEE Conference on Energy Internet and Energy System Integration (EI2)*, 2018, pp. 1–5.

[61] Weijia Tang, Daozhuo Jiang, Rui Yin, Yufen Wang, and Yuebin Zhou, "A novel ccsc for circulating current suppression in modular multilevel converters," in *2016 IEEE Power and Energy Society General Meeting (PESGM)*, 2016.

[62] J. Li, G. Konstantinou, H. R. Wickramasinghe, and J. Pou, "Operation and control methods of modular multilevel converters in unbalanced ac grids: A review," *IEEE Journal of Emerging and Selected Topics in Power Electronics*, vol. 7, no. 2, pp. 1258–1271, June 2019.

[63] S. Akkari, "Control of a multi-terminal HVDC (MTDC) system and study of the interactions between the MTDC and the AC grids." Ph.D. dissertation, , 2016.

[64] W. Wu, D. Wang, Z. Peng, and X. Liu, "Model predictive direct power control for modular multilevel converter under unbalanced conditions with power compensation and circulating current reduction," *ISA Transactions*, 2020. [Online]. Available: http://www.sciencedirect.com/science/article/pii/S0019057820302895

[65] K. Ilves, A. Antonopoulos, S. Norrga, and H. Nee, "Steady-state analysis of interaction between harmonic components of arm and line quantities of modular multilevel converters," *IEEE Transactions on Power Electronics*, vol. 27, no. 1, pp. 57–68, 2012.

[66] Q. Tu, Z. Xu, and L. Xu, "Reduced switching-frequency modulation and circulating current suppression for modular multilevel converters," *IEEE Transactions on Power Delivery*, vol. 26, no. 3, pp. 2009–2017, 2011.

[67] D. Sharma, A. H. Bhat, A. Ahmad, and N. Langer, "Capacitor voltage balancing in neutral-point clamped rectifier using modified modulation index technique," *Computers Electrical Engineering*, vol. 70, pp. 137 – 150, 2018. [Online]. Available: http://www.sciencedirect.com/science/article/pii/S0045790617303439

[68] Z. Liu, W. Yu, H. Guo, W. Kong, C. Gan, and R. Qu, "A capacitor voltage sorting algorithm for modular multilevel converters(mmc) under low-frequency carrier modulation," in *2019 22nd International Conference on Electrical Machines and Systems (ICEMS)*, 2019, pp. 1–4.

[69] H. Peng, Q. Mu, C. Wang, X. Zhang, F. He, and D. Xu, "Capacitor voltage balancing control algorithm for modular multilevel converter based on the dynamic tiered sorting," in *2018 International Conference on Power System Technology (POWERCON)*, 2018, pp. 2752–2757.

[70] D. Wang and B. Zhang, "A optimized capacitor voltage balance strategy using binary number sorting algorithm for modular multilevel converter," in *2019 8th International Symposium on Next Generation Electronics (ISNE)*, 2019, pp. 1–3.

[71] P. Hu, R. Teodorescu, and J. M. Guerrero, "State observer based capacitor-voltage-balancing method for modular multilevel converters without arm-current sensors," *International Journal of Electrical Power Energy Systems*, vol. 113, pp. 188 – 196, 2019. [Online]. Available: http://www.sciencedirect.com/science/article/pii/S0142061518339243

[72] L. Angquist, A. Antonopoulos, D. Siemaszko, K. Ilves, M. Vasiladiotis, and H. Nee, "Open-loop control of modular multilevel converters using estimation of stored energy," *IEEE Transactions on Industry Applications*, vol. 47, no. 6, pp. 2516–2524, 2011.

[73] S. Almasabi, N. Nguyen, and J. Mitra, "Control of a multilevel modular converter using a state observer," in *2015 Annual IEEE India Conference (INDICON)*, 2015, pp. 1–5.

[74] G. Bergna, E. Berne, P. Egrot, P. Lefranc, A. Arzande, J. Vannier, and M. Molinas, "An energy-based controller for hvdc modular multilevel converter in decoupled double synchronous reference frame for voltage oscillation reduction," *IEEE Transactions on Industrial Electronics*, vol. 60, no. 6, pp. 2360–2371, 2013.

[75] L. Harnefors, A. Antonopoulos, S. Norrga, L. Angquist, and H. P. Nee, "Dynamic analysis of modular multilevel converters," *IEEE Transactions on Industrial Electronics*, vol. 60, no. 7, pp. 2526–2537, July 2013.

[76] K. Ogata, *Modern Control Engineering*, ser. Instrumentation and controls series. Prentice Hall, 2010. [Online]. Available: https://books.google.com.br/books?id=Wu5GpNAelzkC

[77] P. Münch, D. Görges, M. Izák, and S. Liu, "Integrated current control, energy control and energy balancing of modular multilevel converters," in *IECON 2010 - 36th Annual Conference on IEEE Industrial Electronics Society*, Nov 2010, pp. 150–155.

[78] H. Bärnklau, A. Gensior, and J. Rudolph, "A model-based control scheme for modular multilevel converters," *IEEE Transactions on Industrial Electronics*, vol. 60, no. 12, pp. 5359–5375, 2013.

[79] H. Khalil, *Nonlinear Control, Global Edition*. Pearson Education Limited, 2015.

[80] M. J. Carrizosa, G. Damm, A. Benchaib, P. Alou, M. Netto, and F. Lamnabhi-Lagarrigue, "Bilinear and nonlinear control algorithms for a dc/dc converter for multi-terminal hvdc networks," *IFAC Proceedings Volumes*, vol. 47, no. 3, pp. 523 – 528, 2014, 19th IFAC World Congress.

[81] J. Slotine and W. Li, *Applied Nonlinear Control*, ser. Prentice-Hall International Editions. Prentice-Hall, 1991. [Online]. Available: https://books.google.com.br/books?id=HddxQgAACAAJ

[82] P. Pardalos and V. Yatsenko, *Optimization and Control of Bilinear Systems: Theory, Algorithms, and Applications*, ser. Springer Optimization and Its Applications. Springer US, 2008.

[83] R. Mohler, *Bilinear Control Processes: with Applications to Engineering, Ecology, and Medicine*, ser. Mathematics in Science and Engineering. Elsevier Science, 1974.

[84] B. Tibken, F. Lehn, and E. Hofer, "Quadratic control lyapunov functions for bilinear systems," 07 1999.

[85] E. D. Sontag, "A 'universal' construction of artstein's theorem on nonlinear stabilization," *Systems Control Letters*, vol. 13, no. 2, pp. 117 – 123, 1989. [Online]. Available: http://www.sciencedirect.com/science/article/pii/0167691189900285

[86] Z. Artstein, "Stabilization with relaxed controls," *Nonlinear Analysis: Theory, Methods Applications*, vol. 7, no. 11, pp. 1163 – 1173, 1983. [Online]. Available: http://www.sciencedirect.com/science/article/pii/0362546X83900494

[87] M. Guan, W. Pan, J. Zhang, Q. Hao, J. Cheng, and X. Zheng, "Synchronous generator emulation control strategy for voltage source converter (vsc) stations," *IEEE Transactions on Power Systems*, vol. 30, no. 6, pp. 3093–3101, 2015.

[88] A. Yazdani and R. Iravani, *Voltage-Sourced Converters in Power Systems: Modeling, Control, and Applications*, ser. Wiley - IEEE. Wiley, 2010. [Online]. Available: https://books.google.com.br/books?id=_x_4Cu-BKwkC

[89] A. Taffese, E. de Jong, S. Arco, and E. Tedeschi, "Online parameter adjustment method for arm voltage estimation of the modular multilevel converter," 04 2019.

[90] I. Landau, "On the optimal regulator problem and stabilization of bilinear systems," in *Laboratoire d'Automatique (CNRS)*, 1979.

[91] S. Bacha, I. Munteanu, and A. Bratcu, *Power Electronic Converters Modeling and Control: with Case Studies*, ser. Advanced Textbooks in Control and Signal Processing. Springer London, 2013.

[92] V. Y. P.M. Pardalos, *Optimization and Controlof Bilinear Systems*, ser. P.M. Pardalos, V. Yatsenko. Springer, 2009.

[93] E. Panteley and A. Loría, "Synchronization and dynamic consensus of heterogeneous networked systems," *IEEE Transactions on Automatic Control*, vol. 62, no. 8, pp. 3758–3773, Aug 2017.

Appendices

APÊNDICE A

Introduction en Français

A.1 Contrôle des convertisseurs modulaires à plusieurs niveaux

Le contrôle de MMC présente des défis supplémentaires par rapport à la topologie d'autres convertisseurs. La méthode de contrôle doit faire face à:

- ❏ En externe, la gestion du flux de puissance active et réactive, ainsi que les tensions AC et DC;
- ❏ En interne, la gestion de la dynamique du convertisseur comme les courants de circulation, la tension du condensateur SM, l'équilibrage des demi-bras, l'équilibrage de phase et le contrôle de l'énergie du convertisseur.

MMCs ont également une technique de modélisation complexe en raison du nombre élevé de Submodule (SM), qui nécessite un contrôle simultané pour atteindre l'équilibrage de la tension du condensateur. Il existe de nombreuses approches de modélisation MMC et les modèles affectent directement la conception des commandes. Dans cette thèse, un modèle mathématique basé sur le demi-bras moyen est utilisé pour développer les contrôleurs, et un modèle de commutation est utilisé pour vérifier les performances des contrôles. Concernant le modèle moyen, il existe de nombreuses approches dans la littérature. Dans [25], le modèle moyen considère un modèle de fonction de commutation qui inclut avec précision la dynamique des condensateurs de chaque SM.

De plus, dans [26], il existe un modèle continu où les demi-bras sont représentés par la fonction de sources de tension variables. Cependant, un modèle moyen plus complexe augmentera l'ordre du système, donc la complexité de la solution proposée. De cette façon, le modèle moyen utilisé dans cette recherche est basé sur [27], qui utilise une tension SM équivalente, par demi-bras.

Un modèle de commutation est simulé à l'aide du contrôleur proposé pour vérifier les performances du contrôle. Le modèle de commutation a un contrôleur de bas niveau, qui atteint

correctement l'équilibrage de tension des SM. L'algorithme de tri implémenté dans le contrôle de bas niveau est basé sur la technique standard proposée par [24].

Concernant le contrôle, la plupart des résultats existants sur la stratégie de contrôle pour MMCs consistent en des contrôleurs linéaires, en tant que contrôle vectoriel. Ainsi, un seul point de fonctionnement est pris en compte dans sa conception puisque les non-linéarités du système sont ignorées [28; 29; 30].

De ce point de vue-là, on peut citer des travaux comme [31], où le modèle non linéaire MMC est d'abord linéarisé, puis des contrôleurs linéaires sont conçus pour cela. D'une manière différente, [27] propose un modèle bilinéaire en temps discret d'une MMC, contrôlé par une méthode de décomposition en somme des carrés, suite à une analyse non linéaire.

Ces études sont motivées par la pertinence de concevoir des contrôleurs non linéaires qui peuvent assurer la stabilité dans les grandes régions d'exploitation du réseau électrique, y compris une analyse de stabilité rigoureuse [32; 33]. Le chapitre suivant abordera plus en détail la modélisation et le contrôle de MMC.

A.2 Objectif principal de la thèse

L'objectif principal de cette thèse est de développer une méthode de contrôle MMC adaptée pour assurer la stabilité de l'état du système, en particulier les courants de circulation et l'énergie stockée par le convertisseur.

Objectifs spécifiques

Les objectifs spécifiques suivants doivent être atteints:

- ❏ Développer une méthode de contrôle capable de minimiser les courants de circulation et l'énergie stockée par le convertisseur pour un convertisseur MMC;
- ❏ Prouver la stabilisation du système;
- ❏ Évaluer la robustesse du contrôle pour la variation des paramètres du convertisseur;
- ❏ Évaluer les impacts des gains de contrôle sur la dynamique du convertisseur.

A.3 Principales contributions

Les principales contributions de cette thèse sont de présenter deux nouveaux contrôleurs non linéaires appliqués à la MMC. Les techniques proposées permettent de contrôler les tensions AC et DC, les courants de circulation et l'énergie totale et d'équilibrage du convertisseur. Des preuves mathématiques sont présentées pour sa stabilité, qui est basée sur la théorie de Lyapunov. Ces contrôleurs fournissent une stabilisation asymptotique pour les triphasés MMC.

A.4 Conclusion générale

Les réseaux électriques sont de plus en plus complexes dans le monde en raison d'une diversité de production d'électricité, de systèmes plus interconnectés et d'un marché de l'énergie intense. La production d'électricité d'origine renouvelable augmente le nombre de barres faibles dans le système. Un nombre élevé de bus faibles peut augmenter le risque de perte de stabilité. De cette manière, la demande de services auxiliaires augmente, par exemple, augmentant le besoin de systèmes à inertie synthétique. Une solution pourrait être l'incorporation pour alimenter les appareils électroniques pour des fonctionnalités supplémentaires via le système de contrôle. Cependant, dans le domaine des convertisseurs HVDC, il reste encore beaucoup à faire pour contrôler la stabilité globale du système de transmission. C'est une question essentielle dans la planification du réseau électrique, en particulier avec l'énorme pénétration des énergies renouvelables connectées au réseau principal via HVDC. Par conséquent, cette thèse fournit des résultats qui contribuent au domaine du contrôle des convertisseurs ac MMC, ce qui pourrait permettre d'autres services auxiliaires.

Le chapitre 1 explique les caractéristiques actuelles du réseau électrique, en raison du système plus interconnecté et de l'augmentation de la production d'énergie renouvelable. De plus, il présente le contexte du développement de l'électronique de puissance et un aperçu des caractéristiques techniques atteintes par chaque type de dispositif de commutation. Le chapitre souligne la dernière réalisation dans ce domaine, comme la mise à niveau du VSC qui produit le MMC. Cette mise à niveau apporte des avantages tels que l'évolutivité et abaisse la fréquence de commutation au niveau des appareils, par rapport au VSC. Enfin, un bref aperçu du contrôle met en évidence les inconvénients du contrôleur MMCs et justifie le développement de la thèse.

Le chapitre 2 passe en revue les aspects techniques du convertisseur MMC. Ce chapitre comprend également un aperçu de la modélisation et indique les compromis sur la vitesse de simulation lors de l'utilisation de modèles d'ordre complet ou de modèles d'ordre réduit. En outre, la vue d'ensemble détaillée de la conception de commande pour MMC est présentée, où les réalisations obtenues par les contrôleurs non linéaires développés sont soulignées.

Le chapitre 3 montre la conception d'un contrôle linéaire qui est utilisé à des fins de comparaison. Les deux systèmes d'essais sont présentés, l'un en moyenne tension et l'autre en haute tension. De plus, une comparaison entre le modèle moyen et le modèle de commutation à l'aide du contrôleur PI est effectuée. Cette comparaison prouve la fidélité entre les modèles pour les variables d'état MMC. Ensuite, un système haute tension est simulé par un modèle de commutation et la dynamique interne est analysée. A partir de la dynamique interne, l'équilibrage d'énergie supérieur et inférieur est rapidement réalisé après les transitoires. Malgré ce fait, le fait que le contrôleur ne permet pas de contrôler directement l'énergie par demi-bras, ceci est réalisé en $400\ ms$. Enfin, l'équilibrage de tension des condensateurs est bien réalisé par l'algorithme de tri mis en œuvre.

Le chapitre 4 présente un contrôleur non linéaire pour un convertisseur MMC appliqué à des

fins de transmission HVDC. La stratégie de contrôle est conçue pour contrôler non seulement les courants alternatifs et circulants, mais également l'énergie stockée et l'équilibre énergétique du convertisseur. La théorie de Lyapunov est la base pour développer le contrôle non linéaire présenté dans cette recherche, où une analyse de stabilité rigoureuse est effectuée pour assurer le bon fonctionnement de la grille.

Les performances de commande proposées sont testées dans un modèle moyen et dans un modèle MMC de commutation détaillé sur la plate-forme Matlab Simscape Electrical. Pour le contrôle proposé, il est à noter que les gains sont basés sur les performances de l'état souhaité et sont simples à régler. Les contrôles PI et non linéaires ont des performances similaires. De plus, le contrôleur non linéaire a un comportement approprié compte tenu d'une vaste région de fonctionnement pour la MMC limitée par les limitations physiques du système.

Les incertitudes de robustesse sur les paramètres sont analysées. Pour les changements dans R, R_c, L et L_c, les variables d'état du variateur de commande à leurs valeurs souhaitées à l'état fixe. Cependant, l'augmentation de la valeur des condensateurs SM C, les composantes dq du courant de circulation (i_{cirdq}) et par conséquent l'équilibrage d'énergie W_v présentent une réponse oscillatoire.

Les fluctuations des tensions DC et AC affectent la vitesse de convergence de l'état du système. Pendant ce temps, le courant de circulation a une grande oscillation lorsque V_{ac} augmente, et oscille également pour les changements de V_{dc}.

Les simulations montrent que le contrôleur non linéaire présente des performances appropriées, avec un faible sur-signal dans les transitoires. Le contrôle non linéaire pilote avec succès les variables contrôlées vers leurs références, ainsi que les états d'énergie. Ces derniers étant à dynamique libre, ils sont contrôlés par les entrées virtuelles conçues.

Le chapitre 5 présente un contrôle bilinéaire pour un convertisseur MMC, qui contrôle directement les courants alternatifs et circulants et l'énergie MMC. Une preuve mathématique rigoureuse est donnée pour sa stabilité, qui est basée sur la théorie de Lyapunov. Ce résultat fournit une stabilisation asymptotique pour les trois phases MMC, et l'utilisation d'une fonction de Lyapunov implique une vérification formelle de la stabilité et d'une région d'attraction spécifique pour le modèle considéré. De plus, des directives de réglage sont également présentées, en tenant compte du compromis entre la vitesse de réponse, l'effet de couplage et l'effort de contrôle. Une analyse de sensibilité est également présentée. Il présente de fortes propriétés de robustesse pour les erreurs de paramètres réalistes.

La technique de contrôle bilinéaire est simulée à l'aide d'un modèle moyen et d'un modèle de commutation dans l'environnement Simscape Electrical. Les résultats théoriques et de simulation montrent que le contrôleur proposé est adapté aux exigences MMC comme temps de réponse et de dépassement, et permet un compromis utile entre la commande de puissance et d'énergie dans le convertisseur. En outre, la gestion de l'énergie de la commande bilinéaire ouvre la voie à de nouveaux services auxiliaires pour la prise en charge du réseau, aussi bien pour les réseaux AC que DC, aussi vite que la réponse en fréquence ou l'inertie synthétique.

Le contrôle bilinéaire présente une preuve de stabilité rigoureuse et possède une zone de fonctionnement bien établie. Dans les simulations, le contrôle bilinéaire fonctionne bien.

Enfin, les contrôleurs proposés, non linéaires et bilinéaires, stabilisent bien les variables d'état MMC. De plus, l'implémentation non linéaire est simple une fois que la relation entre les performances des variables d'état et les gains est claire. Cependant, Bilinear a une solution simple par une loi de contrôle unique.

A.4.1 Résultats principaux

- ❑ Deux algorithmes de contrôle non linéaires, basés sur un modèle mathématique bilinéaire, sont conçus pour les convertisseurs MMC;

- ❑ Ces algorithmes sont capables de contrôler les flux d'alimentation CA et CC, l'énergie totale du convertisseur et l'équilibrage de l'énergie du convertisseur au modèle MMC de commutation;

- ❑ Il existe une analyse de stabilité formelle par la théorie de Lyapunov pour les deux contrôleurs;

- ❑ Une fois que les contrôles proposés ne sont pas basés sur un modèle linéarisé, une vaste zone d'opération est accessible;

- ❑ Pour le bilinéaire, par rapport aux autres techniques de contrôle des MMC, la stratégie de contrôle proposée permet de stabiliser toutes les variables d'état du convertisseur par une seule loi de contrôle. Le fait qu'il existe une loi de contrôle unique rend le contrôleur beaucoup plus facile à régler que les contrôleurs PI en cascade standard de l'industrie.

A.4.2 Perspectives pour les recherches futures

À ce stade, la thèse a relevé certains défis liés au contrôleur d'énergie du convertisseur, et les futurs sujets à aborder sont:

- ❑ Utiliser le contrôle dans une grille MTDC, contrôlant également V_{DC};
- ❑ Étendre à une grille MTDC entièrement contrôlée par bilinéaire;
- ❑ Utiliser la commande MMC comme détecteur de défaut et protection;
- ❑ Pour certains points de fonctionnement MTDC, il sera défini la distance jusqu'à ce que la tension s'effondre dans chaque barre;

- ❏ Utiliser le stockage d'énergie SM pour fournir des services auxiliaires, tels que le support inertiel, de fréquence et de tension pour le réseau.

APÊNDICE **B**

Nonlinear Control Code at Wolfram Mathematica

APPENDIX A: Nonlinear control code at Wolfram Mathematica 11.2

STATE 1 Com integrador

```
Clear["Global`*"]
xdot1 = -Req/Leq * x1 + w * x2 + (u1 - u3)/Leq + (2 * vfd)/Leq;
precontrolinput1 = Solve[
   alpha1 * xtilde1 - Req/Leq * x1 + w * x2 + (u1 - u3)/Leq + (2 * vfd)/Leq + b1 * ξ1 == 0, u1]
```

$$\{\{u1 \to u3 - 2\,vfd + Req\,x1 - Leq\,w\,x2 - alpha1\,Leq\,xtilde1 - Leq\,b_1\,\xi_1\}\}$$

STATE 2 Com integrador

```
xdot2 = -w * x1 - Req/Leq * x2 + (u2 - u4)/Leq + (2 * vfq)/Leq;
precontrolinput2 = Solve[
   alpha2 * xtilde2 - w * x1 - Req/Leq * x2 + (u2 - u4)/Leq + (2 * vfq)/Leq + b2 * ξ2 == 0, u2]
```

$$\{\{u2 \to u4 - 2\,vfq + Leq\,w\,x1 + Req\,x2 - alpha2\,Leq\,xtilde2 - Leq\,b_2\,\xi_2\}\}$$

STATE 3 Com integrador

```
xdot3 = -R/L * x3 + w * x4 - (u1 + u3)/(2 * L);
precontrolinput3 =
  alpha3 * xtilde3 - R/L * x3 + w * x4 - (u1 + u3)/(2 * L) /. precontrolinput1
```

$$\left\{-\frac{R\,x3}{L} + w\,x4 + alpha3\,xtilde3 - \frac{2\,u3 - 2\,vfd + Req\,x1 - Leq\,w\,x2 - alpha1\,Leq\,xtilde1 - Leq\,b_1\,\xi_1}{2\,L}\right\}$$

DEFININDO U3 COMO CONTROLINPUT3

```
controlinput3 =
  Expand[Solve[precontrolinput3 == 0, u3]] /. precontrolinput1
```

$$\left\{\left\{\left\{u3 \to vfd - \frac{Req\,x1}{2} + \frac{Leq\,w\,x2}{2} - R\,x3 + L\,w\,x4 + \frac{alpha1\,Leq\,xtilde1}{2} + alpha3\,L\,xtilde3 + \frac{1}{2}Leq\,b_1\,\xi_1\right\}\right\}\right\}$$

STATE 4 Com integrador

```
xdot4 = -w * x3 - R/L * x4 - (u2 + u4)/(2 * L);
precontrolinput4 =
 alpha4 * xtilde4 - w * x3 - R/L * x4 - (u2 + u4)/(2 * L) + b4 * ξ4 /. precontrolinput2
```

$$\left\{-w\,x3 - \frac{R\,x4}{L} + \text{alpha4}\,\text{xtilde4} - \frac{1}{2\,L}\right.$$
$$\left.(2\,u4 - 2\,vfq + Leq\,w\,x1 + Req\,x2 - \text{alpha2}\,Leq\,\text{xtilde2} - Leq\,b_2\,\xi_2) + b_4\,\xi_4\right\}$$

DEFININDO U4 COMO CONTROLINPUT4

```
controlinput4 =
 Expand[Solve[precontrolinput4 == 0, u4]] // Flatten // First
```

$$u4 \to vfq - \frac{Leq\,w\,x1}{2} - \frac{Req\,x2}{2} - L\,w\,x3 - R\,x4 +$$
$$\frac{\text{alpha2}\,Leq\,\text{xtilde2}}{2} + \text{alpha4}\,L\,\text{xtilde4} + \frac{1}{2}\,Leq\,b_2\,\xi_2 + L\,b_4\,\xi_4$$

STATE 5 ----------DEFININDO U5 COMO CONTROLINPUT5

```
xdot5 = -R/L * x5 - u5/(2 * L) + vdc/(2 * L);
controlinput5 =
 Expand[Solve[alpha5 * xtilde5 - R/L * x5 - u5/(2 * L) + vdc/(2 * L) == 0, u5]]
```

$$\{\{u5 \to vdc - 2\,R\,x5 + 2\,\text{alpha5}\,L\,\text{xtilde5}\}\}$$

DEFININDO U1 COMO CONTROLINPUT1

```
controlinput1 = Expand[precontrolinput1 /. controlinput3]
```

$$\left\{\left\{\left\{\left\{u1 \to -vfd + \frac{Req\,x1}{2} - \frac{Leq\,w\,x2}{2} - R\,x3 + L\,w\,x4 -\right.\right.\right.\right.$$
$$\left.\left.\left.\left.\frac{\text{alpha1}\,Leq\,\text{xtilde1}}{2} + \text{alpha3}\,L\,\text{xtilde3} - \frac{1}{2}\,Leq\,b_1\,\xi_1\right\}\right\}\right\}\right\}$$

DEFININDO U2 COMO CONTROLINPUT2

```
controlinput2 = Expand[precontrolinput2 /. controlinput4]
```

$$\left\{\left\{u2 \to -vfq + \frac{Leq\,w\,x1}{2} + \frac{Req\,x2}{2} - L\,w\,x3 - R\,x4 -\right.\right.$$
$$\left.\left.\frac{\text{alpha2}\,Leq\,\text{xtilde2}}{2} + \text{alpha4}\,L\,\text{xtilde4} - \frac{1}{2}\,Leq\,b_2\,\xi_2 + L\,b_4\,\xi_4\right\}\right\}$$

V tilde dot para os estados de 1 a 5

```
lyapunovequation1 =
 Expand[xtilde1 * (-Req/Leq * x1 + w * x2 + (u1 - u3)/Leq + (2 * vfd)/Leq) + ξ1 * xtilde1 /.
    controlinput1 /. controlinput3]
```

$$\{\{\{\{\{-\text{alpha1}\ \text{xtilde1}^2 + \text{xtilde1}\ \xi_1 - \text{xtilde1}\ b_1\ \xi_1\}\}\}\}\}$$

```
lyapunovequation2 =
 Expand[xtilde2 * (-w * x1 - Req/Leq * x2 + (u2 - u4)/Leq + (2 * vfq)/Leq) + ξ2 * xtilde2 /.
    controlinput2 /. controlinput4]
```

$$\{-\text{alpha2}\ \text{xtilde2}^2 + \text{xtilde2}\ \xi_2 - \text{xtilde2}\ b_2\ \xi_2\}$$

```
lyapunovequation3 = Expand[
  xtilde3 * (-R/L * x3 + w * x4 - (u1 + u3)/(2 * L)) /. controlinput1 /. controlinput3]
```

$$\{\{\{\{\{-\text{alpha3}\ \text{xtilde3}^2\}\}\}\}\}$$

```
lyapunovequation4 =
 Expand[xtilde4 * (-w * x3 - R/L * x4 - (u2 + u4)/(2 * L)) + ξ4 * xtilde4 /.
    controlinput2 /. controlinput4]
```

$$\{-\text{alpha4}\ \text{xtilde4}^2 + \text{xtilde4}\ \xi_4 - \text{xtilde4}\ b_4\ \xi_4\}$$

```
lyapunovequation5 =
 Expand[xtilde5 * (-R/L * x5 - u5/(2 * L) + vdc/(2 * L)) /. controlinput5]
```

$$\{-\text{alpha5}\ \text{xtilde5}^2\}$$

Derivada da lyapunov de x6 com os controles pré-definidos; Derivada de vdottilde6 em relação a xtilde 6 e xtilde 5. Lembrando que xtilde5→0 e xtilde6→0 no ponto de equilibrio.

```
previa =
  Expand[((-3 * u1)/4 * x1 + (3 * u1)/2 * x3 - (3 * u2)/4 * x2 + (3 * u2)/2 * x4 + (3 * u3)/4 * x1 +
      (3 * u3)/2 * x3 + (3 * u4)/4 * x2 + (3 * u4)/2 * x4 + 3 * u5 * x5 + ξ6) /.
    controlinput1 /. controlinput2 /. controlinput3 /.
   controlinput4 /. controlinput5 /. x1 → xtilde1 + xbar1 /.
  x2 → xtilde2 + xbar2 /. x3 → xtilde3 + xbar3 + b7 * ξ7 /.
 x4 → xtilde4 + xbar4 /. x5 → xtilde5 + xbar5 -
  alpha6 * xtilde6 - b6 * ξ6];
dottx6 := previa - ((3 vfd xbar1)/2 - (3 Req xbar1^2)/4 + (3 vfq xbar2)/2 - (3 Req xbar2^2)/4 -
    3 R xbar3^2 - 3 R xbar4^2 + 3 vdc xbar5 - 6 R xbar5^2) /.
   xtilde1 → 0 /. xtilde2 → 0 /. xtilde3 → 0 /.
  xtilde4 → 0 /. xtilde5 → 0 /. xtilde6 → 0 /.
 ξ1 → 0 /. ξ2 → 0 /. ξ3 → 0 /. ξ4 → 0 /. ξ5 → 0
edotx6 := xtilde6;
dottildex5 := -alpha5 * xtilde5 + alpha6 * dottx6;
m =
 D[{edotx6, dottx6, dottildex5}, {{ξ6, xtilde6, xtilde5}}] // Flatten

{0, 1, 0, 1 - 3 vdc b6 + 12 R xbar5 b6 - 12 R b6^2 ξ6, 0, 0,
 alpha6 (1 - 3 vdc b6 + 12 R xbar5 b6 - 12 R b6^2 ξ6), 0, -alpha5}


equilibriumM =
 m /. xtilde5 -> 0 /. xtilde6 -> 0 /. R → 0.5 /. vdc → 90 /. L → 0.0014 /.
  xbar5 → 0.22 /. alpha5 → 100 /. alpha6 → 100 /. ξ6 → 0
{0, 1, 0, 1. - 268.68 b6, 0, 0, 100 (1. - 268.68 b6), 0, -100}
```

```
Eig = Expand[Eigenvalues[
    {{equilibriumM[[1]], equilibriumM[[2]], equilibriumM[[3]]},
     {equilibriumM[[4]], equilibriumM[[5]], equilibriumM[[6]]},
     {equilibriumM[[7]], equilibriumM[[8]], equilibriumM[[9]]}}]];
Eig /. b → 1
Eig /. b → 10
Eig /. b → 100
Eig /. b → 0.01
```

```
{-100, 0. - 16.3915 i, 0. + 16.3915 i}

{-100, 0. - 51.8344 i, 0. + 51.8344 i}

{-100, 0. - 163.915 i, 0. + 163.915 i}

{-100, 0. - 1.63915 i, 0. + 1.63915 i}
```

```
Eigenvalues[{{0, 1, 0}, {b, alpha6 * (-3 * vdc + 12 * R * xbar5), 3 * vdc - 12 * R * xbar5 +
               6 * L * alpha5 * xbar5}, {b, -3 * vdc + 12 * R * xbar5 + 6 * L * alpha5 * xbar5,
              3 * vdc - 12 * R * xbar5 + 6 * L * alpha5 * xbar5 - alpha5}}] /.
         xtilde5 -> 0 /. xtilde6 -> 0 /. R → 0.5 /. vdc → 90 /. L → 0.0014 /.
    xbar5 → 0.22 /. alpha5 → 100 /. alpha6 → 100 /. b → 1
```

```
{-26 865.3, -0.0000223971, 166.195}
```

```
Expand[CharacteristicPolynomial[
  {{m[[1]], m[[2]], m[[3]]}, {m[[4]], m[[5]], m[[6]]}, {m[[7]], m[[8]], m[[9]]}}, s]]
```

$$-\text{alpha5}\, s^2 - s^3 - 3\,\text{alpha5}\, b\, \text{vdc} - 3\, b\, s\, \text{vdc} + 12\,\text{alpha5}\, b\, R\, \text{xbar5} + 12\, b\, R\, s\, \text{xbar5} - 12\,\text{alpha5}\, b^2\, R\, \xi_6 - 12\, b^2\, R\, s\, \xi_6$$

```
lyapunovequation6 =
 Expand[xtilde6 * (dottx6)] /. ξ1 → 0 /. ξ2 → 0 /. ξ4 → 0 /. ξ5 → 0 /. ξ6 → 0 /.
       vdc → 90 /. R → 0.5 /. L → 0.014 /. xtilde5 → 0 // Flatten
```

```
{0}
```

```
Plot3D[lyapunovequation6 /. alpha6 → 1, {xbar5, -0.2, 0.2},
 {xtilde6, -110, 100}, PlotRange → Automatic, AxesLabel → Automatic]
Plot3D[lyapunovequation6 /. alpha6 → 10, {xbar5, -0.2, 0.2},
 {xtilde6, -110, 100}, PlotRange → Automatic, AxesLabel → Automatic]
```

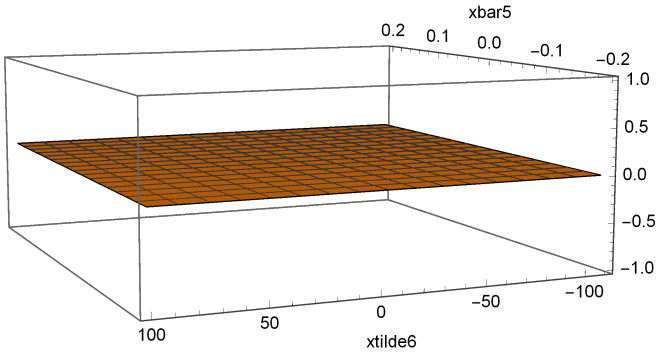

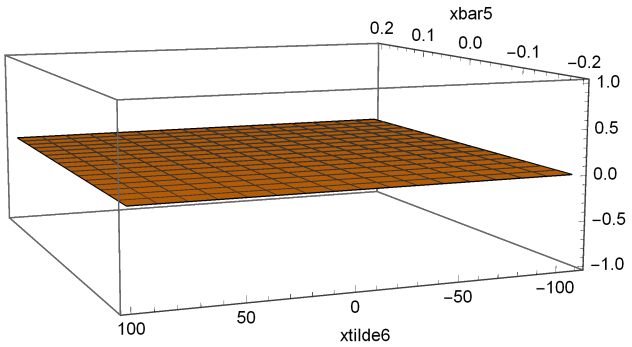

APÊNDICE C

Bilinear Control Code at Wolfram Mathematica

APPENDIX B : Bilinear control code at Wolfram Mathematica 11.2

```
Clear["Global`*"]
Clear[u1b, u2b, u3b, u4b, u5b, q5]
req = R + 2 * Rc;
leq = L + 2 * Lc;
```

$$A = \begin{pmatrix} -\frac{req}{leq} & w & 0 & 0 & 0 & 0 & 0 \\ -w & -\frac{req}{leq} & 0 & 0 & 0 & 0 & 0 \\ 0 & 0 & -\frac{R}{L} & w & 0 & 0 & 0 \\ 0 & 0 & -w & -\frac{R}{L} & 0 & 0 & 0 \\ 0 & 0 & 0 & 0 & -\frac{R}{L} & 0 & 0 \\ 0 & 0 & 0 & 0 & 0 & 0 & 0 \\ 0 & 0 & 0 & 0 & 0 & 0 & 0 \end{pmatrix};$$

$$B_1 = \begin{pmatrix} 0 & 0 & 0 & 0 & 0 & 0 & 0 \\ 0 & 0 & 0 & 0 & 0 & 0 & 0 \\ 0 & 0 & 0 & 0 & 0 & 0 & 0 \\ 0 & 0 & 0 & 0 & 0 & 0 & 0 \\ 0 & 0 & 0 & 0 & 0 & 0 & 0 \\ -\frac{3}{4} & 0 & \frac{3}{2} & 0 & 0 & 0 & 0 \\ -\frac{3}{4} & 0 & \frac{3}{2} & 0 & 0 & 0 & 0 \end{pmatrix};$$

$$B_2 = \begin{pmatrix} 0 & 0 & 0 & 0 & 0 & 0 & 0 \\ 0 & 0 & 0 & 0 & 0 & 0 & 0 \\ 0 & 0 & 0 & 0 & 0 & 0 & 0 \\ 0 & 0 & 0 & 0 & 0 & 0 & 0 \\ 0 & 0 & 0 & 0 & 0 & 0 & 0 \\ 0 & -\frac{3}{4} & 0 & \frac{3}{2} & 0 & 0 & 0 \\ 0 & -\frac{3}{4} & 0 & \frac{3}{2} & 0 & 0 & 0 \end{pmatrix};$$

$$B_3 = \begin{pmatrix} 0 & 0 & 0 & 0 & 0 & 0 & 0 \\ 0 & 0 & 0 & 0 & 0 & 0 & 0 \\ 0 & 0 & 0 & 0 & 0 & 0 & 0 \\ 0 & 0 & 0 & 0 & 0 & 0 & 0 \\ 0 & 0 & 0 & 0 & 0 & 0 & 0 \\ \frac{3}{4} & 0 & \frac{3}{2} & 0 & 0 & 0 & 0 \\ -\frac{3}{4} & 0 & -\frac{3}{2} & 0 & 0 & 0 & 0 \end{pmatrix};$$

$$B_4 = \begin{pmatrix} 0 & 0 & 0 & 0 & 0 & 0 & 0 \\ 0 & 0 & 0 & 0 & 0 & 0 & 0 \\ 0 & 0 & 0 & 0 & 0 & 0 & 0 \\ 0 & 0 & 0 & 0 & 0 & 0 & 0 \\ 0 & 0 & 0 & 0 & 0 & 0 & 0 \\ 0 & \frac{3}{4} & 0 & \frac{3}{2} & 0 & 0 & 0 \\ 0 & -\frac{3}{4} & 0 & -\frac{3}{2} & 0 & 0 & 0 \end{pmatrix};$$

$$B_5 = \begin{pmatrix} 0 & 0 & 0 & 0 & 0 & 0 & 0 \\ 0 & 0 & 0 & 0 & 0 & 0 & 0 \\ 0 & 0 & 0 & 0 & 0 & 0 & 0 \\ 0 & 0 & 0 & 0 & 0 & 0 & 0 \\ 0 & 0 & 0 & 0 & 0 & 0 & 0 \\ 0 & 0 & 0 & 0 & 3 & 0 & 0 \\ 0 & 0 & 0 & 0 & 0 & 0 & 0 \end{pmatrix};$$

$$b_1 = \begin{pmatrix} \frac{1}{leq} \\ 0 \\ -\frac{1}{2 \times L} \\ 0 \\ 0 \\ 0 \\ 0 \end{pmatrix};$$

$$b_2 = \begin{pmatrix} 0 \\ \frac{1}{leq} \\ 0 \\ -\frac{1}{2 \times L} \\ 0 \\ 0 \\ 0 \end{pmatrix};$$

$$b_3 = \begin{pmatrix} -\frac{1}{leq} \\ 0 \\ -\frac{1}{2 \times L} \\ 0 \\ 0 \\ 0 \\ 0 \end{pmatrix};$$

$$b_4 = \begin{pmatrix} 0 \\ -\frac{1}{leq} \\ 0 \\ -\frac{1}{2 \times L} \\ 0 \\ 0 \\ 0 \end{pmatrix};$$

$$b_5 = \begin{pmatrix} 0 \\ 0 \\ 0 \\ 0 \\ -\frac{1}{2 \times L} \\ 0 \\ 0 \end{pmatrix};$$

$$d = \begin{pmatrix} \frac{2 \times vfd}{leq} \\ \frac{2 \times vfq}{leq} \\ 0 \\ 0 \\ \frac{vdc}{2 \times L} \\ 0 \\ 0 \end{pmatrix};$$

$$u = \begin{pmatrix} vud \\ vuq \\ vld \\ vlq \\ vu0 \end{pmatrix};$$

$$uB = \begin{pmatrix} vudB \\ vuqB \\ vldB \\ vlqB \\ vd0B \end{pmatrix};$$

$$x = \begin{pmatrix} x1 \\ x2 \\ x3 \\ x4 \\ x5 \\ x6 \\ x7 \end{pmatrix};$$

$$xt = \begin{pmatrix} x1t \\ x2t \\ x3t \\ x4t \\ x5t \\ x6t \\ x7t \end{pmatrix};$$

$$xb = \begin{pmatrix} x1b \\ x2b \\ x3b \\ x4b \\ x5b \\ x6b \\ x7b \end{pmatrix};$$

```
Rc = 3 / 100;
Lc = 5 / 1000;
R = 5 / 10;
L = 14 / 1000;
capa = 3 / 1000;
w = 2 * Pi * 60;
$Assumptions = u1b ∈ Reals;
$Assumptions = u2b ∈ Reals;
$Assumptions = u3b ∈ Reals;
$Assumptions = u4b ∈ Reals;
$Assumptions = u5b ∈ Reals;
$Assumptions = {P, Q, p1, p2, a, b} ∈ Reals;
Atilde = A + B1 × u1b + B2 × u2b + B3 × u3b + B4 × u4b + B5 × u5b /. {u3b → -u1b, u4b → -u2b};
Simplify[Eigenvalues[Atilde]];
```

```
{E, Λ} = JordanDecomposition[Atilde];
```

$$T = \begin{pmatrix} 0 & 0 & 0 & 0 & 1 & 0 & 0 \\ 0 & 0 & 0 & 0 & 0 & 1 & 0 \\ 0 & 0 & 0 & 0 & 0 & 0 & 1 \\ 0 & 0 & 0 & 1 & 0 & 0 & 0 \\ 0 & 0 & 1 & 0 & 0 & 0 & 0 \\ 0 & 1 & 0 & 0 & 0 & 0 & 0 \\ 1 & 0 & 0 & 0 & 0 & 0 & 0 \end{pmatrix};$$

```
Λstar = Simplify[Transpose[T].Λ.T];
```

$$Qm = \begin{pmatrix} q & 0 & 0 & 0 & 0 \\ 0 & q & 0 & 0 & 0 \\ 0 & 0 & q & 0 & 0 \\ 0 & 0 & 0 & q & 0 \\ 0 & 0 & 0 & 0 & q \end{pmatrix};$$

```
Q7 = DiagonalMatrix[{1, 1, 1, 1, 1, 0, 0}];
Q7[[1 ;; 5, 1 ;; 5]] = Qm[[1 ;; 5, 1 ;; 5]];
Γ = LyapunovSolve[Re[Λstar[[1 ;; 5, 1 ;; 5]]], -Qm];

Γ7 = DiagonalMatrix[{1, 1, 1, 1, 1, p1, p2}];

Γ7[[1 ;; 5, 1 ;; 5]] = Γ[[1 ;; 5, 1 ;; 5]];
Γ.Re[Λstar[[1 ;; 5, 1 ;; 5]]] + Re[Λstar[[1 ;; 5, 1 ;; 5]]].Transpose[Γ];
Γ7.Re[Λstar] + Re[Λstar].Transpose[Γ7];
Γ7.Λstar + Λstar.Transpose[Γ7];
U = Simplify[E.T];
```

```
Rc = 3 / 100;
Lc = 5 / 1000;
R = 5 / 100;
L = 14 / 100;
capa = 3 / 1000;
w = 2 * Pi * 60;
vfd = 30;
vfq = 0;
vdc = 90;
x1b = (2 × P) / (3 × vfd);
x2b = (-2 × Q) / (3 × vfd); x3b = 0; x4b = 0;
x6b = (3 × cap × (vdc - 2 × R × x5b)^2) / 20;
x7b = 0;
u1b = (req × x1b) / 2 - (w × leq × x2b) / 2 - vfd;
u2b = (req × x2b) / 2 + (w × leq × x1b) / 2 - vfq;
x5b = Simplify[1 / (4 × R) (vdc - √(vdc^2 - 8 × R × (0.5 × x1b × u1b + 0.5 × x2b × u2b)))];
u5b = Simplify[-2 × R × x5b + vdc];

Qteste = U.Q7.Inverse[U];

Pteste = Re[ConjugateTranspose[Inverse[U]].Γ7.Inverse[U]];

(*u1t=ComplexExpand[Simplify[(Transpose[B1.xt+b1+B1.xb])].P2.xt]*)
(*u2t=ComplexExpand[Simplify[(Transpose[B2.xt+b2+B2.xb])].P2.xt]*)
(*u3t=ComplexExpand[Simplify[(Transpose[B3.xt+b3+B3.xb])].P2.xt]*)
(*u4t=ComplexExpand[Simplify[(Transpose[B4.xt+b4+B4.xb])].P2.xt]*)
(*u5t=ComplexExpand[Simplify[(Transpose[B5.xt+b5+B5.xb])].P2.xt]*)

(*Block[{$Assumptions=n∈Integers&&p∈Primes&&n>0},operations]*)

u1t = Expand[FullSimplify[
    Block[{$Assumptions = P < 30 && P > -30 && Q < 30 && Q > -30 && p1 > 0 && p2 > 0 && q > 0},
     Refine[(Transpose[B1.xt + b1 + B1.xb]).Pteste.xt]]]] /. x_ /; Abs[x] ≤ 10^-5 → 0
```

$$\{\{6.66667\,x1t - 0.0166667\,P\,x1t - \frac{3\,x1t^2}{4} - 0.0166667\,P\,x2t - 0.75\,x1t\,x2t - 3.57143\,x3t + 1.5\,x1t\,x3t + 1.5\,x2t\,x3t + 0.015\,P\,x4t + 0.675\,x1t\,x4t - 1.35\,x3t\,x4t - 0.00666667\,P\,x5t - 0.3\,x1t\,x5t + 0.6\,x3t\,x5t - 0.0166667\,P\,x6t - 0.75\,x1t\,x6t + 1.5\,x3t\,x6t + 3.21429\,x7t - 0.0166667\,P\,x7t - 0.75\,x1t\,x7t + 1.5\,x3t\,x7t\}\}$$

```
u2t = Expand[FullSimplify[
    Block[{$Assumptions = P < 30 && P > -30 && Q < 30 && Q > -30 && p1 > 0 && p2 > 0 && q > 0},
     Refine[(Transpose[B2.xt + b2 + B2.xb]).Pteste.xt]]]] /. x_ /; Abs[x] ≤ 10^-5 → 0
```

$$\left\{\left\{0.0166667\,Q\,x1t + 6.66667\,x2t + 0.0166667\,Q\,x2t - 0.75\,x1t\,x2t - \frac{3\,x2t^2}{4} - \frac{25\,x4t}{7} - 0.015\,Q\,x4t + \frac{3\,x1t\,x4t}{2} + 2.175\,x2t\,x4t - 1.35\,x4t^2 + 0.00666667\,Q\,x5t - 0.3\,x2t\,x5t + 0.6\,x4t\,x5t + 0.0166667\,Q\,x6t - 0.75\,x2t\,x6t + \frac{3\,x4t\,x6t}{2} + 0.0166667\,Q\,x7t - 0.75\,x2t\,x7t + \frac{3\,x4t\,x7t}{2}\right\}\right\}$$

```
u3t = Expand[FullSimplify[
    Block[{$Assumptions = P < 30 && P > -30 && Q < 30 && Q > -30 && p1 > 0 && p2 > 0 && q > 0},
     Refine[(Transpose[B3.xt + b3 + B3.xb]).Pteste.xt]]]] /. x_ /; Abs[x] ≤ 10^-5 → 0
```

$$\left\{\left\{-6.66667\,x1t - 0.0166667\,P\,x1t - \frac{3\,x1t^2}{4} + 0.0166667\,P\,x2t + 0.75\,x1t\,x2t - 3.57143\,x3t - 1.5\,x1t\,x3t + 1.5\,x2t\,x3t + 0.015\,P\,x4t + 0.675\,x1t\,x4t + 1.35\,x3t\,x4t + 0.00666667\,P\,x5t + 0.3\,x1t\,x5t + 0.6\,x3t\,x5t + 0.0166667\,P\,x6t + 0.75\,x1t\,x6t + 1.5\,x3t\,x6t + 3.21429\,x7t - 0.0166667\,P\,x7t - 0.75\,x1t\,x7t - 1.5\,x3t\,x7t\right\}\right\}$$

```
u4t = Expand[FullSimplify[
    Block[{$Assumptions = P < 30 && P > -30 && Q < 30 && Q > -30 && p1 > 0 && p2 > 0 && q > 0},
     Refine[(Transpose[B4.xt + b4 + B4.xb]).Pteste.xt]]]] /. x_ /; Abs[x] ≤ 10^-5 → 0
```

$$\left\{\left\{0.0166667\,Q\,x1t - 6.66667\,x2t - 0.0166667\,Q\,x2t - 0.75\,x1t\,x2t + 0.75\,x2t^2 - \frac{25\,x4t}{7} - 0.015\,Q\,x4t - 1.5\,x1t\,x4t + 2.175\,x2t\,x4t + 1.35\,x4t^2 - 0.00666667\,Q\,x5t + 0.3\,x2t\,x5t + 0.6\,x4t\,x5t - 0.0166667\,Q\,x6t + 0.75\,x2t\,x6t + 1.5\,x4t\,x6t + 0.0166667\,Q\,x7t - 0.75\,x2t\,x7t - 1.5\,x4t\,x7t\right\}\right\}$$

```
u5t = Expand[FullSimplify[
    Block[{$Assumptions = P < 30 && P > -30 && Q < 30 && Q > -30 && p1 > 0 && p2 > 0 && q > 0},
     Refine[(Transpose[B5.xt + b5 + B5.xb]).Pteste.xt]]]] /. x_ /; Abs[x] ≤ 10^-5 → 0
```

$$\left\{\left\{1350.\,x2t - 15.\,\sqrt{8100. + 0.133333\,P}\;x2t - 3.57143\,x3t + 536.429\,x5t - 6.\,\sqrt{8100. + 0.133333\,P}\;x5t + 3.\,x2t\,x5t + 1.2\,x5t^2 + 1348.57\,x6t - 15.\,\sqrt{8100. + 0.133333\,P}\;x6t + 3.\,x5t\,x6t\right\}\right\}$$

```
u7t = Expand[FullSimplify[
    Block[{$Assumptions = P < 30 && P > -30 && Q < 30 && Q > -30 && p1 > 0 && p2 > 0 && q > 0},
     Refine[(Transpose[B1.xt + b1 + B1.xb]).Pteste.xt]]]] /. x_ /; Abs[x] ≤ 10^-6 → 0
```

$$\left\{\left\{6.66667\,x1t - 0.0166667\,P\,x1t - \frac{3\,x1t^2}{4} - 0.0166667\,P\,x2t - 0.75\,x1t\,x2t - 3.57143\,x3t + 1.5\,x1t\,x3t + 1.5\,x2t\,x3t + 0.015\,P\,x4t + 0.675\,x1t\,x4t - 1.35\,x3t\,x4t - 0.00666667\,P\,x5t - 0.3\,x1t\,x5t + 0.6\,x3t\,x5t - 0.0166667\,P\,x6t - 0.75\,x1t\,x6t + 1.5\,x3t\,x6t + 3.21429\,x7t - 0.0166667\,P\,x7t - 0.75\,x1t\,x7t + 1.5\,x3t\,x7t\right\}\right\}$$

U

$$\left\{\left\{0, 0, \frac{20\left(7-36\,i\,\pi\right)}{9\left(-30+\frac{11\,P}{9000}+i\left(\frac{P\,\pi}{5}-\frac{11\,Q}{9000}\right)+\frac{\pi\,Q}{5}\right)}, \frac{20\left(7+36\,i\,\pi\right)}{9\left(-30+\frac{11\,P}{9000}-i\left(\frac{P\,\pi}{5}-\frac{11\,Q}{9000}\right)+\frac{\pi\,Q}{5}\right)}, 0, 0, 0\right\},\right.$$

$$\left\{0, 0, \frac{20\left(7\,i+36\,\pi\right)}{9\left(-30+\frac{11\,P}{9000}+i\left(\frac{P\,\pi}{5}-\frac{11\,Q}{9000}\right)+\frac{\pi\,Q}{5}\right)}, \frac{20\left(-7\,i+36\,\pi\right)}{9\left(-30+\frac{11\,P}{9000}-i\left(\frac{P\,\pi}{5}-\frac{11\,Q}{9000}\right)+\frac{\pi\,Q}{5}\right)}, 0, 0, 0\right\},$$

$$\left\{\frac{10\,i\left(25\,i+84\,\pi\right)}{21\left(-30+\frac{11\,P}{9000}+i\left(\frac{P\,\pi}{5}-\frac{11\,Q}{9000}\right)+\frac{\pi\,Q}{5}\right)}, -\frac{250+840\,i\,\pi}{21\left(-30+\frac{11\,P}{9000}-i\left(\frac{P\,\pi}{5}-\frac{11\,Q}{9000}\right)+\frac{\pi\,Q}{5}\right)}, 0, 0, 0, 0, 0\right\},$$

$$\left\{-\frac{10\left(25\,i+84\,\pi\right)}{21\left(-30+\frac{11\,P}{9000}+i\left(\frac{P\,\pi}{5}-\frac{11\,Q}{9000}\right)+\frac{\pi\,Q}{5}\right)},\right.$$

$$\left.\left(250\,i-840\,\pi\right)\Big/\left(-21\,i\left(\frac{P\,\pi}{5}-\frac{11\,Q}{9000}\right)+21\left(-30+\frac{11\,P}{9000}+\frac{\pi\,Q}{5}\right)\right), 0, 0, 0, 0, 0\right\},$$

$$\left\{0, 0, 0, 0, -\left(500\Big/\left(21\left(90+\sqrt{\left(8100.+0.133333\,P-5.4321\times10^{-6}\,P^2-5.4321\times10^{-6}\,Q^2\right)}\right)\right)\right),\right.$$

$$\left.0, 0\right\}, \{0, 0, 1, 1, 1, 0, 1\}, \{1, 1, 0, 0, 0, 1, 0\}\Big\}$$